1-1-2010

Activation Of Tumor Cell Death Program By Targeting The Ubiquitin-Proteasome Pathway: Significance In Cancer Treatment And Prevention

Michael Joseph Frezza
Wayne State University

ACTIVATION OF TUMOR CELL DEATH PROGRAM BY TARGETING THE UBIQUITIN-PROTEASOME PATHWAY: SIGNIFICANCE IN CANCER TREATMENT AND PREVENTION

by

MICHAEL FREZZA

DISSERTATION

Submitted to the Graduate School

of Wayne State University,

Detroit, Michigan

in partial fulfillment of the requirements

for the degree of

DOCTOR OF PHILOSOPHY

2010

MAJOR: CANCER BIOLOGY

Approved by:

_____

Advisor Date

_____

_____

_____

_____

DEDICATION

For my father, who instilled in me the virtues of science and all its possibilities, and whose creative passion played a pivotal role in my pursuit of a scientific career. For my mother, who always believed in and supported me, and whose love, strength, and encouragement have been a source of inspiration. For my wife, whose unwavering love and source of strength, allowed my dream to become a reality. For my unborn daughter, your impending arrival has brought tremendous joy and fulfillment into my life. For my late grandparents, whose encounter with cancer was a catalyst in my decision to pursue a career in cancer research. To my entire family and close circle of friends, your unwavering support and encouragement has not only helped me realize my full potential, but has made me a better person. To all of these important people in my life, I am most grateful and indebted to.

ACKNOWLEDGEMENTS

I would like to thank Dr. Q. Ping Dou, for the guidance and support as my research mentor over the last five years. Your thoughtful insight and criticisms have been indispensable as I've progressed from an ambitious student to a thoughtful scientist, and will serve me well throughout my career development. A special thank you goes to my committee members who have raised important questions and provided direction throughout my graduate studies: Dr. Claudio Verani, Dr. Ramzi Mohammad, and Dr. Ye-Shih Ho.

Thank you to the entire laboratory of Dr. Claudio Verani, who synthesized and provided the different analogs of gallium, copper, zinc, and nickel in [NN'O]- containing ligands, which made this work possible. A special thanks to Dr. Verani, Dajena Tomco and Sarmad Hindo who played an important role in my dissertation research, and made we realize the importance of chemistry in approaching cancer research.

Thank you to Dr. Dolores Fregona for synthesizing and providing the various gold-containing compounds that were important to my dissertation work. Thanks to Dr. Shumei Zhai and Dr. Haijun Zhang for assistance with gene clone and recombination for the AR project.

Thanks to Eric Van Buren, Alden Wong and the Flow Cytometry Core at the Karmanos Cancer Institute for help with the ROS and apoptosis assays. Thanks to the Karmanos Cancer Institute Pathology Core Facility for assisting with different immunohistochemistry assays.

A special thanks to the entire Dou lab, both current and present members, who have provided help and encouragement throughout my graduate studies and helped make me a better scientist. Thank you to Dr. Di Chen and Cindy Cui, who have helped me immensely

over the years in overcoming obstacles in my research work. Your support and friendship means a great deal to me, for which I'm most grateful. Thank you to our administrator Carol Maconochie who was always there to lend assistance in any capacity.

A final thank you goes to the Ruth L. Kirschstein National Research Service Award from the National Cancer Institute. I am most honored and grateful to have been chosen for such a prestigious award that was instrumental in facilitating the progress of my dissertation research.

TABLE OF CONTENTS

LIST OF TABLES

LIST OF FIGURES

CHAPTER 1

INTRODUCTION

Cancer remains a major health problem in the United States and throughout many parts of the world, accounting for 1 in 4 deaths in the United States [Jemal et al., 2009]. Cancer is the second leading cause of death in the United States after heart disease [Jemal et al., 2008]. The highest incidence of new cancer cases of men and women in the United States are found in prostate and breast, respectively. However, lung cancer is responsible for the most deaths due to malignancy in both men and women [Jemal et al., 2009]. Although progress has been made in reducing incidence and mortality rates over the years, continuing this positive trend will require sustained advancements in the prevention, detection and treatment of human cancer.

The process by which a normal cell develops into a malignant cell with the capacity for tumor development requires multiple cellular events. Cancer is a highly heterogeneous disease arising from multiple tissue types and displaying great phenotypic and genotypic diversity [Hanahan and Weinberg, 2000]. There are more than 100 distinct types of cancer and subtypes of tumors that can be found within different organs. Six essential alterations have been proposed a decade ago that govern the biological changes acquired during tumor development that are characteristic for malignant cells: self-sufficiency in growth signals, insensitivity to growth-inhibitory signals, evasion of programmed cell death (apoptosis), limitless replicative potential, sustained angiogenesis, and tissue invasion and metastasis [Hanahan and Weinberg, 2000]. Indentifying these alterations has allowed investigators to probe these complex pathways to gain a better understanding of the initiation, growth, and

progression of carcinogenesis. Moreover, these findings have had profound implications in the generation of new therapies for the intervention and treatment of cancer.

The most common modalities in the treatment of cancer involve surgery, radiation therapy, and chemotherapy [Abou-Jawde et al., 2003; Jabbour et al., 2007]. Although these treatment options can result in a positive clinical outcome, they do not represent a curative strategy in most cases. For example, chemotherapy is often effective against many tumors, but its clinical success is often limited by factors such as drug resistance and toxicity [Sarkar and Li, 2009]. More recently, strategies toward the treatment of human cancer have been pursued that can overcome the dysregulated cell machinery of tumor cells and induce cell death without the added systemic toxicity.

Due to the importance of the ubiquitin-proteasome pathway in regulating protein turnover, including those involved in tumorigenesis, the proteasome has emerged as an attractive target in cancer therapy [Goldberg, 2003; Nalepa et al., 2006]. Cancer cells have been shown to exhibit higher proteasome activity compared to normal cells, thus making tumor cells more sensitive to its blockade. Importantly, proteasome inhibition has been shown to induce cell cycle arrest and apoptosis selectively in malignant cells compared to its normal counterpart [An et al., 1998; Dou and Li, 1999]. These important attributes make proteasome inhibitors attractive drug candidates in the treatment of human cancer. Due to the significant challenges of anti-cancer drug discovery, exploring the interface between structural biology and chemistry may provide the most productive means for discovering and improving upon novel anticancer agents [Neidle and Thurston, 2005].

The following dissertation focuses on different metal-containing complexes from a class of [NN"O]-containing ligands with substitutions made at the 4th and 6th positions.

These metal-containing complexes were tested for their abilities to inhibit the proteasome and induce apoptosis in tumor cells. Special emphasis will be given to discerning structure activity relationships as they relate to the nature of the ligand and metal. Additionally, chapters 5 and 6 of this dissertation focus on mechanistic studies relating to the involvement of proteasome inhibition-mediated events in tumor cells. Importantly, how the oxidation state of the metal can influence the cellular events culminating in tumor cell death. To build upon the mechanistic studies in this body of work, special emphasis is given to understanding the role of the androgen receptor, and how it influences regulatory events involved in prostate tumor cell death upon exposure to therapeutic stimuli.

The ubiquitin-proteasome pathway

The balance between protein synthesis and degradation is a tightly regulated process, and is essential to the maintenance of normal cellular function [Goldberg, 2003]. The ubiquitin-proteasome pathway (UPP) is responsible for the proteolytic processing of proteins essential for the regulation of biological processes, such as development, differentiation, cell proliferation, signal transduction, and apoptosis [Nalepa et al., 2006]. The majority of intracellular protein degradation is facilitated through the UPP, which represents the final common effector for proteolysis (Fig. 1) [Ciechanover et al., 2000; Orlowski and Kuhn, 2008]. The UPP involves two critical steps: conjugation of multiple ubiquitin molecules to the protein substrate, followed by degradation of the tagged protein by the 26S proteasome (Fig. 1) [Ciechanover, 1998].

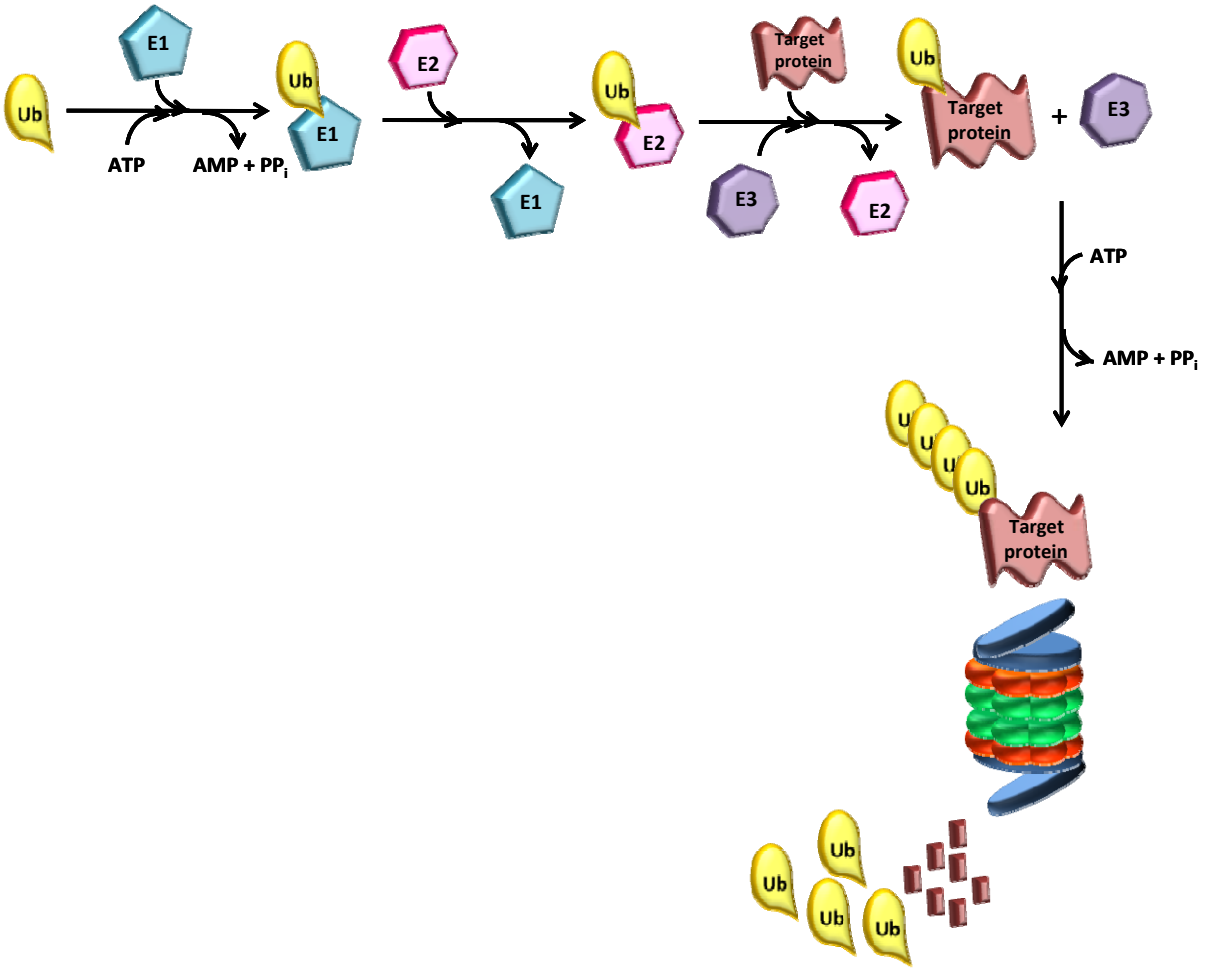

Figure 1. Schematic representation of the ubiquitin-proteasome pathway.

Proteins marked for destruction by the proteasome are first tagged with polyubiquitin molecules in an ATP-dependent process. Ubiquitin (Ub) is covalently linked to target proteins by a multi-enzymatic system consisting of Ub-activating (E1), Ub-conjugating (E2), and Ub-ligating (E3). E1 activates an Ub monomer through adenylation and formation of high-energy thiol ester bond and then transferred to Ub-conjugating (E2) enzyme. Transfer of Ub to a reactive lysine residue of a target protein is facilitated by ubiquitin (E3) ligating enzyme. Polyubiquitinated proteins are recognized by the 19S regulatory complex of the 26S proteasome and fed into the 20S catalytic core for degradation into oligopeptides and the ubiquitin molecules recycled.

The 26S proteasome is a multisubunit protease (2.5 MDa), that resides in the nucleus and cytosol, and selectively degrades intracellular proteins. The 26S proteasome contains the 20S proteasome which serves as the catalytic core and two 19S regulatory subunits, which acts as a recognition site for protein turnover (Fig. 2) [Adams, 2004; Peters et al., 1993]. The 20S core particle contains 4 stacked rings that form a barrel-like structure with a central cavity composed of a total of 28 subunits [Baumeister et al., 1998; Groll et al., 1997]. These stacked rings include two non-catalytic α rings outside of two catalytic β rings, and together form a special αββα arrangement (Fig. 2). The α subunits bar the direct access to the active site of the complex by allowing access to only unfolded substrate polypeptides. The proteolytic activities are confined to the β subunits that harbor the features of the multiple enzymatic activities [Groll et al., 1999]. These are best represented by the β1, β2, and β5 subunits which are responsible for the caspase or peptidyl-glutamyl peptide-hydrolyzing-like (PGPH), trypsin-like, and chymotrypsin-like (CT-like) proteolytic activities of the 20S catalytic core, respectively (Fig. 2) [DeMartino and Slaughter, 1999]. In all three of these β-subunits, the catalytically active residue (Thr1) at the amino terminal is responsible for catalysis, which could be targeted by proteasome inhibitors through nucleophilic attack [Goldberg et al., 2002; Groll et al., 1997].

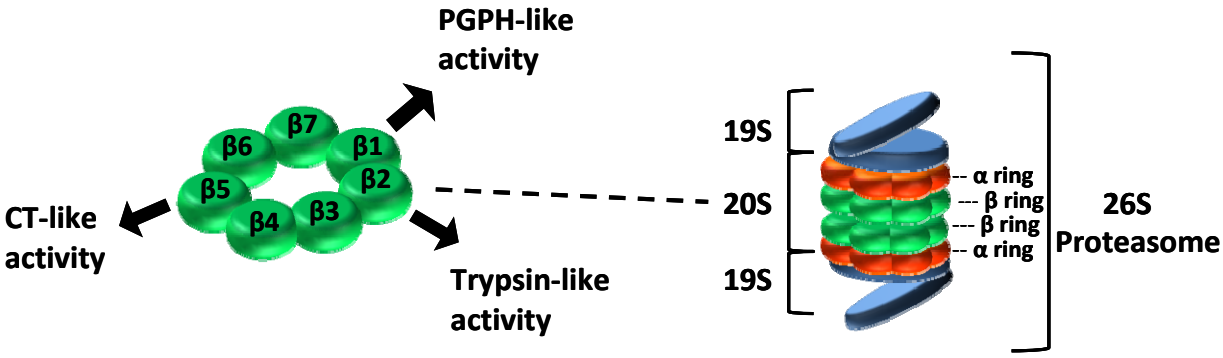

Figure 2. Schematic representation of the 26S proteasome

The 26S proteasome consists of the 20S catalytic core and two 19S caps located on each side of the core. The 19S caps act as a recognition site for ubiquitinated proteins and regulate protein entry into the 20S core. The 20S core is a barrel-like structure containing the primary sites of proteolytic activities. The outer α subunits serve as a gate to regulate protein entry into the inner catalytic site. The inner β subunits line the central cavity and are responsible for the chymotrypsin-like (β-5), trypsin-like (β-2), and the PGPH-like (β-1) activities.

In addition, the 19S particle (700 kDa) serves as a regulatory subcomplex of the 26S proteasome (Fig. 2) which consists of six ATPase and at least eight non-ATPase subunits which are required for recognition, deubiquitination, unfolding and translocation of marked proteins before proteolytic degradation within the 20S proteasome [Coux et al., 1996]. Furthermore, the 11S particle is typically associated with the immunoproteasome, which contains a heptameric ring structure that binds to each end of the 20S core, acting as a potent activator of the proteasome [Whitby et al., 2000].

Proteins marked for degradation are first recognized and tagged with a chain of ubiquitin molecules (Fig. 1). Ubiquitin is a highly conserved 76 amino acid protein that serves as a tag for target proteins that are destined for destruction through the proteasome. The ubiquitin system is characterized by three different enzymes, Ub-activating (E1), Ub-conjugating (E2), and Ub-ligating (E3) which links to protein substrates through covalent binding to create polyubiquitinated proteins (Fig. 1) [Hershko and Ciechanover, 1998]. Initiation of this process is facilitated by the E1 enzyme which activates ubiquitin in an ATP-requiring step by forming a high energy thiol-ester bond at its C-terminus. Activated ubiquitin is then transferred from E1, to one of several distinct ubiquitin-conjugating enzymes (E2) through an additional thiol-ester intermediate. Finally, the ubiquitin-ligating enzyme (E3) facilitates the transfer of activated ubiquitin to the specific substrate at the lysine residues of target proteins (Fig. 1) [Adams, 2003; Ciechanover et al., 2000]. It has been well recognized that the ubiquitin conjugating system plays a critical role in the protein quality control machinery by acting as a cascade to control the precise degradation of intracellular proteins. However, evidence also suggests that several protein substrates, including ornithine decarboxylase, p21, IκB-α, retinoblastoma protein (RB), as well as

hypoxia-inducible factor may be degraded by the proteasome without the added necessity for ubiquitin marking [Hoyt and Coffino, 2004; Kong et al., 2007].

Molecular targets of the proteasome

Cell cycle

The proteasome is an important cellular contributor to many pathological disorders including cancer in which some regulatory proteins are either stabilized or degraded [Ciechanover, 1998]. Many important cellular targets of the proteasome have also been identified as important players in tumorigenesis, including cyclins [Chen et al., 2004b; Diehl et al., 1997], tumor suppressor protein p53 [Blagosklonny, 2002], Retinoblastoma protein (Rb) [Kalejta and Shenk, 2003], pro-apoptotic protein Bax [Li and Dou, 2000], cyclin dependent kinase inhibitor (CKI) p27 [Pagano et al., 1995], and the NF-κB inhibitor, IκB-α [Chen, 2005].

It has been well known that cyclins, cyclin-dependent kinases (CDKs), and CDK inhibitors (CKIs) are critical components involved in controlling the timely progression of the cell cycle [King et al., 1996; Sherr and Roberts, 1995]. It has been demonstrated that CKIs are associated with growth arrest [Serrano et al., 1995], and numerous studies support the role of CDK inhibitors p16, p21 and p27 as tumor suppressor proteins [Deng et al., 1995; Serrano et al., 1995; Sherr and Roberts, 1995]. Since CKIs, especially p27 are degraded through the ubiquitin-proteasome pathway, proteasome function has been implicated in tumor cell survival. Accordingly, pharmacological inhibition of proteasome activity leads to the accumulation of p27 and p21 followed by induction of cell cycle arrest and apoptosis [Dou and Li, 1999; Orlowski, 1999].

The rapid turnover of cyclins is also controlled by the ubiquitin-proteasome pathway and is an essential regulator of cell cycle progression. The degradation of cyclin D1 facilitates the exit out of G_1 phase of the cell cycle and is mediated by phosphorylation-dependent proteolysis [Diehl et al., 1997]. Cyclin E synthesis controls late G_1 progression and entry into S phase requires the degradation of cyclin E protein by the UPP [Won and Reed, 1996]. In addition, the passage of cells through S phase into G_2 requires the degradation of cyclin A, while cyclin B turnover is required for the completion of mitosis [Glotzer et al., 1991]. The proteasome has also been implicated in regulating the stability of CDC25A, CDC25B, and CDC25C phosphatases during cell cycle progression [Baldin et al., 1997; Bernardi et al., 2000; Chen et al., 2002]. Inhibition of proteasome function leads to the accumulation of many of these critical cellular targets leading to the blockade of cell cycle progression.

NF-κB

Another important proteasome target protein is NF-κB. Activation of NF-κB by the proteasome is *via* the processing of the p105 precursor into the p50 subunit of NF-κB and degradation of the NF-κB inhibitor, IκB [Chen et al., 1996; Palombella et al., 1994]. Liberated NF-κB translocates to the nucleus and activates target genes responsible for oncogenesis, angiogenesis, apoptosis inhibition, and other cellular processes [Adams, 2002]. Some of the direct transcriptional targets of NF-κB that block apoptosis have been identified as the prosurvival proteins Bcl-2 and Bcl-X_L [Chen et al., 2000; Grumont et al., 1999], the inhibitors of apoptosis c-IAP1 and c-IAP2, and TNF Receptor associated Factors 1 and 2 [Wang et al., 1998; Zhou et al., 1999]. One of the early mechanisms attributed to proteasome

inhibitors is that they disrupt NF-κB signaling by stabilizing IκB, which prevents nuclear translocation and activation of genes involved in carcinogenesis and cancer cell survival. Accumulation of IκB-α *via* proteasome inhibition prevents the activation of the anti-apoptotic NF-κB resulting in tumor cell apoptosis [Biswas and Iglehart, 2006]. This is best illustrated in multiple myeloma where constitutive activation of NF-κB has been observed in both cell culture and patients samples, and inhibition of its activity is associated with cell cycle arrest and apoptosis [Chauhan et al., 1996; Hideshima et al., 2001].

Proteasome and apoptosis

An important role of proteasome inhibitors is their ability to induce apoptosis preferentially in tumor cells and not in normal tissue [An et al., 1998; Ma et al., 2003]. Although the exact mechanism of action has remained elusive, many have demonstrated the ability of proteasome inhibitors to induce apoptosis by stabilizing pro-apoptotic proteins such as p53 and Bax, while reducing levels of some antiapoptotic proteins, such as Bcl-2 [Mortenson et al., 2005]. Bax, a member of the Bcl-2 family of proteins is distributed in the cytosol as a monomeric protein. Upon induction of apoptosis by proteasome inhibitors, Bax undergoes a conformational change to form a dimer which translocates to the mitochondria resulting in the loss of the mitochondrial membrane potential and release of cytochrome c [Li and Dou, 2000]. Furthermore, the tripeptidyl proteasome inhibitor *N*-carbobenzoxy-*L*-Leucyl-*L*-leucyl-norvalinal (LLnV) accumulates Bax to the mitochondria, where it interacts with the anti-apoptotic Bcl-2 protein to overcome Bcl-2-mediated protection from apoptosis [An et al., 1998; Li and Dou, 2000]. Therefore Bax degradation *via* the proteasome pathway is critical in regulating cell survival, and its accumulation is essential for blocking the growth

of some tumors [Li and Dou, 2000]. Conversely, turnover of the anti-apoptotic proteins, such as Bcl-2 and Bcl-X_L is critical in mitigating tumor growth and progression [Green and Reed, 1998]. In addition, proteasome inhibition has been accompanied by c-Jun-NH2 terminal kinase induction, generation of reactive oxygen species, activation of intrinsic caspase 9-mediated, and extrinsic caspase 8-mediated apoptosis [Nencioni et al., 2007; Orlowski and Kuhn, 2008]. These interesting findings coupled with the observation that highly proliferating tumor cells are more sensitive to the apoptotic stimuli of proteasome inhibitors, makes these drug candidates highly desirable in the treatment of human cancer.

Bortezomib

Bortezomib (Velcade, PS-341) (Fig. 3) is the first proteasome inhibitor to gain approval by the US Food and Drug Administration and is currently in use for the treatment of relapsed multiple myeloma (MM) and mantle cell lymphoma [Kane et al., 2003; Kane et al., 2007]. Bortezomib is a dipeptide boronic acid derivative that demonstrates considerable apoptotic inducing activity in a range of tumor cell lines and animal models [Adams et al., 1999; Frankel et al., 2000]. It is a slowly reversible inhibitor directed mostly against the β5- (chymotrypsin-like) and β1- (PGPH-like) subunits, with the β5 subunit inhibition responsible for its cell-death inducing capabilities (Fig. 4) [Crawford et al., 2006]. A major mechanism of action of bortezomib resides in its suppression of NF-κB activity by stabilizing its inhibitory molecule I-κB, resulting in the down-regulation of its target genes. This leads to decreased expression of myeloma cell adherence factors, and interference with adherence-mediated induction of interleukin-6 production [Hideshima et al., 2001; Orlowski and Baldwin, 2002]. Although the majority of success achieved with bortezomib has been in

hematological malignancies, its effect toward solid tumors has been investigated, but with less than encouraging results [Engel et al., 2007; Yang et al., 2006a]. Additionally, the antitumor effects of bortezomib has been evaluated as a single agent, or in combination with conventional therapies as a means to induce chemosensitization or overcome chemoresistance in various malignancies such as multiple myeloma, solid tumors, or other hematological malignancies [Orlowski and Kuhn, 2008].

Clinical studies have demonstrated that circulating proteasome levels could provide insight as a potential prognostic indicator for MM, lending support to the concept of targeting the proteasome in the treatment of MM [Jakob et al., 2007]. After a "proof of concept" study demonstrated the correlation of proteasome inhibition by bortezomib with tumor cell death, clinical trials evaluating bortezomib for the treatment of MM were initiated. Phase 1 trials using bortezomib as a single agent revealed remarkable efficacy for the treatment of various hematological malignancies [Orlowski et al., 2002]. As a result, bortezomib was further evaluated in two Phase II trials against relapsed multiple myeloma, the Clinical Response and Efficacy Study of Bortezomib in the Treatment of Relapsing Multiple Myeloma (CREST) and the larger Study of Uncontrolled Multiple Myeloma Managed with Proteasome Inhibition Therapy (SUMMIT).

Two doses of bortezomib were compared in the CREST trial (1.3 mg/m^2 and 1.0 mg/m^2) and the addition of Dexamethasone was permitted in cases of inadequate response after 2-4 cycles of therapy. Results showed a higher response in patients receiving the higher dose administration of bortezomib (50% vs. 37%) [Jagannath et al., 2004]. The appearance of side effects included myelosuppression, particularly thrombocytopenia, gastrointestinal irritation, and peripheral sensory neuropathy. An extended follow up report on the CREST

study reported a 5-year-overall survival of 45% in the 1.3 mg/m^2 group and 32% in the 1.0 mg/m^2 group [Jagannath et al., 2008]. The SUMMIT trial found a response rate of 35% when 202 patients with relapsed MM were being treated with bortezomib at 1.3 mg/m^2, with dexamethasone added as needed [Richardson et al., 2003]. Following the remarkable clinical results from phase I and II trials, a large phase III trial APEX (Assessment of Proteasome Inhibition for Extending Remissions) was initiated comparing bortezomib with high-dose dexamethasone in patients with previously treated myeloma. These results demonstrated the superior clinical efficacy over dexamethasone in hematological malignancy patients in terms of response rate, time to progression, and survival [Richardson et al., 2007; Richardson et al., 2005].

Many cytotoxic agents have been found to induce the anti-apoptotic proteins, NF-κB and Bcl-2, which suggests that the use of proteasome inhibitors may be an effective strategy in inducing chemosensitization or overcoming chemoresistance [Ma et al., 2003; Mitsiades et al., 2003]. Moreover, bortezomib has been clinically investigated in combination with a variety of chemotherapeutics, and results from these studies show that bortezomib has generally been tolerable without significantly increased toxicity or large dose adjustments [Aghajanian et al., 2005; Messersmith et al., 2006].

Bortezomib has also shown to have activity against other hematological malignancies. In a phase 1 trial, one patient with refractory mantle cell lymphoma (MCL) and another with follicular center cell lymphoma (FCCL) responded to treatment with single-agent bortezomib [Orlowski et al., 2002]. In a phase II clinical trial of patients with refractory B-cell non-Hodgkins lymphoma (NHL) using bortezomib at a dose of 1.5 mg/m^2 on days 1, 4, 8, and 11 of repeating 21 day cycles, 41% of 33 patients with MCL responded

to treatment [Goy et al., 2005]. Another phase II trial involving MCL patients and other patients with indolent NHL showed responses in patients with FCCL [O'Connor et al., 2005]. Two additional Phase II trials demonstrated the superior efficacy of bortezomib, leading to its FDA approval for the treatment of previously treated MCL [Belch et al., 2007; Fisher et al., 2006].

Although significant efficacy has been achieved in clinical trials with bortezomib against a number of hematological malignancies, its activity toward solid tumors has yielded disappointing results. Bortezomib was tolerated but no responses were observed in patients with metastatic breast cancer [Engel et al., 2007; Yang et al., 2006a]. Single agent bortezomib exhibited only modest efficacy against androgen-independent prostate cancer [Papandreou et al., 2004]. A phase I/II dose escalation study showed that bortezomib/docetaxel combination therapy demonstrated antitumor activity, but its results were similar to docetaxel alone [Hainsworth et al., 2007]. Similarly, bortezomib in combination with pemetrexed did not demonstrate a clinical advantage in patients with non-small lung carcinoma (NSCLC) [Davies et al., 2007], gemcitabine in pancreatic cancer [Alberts et al., 2005], irinotecan in various advanced solid tumors [Ryan et al., 2006], or carboplatin in ovarian cancer [Aghajanian et al., 2005].

In the early development of proteasome inhibitors as potential drug candidates, there was great concern that the proteasome could not be inhibited without dire consequences because of the essential role it plays in cellular processes. Fortunately, an acceptable therapeutic index was achieved, but the appearance of toxic side effects have been documented throughout clinical testing. The most frequent toxic side effects associated with bortezomib treatment are nausea, fatigue, and diarrhea, and more serious ones include

thrombocytopenia, peripheral neuropathy, neutropenia, and lymphopenia [Shah and Orlowski, 2009]. These problems associated with bortezomib, plus development of resistance to this proteasome inhibitor drug in some solid tumors, have encouraged researchers to broaden the search for and discover new proteasome inhibitors with similar potency but decreased toxicity.

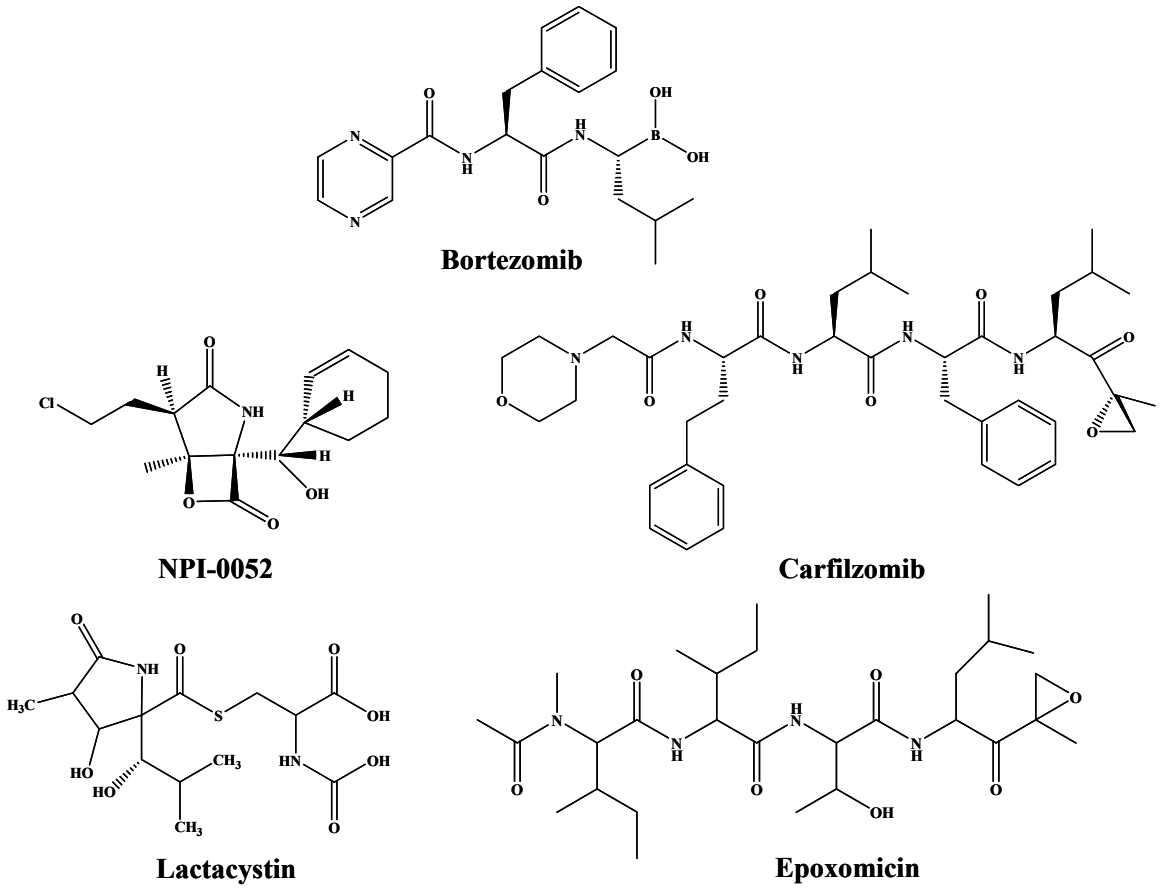

Figure 3. Chemical structures of proteasome inhibitors

The chemical structures depicted are currently in clinical use or under going clinical trials. Bortezomib is a dipeptide boronate analog currently in use for the treatment of multiple myeloma and mantle cell lymphoma. NPI-0052, is a natural product derivative resembling Lactacystin, the first proteasome inhibitor identified in nature. Carfilzomib is a peptide epoxyketone derived from epoxomicin. Both NPI-0052 and Carfilzomib are currently undergoing clinical trials for the treatment of multiple myeloma and other hematological malignancies.

Other clinically investigated proteasome inhibitors

NPI-0052 (Fig. 3), also referred to as salinosporamide A, is currently being developed by Nereus Pharmaceuticals, Inc. (San Diego, CA). This natural product derivative resembles lactacystin (Fig. 3); the first proteasome inhibitor identified in nature, and irreversibly targets all three active sites of the proteasome (Fig. 4) [Chauhan et al., 2006; Joazeiro et al., 2006]. Preclinical studies have suggested significantly stronger and more durable effects on the chymotrypsin-like and trypsin-like activities of the proteasome compared to bortezomib (Fig. 4) [Chauhan et al., 2005; Groll et al., 2006]. It has been suggested that the increased potency of NPI-0052 may be directly related to its emphasis on caspase 8-mediated apoptosis compared to bortezomib [Chauhan et al., 2005]. Perhaps, due to these properties, NPI-0052 was able to overcome bortezomib resistance and act synergistically with conventional therapy in various MM cell lines, as well as in primary lymphocytes from patients with chronic lymphocytic leukemia (CLL) [Chauhan et al., 2008; Chauhan et al., ; Sterz et al., 2008]. Phase 1 studies aimed at establishing optimal dosing of NPI-0052 against advanced solid tumors or refractory lymphomas and MM have been conducted [Yang et al., 2009]. Preliminary studies have shown it to be well tolerated with toxicities comparable to that of bortezomib in patients with myeloma [Shah and Orlowski, 2009]. Furthermore, clinical studies investigating NPI-0052 in combination with vorinostat are ongoing in a Phase Ib open-label study in patients with advanced non-small lung cancer (NCT00667082, Nereus Pharmaceuticals).

Carfilzomib (Fig. 3) is a peptide epoxyketone derived from epoxomicin (Fig. 3) that was developed by Proteolix, Inc. (South San Francisco, CA) and has entered clinical trials. Carfilzomib binds irreversibly to the proteasome, with increased specificity toward the

chymotryptic activity over the caspase-like or trypsin-like activities (Fig. 4) [Kuhn et al., 2007]. Preclinical studies suggest that carfilzomib showed higher apoptotic-inducing indices compared to bortezomib in primary plasma cell models, and were able to overcome resistance to bortezomib [Kuhn et al., 2007]. In tumor xenograft models, carfilzomib showed antitumor activity that was both dose and schedule dependent, with efficacy stronger than bortezomib when administered on its clinical dosing schedule [Demo et al., 2007]. Phase II clinical trials in patients with previously treated myeloma showed response rates in the range of 25-54 % [Yang et al., 2009]. Another clinical trial has been initiated to evaluate the efficacy and safety of carfilzomib with lenalidomide and dexamethasone in patients with relapsed MM (NCT00603447, Proteolix). Despite these encouraging results, there remains an unmet need to develop proteasome inhibitors with a broader spectrum of activity, especially toward solid tumors, as potential drug candidates. These include compounds harvested from nature, or harnessing the unique properties of metal-based compounds as potential proteasome inhibitors.

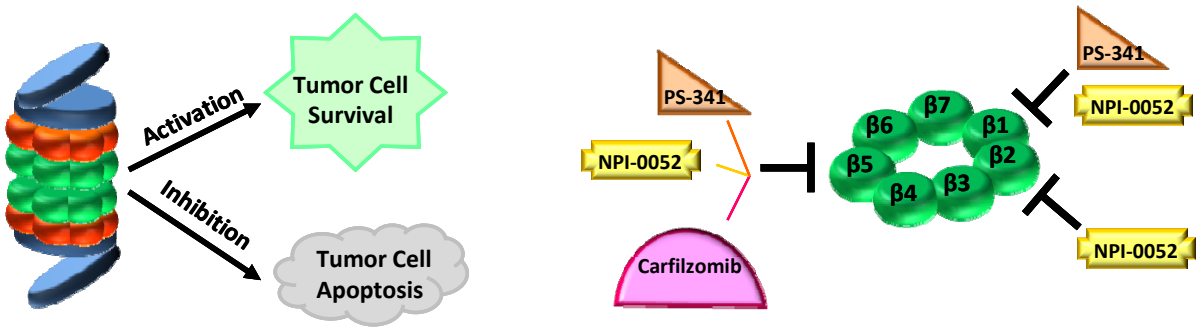

Figure 4. Proteasome inhibition by clinically used and tested proteasome inhibitors

The β-subunits of the 20S core contain three catalytic sites: β-1 (responsible for the caspase-like activity), β-2 (responsible for the trypsin-like activity), and β-5 (responsible for the chymotrypsin-like activity). Bortezomib is commonly used in the treatment of multiple myeloma, whereas NPI-0052 and Carfilzomib are undergoing clinical trials. These proteasome inhibitors predominantly affect the β-5 chymotryptic-like site which is associated with tumor cell growth, although their mechanisms of action may also play a role in binding to other sites.

Apoptosis

Apoptosis (programmed cell death) is a highly regulated form of cell death that is important in many biological processes, and plays an important role in the maintenance of tissue homeostasis. Deregulation of this process can disrupt the delicate balance between cell proliferation and cell death and lead to pathological disorders, including cancer [Fesik, 2005; Roth and Reed, 2002]. Apoptosis can be characterized by typical biochemical and morphological hallmarks, including cell shrinkage, nuclear DNA fragmentation, and membrane blebbing [Hengartner, 2000]. Induction of apoptosis by anticancer drugs converges in the activation of intracellular caspases which cleave various substrates in the cytoplasm and nucleus leading to the many of the morphological features of apoptotic cell death [Fulda and Debatin, 2006].

Apoptosis predominantly operates through two main intracellular cascades and is characterized by three fundamental steps: initiation, commitment and execution [Reed, 1997]. The intrinsic pathway or mitochondrial pathway is initiated by the release of apoptogenic factors such as cytochrome c from the mitochondria and forming the apoptosome, consisting of dATP (2'deoxyadenosine 5'triphosphate), apoptotic protease-activating factor 1 (APAF-1), and caspase 9 [Budihardjo et al., 1999; Fesik, 2005]. Formation of the apoptosome functions in promoting the processing of caspase 9 which leads to the recruitment and activation of the effector caspase 3, which in turn facilitates the proteolytic degradation of its target substrates [Hunter et al., 2007]. Conversely, Bcl-2 and Bcl-XL inhibit programmed cell death by preventing the release of cytochrome c, whereas pro-apoptotic Bcl-2 family members (such as Bak, Bax, Bad and Bid) promote the release of cytochrome c [Huang and Strasser, 2000].

The extrinsic pathway is activated by the engagement of death receptors such as CD95/Fas, the tumor necrosis factor (TNF) or TNF related apoptosis-inducing ligand (TRAIL) that are found at the cell surface. The intracellular death domains of these receptors recruit adaptor proteins (such as FADD and TRADD) along with the initiator caspase-8 and together comprise the death-inducing signaling complex (DISC) [Fesik, 2005]. Stimulation of death receptors results in the activation of caspase 8 which can propagate the apoptotic stimuli via the direct activation of the effector caspase-3 [Adams and Cory, 2007]. Additionally, connections exist at different levels linking the intrinsic and extrinsic pathways. Death receptor-mediated activation of caspase 8 may result in the cleavage of the Bcl-2 family member, Bid. Truncated Bid can then translocate to the mitochondria to release cytochrome c thereby triggering the apoptotic stimuli [Fulda and Debatin, 2004]. In addition to apoptosis, other mechanisms of cell death have been identified that operate independently of caspase activation. These nonapoptotic forms of cell death include among others, necrosis and autophagy.

Metals and metal complexes

The field of medicinal inorganic chemistry encompasses, but is not limited to, the administration (or removal) of a metal ion into (or from) a biological system for either therapeutic or diagnostic purposes [Scott and Orvig, 2009]. An important property of metals is that they form positively charged ions in aqueous solution that can bind to negatively charged biological molecules. Thus, the charge can be fine-tuned depending on the coordination environment involved, leading to the generation of a species that can be cationic, anionic, or neutral [Haas and Franz, 2009; Orvig and Abrams, 1999]. Additionally,

metal ions with high electron affinity can significantly polarize groups that are coordinated to them, fostering the generation of hydrolysis reactions [Haas and Franz, 2009].

In recent years, the field of medicinal inorganic chemistry has received considerable attention in the design of anticancer agents [Jakupec et al., 2008; Zhao and Lin, 2005]. Although metals have been used throughout human history in treating various pathological disorders, it has only been since the landmark discovery of cisplatin (Fig. 5) in the 1960's that the full impact of metal-based compounds in the treatment of cancer has been fully realized. Because the presence of metals under cellular conditions is a tightly regulated process, appropriate administrations of metal-containing drugs must be carefully defined to achieve an optimal therapeutic response [Holm et al., 1996; Mertz, 1993]. Otherwise, both excess and deficiency of metals may result in undesirable toxicity.

Metal-containing compounds offer many advantages over conventional carbon-based compounds in the development of new medicinal compounds. These advantages are due to their ability to coordinate ligands in a three dimensional configuration, thus allowing functionalization of groups that can be tailored to defined molecular targets [Fricker, 2007; Meggers, 2009]. Metal-based complexes offer a rich environment to build upon a variety of distinct molecular structures that confer a wide spectrum of coordination numbers and geometries, as well as kinetic properties, that cannot be realized with conventional carbon-based structures [Cohen, 2007; Ott and Gust, 2007; Yan et al., 2005]. The partially filled *d* orbitals in transition metals impart interesting electronic properties that can act as suitable probes in the design of anticancer agents [Hambley, 2007]. The oxidation state of a metal is also an important consideration in the design of coordination compounds, given that it allows the participation in biological redox chemistry and plays an influential role in optimal dose

and bioavailability of the agent administered [Orvig and Abrams, 1999; Thompson and Orvig, 2003]. Furthermore, the ability to undergo ligand exchanged reactions offers a myriad of opportunities for metals to interact and coordinate to biological molecules, as demonstrated by the widely used drug cisplatin [Fricker, 2007].

Platinum-based complexes

The discovery of cisplatin (Fig. 5) more than four decades ago represented a significant achievement in cancer therapy and stimulated efforts to investigate other platinum and non platinum metal-containing compounds for their potential use in the treatment of cancer [Desoize, 2004; Ott and Gust, 2007]. Cisplatin has been widely employed to treat a variety of tumors including ovarian, cervical, head and neck, non-small cell lung carcinoma, and testicular cancers, and is commonly used in combination regimens [Jamieson and Lippard, 1999; Kelland, 2007]. However, its widespread clinical use has been hampered by increased toxicity, and the appearance of intrinsic and acquired resistance [Galanski et al., 2003]. In an effort to address these shortcomings, 2nd and 3rd generation platinum analogs, namely carboplatin and oxaliplatin (Fig. 5), have been designed and clinically approved that maintain a more manageable toxicity profile [Alama et al., 2009]. Carboplatin is effective in the treatment of ovarian carcinoma, lung, and head and neck cancers [Harrap, 1985], while oxaliplatin (Fig. 5) is clinically approved for the treatment of colorectal cancer, which is resistant to cisplatin [de Gramont et al., 2000].

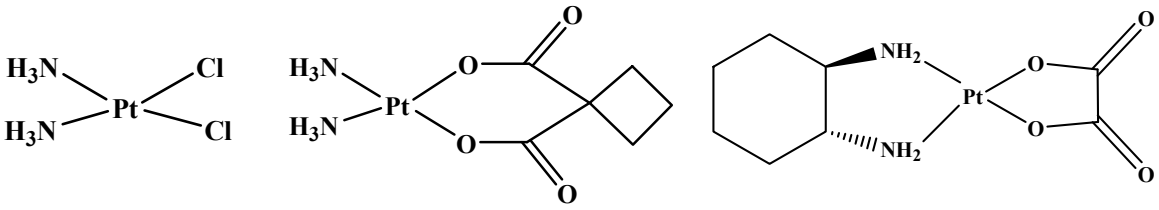

Cisplatin **Carboplatin** **Oxaliplatin**

Figure 5. Chemical structures of platinum-based anticancer agents.

The chemical structures depicted are platinum drugs used in the treatment of various malignancies. Carboplatin and Oxaliplatin are next generation platinum compounds that are currently used in the clinic.

A key factor underlying the antitumor effect of platinum-based compounds is related to its ligand exchange kinetics. Although the platinum-ligand bond exhibits similar thermodynamic durability (less than 100 kJ/mol) and is much weaker than typical coordination bonds, such as C-C, C-N, or C-O single and double bonds (between 250 and 500 kJ/mol) , the ligand exchange behavior is rather slow [Reedijk, 2003]. This gives them a high kinetic stability and allows much slower ligand exchange reactions on the order of minutes to days rather than seconds [Kostova, 2006; Montana and Batalla, 2009].

Upon binding of platinum-based compounds, various signal transduction pathways are activated, which interfere with different cellular processes including transcription and DNA replication, thereby triggering apoptotic cell death [Siddik, 2003]. The antitumor activity of cisplatin and carboplatin (Fig. 5) is derived from the formation of identical 1,2-intrastrand DNA cross-links [Fuertes et al., 2002; Galanski, 2006]. In contrast, the bulky diaminocyclohexane (DACH) carrier ligand of oxaliplatin (Fig. 5) is thought to confer less cross-resistance and a more favorable toxicity profile [Wang and Lippard, 2005].

In an effort to improve upon the limitations of platinum anticancer drugs, different metals and metal complexes that pose different mechanisms of action has been the subject of investigation as potential anticancer drugs.

Gallium

Investigation into the therapeutic utility of gallium was not pursued until the 1970's, when Group 13 (previously IIIA) elements including aluminum, indium, thallium and gallium were considered for efficacy in various experimental models for tumor growth inhibition. Only gallium represented a suitable therapeutic and toxicity profile that allowed

for further clinical development [Hart and Adamson, 1971; Hart et al., 1971]. Gallium was subsequently found to be active against accelerated bone turnover, tumor growth and immune disease [Blair et al., 1992; Orosz et al., 1996]. Based on positive clinical activity of gallium nitrate [$Ga(NO_3)_3$] against accelerated bone turnover, research efforts involving this metal salt was refocused toward its effects on bone breakdown and was subsequently approved for the treatment of hypercalcemia related to malignancy [Chitambar, 2004b]. Excitement toward gallium nitrate in anti-cancer therapy has only reappeared recently, fostering resurgence in investigating gallium-based compounds as anti-tumor agents [Chitambar, 2004b]. Gallium nitrate and other gallium compounds are currently being investigated in clinical trials to be used as single agents, or in combination with pre-existing chemotherapeutic agents against various malignancies [Einhorn, 2003; Weick et al., 1983]. Gallium nitrate is especially effective in lymphomas and in bladder cancer.

Because gallium (II) would exhibit an energetically unfavorable [Ar]3d104s1 configuration, and because the process $Ga^{3+} \rightarrow Ga^{4+} + e^-$ would require considerable energy (6200 kJ/mol), the trivalent form of gallium is redox-inactive, often being used as a probe for electroactive ligands [Imbert et al., 2005; Lanznaster et al., 2006].

The therapeutic application of gallium appears to be underscored by its biochemical similarities to the ferric ion, specifically its protein binding modes, but with a distinct physiological effect [Bernstein, 1998]. Mutually shared chemical characteristics include ionic radius, electronegativity and electron affinity [Green and Welch, 1989]. Therefore, gallium is expected to pursue similar biochemical pathways found in iron metabolism. However, it is the difference between these two ions that allows for gallium to be exploited as a therapeutic agent. Gallium, unlike iron, is redox inactive. This property prevents gallium

insertion into certain proteins involved with oxygen transport and precludes participation in other redox reactions of biological relevance [Hedley et al., 1988]. However, gallium is able to bind to proteins that require the trivalent form of iron, such as transferin, therefore disrupting normal cellular homeostasis. Increasing evidence suggests that this mimicking effect of gallium plays a pivotal role in the cytotoxicity of the metal [Jakupec and Keppler, 2004a]. Targeting of the transferin receptor (TFR) by metal-bound transferrin is achieved in a highly competitive fashion and is incorporated into cells *via* receptor mediated endocytosis, leading to intracellular accumulation of gallium [Chitambar, 2004a].

One of the critical targets for intracellular gallium appears to be ribonucleotide reductase, which catalyzes the rate-limiting step in DNA synthesis and is up-regulated in highly proliferating cells. Iron plays a key role in stabilizing the tyrosyl free radical in the R2 subunit of ribonucleotide reductase. However, the binding of gallium to this subunit serves as a destabilizing effector resulting in inhibition of DNA synthesis [Chitambar et al., 1988; Chitambar and Narasimhan, 1991]. This gallium-dependent inhibition of ribonucleotide reductase is in part related to the inhibition of cellular proliferation. Although the mechanism of cellular uptake is more readily understood, its downstream effects regulating its antiproliferative activity have been open to investigation.

Several gallium complexes have been synthesized and evaluated in clinical trials which have shown an increase in bioavailability and superior anti-tumor efficacy compared to gallium nitrate and other gallium based salts [Collery et al., 1996]. These findings provide evidence for developing gallium-based complexes with various ligand moieties that maximizes the therapeutic index. However, a full understanding of their molecular targets and the underlying mechanism responsible for their anticancer activity has yet to be

elucidated. Since our lab has previously shown that other metal-containing complexes such as copper, zinc, and gold could potently target and inhibit the cellular proteasome [Chen et al., 2006; Milacic et al., 2008a; Milacic et al., 2006], we hypothesize that gallium could have a similar effect. This dissertation will highlight the cellular proteasome as a molecular target for gallium-based complexes that is atleast partially responsible for their biological effects. The introductory section on tridentate ligands will explore the evolution of this ligand platform and it suitability as a metal complex endowed with anticancer activity.

Copper

Copper is another essential trace metal that has been selected by nature to be a driving force in many biochemical processes including chemical redox reactions, cellular growth, development, and angiogenesis [Chen et al., 2009; Tapiero et al., 2003]. Under biological conditions, copper exists in both (Cu^{+}) and (Cu^{2+}), which allows it to serve as a cofactor in redox reactions, such as cytochrome c oxidase (involved in the mitochondrial electron transport chain) and superoxide dismutase (involved in the detoxification of reactive oxygen species) [Gupte and Mumper, 2009; Kim et al., 2008]. The acquisition and distribution of copper is a tightly regulated process to assure proper uptake, distribution, and to avoid unnecessary binding to biomolecules [Chen and Dou, 2008; Radisky and Kaplan, 1999].

Depending on the oxidation state, the coordination chemistry of copper is often distinct: Cu^{+} shows a preference for sulfur donor ligands, such as cysteine or methionine, whereas Cu^{2+} prefers nitrogen donors such as histidine or oxygen donors such as glutamate or aspartate (Kim, 2008, 176). Copper in its reduced form (Cu^{+}) has a filled d^{10} configuration with no preference for geometry based on no LFSE (ligand field stabilization

energy) and thus can exist in a wide range of geometries [Marzano et al., 2009; Rorabacher, 2004]. The d^9 configuration of Cu^{2+} favors a four to six coordination arrangement due to Jahn-Teller distortions. Geometries include four-coordinate square-planar, five-coordinate trigonal bipyramidal, and six-coordinate axially distorted octahedral arrangements [Marzano et al., 2009; Rorabacher, 2004].

The role of copper in the growth and progression of malignancy has been the subject of intense investigation for the last two decades. This was born out of the realization that copper levels are altered in tumor bearing mice and humans [Apelgot et al., 1986; Zowczak et al., 2001]. Additionally, high serum and tissue levels of copper were found in various human tumors including breast [Kuo et al., 2002], prostate [Habib et al., 1980], colon [Nayak et al., 2003], lung [Diez et al., 1989], and brain [Turecky et al., 1984], compared to healthy subjects. The reasons for this elevation have not been fully elucidated and no firm conclusions could be established. Moreover, a number of clinical trials have shown promising results using copper chelation as an anticancer strategy [Brewer et al., 2000; Redman et al., 2003]. We have shown that copper binding compounds, such as CQ (Clioquinol) and DSF (Disulfiram) (Fig. 6), when complexed with copper, could target the and inhibit the proteasome *in vitro* and *in vivo* associated with apoptosis induction [Chen et al., 2007a; Chen et al., 2006]. Our hypothesis is predicated on the following observations: (i) tumor cells *in vivo* contains high levels of copper, (ii) this *in vivo* finding can be emulated under cell culture conditions (which contain low levels of copper) by supplementing exponentially growing cells with copper, (iii) treatment of tumor cells-containing heightened levels of copper with a copper chelating ligand can generate a copper complex which can target the tumor proteasome and induce cell death, (iv) alternatively, treating tumor cells

under cell culture conditions (containing low levels of copper) with a copper complex could mimic the biological effect observed under *in vivo* conditions. Due to the importance of copper in the growth and development of cancer, coupled with the anticancer activity of the copper metal, the use of copper complexes that target the tumor proteasome may have potential clinical relevance in the treatment of human cancer.

This dissertation will explore a series of copper-containing complexes with tridentate [NN'O] ligands appended with iodo groups at the 4^{th} and 6^{th} position as potential proteasome inhibitiors by taking a interdisciplinary apporoach of biology and inorganic chemistry. The introductory section on tridentate ligands will further elaborate on the proposed studies of this dissertation.

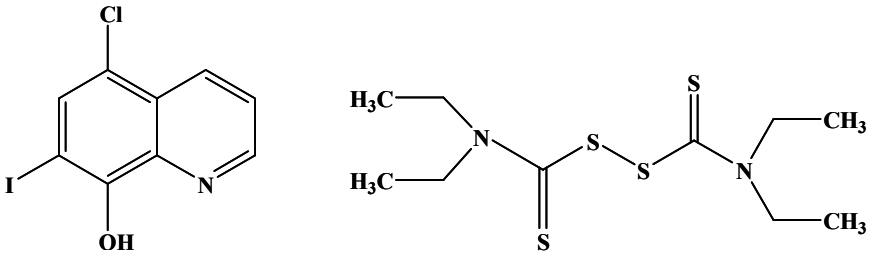

Clioquinol **Disulfiram**

Figure 6. Chemical structures of copper binding compounds.

The depicted chemical structures Disulfiram and Clioquinol are copper-binding compounds with proteasome inhibitory activity.

Zinc

Zinc is an indispensable trace element that plays a critical role in a wide range of cellular processes including cell proliferation, differentiation, and defense against free radicals [Ho, 2004; Stefanidou et al., 2006]. Zinc acts as a key structural component in many proteins and enzymes, including transcription factors, cellular signaling proteins, and DNA repair enzymes [Prasad, 1995].

It has also been well established that zinc plays a critical role in the regulation of apoptosis in mammalian cells [Chang et al., 2006; Fraker and Lill-Elghanian, 2004]. However the precise role of zinc in modulating this response appears to be cell specific, highly complex, and lacking firm conclusion [Franklin and Costello, 2009]. In many cell types, including prostate epithelial, glial cells, ovarian epithelial cells, and others, zinc has been reported to induce apoptosis. However, in breast cells, lung epithelial cells, renal cells, macrophages, and Hela cells, zinc exhibits antiapoptotic effects [Franklin and Costello, 2009]. This has been supported by evidence showing that in some cells, exposure to low levels of zinc induces apoptosis, whereas exposure to high zinc levels inhibits apoptosis [Provinciali et al., 1995]. These seemingly contradictory results have been the subject of intense investigation and currently remain unanswered.

Given the indispensible role of Zn in a myriad of biochemical processes, it is not surprising that altered levels of Zn are associated with systemic abnormalities, including the development of cancer [Murakami and Hirano, 2008]. Although the levels of zinc have been found to be compromised in cancer patients as compared to normal subjects, the relationship between tumor development and Zn levels appears to lack discernable conclusions and is dependent on tumor type [Federico et al., 2001; Franklin and Costello, 2009; Prasad et al.,

1998]. Zinc levels have been found to be reduced in patients afflicted with cancer of the liver, gallbladder, digestive tract, or prostate [Chakravarty et al., 1986; Franklin and Costello, 2007; Gupta et al., 2005], whereas breast cancer patients showed decreased and elevated Zn levels in serum and malignant tissues [Chakravarty et al., 1986; Margalioth et al., 1983; Schwartz et al., 1974]. Emerging evidence suggests that expression levels of Zn transporters are associated with cancer progression [Murakami and Hirano, 2008; Zhao and Eide, 1996]. In addition to the critical role that zinc plays in biological systems, the unique properties of zinc have allowed it to gain favor as potential anticancer agents. Our lab has previously shown that zinc-containing complexes can inhibit the proteasome and apoptosis in tumor cells [Cvek et al., 2008; Milacic et al., 2008a]. Based on the anticancer properties of zinc, and previous studies from our lab, this dissertation investigates the potential of zinc-containing complexes with [NN'O] tridentate ligands as potential proteasome inhibitors as explained further in the following section.

Metals with tridentate [NN'O]-containing ligands

Our groups have been actively pursuing a strategy of developing novel complexes of well defined stoichiometry formed between asymmetric [NN'O] tridentate ligands-containing metals as potential anticancer drug candidates (Fig. 7). Such ligands are an evolution from terbutylated analogues used as biomimetic models for galactose-oxidase [Itoh et al., 1999; Vaidyanathan et al., 1998]. Moreover, a secondary amine in this ligand allows for the design of complexes with appended moieties to enhance water solubility [Melchior et al., 2001; Storr et al., 2005] or lipophilicity [Kirin et al., 2005; Shakya et al., 2006b] to address concerns for drug design purposes (Fig. 7). Our studies initially focused on the development

of a series of gallium complexes described as $[Ga^{III}(^{Lx\text{-}NN'O})_2]ClO_4$, with asymmetric NN'O-containing pyridine amino phenolate ligands (Fig. 7) [Shakya et al., 2006b]. The phenolate moiety groups were appended with electron withdrawing and donating groups such as methoxy (**1**), nitro (**2**), chloro (**3**) bromo (**4**), and iodo (**5**) positioned at the 4^{th} and 6^{th} positions (Fig. 7). The geometry of the final complex is distorted octahedrally, but owing to the flexibility of the ligands, facial coordination takes place (Fig. 7) [Shakya et al., 2006b].

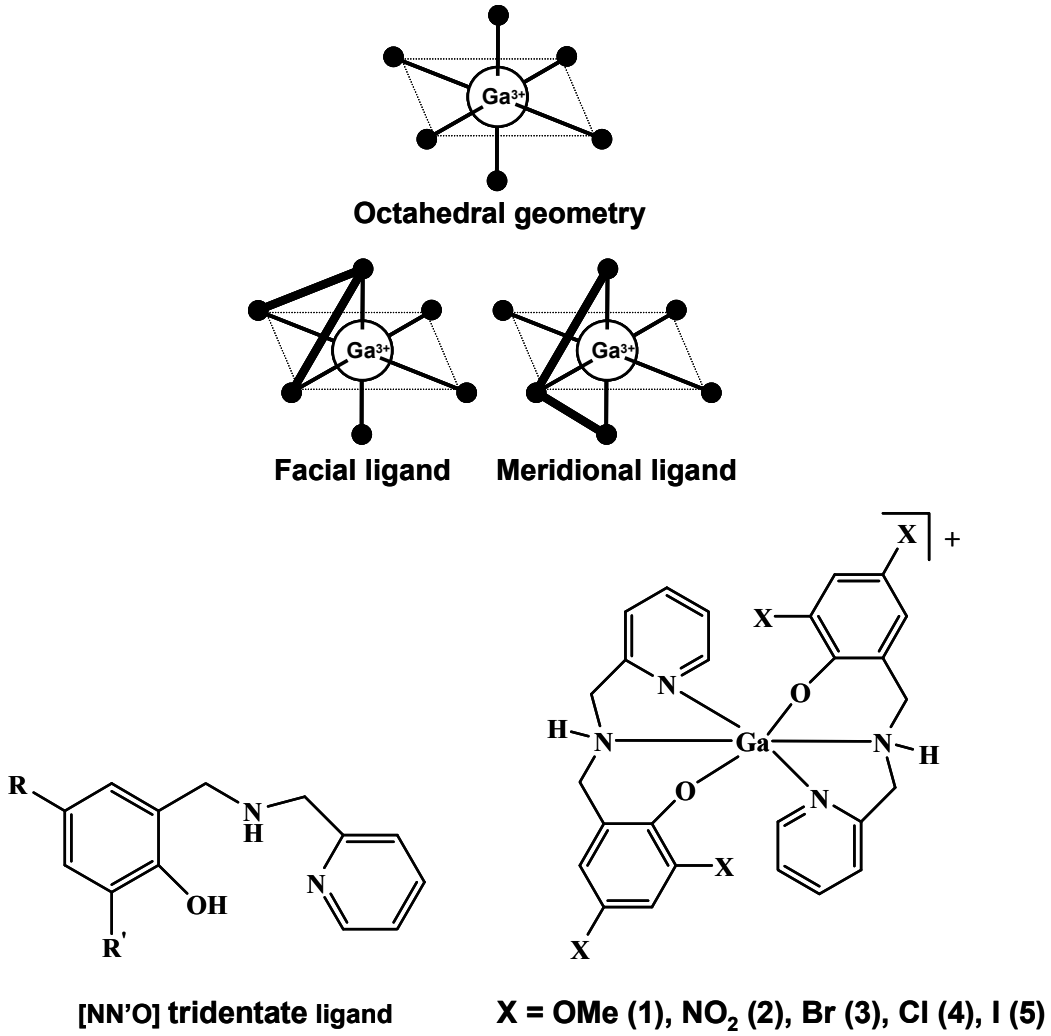

Figure 7. Chemical structure of gallium complexes with [NN'O] tridentate ligands

The chemical structures represented are gallium complexes with [NN'O] tridentate ligands appended with substitutions at the 4th and 6th position. These complexes can take on a facial or meridional coordination. The geometry of the final complex is distorted octahedrally.

Our initial studies revealed, in ranking order, methoxy (**1**) = nitro (**2**) < chloro (**3**) < bromo (**4**) < iodo (**5**), that the species containing halogen substituents showed preferential growth inhibition in human neuroblastoma cells with activity superior to that of cisplatin (Fig. 7) [Shakya et al., 2006b]. Interestingly, these gallium(III) complexes were associated with only minor toxicity. Thus, the formation of a coordination complex appended with halogen substituents appears to influence the cytotoxicity of these complexes.

This dissertation sets out to investigate a possible molecular mechanism for these gallium complexes that could provide insight into their growth inhibitory properties. Our studies reveal that complexes (**3** Chloro) < (**4** Bromo) < (**5** Iodo) are able to target and inhibit proteasomal activity and induce apoptosis in various prostate cancer cell lines. Importantly, complex (**5**) exhibited superior anticancer activity, and was able to exert the same effect *in vivo* by inhibiting the growth of mice-bearing xenografts.

Since one of the important focuses in our labs involves investigating the use of copper chelating ligands and other transition metal-based complexes as proteasome inhibitors (discussed above) [Chen et al., 2007a; Chen et al., 2006; Chen and Dou, 2008], we decided to extend our work by investigating the role of bivalent transition metals, such as copper and zinc complexed to our same HL^I platform to gain insight into their potential as anticancer agents. Based on the significantly higher potency conferred by the HL^I ligand when formed in a coordination complex with gallium, subsequent studies relied on this model architecture with other bivalent transition metals, with emphasis on mechanistic properties.

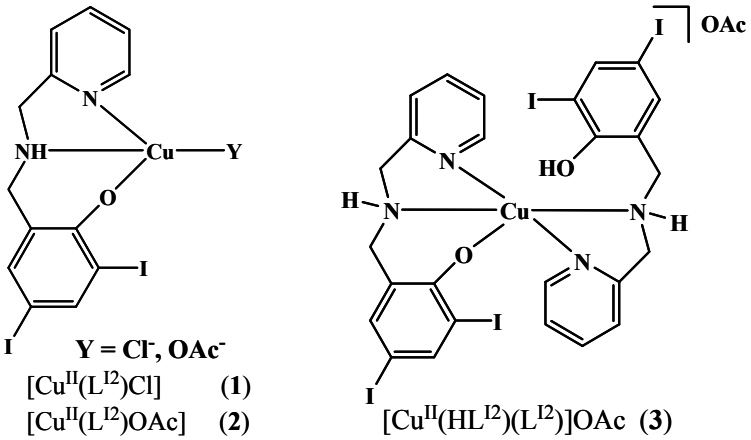

Figure 8. Copper complexes with [NN'O] tridentate ligands.

Evaluation of a stoichiometric HL^{I}:Cu:DMSO mixture led to the identification of both fragments (**1**) and (**2**) that may act as pharmacophores responsible for their biological activity. Species (**1**) was (**2**) were mixed with copper chloride and acetate, respectively. Species (**3**) was synthesized in a 2:1 ligand to metal ratio.

Evaluation of a stoichiometric HL^{I}:$CuCl_2$:DMSO mixture led to the identification of both monomeric and dimeric fragments that may act as pharmacophores responsible for their biological activity [Hindo et al., 2009]. These initial studies formed the basis of developing a series of copper(II) complexes with the ligand HL^{I}, which were synthesized and characterized as (**1**), (**2**), and (**3**) (Fig. 8). The results from this dissertation show that these copper complexes function as proteasome inhibitors and apoptosis inducers in human prostate cancer cells. Furthermore, this study also provides insight into the potential pharmacophore needed for inhibition of proteasomal activity.

To further build upon our studies and further investigate our hypothesis that species $[ML^{IA}]^{+}$ is the necessary pharmacophore for proteasome inhibition, data in this dissertation compared the proteasome inhibition capabilities of two divalent transition metals, namely zinc and nickel as coordination complexes utilizing the same HL^{I} ligand as a platform (Fig. 9). Initial comparison studies considering coordination of a 1:1 $[Zn(L)]^{+}$ fragment with threonine suggest a favorable coordination through the terminal hydroxyl group. This dissertation shows that the zinc complex could significantly inhibit the cellular proteasome compared to its nickel counterpart [Frezza et al., 2009]. The data provided in this dissertation seeks to dissect the underlying disparity in biological activity between the two metals and provide some mechanistic insight into its proteasome inhibitory effects by using a chemical biology approach.

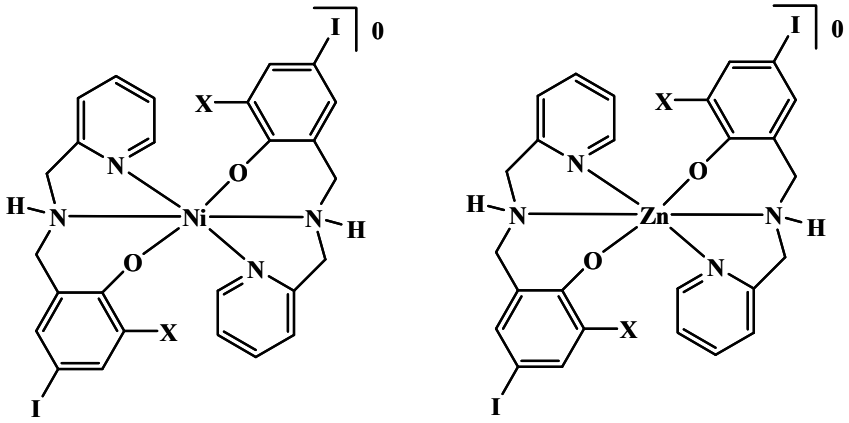

Figure 9: Zinc and Nickel complexes synthesized with [NN'O] tridentate ligands

The Chemical structures of zinc and nickel complexes depicted were synthesized in a 2:1 ligand: metal ratio with tridentate ligands.

Gold and gold complexes

Gold was first recognized for its medicinal and therapeutic applications thousands of years ago, but its rational use in medicine didn't begin until the early twentieth century. The gold(I) triethylphosphine compound, auranofin (Fig. 10) was the first clinically approved gold drug for the treatment of rheumatoid arthritis. Although no other gold-containing complex has been approved clinically, its therapeutic value continues to be the subject of investigation [Milacic et al., 2008b].

Based on the finding that auranofin displayed cytotoxic effects toward cancer cells *in vitro*, various gold(I) compounds were synthesized and shown to have strong cytotoxic activity against melanoma and leukemia cell lines *in vitro* and anti-tumor activity against leukemia *in vivo* [Mirabelli et al., 1986]. Although the phosphine-coordinated gold(I) thiosugar complexes appeared to be the most potent of them, they were found to be completely inactive against solid tumors [Chen et al., 2009].

Primarily because of their high reactivity, gold(III) complexes have not been as thoroughly investigated as gold(I) complexes. Having a high redox potential and relatively poor stability, the use of gold(III) complexes as anti-cancer drugs under physiological conditions was questioned [Ronconi et al., 2005]. Given that the cellular environment is generally reducing, compounds with gold(III) were expected to be reduced *in vivo* to gold(I) and metallic gold, which makes them less effective as drugs [Ronconi et al., 2005].

However, the interest for gold(III) complexes was markedly increased after platinum(II) complexes exhibited promising results against selected types of cancers. Since gold(III) is isoelectronic (d^8) with platinum(II) and tetracoordinate gold(III) complexes have

the same square-planar geometries as cisplatin [Ronconi et al., 2006], the anti-cancer activity of gold(III) compounds has been investigated.

In recent years, a selection of more stable gold(III) compounds have been synthesized using better ligand platforms that contain nitrogen atoms as donor groups [Messori et al., 2003]. Ronconi et al. synthesized various gold(III) dithiocarbamate derivatives that display superior chemotherapeutic index in terms of increased bioavailability, higher cytotoxicity, and more tolerable side effects compared to cisplatin [Ronconi et al., 2005]. These different gold(III) dithiocarbamate derivatives, particularly, *N*,*N*-dimethyldithiocarbamate and ethylsarcosinedithiocarbamate analogs were shown to display significantly higher cytotoxicity and were able to overcome resistance to cisplatin (Fig. 10).

Studies with gold(III) complexes have shown that their interaction with DNA, the primary target of platinum compounds, was less than favorable, suggesting a different mechanism of action [Marcon et al., 2002; Messori et al., 2001]. This observation has prompted the search a new search for gold-protein interactions in an attempt to identify possible targets for the biological effects of gold-containing compounds.

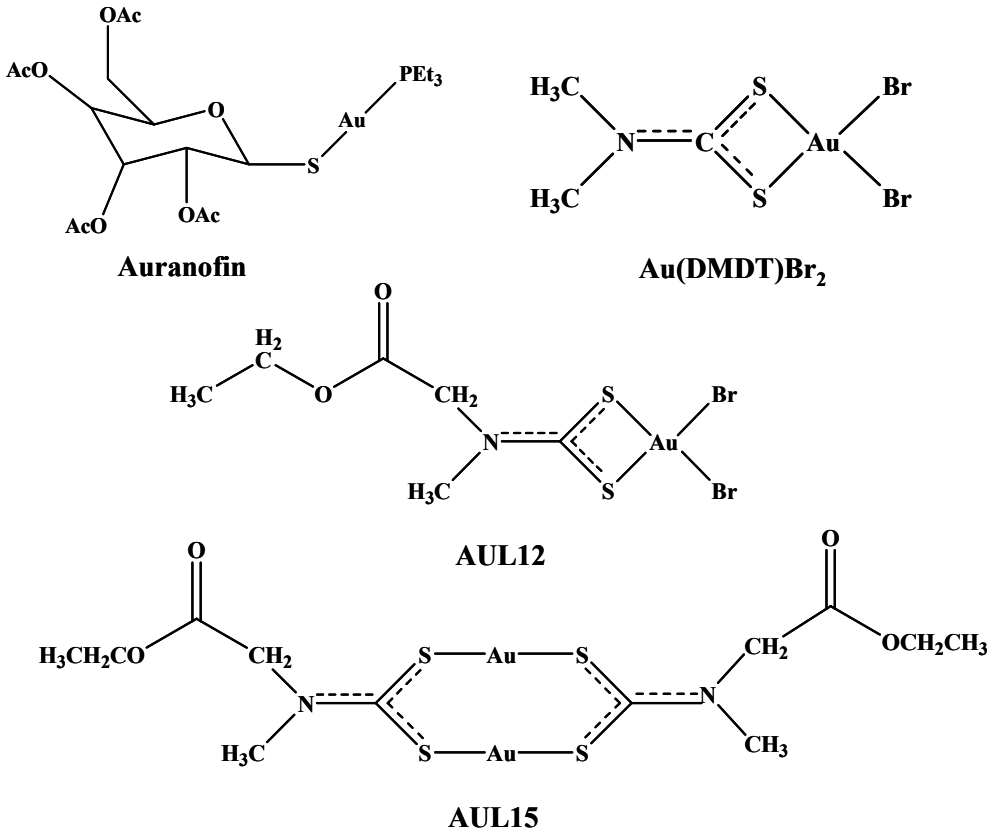

Figure 10. Chemical structures of gold-containing compounds.

Auranofin was the first and only gold compound used clinically. $Au(DMDT)Br_2$ with 3+ charge; AUL12 with a 3+ charge, and AUL15 with 1+ charge are gold-containing dithiocarbamate compounds with proteasome inhibitory activity.

Our lab has shown that a gold(III) dithiocarbamate derivative, namely [Au(DMDT)Br_2] (Fig. 10) could target and inhibit the chymotrypsin-like activity of a purified 20S proteasome (IC_{50}= 7.4 μM) and 26S proteasome in intact MDA-MB-231 breast cancer cells [Milacic et al., 2006]. PGPH-like and trypsin-like activities were also inhibited, but the CT-like inhibition was the most significant, indicating that this complex preferentially binds to and inhibits the chymotrypsin-like β5 subunit of the proteasome. Associated with proteasomal inhibition, an accumulation of ubiquitinated proteins, p27, and induction of apoptosis was observed in breast cancer cells. Additionally, Au(DMDT)Br_2 was able to potently inhibit tumor growth (~50%) associated with inhibition of proteasomal activity and apoptosis induction [Milacic et al., 2006]. However, whether the nature of the metal and dithiocarbamate ligand is instrumental in influencing its biological activity could not be established.

In this dissertation we investigate the importance of the oxidation state of gold and the involved mechanism of action of two gold containing complexes toward human breast cancer cells (Fig. 10). The data provides strong evidence that the cellular proteasome is an important target of both gold(I) and gold(III) dithiocarbamates, but distinct cellular mechanisms are responsible for their different overall effect.

Androgen Receptor Signaling in Prostate Cancer

Prostate cancer is the most frequently diagnosed cancer and the second leading cause of cancer death among american males [Jemal et al., 2008]. Prostate cancer can be effectively treated by androgen-ablation therapy through medical or surgical castration. However, this effect is transient and the majority of prostate cancer patients eventually

relapse to a hormone refractory state that no longer responds to androgen withdrawal [Heinlein and Chang, 2004]. Treatment options for hormone refractory prostate cancer are an unmet need with only docetaxel being the only agent that has been shown to prolong survival [Chen et al., 2008].

Androgen Receptor (AR) appears to be a critical component of the transition from a hormone sensitive to a hormone refractory state that remains dependent on AR signaling. Despite decreased androgen levels, AR remains highly expressed and active in hormone-refractory tumors, implying a switch to alternative mechanisms of action [Burnstein, 2005; Steinkamp et al., 2009]. Clinical observations have provided clues that AR signaling remains active and engaged in hormone refractory prostate cancer. The AR-dependent gene, PSA has been successfully used as a clinical marker to assess disease activity. PSA declines after hormone deprivation therapy and a subsequent rise is commonly the first sign of disease progression, indicating the reactivation of AR signaling accompanies the development of HRPC [Attard et al., 2009a]. Recently it was discovered that up to 90% of all prostate cancers overexpress an ets oncogene, including ERG, ETV1, ETV5, and ETV6 via a variety of mechanisms (Petrovics, 2005, 3847). The most common mechanism of overexpression is fusion of the ets gene (ERG) to the 5'-untranslated region of highly AR-regulated TMPRSS2 gene. Thus, in addition to the lineage dependence of prostate cells on AR signaling, prostate cancer has additional selection pressure to maintain TMPRSS2 expression and AR activity [Tomlins et al., 2007; Tomlins et al., 2005]. It has been reported that 40%-70% of prostate cancers have chromosomal rearrangement that results in hormonal regulation of oncogenic ETS gene expression, highlighting one mechanism by which AR becomes oncogenic [Tomlins et al., 2005].

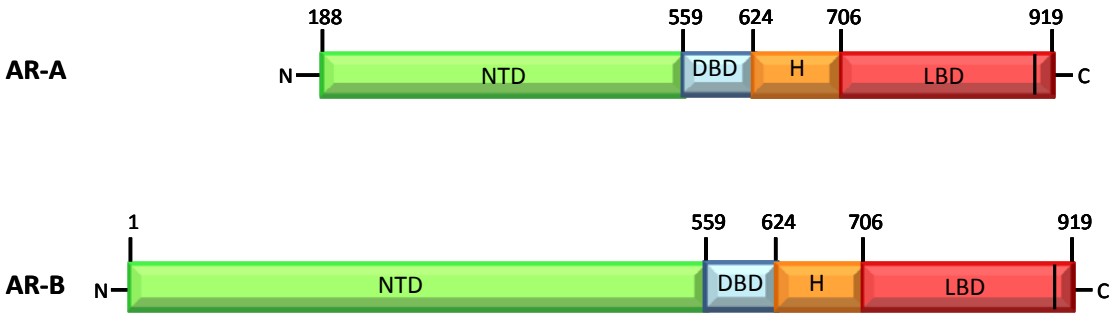

Figure 11. Schematic representation of the androgen receptor (AR)

Two isoforms of AR, AR-A and AR-B, exist. AR is a member of the steroid superfamily of transcription factors and shares a similar organization of functional domains. AR contains an amino-terminal domain (NTD), a DNA-binding domain (DBD), a hinge region (H) containing a proline-, glutamate-, serine-, threonine-rich (PEST) motif, and a carboxy-terminal ligand-binding domain (LBD). AR-A differs from AR-B in that its NTD is shorter than that of AR-B. The additional portion of NTD present in AR-B (missing from AR-A) contains a motif necessary for full ligand activated transcriptional activity.

AR is a member of the steroid superfamily of ligand activated transcription factors sharing a similar organization of functional domains. Like other members of this family, AR contains three domains; an NH_2-terminal domain (ATD), a central DNA binding domain (DBD), and a carboxy-terminal ligand binding domain (LBD) (Fig. 11) [Lee and Chang, 2003; Tsai and O'Malley, 1994]. The DBD and LBD are separated by a hinge region containing a PEST (proline-, glutamate-, serine-, and threonine-rich) motif (Fig. 11). Unliganded AR remains inactive in the cytosol and associates with the HSP chaperone complex which maintains AR competent for binding androgens [Shen and Balk, 2009]. Testosterone is the predominant circulating androgen in mammals and is converted to dihydrotestosterone (DHT) by 5α-reductase in certain tissues including the prostate. DHT binds with the highest affinity to AR and together with testosterone promotes AR transcriptional activity through receptor nuclear translocation, dimerization, and binding to androgen response elements in DNA of target genes (Fig. 12) [Burnstein, 2005; Taplin, 2008]. AR homodimers recruit a myriad of factors including coactivators and mediator proteins whose enzymatic activities promote chromatin remodeling and transcriptional regulation of target genes leading to cell differentiation, survival, and proliferation (Fig. 12) [Heinlein and Chang, 2002]. Androgen stimulation of the AR is not only essential, but is also sufficient for the development of the prostate gland and is strongly implicated in the growth and progression of prostate cancer [Burnstein, 2005].

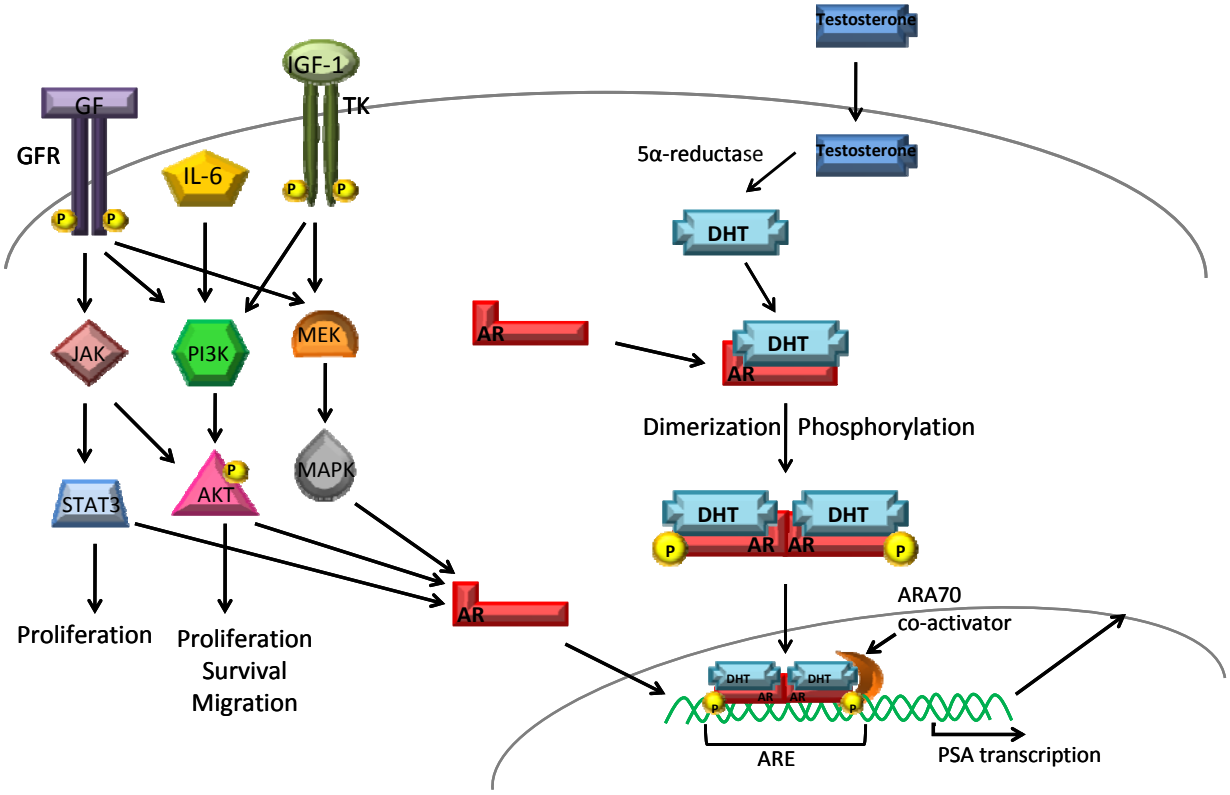

Figure 12. Schematic description of androgen receptor signaling

Androgen receptor signaling mediated by testosterone, or its more potent form, dihydrotestosterone by 5α-reductase (right). Upon activation, AR translocates to the nucleus and binds to the promoters of AR target genes such as PSA regulating cell survival and proliferation. AR may become promiscuous and respond to other ligands, such as growth factors and other steroids. AR may also be responsive to other signaling pathways such as PI3K and MAPK. These AR-mediated events are associated with cell migration, proliferation and survival (left).

There is well established evidence that the AR gene undergoes alterations from a hormone sensitive to a hormone refractory state. AR gene amplification has been reported in 25-30% of patients with HRPC but, but is present at a very low rate in primary prostate cancer [Edwards et al., 2003; Ford et al., 2003]. Additionally, AR mutations have been found in prostate cancer and its incidence has been known to occur in the 10%-40% range [Taplin and Balk, 2004]. As a result, these hormone-independent tumor cells become very sensitive to low or no androgen environments, and are responsive to a broad range of ligands such as growth factors, other steroid hormones, anti-androgens, etc [Chen et al., 2004a; Culig et al., 1994]. It has also been reported that wild type AR can be activated by other signal transduction pathways in a ligand independent manner [Chen et al., 2004a; Culig, 2004]. Furthermore, ligand-independent AR can bind the enhancer elements on the promoters of target genes and mediated their expression even in the absence of androgen as seen with the prostate specific antigen (PSA) gene in androgen-independent prostate cancer cells [Jia et al., 2006]. Finally, Alterations in the balance of between AR coactivator and co-repressor proteins may result in a growth advantage of prostate cancer cells, thus making these potential drug targets [Gregory et al., 2001].

Approaches in prostate cancer treatment

Standard hormone therapy for prostate cancer includes a variety of approaches to directly reduce ligand (androgen) concentrations or block the ability of ligand to interact with AR. Approved antiandrogens, include bicalutamide, or hydroxyflutamide and nilutamide, and adrenal androgen synthesis is commonly inhibited with corticosteroids. These Conventional approaches reduce but fail to completely eliminate circulating levels of

androgen. Serum testosterone is reduced to 90-95%, while intraprostatic androgen, concentration is reduced only about 75% and is sufficient to activate AR [Chen et al., 2008; Montgomery et al., 2008]. However, despite an initial response, the time to progression is usually short in the majority of patients. This has stimulated significant efforts to develop novel therapeutic strategies for the treatment of hormone-resistant prostate cancer (HRPC).

HSP-90 is a chaperone protein required for refolding denatured proteins and protein maturation, and inhibitors of HSP-90 have been in clinical testing as prostate cancer therapeutics [Solit and Rosen, 2006]. Histone deacetylases are enzymes that modulate chromatin remodeling and regulate gene transcription. HDAC inhibitors are currently in clinical testing for leukemia and solid tumors, including prostate cancer and exert their activity by inducing cell cycle arrest and apoptosis. In a manner similar to HSP-90 inhibitors, HDAC inhibitors destabilize the AR by interfering with the binding of HSP90 to the AR and also to ERBB2 [Minucci and Pelicci, 2006]. More recently, Abiraterone acetate has been developed, which acts as a highly specific inhibitor of CYP17 and results in significant suppression of serum androgenic steroids and estrogens which was associated with significant reductions in PSA associated with tumor regression in patients with HRPC [Attard et al., 2009b; Attard et al., 2008]. MDV-3100 is a novel small molecule antagonist being testing in clinical trials for patients with HRPC that have failed other treatments. Its mechanism of action involves blockade of nuclear translocation of AR, DNA binding, and exhibits no agonist activity when AR is overexpressed [Tran et al., 2009]. These encouraging findings suggest that further understanding the role of AR in the growth and progression of prostate cancer could lead to the more effective design of therapeutic strategies in the treatment of prostate caner.

We have previously reported that proteasome inhibitors caused downregulation of AR in both androgen-dependent LNCaP cells and androgen-independent C4-2B cells [Chen et al., 2007b; Yang et al., 2006b], and that calpain involvement is at least partially responsible for this effect [Yang et al., 2008]. However, whether AR stability is directly implicated in modulating the cell death pathway in prostate cancer cells has yet to be established. The data in this dissertation provides compelling evidence that AR can influence the regulatory events associated with cell death in response to proteasome inhibition and chemotherapy. Although both AR-independent prostate cancer cells and AR transfected cells showed similar sensitivity to growth inhibition, the mechanism underlying this effect appears to be distinct and regulated by AR-mediated events. The data provided in this dissertation could have important prognostic and clinical relevance in the treatment of prostate cancer.

CHAPTER 2

Inhibition of the Proteasome Activity by Gallium(III) Complexes Contributes to Their Anti-Prostate Tumor Effects

Adapted from published material in Cancer Research, 2007; 67(19): 9258-65.

The investigation of metal-based complexes with potential antitumor activity has been of paramount importance in recent years due to the successful use of cisplatin against various cancers. Gallium(III) and subsequently developed gallium(III)-containing complexes have shown promising antineoplastic effects when tested in a host of malignancies, specifically in lymphomas and bladder cancer. However, the molecular mechanism responsible for their anticancer effect is yet to be fully understood. The data in this dissertation shows for the first time that the proteasome is a molecular target for gallium complexes in a variety of prostate cancer cell lines and in human prostate cancer xenografts. Five gallium complexes (**1**–**5**) were tested in which the gallium ion is bound to an NN'O asymmetrical ligand containing pyridine and substituted phenolate moieties in a 1:2 (M/L) ratio. The data shows that complex **5** showed superior proteasome inhibitory activity against both 26S proteasome (IC50, 17 μmol/L) and purified 20S (IC50, 16 μmol/L) proteasome. Consistently, this effect was associated with apoptosis induction in prostate cancer cells. Additionally, complex **5** was able to exert the same effect *in vivo* by inhibiting growth of PC-3 xenografts in mice (66%), which was associated with proteasome inhibition and apoptosis induction. The data presented in this dissertation strongly suggest that gallium complexes,

acting as potent proteasome inhibitors, have great potential to be developed into novel anticancer drugs.

Materials and Methods

Materials. The gallium complexes **1 – 5** were synthesized as described previously [Shakya et al., 2006b]. Hoechst 33258 and cremophor were purchased from Sigma-Aldrich (St. Louis, MO). Purified rabbit 20S proteasome, fluorogenic peptide substrates Suc-LLVY-AMC and Ac-DEVD-AMC were obtained from Calbiochem Inc (San Diego, CA). Peptide substrate Z-GGL-AMC was from BIOMOL International LP (Plymouth Meeting, PA). Apoptag Peroxidase *In Situ* Apoptosis Detection Kit was from Chemicon International, Inc. (Temecula, CA).

Cell cultures and whole cell extract preparation. Human prostate cancer cells, LNCaP, C4-2B and PC-3, were grown in RPMI 1640 medium supplemented with 10% FBS and maintained at 37 °C and 5% CO_2. A whole cell extract was prepared as described previously [An et al., 1998; Chen et al., 2006].

Inhibition of purified 20S proteasome activity. Purified rabbit 20S proteasome (17.5 ng) was incubated in 100 μl of assay buffer (50 mmol/L Tris–HCl, pH 7.5) with gallium complexes and 10 μmol/L fluorogenic peptide substrate Suc-LLVY-AMC for 2 h at 37 °C. After incubation, production of hydrolyzed AMC groups was measured as previously described [Daniel et al., 2004].

Inhibition of the proteasome activity in intact cells. C4-2B cells were cultured in a 96-well plate (1×10^4 cells/well) and treated with various concentrations of gallium complexes for 18 h. After the additional 2 h incubation with the fluorogenic peptide

substrate Z-GGL-AMC, specific for the proteasomal chymotrypsin-like activity, production of hydrolyzed AMC groups was measured as described above.

Caspase-3 and proteasomal CT-like activity assays. Proteins extracted from cells or tumor tissue were incubated for 1 h at 37°C in 100 μl of assay buffer (50 mmol/L Tris-HCl, pH 7.5) with 10 μmol/L fluorogenic substrate Suc-LLVY-AMC (for CT-like activity in cultured cells) or Z-GGL-AMC (for CT-like activity in tumor tissues) or Ac-DEVD-AMC (for Caspase–3/7 activity) as described previously [Daniel et al., 2005].

Cellular and nuclear morphology analysis. A Zeiss Axiovert 25 microscope was used for all microscopic imaging with either phase contrast for cellular morphology or fluorescence for nuclear morphology with Hoechst 33258 staining as described previously [Daniel et al., 2005].

Western blot analysis. The cell or tissue extracts were separated by SDS-PAGE and transferred to a nitrocellulose membrane. Western blot analysis was performed using specific antibodies against ubiquitin, p27, AR, β-actin (Santa Cruz Biotechnology Inc, Santa Cruz, CA) or PARP (BIOMOL International LP, Plymouth Meeting, PA), followed by visualization using the enhanced chemiluminescence (ECL) reagent (Amersham Biosciences, Piscataway, NJ).

Human prostate tumor xenograft experiments. Five-week-old male athymic nude mice were purchased from Taconic Research Animal Services (Hudson, NY) and housed under pathogen-free conditions according to Wayne State University animal care guidelines. The protocols of animal experiments were reviewed and approved by Institutional Laboratory Animal Care and Use Committee of Wayne State University. PC-3 cells (2×10^6) were injected subcutaneously (*s.c.*) at one flank of the mice. The mice were then randomly

grouped and injected *s.c.* daily with either solvent (PBS: Cremophor: Ethanol: DMSO = 5: 2.7: 1.3: 1) as a control (n=9), 20 mg/kg of complex **5** (n=9), or 20 mg/kg of L**5** (n=5) for 29 days. Tumor size was measured every other day using calipers. Tumor volume (V) was determined by the equation: $V= (L \times W^2) \times 0.5$, where L is the length and W is the width of the tumor.

Terminal deoxyribonucleotidyl transferase-mediated dUTP nick end labeling (TUNEL), immunostaining and Hematoxylin and Eosin (H&E) assays. TUNEL assay using *in situ* apoptosis detection kit and immunostaining of p27 were done as previously described [Chen et al., 2006]. H&E staining in tumor tissues was done following manufactory protocols [Chen et al., 2006]. Briefly, paraffin-embedded sample slides were deparafinized and hydrated, and then stained with Hematoxylin for 1 minute. After rinsing, the slides were stained with Eosin for 1 minute, rinsed and mount of cover slips onto slides with Permount.

Statistical analysis. Statistical analysis was performed with Microsoft Excel™ software. Student's *t* test for independent analysis was applied to evaluate differences between treatments and control.

Results

Structural relationships of several synthetic gallium complexes with their activities to inhibit purified 20S proteasome and cellular 26S proteasome. We have previously reported that certain copper complexes are potent proteasome inhibitors [Chen et al., 2007a; Chen et al., 2006; Daniel et al., 2004]. Therefore, we hypothesized that gallium complexes might be similarly capable of targeting and inhibiting the proteasome in human tumor cells. To test this hypothesis, proteasome-inhibitory potencies of five gallium complexes were analyzed (Fig. 13) under cell-free conditions, and found that the complexes **3**, **4** and **5** inhibited CT-like activity of the purified 20S proteasome with IC_{50} values 46, 27 and 16 μmol/L, respectively (Fig. 14A). In contrast, complex **2** demonstrated very weak inhibitory potential, while complex **1** had no effect at the highest concentration used (50 μmol/L; Fig. 14B). The rank of the inhibitory potencies of the gallium complexes against the purified 20S proteasome is: **5** > **4** > **3** > **2** ≥ **1**.

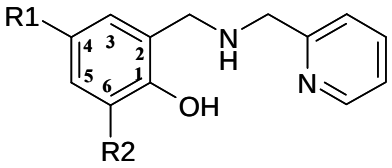

1: $[Ga^{III}(L^{OCH3})_2]ClO_4$; (R1 = H, R2 = methoxy)
2: $[Ga^{III}(L^{NO2})_2]ClO_4$; (R1 = nitro, R2 = H)
3: $[Ga^{III}(L^{Cl2})_2]ClO_4$; (R1 and R2 = chloro)
4: $[Ga^{III}(L^{Br2})_2]ClO_4$; (R1 and R2 = bromo)
5: $[Ga^{III}(L^{I2})_2]ClO_4$; (R1 and R2 = iodo)

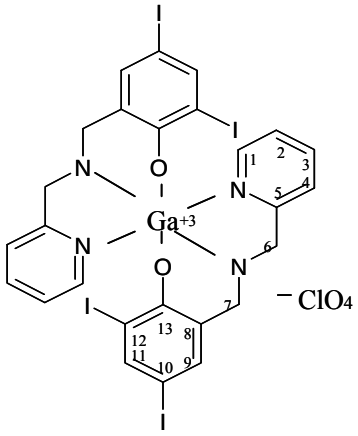

5: Ga-iodo-amine

Figure 13. Chemical structures of gallium complexes.

Gallium complexes **1-5** depicted were synthesized with tridentate ligands in a 2:1 ligand:metal ratio

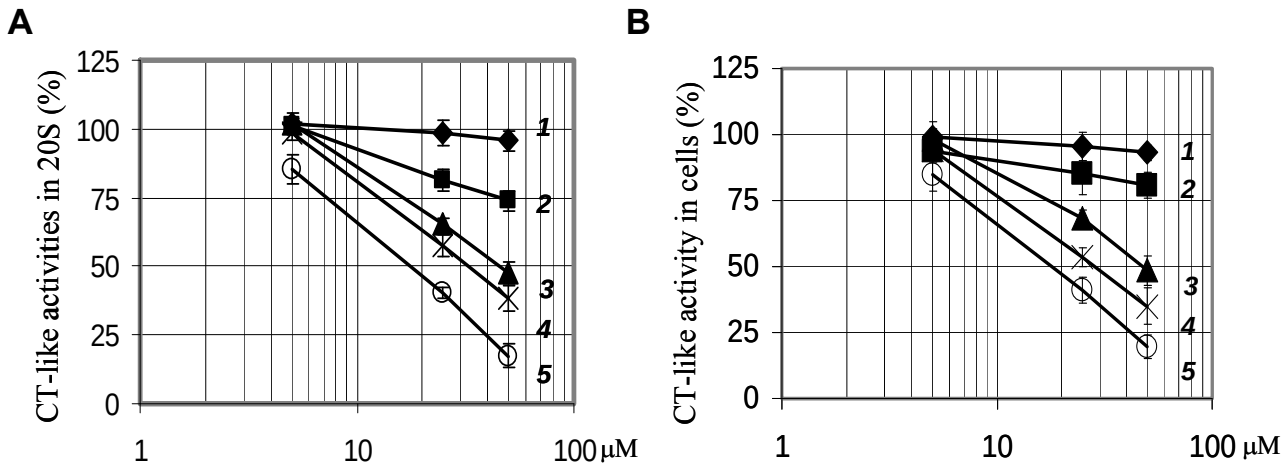

Figure 14. Gallium complexes inhibit the chymotrypsin-like activity of purified 20S proteasome and cellular 26S proteasome.

A. Inhibition of the chymotrypsin-like activity of purified 20S proteasome. **B.** Inhibition of proteasome activities in intact human prostate cancer cells. C4-2B cells were treated with 50 μmol/L of each gallium complex for 18 h, followed by measurement of proteasomal chymotrypsin-like activities.

To determine the potencies of these complexes to inhibit CT-like activity in intact cells, an androgen-independent human prostate cancer line C4-2B [Thalmann et al., 1994] were plated in a 96-well plate and treated with each of the five complexes for 18 h, followed by measuring the proteasome activity. We found that IC_{50} values of the complexes **3**, **4** and **5** in intact C4-2B cells were 48, 28 and 17 μmol/L, respectively (Fig. 14B), consistent with their inhibitory potencies against the purified 20S proteasome. Complexes **1** and **2** again showed only slight inhibitory effect (Fig. 14B).

Inhibition of proteasomal CT-like activity by gallium complexes in androgen-independent human C4-2B prostate cancer cells is associated with down-regulation of androgen receptor (AR) and induction of cell death. To confirm the ability of these gallium complexes to inhibit the proteasomal activity in prostate cancer cells, C4-2B cells were treated with each complex at 50 μmol/L concentrations for 18 h. The cells were harvested and used for cell extract preparation, followed by measurement of the proteasomal CT-like activity and accumulation of ubiquitinated proteins. Complexes **1-5** were found to inhibit 7.5, 14, 38, 58 and 81% of the proteasomal activity, respectively (Fig. 15). Additionally, high levels of accumulated ubiquitinated proteins were detected in C4-2B cells treated with complexes **3**, **4** and **5** (Fig. 16).

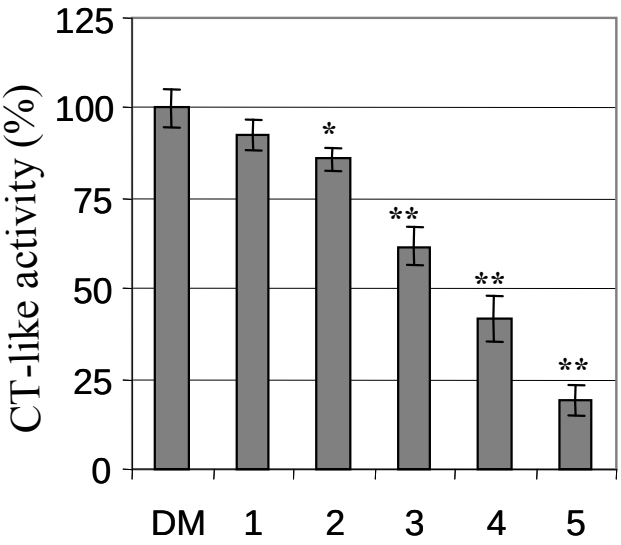

Figure 15. Gallium complexes inhibit proteasome activities in prostate cancer C4-2B cells.

Human prostate cancer C4-2B cells were treated with 50 μM of complex **1-5** for 18 h, followed by measurement of chymotrypsin-like activity. *, $P < 0.05$, **, $P < 0.01$.

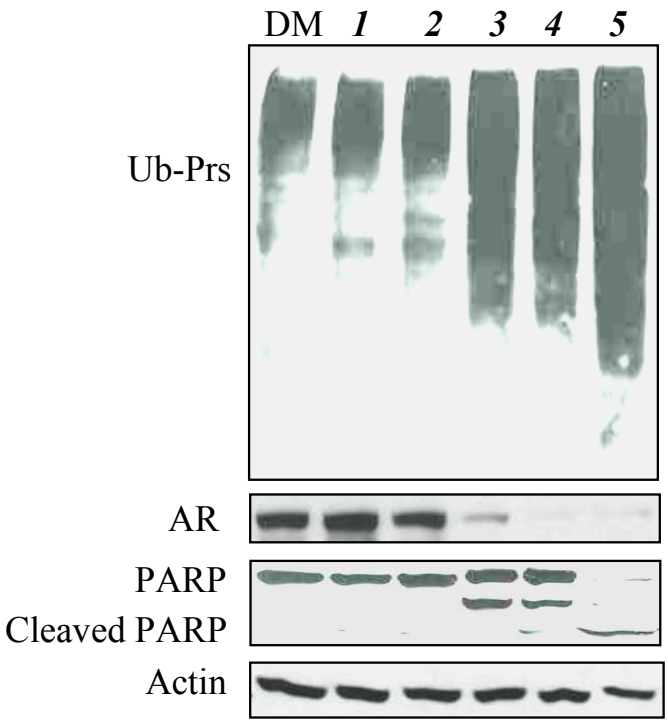

Figure 16. Gallium complexes accumulate ubiquitinated proteins and induce cell death in prostate cancer C4-2B cells.

Human prostate cancer C4-2B cells were treated with 50 μM of complex **1-5** for 18 h, followed by western blot analysis of ubiquitinated proteins (Ub-Prs), androgen receptor (AR), and PARP. DM was used as solvent control.

It has been shown that proteasome inhibition could down-regulate AR expression [Lin et al., 2002]. Therefore, if gallium complexes were able to inhibit proteasomal activity, we would expect a decrease in AR expression level. Indeed, the results in Figure 16 showed that gallium complexes **2** and **3**, but not **1**, down-regulated AR protein (**3** > **2** > **1**), while complexes **4** and **5** completely abrogated AR protein expression (Fig. 16). These results remained consistent with the order of proteasome-inhibitory potency of the gallium complexes.

It has also been shown that inhibition of the proteasomal CT-like activity in malignant cells could result in the induction of apoptosis [An et al., 1998; Lopes et al., 1997]. To investigate whether the proteasomal inhibition and AR level reduction by gallium complexes are associated with cell death, PARP cleavage and morphological and nuclear changes were measured in the same experiment. The results showed that treatment with gallium complexes **3, 4** and **5** caused cell death associated PARP cleavage (Fig. 16), while complexes **1** and **2** failed to do so (Fig. 16). Consistently, morphological changes (shrunken cells and characteristic apoptotic blobbing; Fig. 17) and the presence of apoptotic nuclei after Hoechst staining (condensed or punctuated and brighter nuclei; Fig. 17) were observed in the cells treated for 18 h with the complexes **4** and **5.** While complex **3** induced only moderate level of apoptotic cellular and nuclear changes (Fig. 17), complexes **1** and **2** showed some to no activity (Fig. 17). These results demonstrate that the induction of apoptosis in C4-2B cells by gallium complexes is associated with the inhibition of the proteasomal CT-like activity, and that the apoptosis-inducing potency of these compounds was also ranked as **5** > **4** > **3** > **2** ≥ **1**.

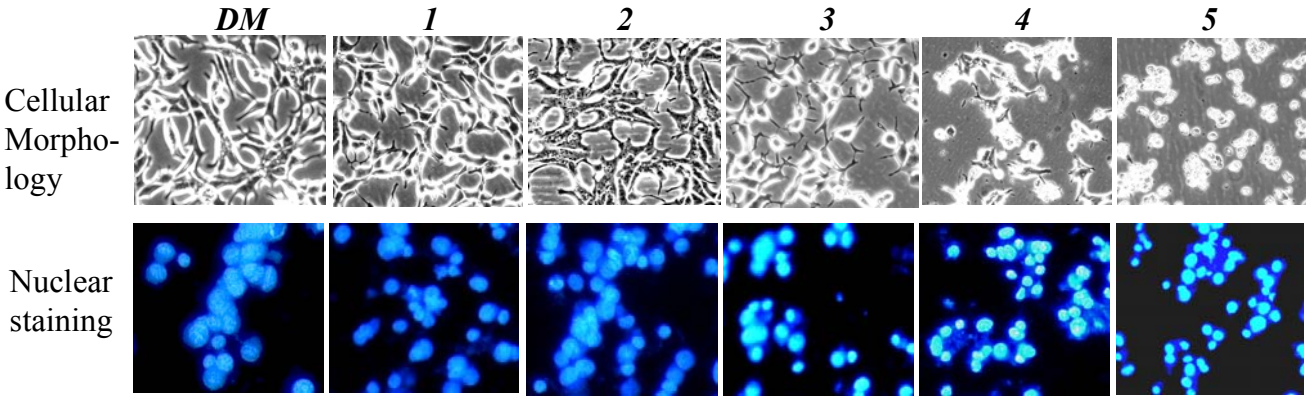

Figure 17. Cellular morphological and nuclear changes.

Human prostate cancer C4-2B cells were treated with 50 μM of complex **1-5** for 18 h, followed by staining for cellular morphological and nuclear changes. (DM) was used as solvent control.

To investigate effects of different concentrations of gallium complexes on prostate cancer cells, we selected the most potent complex **5** and treated C4-2B cells at various concentrations (10, 25, and 50 μmol/L), followed by measurement of proteasome inhibition, AR protein level, and cell death induction. The results showed that complex **5** inhibited the proteasome in a dose-dependent manner, as measured by proteasomal CT-like activity (Fig. 18), accumulation of ubiquitinated proteins and proteasome target protein p27 (Fig.19). A decrease in AR level and cell death associated PARP cleavage were also induced in a dose-dependent manner (Fig.19).

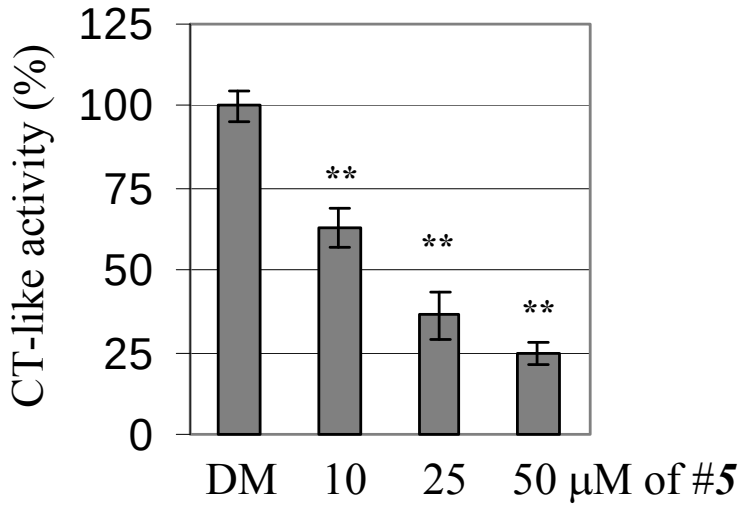

Figure 18. Dose effects of gallium complex 5 on C4-2B cells.

Human prostate cancer C4-2B cells were treated with indicated concentrations of complex **5** for 18 h, followed by measurement of the chymotrypsin-like activity. **, $P < 0.01$.

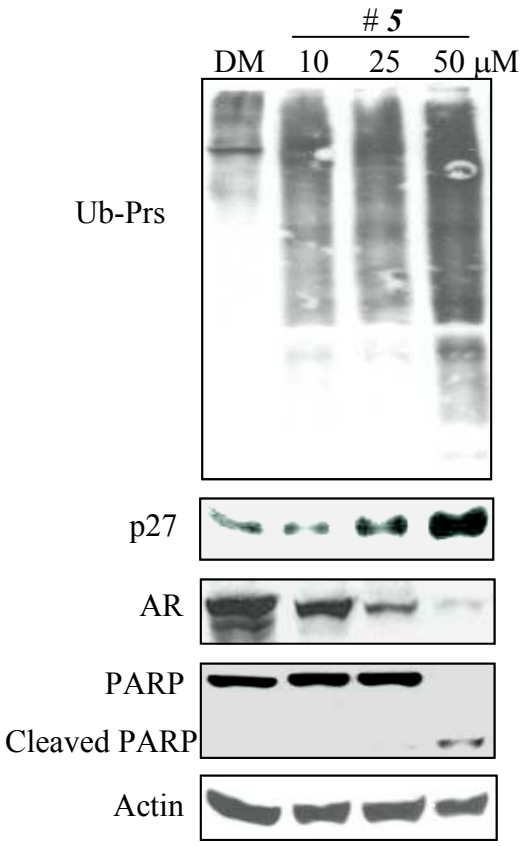

Figure 19. Dose effects of the gallium complex 5 on C4-2B cells.

Human prostate cancer C4-2B cells were treated with indicated concentrations of complex **5** for 18 h, followed by Western blot analysis with antibodies to ubiquitin, p27, androgen receptor, and PARP. DMSO (DM) was used as solvent control.

Inhibition of proteasomal CT-like activity by gallium complexes in androgen-dependent human LNCaP prostate cancer cells is associated with down-regulation of androgen receptor (AR) and induction of cell death. After we showed the ability of the gallium complexes to inhibit proteasome activity and induce cell death in androgen-independent C4-2B prostate cancer cells, we tested the effect of the same gallium complexes on androgen-dependent LNCaP cell line [Thalmann et al., 1994]. LNCaP cells were treated with 50 μmol/L concentration of each complex for 18 h, followed by measurement of the proteasome activity, AR protein level and cell death induction. We found that gallium complexes **2, 3, 4** and **5** inhibited CT-like activity of the proteasome by 12, 39, 62 and 79%, respectively (Fig. 20), while complex **1** showed only slight effect compared to solvent control (Fig.20).

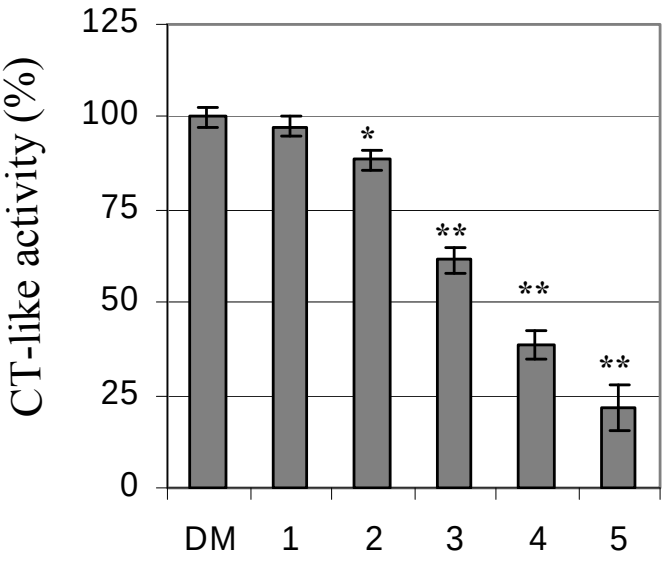

Figure 20. Gallium complexes inhibit proteasome activities in prostate cancer LNCaP cells.

Human prostate cancer LNCaP cells were treated with 50 μM of complex 1-5 for 18 h, followed by measurement of chymotrypsin-like activity. *, $P < 0.05$, **, $P < 0.01$.

Consistent with the inhibition of the proteasomal CT-like activity, significantly increased levels of ubiquitinated proteins were detected in the LNCaP cells treated with the complexes **3-5** (Fig. 21). Complex **5** was also found to be most potent in decreasing AR level, while complex **1** had almost no effect (Fig 21). In the same experiment, treatment with gallium complexes **3**, **4** and **5** resulted in massive cell detachment (data not shown) and PARP cleavage (Fig. 21). Additionally, complexes **3-5** induced caspase-3/7 in a time-dependent manner (data not shown), while complexes **1** and **2** showed only slight effect. These results demonstrate that in androgen-dependent LNCaP cells these gallium complexes have the same rank of proteasome-inhibitory, AR-suppressing and cell death-inducing potencies as in androgen-independent C4-2B cells.

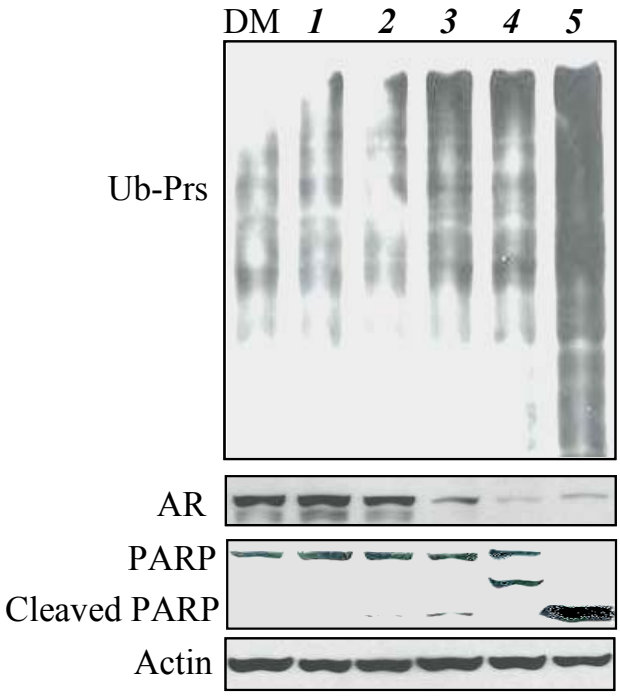

Figure 21. Accumulation of ubiquitinated proteins and cell death induction by gallium complexes in prostate cancer LNCaP cells.

Human prostate cancer LNCaP cells were treated with 50 μM of complex 1-5 for 18 h, followed by western blot analysis of ubiquitinated proteins (Ub-Prs), androgen receptor (AR), and PARP. DM was used as solvent control.

The time-dependent proteasome inhibition and cell death induction by gallium complex 5 in androgen-independent human prostate cancer PC-3 cells. The data in this dissertation reveals that complex **5,** of all tested complexes, had superior proteasome-inhibitory and cell death-inducing abilities in AR-dependent prostate cancer C4-2B and LNCaP cells (Figs. 14-21). To study the effect of these compounds in AR-independent prostate cancer cells, PC-3 cells were treated with 50 μmol/L of complex **5** for various time points (0.5-12 h). The proteasomal CT-like activity was found to be inhibited by 17% after first 30 minutes of treatment (Fig. 22), associated with accumulated level of ubiquitinated proteins (Fig. 23). The proteasome inhibition and accumulation of ubiquitinated proteins were observed during the course of treatment (Fig. 22 and 23). Accumulation of p27 was also found to be time-dependent (Fig. 23). Importantly, cell death associated PARP cleavage was not observed until 4 hours of treatment (Fig. 23). These results clearly show that cell death induced by complex **5** occurs after proteasome inhibition. Therefore, proteasome inhibition seems to be required for cell death induction by gallium complexes.

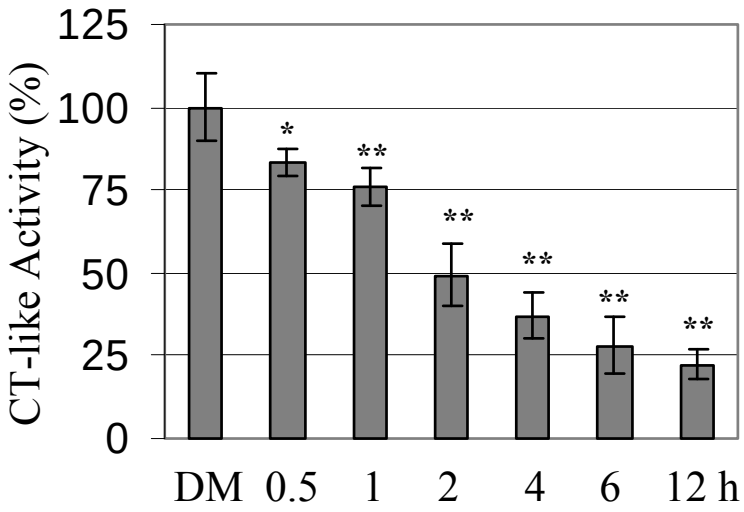

Figure 22. Kinetic effects of complex 5 on PC-3 cells.

Human prostate cancer PC-3 cells were treated with 50 μmol/L of complex 5 for indicated hours, followed by measurement of the chymotrypsin-like activity. *, $P < 0.05$, **, $P < 0.01$.

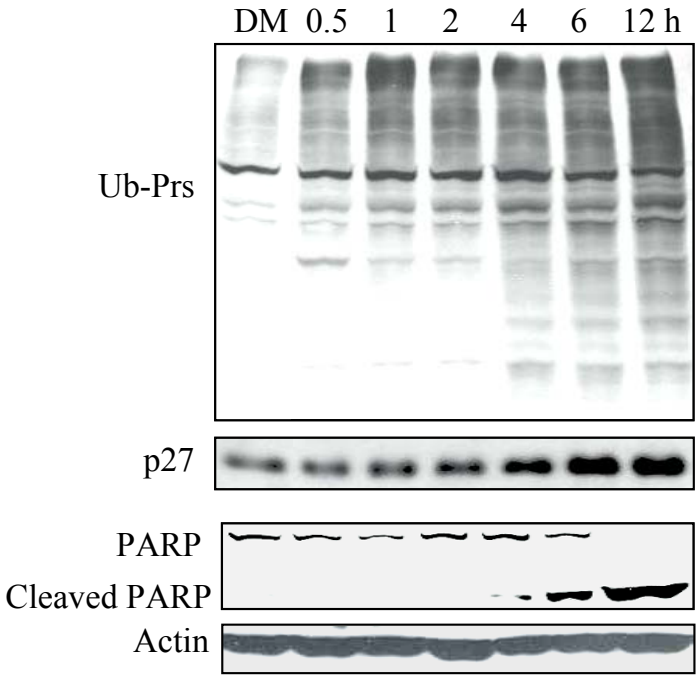

Figure 23. Kinetic effects by complex 5 on PC-3 cells.

Human prostate cancer PC-3 cells were treated with 50 μmol/L of complex 5 for indicated hours, followed by Western blot analysis of Ub (Ub-Prs), p27, and PARP. DMSO (DM) was used as solvent control.

Proteasome-inhibitory and apoptosis-inducing activities of gallium complex 5 and ligand 5 (L5) in human prostate cancer xenografts. The *in vitro* data shown in this dissertation demonstrate that gallium complexes **3, 4** and **5** act as proteasome inhibitors and cell death (*e.g.* apoptosis) inducers in cultured human prostate cancer cells and that complex **5** is the most potent (Figs. 14-23). To investigate whether compound **5** could also inhibit the proteasome and induce apoptosis *in vivo*, we used mice bearing human prostate tumor xenografts. PC-3 cells were implanted *s.c.* into male nude mice and allowed to grow until the appearance of a palpable tumor (~120 mm^3). The mice were then randomly grouped and injected *s.c.* daily with either solvent, 20 mg/kg of complex **5**, or 20 mg/kg of L**5** for 29 days. At the end of the trial, the mice were sacrificed and tumor tissue was harvested and used for multiple assays. The measurement of tumor size showed that tumor growth was inhibited by 66% in complex **5**-treated mice, and by only 30% in L**5**-treated mice, compared to the control mice (Fig. 24). Therefore, complex **5** possesses potent anti-tumor properties *in vivo*. However, the anti-tumor activity of L**5** was also observed (see below).

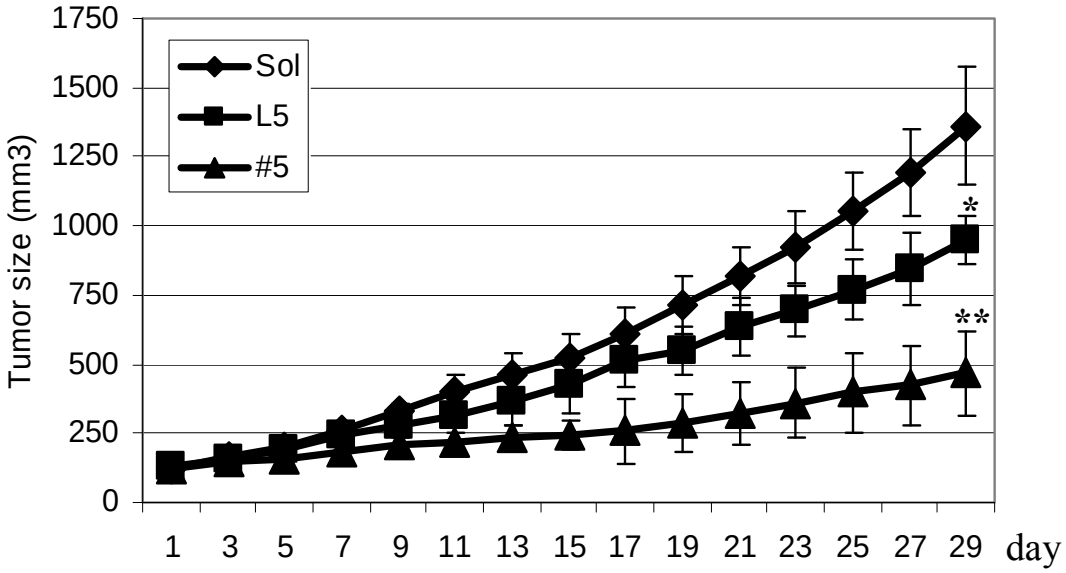

Figure 24. Complex 5 inhibits tumor growth in mice bearing PC-3 xenografts.

Male athymic nude mice were xenografted by injection of PC-3 cells. When tumor size reached to ~120 mm^3, the mice were divided into three groups and treated with either solvent (Sol) control (n=9) or Ligand **5** (L**5**; 20 mg/kg/day; n=5) or Complex **5** (20 mg/kg/day; n=9) for 29 days. Tumor growth was inhibited up to 66% and 30% by Complex **5** and L**5** after 29-day treatment, respectively, when compared to control (*, $P < 0.05$; **, $P < 0.01$). Points represent the means of tumor volume in each experimental group.

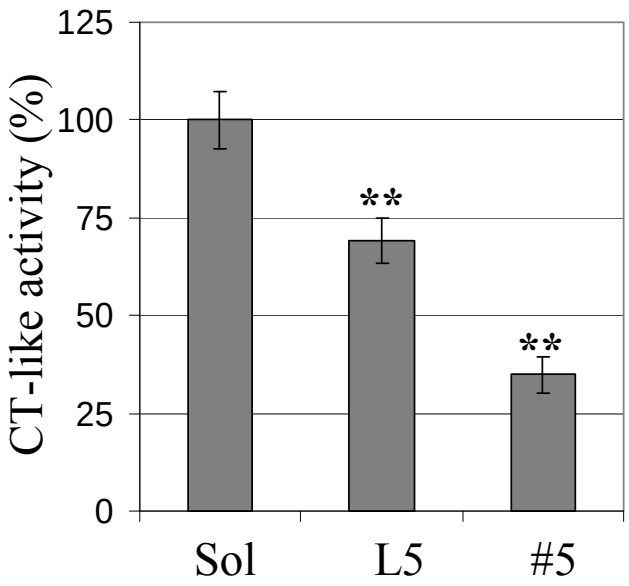

Figure 25. Inhibition of tumor growth by complex 5 is associated with inhibition of chymotrypsin-like activity.

Male nude mice bearing PC-3 xenografts were treated with either solvent (Sol) control (n=9) or Ligand **5** (L**5**; 20 mg/kg/day; n=5) or Complex **5** (20 mg/kg/day; n=9) for 29 days. At the end of 29 days tumors were collected and measured for the proteasomal chymotrypsin-like activity. *, $P < 0.05$; **, $P < 0.01$.

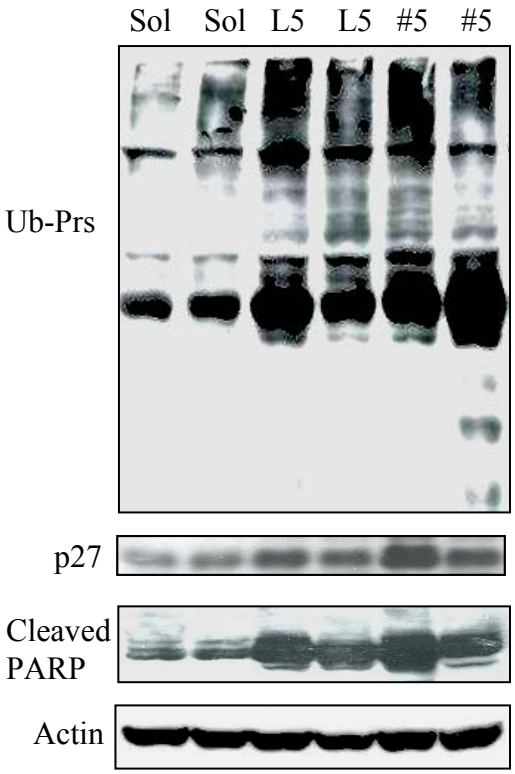

Figure 26. Western blot analysis of tumor extracts

Male nude mice bearing PC-3 xenografts were treated with either either solvent (Sol) control (n=9) or Ligand **5** (L**5**; 20 mg/kg/day; n=5) or Complex **5** (20 mg/kg/day; n=9) for 29 days. At the end of 29 days tumors were collected and measured for protein levels of Ub, p27, and cleaved PARP.

To determine if the observed anti-tumor effects of complex **5** and L**5** are associated with proteasome-inhibitory and apoptosis-inducing activities *in vivo*, the prepared tissue samples were used for several assays. Figure 25 shows inhibition of the proteasomal CT-like activity by 65% in complex **5**-treated tumors, compared to the control, while L**5**-treated tumors showed only 31% inhibition. Consistently, accumulation of ubiquitinated proteins and p27 was found in tumors treated with complex **5,** as measured by Western blot analysis (Fig. 26). L**5**-treated tumors were also able to accumulate ubiquitinated proteins and p27, but to a lesser extent (Fig. 26). This suggests the possibility of L**5** combining with endogenous metal species, such as copper, forming partial proteasome-inhibiting complexes (see Discussion). Increased accumulation of p27 protein in tumors treated by complex **5** or L**5** was further confirmed by immunohistochemistry assay, which showed the increase of p27-positive cells by 64, 25 and 7% in tumors treated with complex **5**, L**5** or solvent, respectively (Fig. 28).

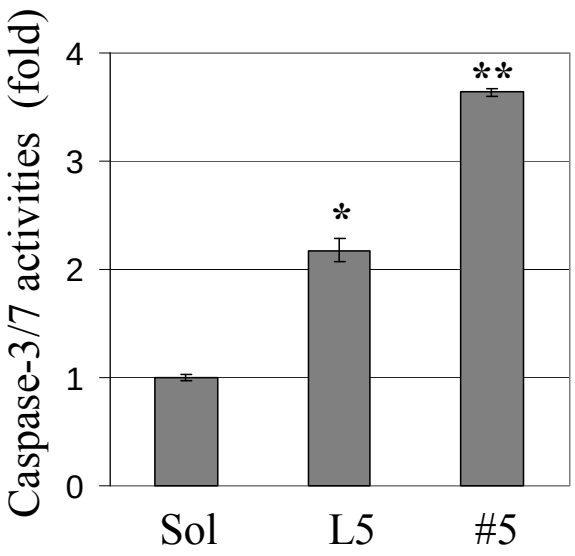

Figure 27. Inhibition of tumor growth by complex 5 is associated with activation of caspase 3/7 activity.

Male nude mice bearing PC-3 xenografts were treated with either solvent (Sol) control (n=9) or Ligand **5** (L**5**; 20 mg/kg/day; n=5) or Complex **5** (20 mg/kg/day; n=9) for 29 days. At the end of 29 days tumors were collected and measured for the caspase 3/7 activity. *, $P < 0.05$; **, $P < 0.01$.

Furthermore, we found that the inhibition of the proteasomal CT-like activity in tumors treated with complex **5** or L**5** was associated with apoptosis, as shown by induction of caspase-3/7 activity (Fig. 27) and the appearance of cleaved PARP fragment (Fig. 26). Induction of apoptosis in tumors treated with complex **5** or L**5** was further confirmed by the presence of TUNEL-positive cells (78 and 19% in complex **5** and L**5**-treated tumors, respectively) (Fig. 28), and high levels of condensed apoptotic nuclei detected by H & E staining (76 and 23% in complex **5**- and L**5**-treated tumors, respectively) (Fig. 28). While L**5** alone was able to induce some level of apoptosis, complex **5** was much more potent, showing superior tumor growth inhibition. We monitored the body weight of mice from each group and the average readings were 25.9, 25.7 and 25.5 grams from the mice treated with the solvent, L**5** and complex **5**, respectively. The data of the body weight showed that there was no toxicity of L**5** and complex **5** observed in the treated mice. Taken together, these results clearly demonstrate that complex **5** was able to target the proteasome *in vivo*, resulting in induction of apoptotic cell death.

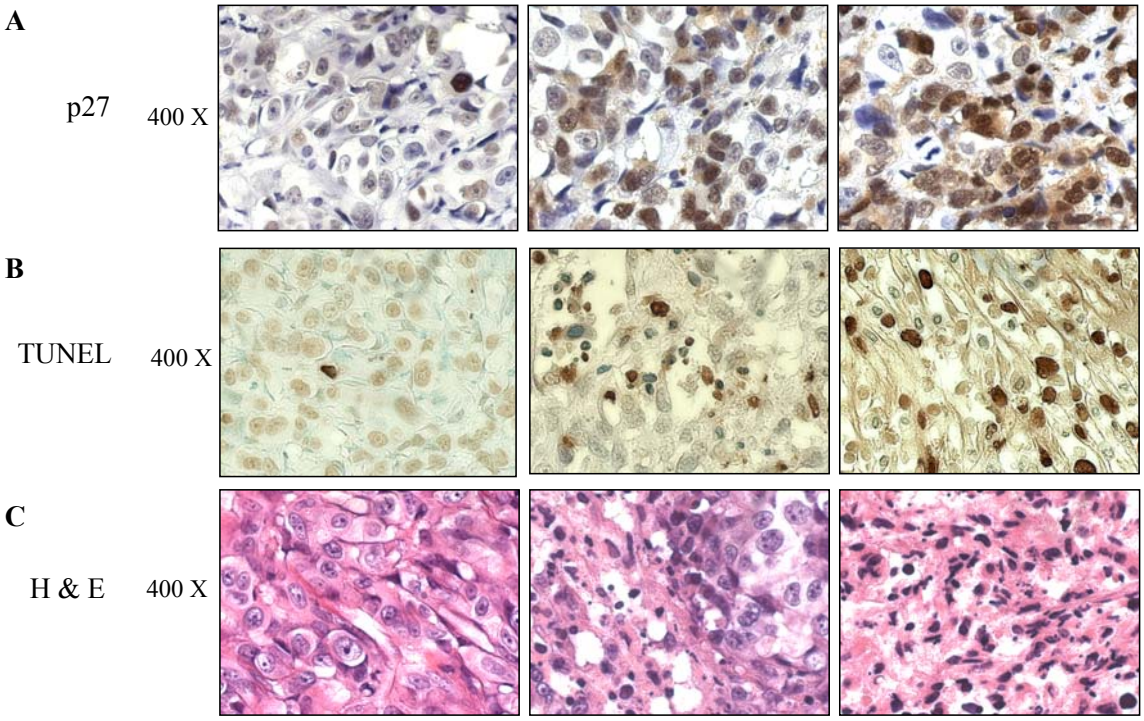

Figure 28. Immunohistochemistry p27, TUNEL and H&E staining assays using mouse tumor samples.

Tumors were collected after 29-day treatment (see Fig. 5 legend), and the prepared tissue slides were used for immunostaining with p27 antibody (*A*), TUNEL (*B*) and H&E staining assays (*C*). Stronger or/and more p27 positive cells and TUNEL positive nuclei as well as apoptotic-condensed nuclei were found in tumor tissue from mice treated with complex **5**. L**5** has the similar effects but weaker. Magnification 400X as indicated.

Discussion

The main problems with conventional metal-based chemotherapeutic strategies are nonspecific interactions and the acquisition of drug resistance. The screening and subsequent development of copper-based compounds as anti-tumor agents has shown promising pre-clinical results, which formed the basis for a potential novel therapeutic strategy [Chen et al., 2006; Chen et al., 2005]. Gallium complexes have been investigated in clinical trials and ongoing studies are trying to optimize drug disposition and pharmacokinetic parameters [Galanski et al., 2003; Jakupec and Keppler, 2004a].

The established anti-tumor activity and therapeutic potential of gallium complexes have renewed our interest in exploring their mechanisms of action [Galanski et al., 2003; Jakupec and Keppler, 2004a; Jakupec and Keppler, 2004b]. Although many studies are investigating biological effects of gallium, they are mainly focused on a transferrin-mediated mode of action, with subsequent inhibition of DNA synthesis [Chitambar, 2004b; Galanski et al., 2003; Jakupec and Keppler, 2004b]. Some studies with gallium have been implicated in the programmed cell death pathway concomitant with iron deficiency and sustained gallium exposure [Chitambar, 2004a; Haq et al., 1995]. However, the mechanism of action triggered by gallium complexes remains unclear.

Since gallium complexes showed inhibition of cell proliferation against cisplatin-resistant neuroblastoma cells [Shakya et al., 2006b], we decided to further investigate their biological activities against prostate cancer cells and tumors. We demonstrate in this dissertation that some of these gallium complexes are very potent cell death inducers in androgen-dependent and androgen-independent prostate cancer cells. Moreover, we reveal

the 26S proteasome as their target, which represents an important step in delineating their mechanism of action.

The gallium complexes investigated here were synthesized by using asymmetric ligands containing pyridine and 2,6 substituted phenol moieties (Fig. 13). While their cell-killing activities have been well-established, their coordination mode and structure activity relationship (SAR) are not well understood. In the current study we have found that complex **5** is much more potent than complexes **1-4,** suggesting that L**5** possesses certain characteristics that, after coordination with gallium, provide an optimal biological response. This optimal response may be governed by the strong π electron-donating iodine group. Considering that all ligands used to synthesize complexes **3-5** contain electron withdrawing halogen substituents, only their π-donating ability could relate to their anti-tumor effects (I > Br > Cl). Iodine retains very weak electron withdrawing ability but is a very strong π-donating group, which can activate the ring system of the complex and influence its ability to bind the proteasome. However, the influence of the coordination mode of the metal ion and phenol substitute group as it relates to its therapeutic effect is purely speculative at this point. The data also showed that L**5** is able to bind other metals, such as copper, and that L**5** mixed with copper potently inhibited the proteasome and induced apoptosis in human prostate cancer cells (data not shown). It has been reported that tumor tissue contains elevated level of copper [Habib et al., 1980; Nayak et al., 2003]. Therefore, one possible explanation for some tumor growth inhibition observed in the mice treated with L**5** could be an effect of the complex made between L**5** and copper.

We also found that the gallium(III) chloride was relatively nontoxic and that concomitant treatment with complex **5** and iron(III) chloride partially precluded the cytotoxic

effect of complex **5** (data not shown). Therefore, we propose that gallium complexes, rather than gallium ions sequestered from the complex, are taken up through the transferrin receptor-mediated pathway. However, the exact mechanism for uptake of gallium complexes and their intracellular trafficking and binding to the proteasome needs to be further investigated.

The most important aspects in this dissertation were to investigate whether these gallium complexes were active *in vivo* and to verify their molecular target(s). Therefore, the effects of complex **5** were tested along with its ligand L**5** in mice bearing human PC-3 xenografts. Our data in this dissertation showed that treatment with complex **5** caused a significant inhibition of PC-3 tumor growth in nude mice (Fig. 24). Importantly, the anti-tumor activity of complex **5** was associated with the proteasomal activity inhibition (Fig. 25), accumulation of the proteasome target proteins p27 (Figs. 26 and 28), and induction of apoptosis, demonstrated by caspapse-3/-7 activation, PARP cleavage, TUNEL positivity and nuclei condensation (Figs. 26, 27, 28B). Taken together, the data in this dissertation suggests that gallium complexes, by acting as potent proteasome inhibitors, have great potential to be developed as novel anti-cancer drugs.

CHAPTER 3

Metals in anticancer therapy: Copper(II) complexes as inhibitors of the 20S proteasome

Adapted from published material in European Journal of Medicinal Chemistry, 2009; 4353-4361

The data presented in this dissertation shows that selective 20S proteasomal inhibition and cell death induction were observed when several lines of cancer cells were treated with a series of copper complexes described as $[Cu(L^I)Cl]$ **(1)**, $[Cu(L^I)OAc]$ **(2)**, and $[Cu(HL^I)(L^I)]OAc$ **(3),** where HL^I is the ligand 2,4-diiodo-6-((pyridine-2-ylmethylamino)methyl)phenol**.** These complexes were synthesized, characterized by means of ESI (Electrospray ionization) spectrometry, infrared, UV-visible and EPR (Electron paramagnetic resonance) spectroscopies, and X-ray diffraction when possible. After full characterization species **1-3** were evaluated for their ability to function as proteasome inhibitors and cell death inducers in C4-2B and PC-3 human prostate cancer cells and MCF-10A normal cells. With distinct stoichiometries and protonation states, this series suggests the assignment of species $[CuL^I]^+$ as the minimal pharmacophore needed for proteasomal chymotrypsin-like activity inhibition and permits some initial inference of mechanistic information.

Materials and Methods

Materials

All reagents were obtained from commercial sources. $CuCl_2 \cdot 2H_2O$ was purchased from Sigma-Aldrich (St. Louis, MO). Solvents were purified by means of an I.T. solvent purification system. RPMI 1640, penicillin and streptomycin were purchased from Invitrogen (Carlsbad, CA). Fetal bovine serum was purchased from Aleken Biologicals (Nash, TX). Fluorogenic peptide substrate Suc-LLVY-AMC (for the proteasomal chymotrypsin-like activity) were from Calbiochem (San Diego, CA). Mouse monoclonal antibody against human poly(AP-ribose) polymerase (PARP), p27, ubiquitin and secondary antibodies were from Santa Cruz Biotechnology, Inc. (Santa Cruz, CA).

Methods

ESI (Electrospray ionization) spectra were measured on a Micromass QuattroLC triple quadrupole mass spectrometer with an electrospray/APCI source and Walters Alliance 2695 LC, autosampler and photodiode array UV (Ultraviolet) detector. Experimental assignments were simulated based on peak location and isotopic distributions. Infrared spectra were measured from 4000 to 400 cm^{-1} as KBr pellets on a Tensor 27 FTIR (Fourier transform infrared)-spectrophotometer. UV (Ultraviolet)-visible spectroscopy from 1.0×10^{-4} methanol or methanol:DMSO solutions were performed using a Cary 50 spectrometer in the range 250 to 1000 nm. The samples were mortar-ground and heat-dried under vacuum overnight to eliminate solvent molecules. First derivative X-Band EPR (Electron paramagnetic resonance) spectra of 1.0×10^{-3} M methanol solutions were performed with a Bruker ESP 300 spectrometer using liquid helium as the coolant. Elemental analyses were

performed by Midwest Microlab, Indianapolis, Indiana. Cellular morphology analyses and imaging with phase contrast were performed on a Zeiss Axiovert 25 microscope.

X-ray Structural Determination for [Cu(L^I)(Cl)] (1). Diffraction data were measured at 100 K on a Bruker X8 APEX-II kappa geometry diffractometer with Mo radiation and a graphite monochromator. Frames were collected as a series of sweeps with the detector at 40 mm and 0.3 degrees between each frame, recorded for 10 or 20 s. APEX-II and SHELX-97 software were used in the collection and refinement (Table 2). Crystals of 1 [$C_{13}H_{11}N_2O_1Cl_1I_2Cu_1$] were blue-green needles; the diffraction sample was 0.4 x 0.02 x 0.01 mm^3. 50251 total reflections were recorded, yielding 7828 independent hkl data. Hydrogen atoms were placed in calculated positions. The asymmetric unit consists of two independent neutral complexes.

Syntheses

The ligand 2,4-diiodo- 6-((pyridine-2-ylmethylamino) methyl)phenol was synthesized according to a previously published procedure [Shakya et al., 2006a; Shakya et al., 2006b]. [Cu(L^I)Cl] **(1).** (0.50 g, 1.1 mmol) of HL^I was dissolved in 15 mL of DMSO. After 5 minutes (0.18 g, 1.2 mmol) of $CuCl_2 \cdot 2H_2O$ was dissolved in 15 mL of DMSO and the resulting solution was added drop wise and stirred at room temperature for 45 min. The green solution was added to 15 mL of cold ethanol to afford dark green needle-like crystals after 48 hours. Yield = 0.15 g (27%). Elemental analysis calc. (%) for $C_{13}H_{11}ClCuI_2N_2O$: C 27.68; H 1.97; N 4.97. Found: C, 27.72; H, 1.88; N, 4.86. IR data (KBr, cm^{-1}): 3073 v(N-H); ESI^+ MS data (MeOH): m/z = 527.9 for $[CuL]^+$, 605.9 $[CuL\text{-}DMSO]^+$.

[Cu(L^I)OAc] (2). (0.50 g, 1.1 mmol) of HL^I was dissolved in 15 mL of DMSO and treated with 1.1 equivalents of triethylamine. While stirring for 5 minutes at room

temperature, (0.27 g, 1.2 mmol) of $Cu(OAc)_2 \cdot 2H_2O$ was dissolved in 15 mL of DMSO and the ligand solution was added drop wise and allowed to react for 45 min. The complex was isolated using suction filtration and washed with cold methanol and ether to afford a green precipitate. Yield = 0.505 g (86%). Elemental analysis calc. (%) for $C_{15}H_{14}CuI_2N_2O_3$: C 30.66; H 2.40; N 4.77. Found: C, 30.82; H, 2.45; N, 4.70. IR data (KBr, cm^{-1}): 3073 v(N-H); 1586 $v_{asym}(OAc^-)$; 1402 $v_{sym}(OAc^-)$. ESI^+ MS (Electrospray ionization mass spectrometry) data (MeOH): m/z = 527.8 for $[CuL]^+$, 606.0 $[CuL\text{-}DMSO]^+$.

$[Cu(HL^I)(L^I)]OAc$ (3). A 15 mL methanol solution of HL^I (1.05 g, 2.1 mmol) was added drop wise to a 15 mL methanol solution of $Cu(OAc)_2 \cdot 2H_2O$ (0.27 g, 1.2 mmol) at 45 ^oC. After 45 minutes a green precipitate was obtained, isolated by frit filtration, and washed with cold methanol and ether. The solid was recrystallized in dichloromethane. Yield = 0.900 g (79%). Elemental analysis calc (%) for **3**•CH_2Cl_2 $C_{29}H_{28}Cl_2CuI_4N_4O_4$: C 30.59; H 2.48; N 4.92. Found: C, 30.82; H, 2.42; N, 4.76. IR data (KBr, cm^{-1}) 3448 v(OH); 3076 v(N-H); 1564 $v_{asym}(OAc^-)$; 1439 $v_{sym}(OAc^-)$. ESI^+ MS (Electrospray ionization mass spectrometry) data (MeOH): m/z = 527.9 for $[CuL]^+$, 994 (minor) for $[Cu(HL)(L)]^+$.

Trypan blue assay

The trypan blue dye exclusion assay was performed by mixing 100 µl of cell suspension with 50 µl of 0.4% trypan glue dye before injecting into a hemocytometer and counting. The number of cells that absorbed the dye and those that excluded the dye were counted, from which the percentage of nonviable cell number to total cell number was calculated.

Cell Cultures and Whole-cell Extract Preparation.

Human prostate cancer cells, C4-2B and PC-3 were grown in RPMI 1640 medium supplemented with 10% FBS and maintained at 37°C and 5% CO_2. MCF-10A cells (normal, derived from benign human breast tissue were obtained and cultured as previously described. A whole cell extract was prepared as previously described [Daniel et al., 2005].

Analysis of the Proteasomal Activity in Whole-cell Extract

C4-2B, PC-3 and MCF-10A whole-cell extract (8 µg) was incubated with 10 µmol/L chymotrypsin-like-substrate (Suc-LLVY-AMC) in 100 µL assay buffer [50 mmol/L Tris-HCl (pH 7.5)] in the presence of different copper complexes, ligand, and inorganic copper salt at various concentrations or solvent DMSO as control. After 2 h incubation at 37° C, production of hydrolyzed AMC groups was measured using a Wallac Victor3^{TM} multilabel counter with an excitation filter of 365 nm and an emission filter of 460 nm [Daniel et al., 2005].

Western Blot Analysis

Cell extracts were separated by SDS-PAGE and transferred to a nitrocellulose membrane. Western blot analysis was performed using specific antibodies to p27, ubiquitin, or PARP (Santa Cruz Biotechnology Inc, Santa Cruz, CA) followed by visualization using the HyGLO reagent (Denville Scientific, Metuchin, NJ)

Results

Ligand design and in situ copper complexation. The iodo-substituted ligand 2,4-diiodo-6-((pyridine-2-ylmethylamino)methyl)phenol, HL^I was synthesized by treatment of 2-hydroxy-3,5-diiodobenzaldehyde with 2-aminomethylpyridine followed by reduction with sodium borohydride [Shakya et al., 2006a; Shakya et al., 2006b]. It can be considered as an evolution from its terbutylated analogues inspired by biomimetic efforts to model redox-active enzymes such as galactose-oxidase [Itoh et al., 1999; Vaidyanathan et al., 1998]. The complexes were designed considering that a metal ion coordinated to the ligand could bind to the 20S core of the proteasome, possibly *via* the terminal threonine residue Thr1 or another available coordination site. Initial exploratory studies on human C4-2B prostate cancer cells, comprised of cell death induced by a stoichiometric mixture of HL^I and copper(II) chloride in DMSO and toward proteasomal activity in whole-cell extracts. These data reported in this dissertation show that the resulting HL^I:$CuCl_2$:DMSO mixture was fourfold more potent than the recently reported gallium species.

Syntheses, Spectrometry, and Spectroscopic Characterization of complexes 1-3. Spectrometric evaluation of the stoichiometric HL^I:$CuCl_2$:DMSO mixture using ESI (Electrospray ionization) in the positive mode led to the identification of monomeric and dimeric fragments that may act as pharmacophores to the inhibition of the proteasome complex (Fig. 29). These fragments fit well with the expected distribution anticipated in systems containing copper and iodine isotopes. The relative ESI-MS (Electrospray ionization-mass spectrometry) profile for the monomeric $[CuL^I]^+$ is m/z = 527.9.

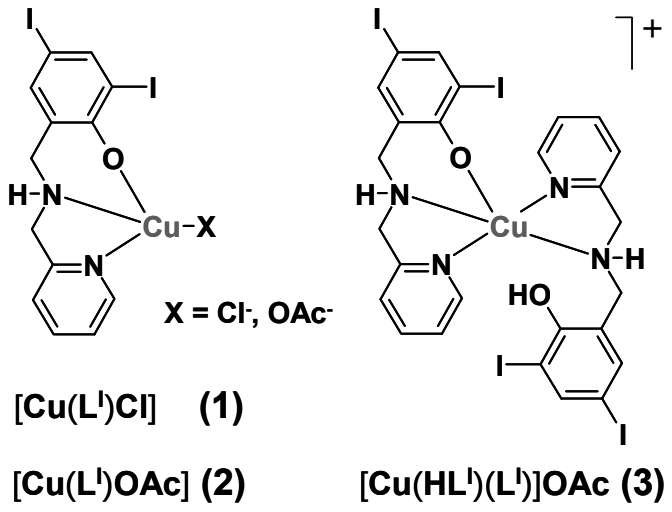

Figure 29. Representative copper(II) complexes with tridentate ligands

Spectrometric evaluation of the stoichiometric HL^I:$CuCl_2$:DMSO mixture led to the identification of monomeric and dimeric fragments depicted as [Cu(L^I)Cl] (1), Cu(L^I)OAc (2), and [Cu(HL^I)(L^I)]OAc (3).

A minor peak at m/z = 994 is also detectable in this mixture suggesting a 2:1 ligand-to-copper complex, where either two fully deprotonated ligands are coordinated to the metal ion as in $[Cu(L^I)_2]+H^{++}$ or one of the ligands remains protonated as in $[Cu(HL^I)(L^I)]^+$, respecting a 5-coordination preference imposed by the Jahn-Teller effect expected by a $3d^9$ species such as the copper(II) ion [Rorabacher, 2004]. Based on similar systems the latter proposition is favored.

With the intent of isolating and testing these species as anticancer agents, reactions with 1:1, and 2:1 ligand-to-metal ratios were performed. Treatment of 1 equiv. of the ligand with 1 equiv. of $CuCl_2 \cdot 2H_2O$ in DMSO yielded a green solution that was precipitated with ethanol in 30% yield as a crystalline material.

The isolated product was characterized as $[Cu(L^I)Cl]$ **(1)**. It is noteworthy that **1** can also be obtained using methanol or ethanol as solvents, and the choice of DMSO was intended to match the experimental conditions of the initially used stoichiometric mixture. The chloride anions from the copper salt seem able to deprotonate the ligand with subsequent formation of hydrochloric acid. Hence, copper chloride was replaced by copper acetate, primarily in order to increase the yield of this reaction, as well as a cautionary measure to avoid HCl build up [Olaleye and Farombi, 2006]. The ligand HL^I (1 equiv.) was treated with $Cu(OAc)_2 \cdot 2H_2O$ (1 equiv.) in presence of triethylamine as a base to support ligand deprotonation yielding the species $[Cu(L^I)OAc]$ **(2)** in 90% yield. The ESI(pos) MS (Electrospray ionization mass spectrometry)spectrum shows the characteristic m/z = 527.8 associated with the fragment $[Cu(L^I)]^+$, whereas the acetate species was detected by infrared spectroscopy at 1586 and 1402 cm^{-1} as a monodentate ligand. Elemental analysis showed excellent agreement with the proposed formula.

The EPR (Electron paramagnetic resonance) spectra taken at 77 K for **1** and **2** reinforce this notion with values of $g_{\|} \approx 2.26$, $g_{\perp} \approx 2.06$, $A_{\|} \approx 174$ G and $A_{\perp} \approx 19$ G, thus typical of $3d^9$ copper(II) ions in nearly square planar environments. Furthermore, the UV-visible spectra of species **1** and **2** in methanol show the presence of a phenolate-to-copper charge transfer band at around 450 nm ($\varepsilon \approx 1250$ L·mol^{-1}·cm^{-1}) [Itoh et al., 1999].

When a reaction of 2:1 stoichiometry between HL^I and the copper acetate salt was carried out in methanol, a green precipitate described as $[Cu(HL^I)(L^I)]OAc$ **(3)** was obtained. The compound was recrystallized in dichloromethane yielding a microcrystalline material. Although crystals suitable for X-ray diffraction were not obtained, infrared spectroscopy reveals the presence of acetate counterions, as displayed by prominent peaks at 1564 and 1439 cm^{-1}. Additional peaks at 3448 are attributed to the presence of OH stretches belonging to a protonated HL^I ligand. ESI (Electrospray ionization) mass spectra in the positive mode shows m/z = 527.9 characteristic of the $[Cu(L^I)]^+$ fragment. In good agreement with the elemental analysis, these data confirm the presence of two ligands coordinated to copper, one of which remaining protonated. This coordination mode for copper has been observed in our laboratories with the analogous ligand HL^{tBu}, where tertiary butyl groups occupy the 2- and 4- positions of the phenol ring. Species **3** shows EPR parameters $g_{\perp}$, $A_{\|}$, and $A_{\perp}$ similar to those of **1** and **2** but with $g_{\|} = 2.30$, thus, evidencing bonding along the z-axis typical of five-coordinate copper(II) ions.

Molecular Structure of complex 1. Needle-like crystals of $[Cu(L^I)Cl]$ **(1)** were isolated and solved diffractometrically by means of X-ray diffraction. The crystal structure of **1** is shown in Figure 30 and confirms its mononuclear nature. One copper(II) ion is coordinated to a deprotonated ligand with distances of 1.93 Å to the oxygen of the phenolate group, 1.99 Å to

the amine nitrogen, and 2.02 Å for the pyridine nitrogen, resembling similar systems [Itoh et al., 1999; Vaidyanathan et al., 1998]. The coordination sphere is completed with the anionic chloro ligand occupying the fourth position 2.24 Å away from the metal. The copper center adopts a distorted square-planar environment. One can, therefore, conclude that contrary to the tetradentate phenol-containing ligands tridentate ligands such as HL^{I} do not foster the formation of stable dimers in the solid state [Brewer, 2007]. **(The spectroscopic, spectrometric and structural analyses were generated by the Verani Lab, WSU Department of Chemistry).**

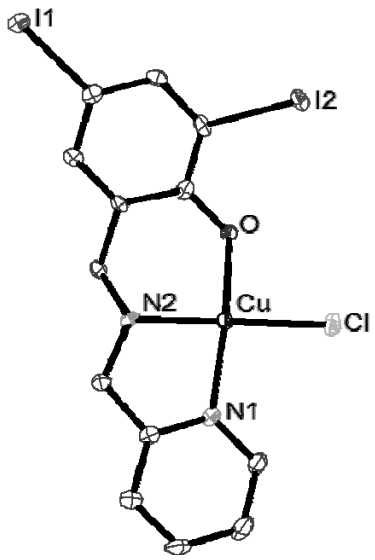

Figure 30. Crystal structure of [Cu(L^I)Cl] (1).

ORTEP (Oak Ridge Thermal Ellipsoid Plot Program) diagram at 50% probability level for [Cu(L^I)Cl] (**1**) with selected bond lengths (Å) and angles (°). Cu(1)-O(1) = 1.929(3), Cu(1)-N(2) = 1.990(4), Cu(1)-N(1) = 2.018(4), Cu(1)-Cl(1) = 2.2488(14), N(2)-Cu(1)-Cl(1) = 162.63(14), O(1)-Cu(1)-N(1) = 66.40(17).

Antiproliferative Effect of 1-3 in Tumor Cells. Our results thus far have allowed us to gain detailed understanding on the coordination chemistry of copper complexes as candidate drugs or prodrugs for cancer therapy. Human leukemia Jurkat T cells were treated with complexes **1-3** at different concentrations for 18 h, followed by trypan blue assay to assess cell death. This is a reliable assay that is reproducible and frequently used in our lab. All species tested demonstrated a dose-dependent increase in cell-killing activity with nearly 100% cell death at 15 μM, compared to a control treated with DMSO. The values given in Table 1 reflect the concentration that each compound induces 50 % cell death.

The 1:1 copper species **1** and **2** demonstrated IC_{50} values of 3.82 and 4.46 μmol/L. Interestingly, complex **3** exerted a similar degree of potency (IC_{50} = 3.98 μmol/L). Because the cation $[Cu^{II}(L^{I})]^{+}$ of **1** is isostructural with that of **2**, this observation suggests the 1:1 ligand-to-metal ratio as the possible pharmacophore and potential therapeutic agent. Furthermore, treatment of the cells with up to 50 μM of the ligand HL^{I} or the copper salt failed to induce death ratios greater than 10%. Due to the small standard deviation values between **1** and **2**, ascertaining the role played by the nature of the anionic ligand (chloride *vs.* acetate) remains unclear and further analysis will be necessary to provide a more conclusive result.

Compound	Cell death induction IC_{50} µmol/L
1	3.82 ± 0.01
2	4.46 ± 0.01
3	3.98 ± 0.01
HL^I	no activity
$CuCl_2$	no activity

Table 1. IC_{50} values for cell death induction by copper compounds.

Human leukemia Jurkat T cells were treated with copper compounds 1-3 for 18h, followed by measurement of cell death in a trypan blue exclusion assay. Standard deviations are indicated.

***In-vitro* Inhibition of Proteasomal Chymotryspin-like Activity by 1-3.** In order to test the role of complexes **1-3** in targeting the cellular proteasome, we compared the independent activity of the salt $CuCl_2 \cdot 2H_2O$, the ligand HL^I, and that of a 1:1 mixture of copper chloride and the ligand HL^I towards C4-2B prostate cancer cell extract. The results indicate that both the copper chloride salt and the copper chloride:ligand mixture inhibit the chymotrypsin-like activity of the 26S proteasome with IC_{50} values of ~3.5 μM (Fig. 31a). In contrast, the ligand HL^I alone had a negligible effect, even at concentrations as high as 25 μM. This seems to be consistent with prior work in our laboratories in which the copper ion [Chen and Dou, 2008; Daniel et al., 2005; Daniel et al., 2004] is the driving force underlying proteasome inhibition. We hypothesize that the ligand is necessary as a carrier to preclude undesired nonspecific interactions of copper in the cell extract [Brewer, 2007]. In order to underscore the role of the ligand, we tested complexes **1-3** under similar conditions. All species inhibited the proteasomal chymotrypsin-like activity in a concentration-dependent manner as shown in Figure 31b.

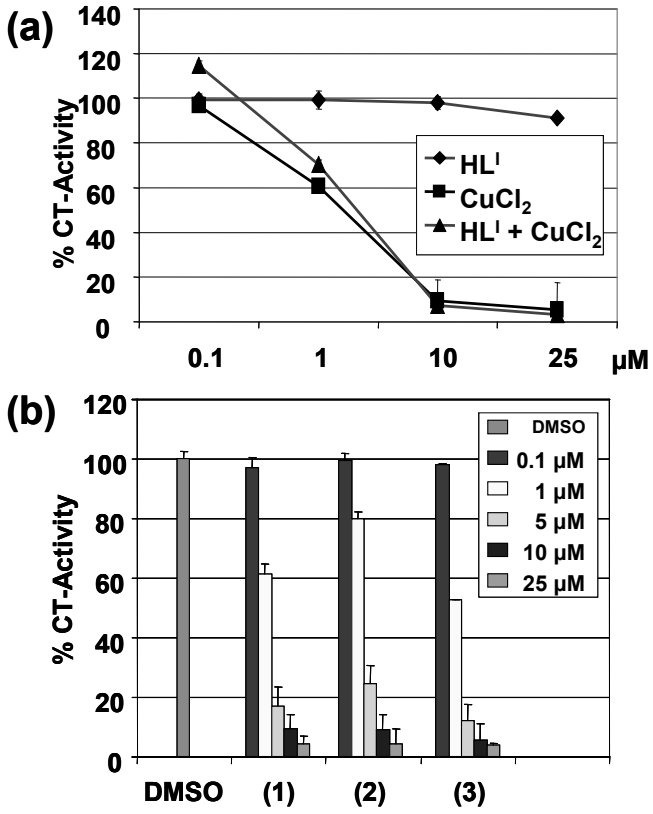

Figure 31. ***In vitro*** **proteasome-inhibitory activity of compounds 1-3 in C4-2B cell extracts.**

A. Proteasomal chymotrypsin-like activity (%CT) of the ligand HL^I, the salt $CuCl_2$, and a 1:1 HL^I:$CuCl_2$ mixture in DMSO at 25 mmol/L stock solution. **B.** Concentration dependent inhibition by **1-3** at 0.1, 1, 5, 10, and 25 µM

Inhibition of Chymotrypsin-like Activity and Induction of Apoptosis by 1-3 in Multiple Prostate Cancer Cell Lines. In the previous section we have discussed the inhibition of proteasomal chymotryspin-like activity under cell-free conditions. When intact prostate cancer cells were treated with HL^I or the Cu^{+2} ion at the 15 μmol/L concentration, less than 20% proteasome inhibition was evident. In order to confirm the ability of the copper complexes to inhibit the proteasomal activity in cancer cells, two distinct prostate cell lines were tested, namely androgen receptor-positive C4-2B and androgen receptor-negative PC-3.

Androgen receptor-positive C4-2B prostate cells were first treated with compound **1** at 5, 10 and 15 μM concentrations for 18 h. The cells were harvested and proteins extracted, followed by measurement of proteasomal inhibition and apoptosis. Cells were also treated with the vehicle DMSO, the ligand HL^I, and the salt $CuCl_2 \cdot 2H_2O$ at the same concentrations to serve as negative controls. Compound **1** inhibited the proteasomal chymotrypsin-like activity in a dose dependent manner by 35% at 5 μM, 62% at 10 μM and 85% at 15 μM (Fig. 32). Consistent with proteasome inhibition by **1**, levels of ubiquitinated proteins were also increased in a dose-dependent fashion in the treated C4-2B cells (Fig. 33). In a sharp contrast, cells treated either with the solvent, the ligand, or the copper salt failed to inhibit significantly the proteasome activity (Figs. 32, 33 and data not shown). Therefore, we hypothesize that the combination of copper(II) ion and ligand is a necessary requirement in order to cross the cellular membrane and reach the proteasome.

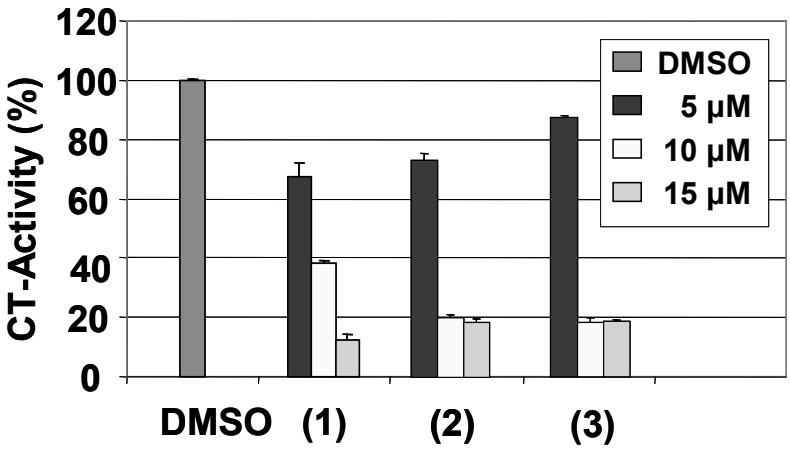

Figure 32. Effects of compounds 1-3 on C4-2B cells are dose-dependent.

Human prostate C4-2B cells were treated with compounds **1**, **2**, or **3** for 18 h followed by measurement of proteasomal chymotrypsin-like activity. DMSO was used as solvent control.

It has been shown that inhibition of the proteasomal chymotrypsin-like activity is associated with apoptosis of tumor cells [Lopes et al., 1997]. To investigate whether the proteasomal inhibition by **1** is associated with cell death, cleavage of the DNA repair protein, poly-(ADP-ribose) polymerase (PARP) and cellular morphological changes were measured in the same experiment. Cells showed a significant decrease in levels of PARP protein (Fig. 33) when treated with **1** at 10 and 15 μM. Consistently, aberrant morphological changes, namely the rounded up shape and detached shown in Figure 34, were also observed in **1** in a concentration-dependent manner. Again, cells treated with DMSO, the ligand HL^{I}, or the salt $CuCl_2$ individually were unable to perturb the full length PARP fragment and no visible aberrant morphological changes were observed up to 15 μM tested (Figs. 33, 34 and data not shown).

Similar results were also obtained from the C4-2B cells treated with compounds **2** and **3:** these two compounds inhibited about 80% of proteasomal activity at concentrations of 10 and 15 μM (Fig. 32), associated with increased levels of ubiquitinated proteins, decreased levels of PARP protein and the appearance of characteristic cell death morphology (Figs. 33, 34). These results show that the inhibition of proteasomal chymotrypsin-like activity in C4-2B cells is associated with the induction of cell death (*e.g.* apoptosis). Due to similar activity, it is also possible that in the 2:1 species **3**, the protonated ligand is labile and easily interchangeable suggesting that the active pharmacophore in both **2** and **3** is the cupric cation $[Cu(L^{I})]^{+}$.

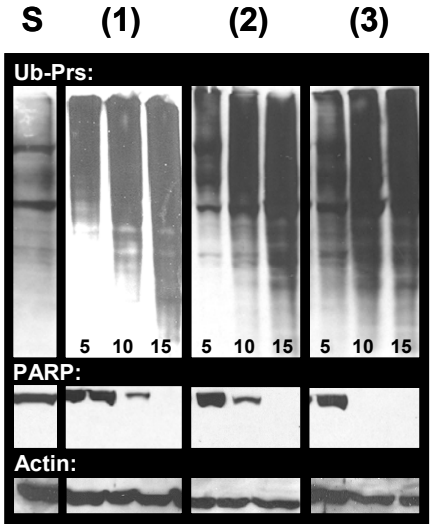

Figure 33. Dose dependent effects of compounds 1-3 on C4-2B cells.

Human prostate C4-2B cells were treated with compounds **1**, **2**, or **3** for 18 h followed by measurement of accumulation of ubiquitinated proteins (Ub-Prs), and cleavage of PARP.

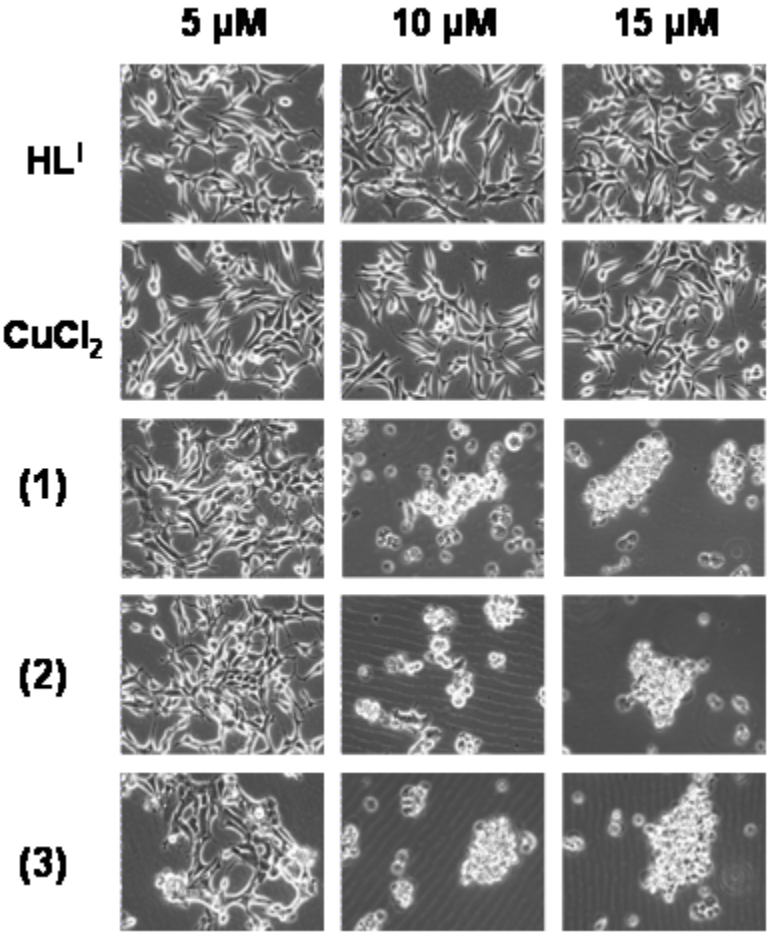

Figure 34. Dose dependent effects of compounds 1-3 on C4-2B cells.

Human prostate cancer C4-2B cells were treated with HL^{I}, $CuCl_2$, **1**, **2**, and **3** followed by visualization of apoptotic morphological changes.

We next tested the effects of these copper compounds toward androgen receptor-negative PC-3 prostate cells: Upon demonstrating the ability of copper compounds to inhibit the proteasomal chymotrypsin-like activity in androgen receptor-positive C4-2B cells, we then tested the effect of compounds **2** and **3** on androgen receptor-negative PC-3 prostate cancer cells. PC-3 cells were treated respectively with different concentrations of **2** and **3**, copper salt, and HL^I for 18 h, followed by measurement of the proteasome activity, accumulated ubiquitinated proteins and cell death induction. We found that **3** could inhibit the chymotrypsin-like activity by ~30% and ~85% at 5 and 10 μmol/L, respectively, whereas **2** could inhibit the chymotrypsin-like activity by ~88% at 10 μmol/L (Fig. 35). Additionally, cells treated with either $CuCl_2$ or HL^I showed no effect toward proteasome activity compared to the DMSO control.

Consistent with the inhibition of proteasomal chymotrypsin-like activity, significantly increased levels of ubiquitinated proteins were detected in the PC-3 cells treated with **2** and **3** but not metal salt or HL^I (data not shown). In the same experiment, treatment with **2** and **3** resulted in significant cellular detachment and cleavage of PARP, associated with cell death induction (Fig. 36). These results show that as in C4-2B prostate cancer cells, copper compounds **2** and **3** could target and inhibit the proteasome in PC-3 cells. Our results in this dissertation remain consistent in that HL^I or the metal salt alone had little effect on proteasome activity and overall cellular integrity.

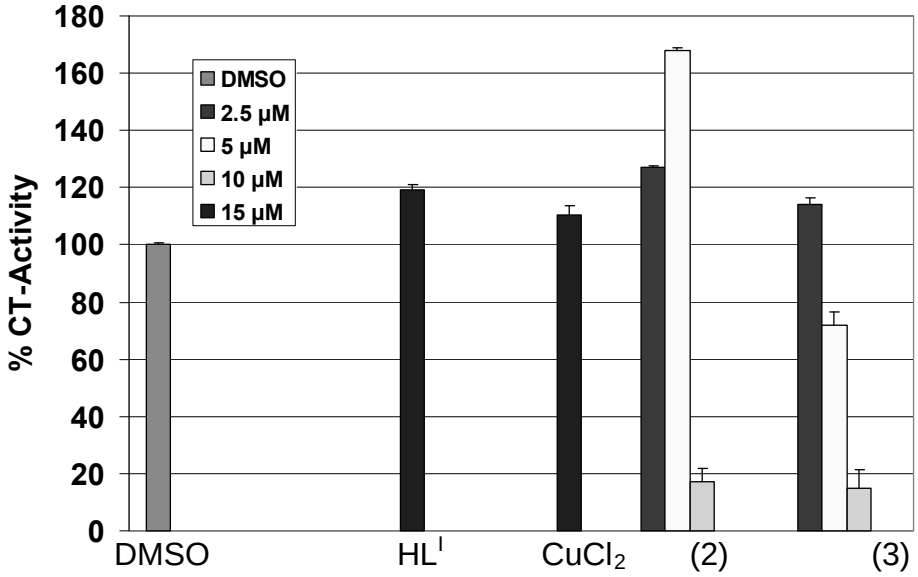

Figure 35. Proteasome inhibitory effects of compounds 2 and 3 on androgen-dependent PC-3 cells.

Human prostate cancer C4-2B cells were treated with HL^{I}, $CuCl_2$, **1**, **2**, and **3** for 18 h followed by measurement of proteasomal chymotrypsin-like activity.

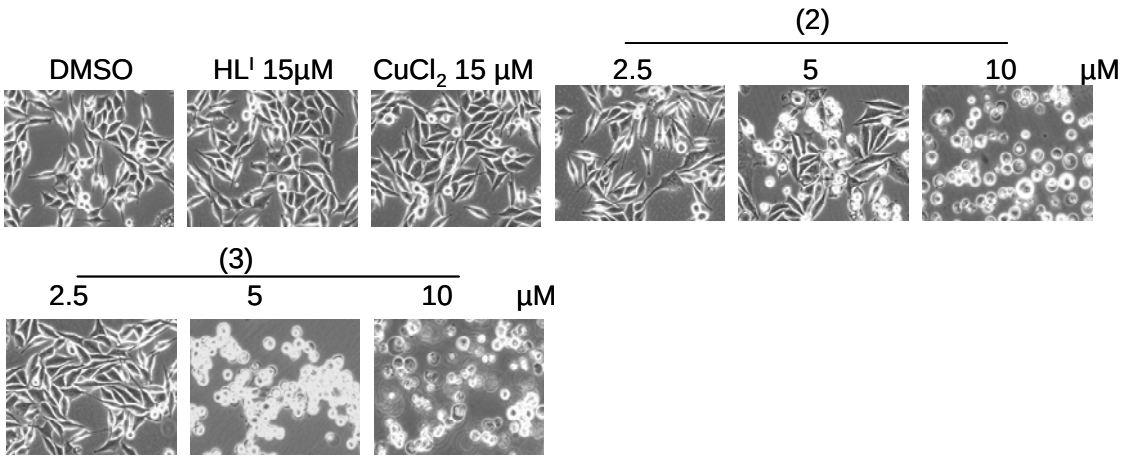

Figure 36. Cell death inducing effects of compounds 2 and 3 on androgen-dependent PC-3 cells.

Human prostate cancer C4-2B cells were treated with HL^{I}, $CuCl_2$, **2**, and **3** for 18 h followed by visualization of cellular morphology.

Kinetic effect of complexes 1-3 on proteasome Inhibition and cell death induction. The previous results show that complexes **1-3** demonstrated potent proteasome-inhibitory and cell death-inducing activities in multiple prostate cancer cell lines. In order to study the kinetic effect of copper complex-induced proteasome inhibition, C4-2B prostate cancer cells were treated with 15 μM of **2** for 2-18 h. The proteasomal chymotrypsin-like activity was inhibited by 45%, 60%, 70% and 80% after 2, 4, 8, and 18 h, respectively, as shown in the graph on Figure 37A. The proteasomal chymotrypsin-like activity inhibition was associated with accumulated levels of ubiquitinated proteins (Fig. 37B). Consistently, cell death associated PARP cleavage was visible after 8 h treatment and full length PARP was completely cleaved into its respective p65 fragment after 18 h (Fig. 37B). This observation is also supported by abnormal morphological changes during later time points, as well as the appearance of rounded up and detached cells indicative of cell death, as shown by selected micrographs in Figure 37C**.** These results presented in this dissertation clearly show that cell death induction occurs following inhibition of proteasomal activity. Therefore, proteasome inhibition appears to be a requirement for cell death (*e.g.* apoptosis) induction.

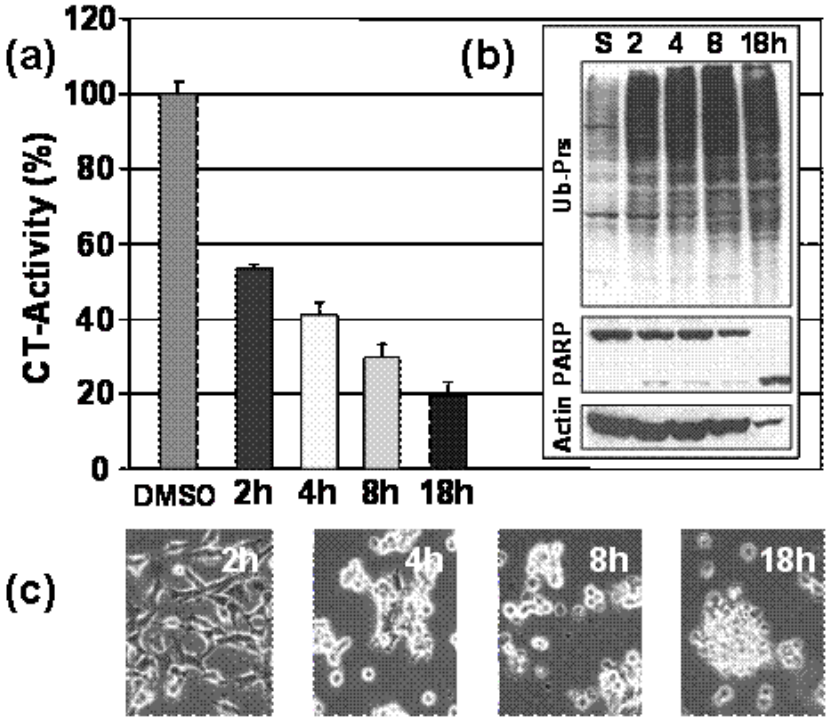

Figure 37. Kinetic effect of proteasome inhibition and cell death induction by compound 2 in C4-2B cells.

Human prostate cancer C4-2B cells were treated with 15 μmol/L of compound **2** for indicated time points followed by measurement of proteasomal chymotrypsin-like activity (A) accumulated ubiquitinated proteins (Ub-Prs) and PARP cleavage (B) and cell death associated morphological changes (C).

Nontoxic Effect of 1-3 in Immortalized Human Breast Cells. The ability to distinguish normal from malignant cells is imperative for developing successful anticancer drugs. To determine whether inhibition of proteasome activity achieved by copper compounds is selective toward malignant cells and not normal cells, we used normal-immortalized human breast cell line, MCF-10A to test this effect. MCF-10A cells were treated with different concentrations of 2 and 3 up to 10 μmol/L for 18 h, followed by measurement of proteasomal chymotrypsin-like activity and cell death. We found that when these nontransformed cells were treated with 2 and 3, no proteasome inhibition was detected (data not shown). Other treatments also had no or little effect on MCF-10A cells. To determine whether the inability of copper compounds to inhibit the proteasome activity is associated with the lack of cell death induction in these normal immortalized breast cells, cell death-associated morphological changes were then assessed in the same experiment. These normal, immortalized MCF-10A cells showed only little, if any, such cell death-related detachment after treatment with 2 and 3 up to 18 h (Fig. 38). Our data suggests that these copper compounds could inhibit the proteasome activity and induce cell death selectively in human cancer cells but not in normal immortalized breast cells.

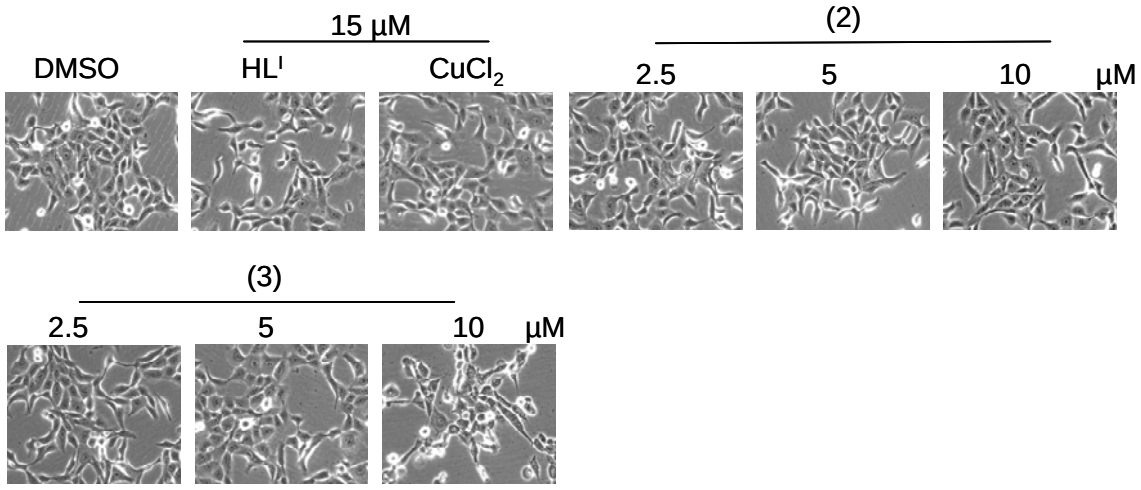

Figure 38. Effects of compounds 2 and 3 on normal, immortalized MCF-10A cells.

Human immortalized MCF-10A breast cells were treated with either HLI, $CuCl_2$, 2, or 3 for 18 h followed by visualization of morphological changes. Abnormal (spherical, detached) morphological changes were not observed in normal breast cells after treatment with $CuCl_2$, HL^{I}, or copper compounds.

Discussion

Following the encouraging results observed for similar gallium(III) complexes [Chen et al., 2007b] this dissertation presented the results of proteasome inhibition by copper(II) complexes of the iodo-substituted ligand HL^I as a potential anticancer therapeutic route. Three compounds with distinctive stoichiometries and nature of the anionic monodentate ligand were compared. On one hand, it has been demonstrated that the non-metallated ligand is incapable of inhibiting the 20S proteasome activity. On the other hand, inhibition does occur by the copper(II) chloride salt, but only under cell-free conditions. Therefore, it is hypothesized that the primary function of the copper complexes is to serve as a carrier to cross the cell membrane. Once inside the cell, this complex is likely to cause proteasome inhibition by coordination of the metal center to available amino acids capable of forming Cu-N, Cu-S, or Cu-O bonds. If this hypothesis is correct, the stoichiometry of the complex is of paramount importance. Consistently, the 1:1 metal-to-ligand complexes **1** and **2** are comparable or slightly more effective than the 1:2 species **3**. Nonetheless, due to the small SD values in terms of cytotoxicity, it seems premature to make such a comparison. Copper(II), being a labile species, can gain in stability by bonding to deprotonated and negatively charged phenolates and the nature of the anionic monodentate ligand *per se* may or may not be relevant. The data in this dissertation shows, that Species **1** and **2** have shown comparable proteasome-inhibitory activity *in vitro*. Therefore, it can be suggested that the pharmacophore to act as an active species can be described as $[CuL^I]^+$ or, more likely, some equivalent solvated species such as $[CuL^I(H_2O)]^+$ or $[CuL^I(H_2O)_2]^+$, where one or more water molecules replace the chloro or acetato ligands. Granted that more detailed studies are necessary to provide final evidence, this pharmacophore would present an open coordination

that facilitates interaction with available amino acids with high affinity for copper. It is viable that the active form of the copper complex binds to the amino-terminal threonine residue of the chymotryptic active center in the 20S proteasome. This hypothesis is based on known mechanisms for different classes of proteasome inhibitors [Adams, 2004; Adams et al., 1999; Groll et al., 2006]. Recent data [Cvek et al., 2008] indicating that the JAMM domain of the 19S caps in the 26S proteasome is another target for copper complexes suggests that further studies are necessary to assess this possibility and to ascertain the precise *locus* of coordination. It is also possible that **3** is a pro-drug and in order to become active, the loss of a ligand must occur. This process would convert this compound into a similar $[CuL^1(H_2O)_n]^+$ species, as described in Figure 39.

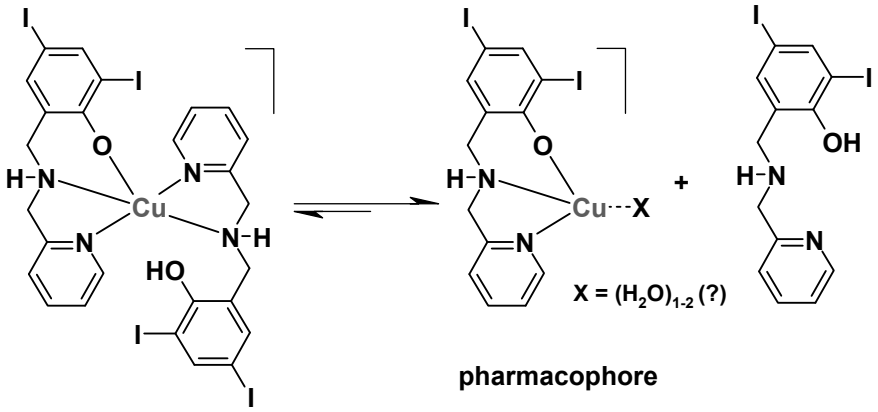

Figure 39. Suggested conversion of 3 into a $[CuL^{I}(H_2O)_n]^+$ species.

This depiction suggests the assignment of species $[CuL^{I}]^+$ as the minimal pharmacophore needed for proteasomal chymotryspin-like activity.

The depth of the therapeutic potential for metal-based proteasome inhibitors is yet to be determined. It is evident, however, that this can become a viable novel route to anticancer therapy. Ongoing work focuses on (i) the metabolic stability and the pharmacokinetic behavior of these compounds, (ii) assessment of the role of anionic ligands, and (iii) on the inclusion of other bivalent metal centers such as cobalt, nickel, and zinc, and trivalent ions such as iron and ruthenium to assess the roles of ligand dissociation, the 1:1 and 1:2 metal-to-ligand stoichiometry, redox activity, and charge. Biomimetic models of the 1:1 gallium and copper species are also being developed towards complexation with threonine and other amino acids and short peptides in order to determine the precise coordination loci within the proteasome.

CHAPTER 4

Comparative Activities of Nickel(II) and Zinc(II) Complexes of Asymmetric [NN'O] Ligands as 26S Proteasome Inhibitors

Adapted from published material in Inorganic Chemistry, 2009; 48: 5928-5937

In this dissertation, we compare the proteasome inhibition capabilities of two anticancer candidates, $[Ni(L^{IA})_2]$ **(1)** and $[Zn(L^{IA})_2]$ **(2)** where L^{IA-} is the deprotonated form of the ligand 2,4-diiodo-6-((pyridine-2-ylmethylamino)methyl)phenol. Species **1** contains Nickel(II), a considerably inert ion that favors covalency, whereas **2** contains Zinc(II), a labile transition metal ion that favors predominantly ionic bonds. We report on the synthesis and characterization of **1** and **2** using various spectroscopic, spectrometric, and structural methods. Furthermore, the pharmacological effects of **1** and **2,** along with the salts $NiCl_2$ and $ZnCl_2$, were evaluated *in vitro* and in cultured human cancer cells in terms of their proteasome-inhibitory and cell death-inducing capabilities. It is shown that neither $NiCl_2$ nor **1** have the ability to inhibit the proteasome activity at any sustained levels. However, $ZnCl_2$ and **2** showed superior inhibitory activity to the chymotrypsin-like activity of both 26S proteasome (IC_{50} = 5.7 and 4.4 μmol/L, respectively) and purified 20S proteasome (IC_{50} = 16.6 and 11.7 μmol/L, respectively) under cell-free conditions. Additionally, inhibition of proteasomal activity in cultured prostate cancer cells by **2** was associated with higher levels of ubiquitinated proteins and cell death. Treatment with either metal complex or salt was relatively non-toxic toward human normal cells. The results presented in this dissertation strengthen the current working hypothesis that fast ligand dissociation is required to generate

an $[ML^{IA}]^+$ pharmacophore capable of interaction. This interaction, possibly via the N-terminal threonine amino acids present in the active sites, renders the proteasome inactive. These results present a compelling rationale for **2**, along with its gallium(III) and copper(II) congeners to be further investigated as potential anticancer drugs that act as proteasome inhibitors.

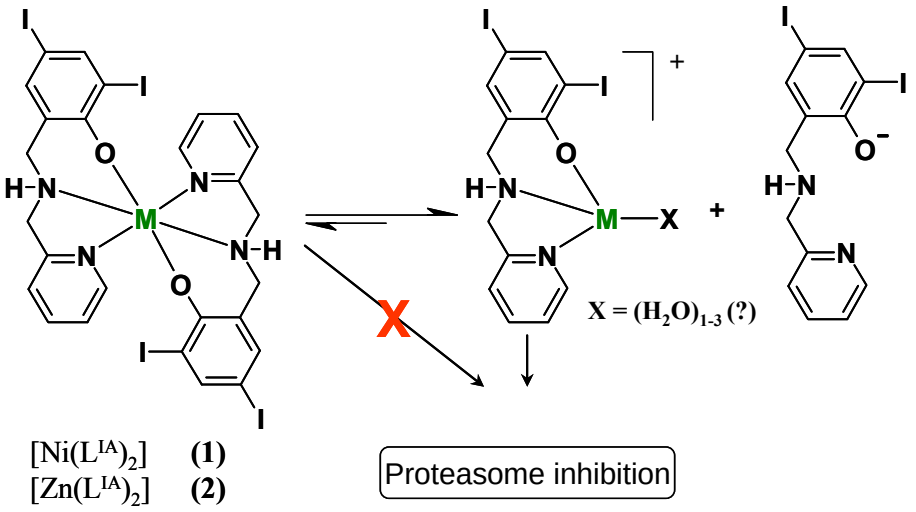

Figure 40. Proposed model of the species responsible for proteasome inhibition

Representation of the equilibrium of $[M(L^{IA})_2] \leftrightarrow [M(L^{IA})]^+ + L^{IA-}$ to generate the $[M(L^{IA})]^+$ pharmacophore.

Materials and Methods

Materials. All reagents were obtained from commercial sources and were used as received. Methanol was distilled over CaH2. IR (Infrared) spectra were measured from 4000 to 400 cm-1 as KBr pellets on a Tensor 27 FTIR-spectrophotometer. ESI spectra on the positive mode were measured in methanol on a Micromass Quattro LC triple quadrupole mass spectrometer with an electrospray/APCI source and Walters Alliance 2695 LC, autosampler and photodiode array UV detector. Experimental assignments were simulated based on peak location and isotopic distributions. The 1H-NMR spectra were measured in CDCl3 in a Varian Unity-300 instrument. Elemental analyses were performed by Midwest Microlab, Indianapolis, Indiana. Trypan blue exclusion dye was purchased from Sigma Aldrich (St. Louis, MO). The peptide substrate Suc-LLVY-AMC (for the proteasomal chymotrypsin-like activity) was purchased from Calbiochem, Inc (San Diego, CA). RPMI 1640, penicillin, and streptomycin were purchased from Invitrogen (Carlsbad, CA). Fetal bovine serum was purchased from Aleken Biologicals (Nash, TX). Antibodies against Ubiquitin, Actin, and secondary antibodies were purchased from Santa Cruz Biotechnology (Santa Cruz, CA). Mouse monoclonal antibody against human poly (ADP-ribose) polymerase (PARP) was purchased from BIOMOL International LP (Plymouth Meeting, PA).

X-ray Structural Determination for $[Ni(L^{IA})_2]$ (1) and $[Zn(L^{IA})_2]$ (2): Diffraction data were measured on a Bruker *X8 APEX-II* kappa geometry diffractometer with Mo radiation and a graphite monochromator. Frames were recorded for 10 s at 100 K with the detector at 40 mm and 0.3 degrees between each frame. *APEX-II* (Bruker AXS INC,

Madison WI, USA, 2005) and *SHELX* software were used in the collection and refinement of the models.

Crystals of **[Ni(L^{IA})$_2$] (1)** were colorless plates. A total of 86456 reflections were counted, which averaged to 10883 independent data. Hydrogen atoms were placed at calculated positions except for those on nitrogen which were observed. The complex crystallized with three equivalents of chloroform. All atoms occupy general positions.

Crystals of **[Zn(L^{IA})$_2$] (2)** appeared as colorless needles. A total of 77377 reflections were measured, yielding 14112 unique data. Hydrogen atoms were placed in calculated positions. The complex crystallized with three equivalents of methylene chloride and one equivalent of water. All atoms occupy general positions.

Electronic Structure Calculations Methods: The B3LYP level of theory [Becke, 1988] with the SDD of the presence of iodine atoms, and all of the calculations were done using the *Gaussian* series of programs. Geometries were fully minimized, without symmetry constraints, using standard methods. Located stationary points were characterized by computing analytic vibrational frequencies. Reported energies include zero-point correction.

Syntheses: The iodo-substituted ligand **HL^{IA}** was synthesized by treatment of 2-hydroxy-3,5-diiodobenzaldehyde with 2-aminomethylpyridine in methanol followed by reduction with sodium borohydride as previously published [Shakya et al., 2006b].

[Ni(L^{IA})$_2$] (1). A 15 mL methanol solution of HL^{I} (0.49 g, 1.1 mmol) was added dropwise to a 15 mL methanol solution of $Ni(OAc)_2 \cdot 2H_2O$ (0.25 g, 1.2 mmol) at 45 ^{o}C. After 45 minutes a purple precipitate was obtained, isolated by frit filtration, and washed with cold methanol and ether. The solid was recrystallized in chloroform. Yield = 0.95 g (88 %). Elemental analysis calculated for **1** $C_{26}H_{22}NiI_4N_4O_2$: C 31.58; H 2.24; N 5.67. Found: C, 31.47; H,

2.30; N, 5.56. IR (KBr, cm^{-1}) 3068 *v*(N-H), 1606, 1593 (C=N from pyridine), 1486 (C-O from phenyl). ESI pos. in MeOH: *m/z* = 988.9 for $[NiL_2+H^+]^+$.

$[Zn(L^{IA})_2]$ (2). A 15 mL methanol solution containing HL^I (0.51 g, 1.1 mmol) was added dropwise to a 15 mL methanol solution of $Zn(OAc)_2 \cdot 2H_2O$ (0.26 g, 1.2 mmol) at 45 °C. A white precipitate was obtained after 1 hour, isolated by frit filtration, and washed with cold methanol and ether. The solid was recrystallized in dichloromethane. Yield = 0.85 g (77 %). Elemental analysis calculated for **2** $C_{26}H_{22}ZnI_4N_4O_2$: C 31.37; H 2.23; N 5.63. Found: C, 31.27; H, 2.38; N, 5.58. IR (KBr, cm^{-1}) 3290 (N-H), 1608 (C=N from pyridine), 3079 *v*(N-H). ESI pos. in MeOH: *m/z* = 994.9 for $[ZnL_2+H^+]^+$.

Cell Cultures and Whole-cell Extract Preparation. Human prostate cancer cells, C4-2B and PC-3, and human leukemia Jurkat T cells were grown in RPMI-1640 supplemented with 10 % fetal bovine serum and maintained at 37° C and 5 % CO_2. MCF-10A (normal, derived from benign human breast tissue) were obtained and cultured as previously described [Daniel et al., 2005]. A whole-cell extract was prepared as previously described [Daniel et al., 2005].

Cell Proliferation Assay. Cells were seeded in quadruplicate in a 96-well plate and grown until 70-80 % confluence, followed by treatment with indicated agents for 18 h. After that, the 3-(4,5-dimethylthiazol-2-yl)-2,5-diphenyltetrazolium bromide (MTT) assay was done as described previously [Daniel et al., 2005].

Trypan Blue Assay. Jurkat T cells were treated with $NiCl_2$, $ZnCl_2$, **1**, and **2** for 18 h at indicated concentrations followed by measurement of cell death. The trypan blue dye exclusion assay was performed by mixing 100 µl of cell suspension with 50 µl of 0.4 % trypan blue dye before injecting into a hemocytometer and counting. The number of cells

that absorbed the dye and those that excluded the dye were counted, from which the percentage of nonviable cell number to total cell number was calculated.

Proteasomal Activity in Whole-cell Extract or Purified 20S proteasome. C4-2B whole-cell extract (8 μg) or a purified 20S rabbit proteasome (35 ng) were incubated with 10 μmol/L CT-substrate, Suc-LLVY-AMC, in 100 μL assay buffer [50 mmol/L Tris-HCl (pH 7.5)] in the presence of $NiCl_2$, $ZnCl_2$, **1**, and **2** at various concentrations or solvent DMSO as control. After 2 h incubation at 37°C, production of hydrolyzed AMC groups was measured using a Wallac Victor3^{TM} multilabel counter with an excitation filter of 365 nm and an emission filter of 460 nm.

Proteasome CT-like Activity in Cells. Proteins extracted from cells after each treatment were incubated for 2 h at 37° C in 100 μl of assay buffer (50 mmol/L Tris-HCL, pH 7.5) with 10 μmol/L fluorogenic substrate Suc-LLVY-AMC as described previously [Daniel et al., 2005].

Western Blot Analysis. Cell extracts were separated by SDS-PAGE and transferred to a nitrocellulose membrane. Western blot analysis was performed using specific antibodies to PARP, Ubiquitin, or AR followed by visualization using the HyGLO reagent (Denville Scientific, Metuchin, NJ).

Cellular Morphology Analysis. A Zeiss Axiovert 25 microscope was used for all microscopic imaging with phase contrast for cellular morphology. Magnification x100.

Results

Ligand Design. The work in this dissertation focuses on the development of discrete complexes of well established stoichiometry, formed between asymmetric [NN'O] ligands and transition metal ions for anticancer therapy. Such ligands are an evolution from terbutylated analogues used as biomimetic models for galactose-oxidase [Itoh et al., 1999; Shimazaki et al., 2000]. The presence of electron-donating and -withdrawing phenol substituents (*i.e.* H, ^{t}Bu, Cl, Br, and I) in such complexes has shown distinctive influence on the apoptosis of cisplatin-resistant neuroblastoma and prostate cancer cell lines [Chen et al., 2007b; Shakya et al., 2006b]. We are mostly engaged with the phenol-based ligand 2,4-diiodo-6-(((2-pyridinylmethyl)amino)methyl)phenol, synthesized by treatment of 2-hydroxy-3,5-diiodobenzaldehyde with 2-aminomethylpyridine followed by reduction with sodium borohydride [Shakya et al., 2006b]. Upon deprotonation, this ligand leads to 2:1 ligand-to-metal [$M(L^{IA})_2$] species with divalent ions, hence, eliminating the required charge balance by counterions. Moreover, a secondary amine in this ligand allows for the design of species with appended moieties to enhance water solubility [Melchior et al., 2001; Storr et al., 2005] (currently at $4.5x10^{-5}$ mol/L for the equivalent gallium complex) or lipophilicity [Kirin et al., 2005; Shakya et al., 2006b]. Such changes can address concerns with future oral administration as therapeutics.

Syntheses, Spectrometric, and Spectroscopic Evaluation. Complexes [$Ni(L^{IA})_2$] **(1)** and [$Zn(L^{IA})_2$] **(2)** were synthesized by treatment of HL^{IA} with the proper acetate salts in methanol and isolated in good yields (~80 %). Triethylamine was used as a base to ensure ligand deprotonation. Spectrometric evaluation of **1** and **2** in methanol using ESIMS (Electrospray Ionization Mass Spectrometry) in the positive mode led to identification with a

good isotropic distribution for the main peaks *m/z* = 988.7 and 994.7 respectively for $[\mathbf{1}+(H^+)]^+$ and $[\mathbf{2}+(H^+)]^+$. The 1:1 ligand-to-metal species were also detected via ESIMS (Electrospray Ionization Mass Spectrometry). Since such species only become prominent at higher cone voltages, they were considered a direct result of fragmentation of **1** and **2**. Infrared spectra confirmed the presence of the ligand and revealed the absence of peaks at *ca.* 1560 and 1450 cm^{-1} associated with potential acetate counterions. This gives further evidence that the 2:1 ligand-to-metal species are the favored products. Furthermore, elemental analyses were in excellent agreement with those expected for **1** and **2**.

The ^{1}H-NMR (Nuclear Magnetic Resonance) spectrum of the ligand shows the expected signals for protons at the pyridine and phenol rings between 7.0 and 9.0 ppm (parts per million) [Shakya et al., 2006b]. Distinctive signals for methylene groups vicinal to the pyridine and phenol rings appear respectively as singlet peaks at 3.94 and 3.91 ppm. At room temperature the ^{1}H-NMR spectrum of the zinc complex **1** is comparable to that of the ligand with further splitting of the peaks between 7-9 ppm, suggestive of two ligands with dissimilar conformation. Equally distinctive is the observation that the methylene signals become broadened and split into 6 ill-defined bands, indicating that the complex is not rigid, and that at least six of the eight methylene protons are non-equivalent. By lowering the temperature to *ca.* -60^{o}C, these signals coalesce into three peaks. The amine proton, originally at 3.49 ppm in the ligand, splits into two broad peaks at 1.77 and 1.18 ppm and appears at 2.20 ppm at low temperature. The nickel species yielded broad and ill-defined ^{1}H-NMR results in agreement with the paramagnetic nature of a $3d^8$ high spin species. A detailed investigation of the ligand dynamics of **1** and its gallium-containing counterpart

using VT-NMR (Variable Temperature-Nuclear Magnetic Resonance) properties is under development.

Molecular Structural Characterization. Good crystals for X-ray diffractometric analyses were isolated for **1** and **2** in chloroform and dichloromethane, respectively, and their molecular structures were determined. The ORTEP (Oak Ridge Thermal Ellipsoid Plot Program) renditions for **1** and **2** are shown in Figure 41, and selected bond lengths and angles are displayed in **Table 2**. Complex **1** crystallizes in a monoclinic space group $P2_1/n$ composed of a nickel(II) ion coordinated to two deprotonated $(L^{IA})^-$ ligands, with each of them containing an $[N_{py}N_{am}O_{phen}]$ set of donors. Both ligands are facially coordinated with the two pyridine rings (Ni - $N_{py} \approx 2.09$ Å), the two amine groups (Ni - $N_{am} \approx 2.09$ Å), and the two phenolate rings (Ni - $O_{phen} \approx 2.04$ Å), arranged trans to one another to yield a pseudo-octahedral geometry. Crystals of **2** appeared as colorless needles and crystallize in an orthorhombic $P2_12_12_1$ space group, also showing a similar facial coordination of the $(L^{IA})^-$ ligands in a pseudo-octahedral geometry**.** However, whereas **1** exhibits a symmetrical all-trans environment described as $[Ni<N_{am1}N_{am2}><N_{py1}N_{py2}><O_{(phO-)1}O_{(phO-)2}>]$ in a bent arrangement (Lesh, 2009, 345), **2** is described as having an all-cis $[Zn<N_{am1}O_{(phO-)2}><N_{py1}N_{am2}><O_{(phO-)1}\ N_{py2}>]$. As observed by the ^{1}H-NMR (Nuclear Magnetic Resonance) spectrum with distinctive signals for methylene groups the two ligands present dissimilar conformations.

We have demonstrated the role played by structural and electronic effects in a series of $3d^{5\text{-}10}$ $[M(L)_2]$ species with such asymmetric NN'O ligands. Although ligand rigidity enforces *meridional* coordination in similar imine ligands, electronic configuration leads to a *facial* coordination mode in flexible amines. The metal centers also dictate the preferential

cis or *trans* orientation of equivalent phenolates and other donor sets in vicinal ligands, with $3d^5_{\text{high spin}}$ ions [Imbert et al., 2005] displaying a cis-arrangement and $3d^6_{\text{low spin}}$ and $3d^7_{\text{high spin}}$ ions, supporting a *trans*-orientation. Species **1** reinforces the notion of an all-trans mode for $3d^8$ configurations, whereas **2** seems to fall within other $3d^{10}$ configurations [Lanznaster et al., 2006; Shakya et al., 2006b] lacking a clear preference. Another remark is that while most of the $O_{\text{phenolate}}$ bond lengths for **1** and **2** are comparable at 2.02-2.05 Å, one of the Zn-$O_{\text{phenolate}}$ bonds for **2** is elongated reaching *ca.* 2.11 Å. This is attributed to the $3d^{10}$ electronic configuration of the zinc(II) ion which favors electrostatic interactions.

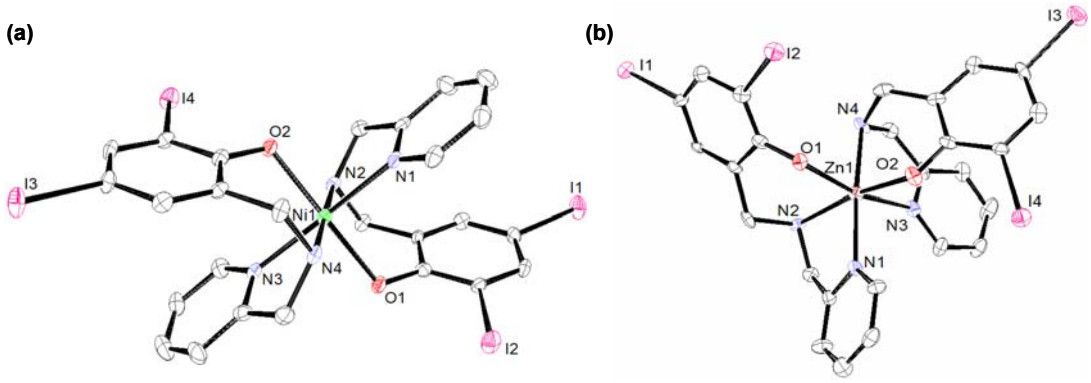

Figure 41. ORTEP (Oak Ridge Thermal Ellipsoid Plot Program) diagrams at 50% probability level for 1(a) and 2(b).

1	2
Ni(1)-O(2) = 2.036(2)	Zn(1)-O(2) = 2.025(6)
Ni(1)-O(1) = 2.057(2)	Zn(1)-O(1) = 2.111(5)
Ni(1)-N(2) = 2.088(3)	Zn(1)-N(1) = 2.149(6)
Ni(1)-N(3) = 2.090(3)	Zn(1)-N(4) = 2.179(6)
Ni(1)-N(4) = 2.096(3)	Zn(1)-N(2) = 2.181(7)
Ni(1)-N(1) = 2.098(3)	Zn(1)-N(3) = 2.259(7)
O(2)-Ni(1)-O(1) = 179.52(10)	O(2)-Zn(1)-O(1) = 92.0(2)
O(2)-Ni(1)-N(2) = 87.86(10)	O(2)-Zn(1)-N(1) = 90.0(2)
O(1)-Ni(1)-N(2) = 91.99(10)	O(1)-Zn(1)-N(1) = 99.6(2)
O(2)-Ni(1)-N(3) = 89.60(10)	O(2)-Zn(1)-N(4) = 92.4(2)
O(1)-Ni(1)-N(3) = 90.87(10)	O(1)-Zn(1)-N(4) = 88.7(2)
N(2)-Ni(1)-N(3) = 99.14(11)	N(1)-Zn(1)-N(4) = 171.3(3)
O(2)-Ni(1)-N(4) = 92.66(10)	O(2)-Zn(1)-N(2) = 168.9(2)
O(1)-Ni(1)-N(4) = 87.49(10)	O(1)-Zn(1)-N(2) = 89.2(2)
N(2)-Ni(1)-N(4) = 179.47(11)	N(1)-Zn(1)-N(2) = 79.0(2)
N(3)-Ni(1)-N(4) = 80.76(11)	N(4)-Zn(1)-N(2) = 98.6(2)
O(2)-Ni(1)-N(1) = 88.86(10)	O(2)-Zn(1)-N(3) = 87.9(2)
O(1)-Ni(1)-N(1) = 90.66(10)	O(1)-Zn(1)-N(3) = 166.7(2)
N(2)-Ni(1)-N(1) = 81.01(11)	N(1)-Zn(1)-N(3) = 93.7(2)
N(3)-Ni(1)-N(1) = 178.45(11)	N(4)-Zn(1)-N(3) = 78.1(3)
N(4)-Ni(1)-N(1) = 99.10(12)	N(2)-Zn(1)-N(3) = 93.5(2)

Table 2. Selected bond lengths (Å) and angles (deg) for **1** and **2**.

Electronic Structure Calculations. A series of electronic structure calculations were carried out for the nickel-containing **1**, and zinc-containing **2**, as well as on isomers with alternative geometries and binding modes aiming at evaluating bond nature, delocalization and energy differences between isomers. These results allowed to gain insight on how the electronic structure of these species may foster the formation of the expected pharmacophores $[ML^{IA}]^{+}$. The optimized geometries for the electronic structures of **1** and **2** are in good agreement with the crystallographic data presented above.

Nickel species: A recent study on similar nickel complexes supports a favorable *trans* facial coordination of the ligands over the *meridional* mode by approximately 5.0 kcal/mol using a comparable level of theory. Therefore, the work in this dissertation was focused on two different all-trans *facial* isomers, namely, the structurally characterized **1** and a hypothetical 1'. Isomer 1 displays both phenolate rings in parallel planes, whereas these same rings are perpendicular to one another in 1' (Figure 42A). The energy difference between the two structures is 3.7 kcal/mol, clearly favoring 1 as the lowest energy state. Interestingly, we recently compared similar isomers with unsubstituted phenolate rings and the energy difference was a mere 1.1 kcal/mol. It can be suggested that the iodine substituents play a significant role in favoring 1 instead of 1'. Furthermore, both isomers display triplet ground states with S=1, consistent with a $3d^8$ high spin configuration where two unpaired electrons populate the $d_{X^2-y^2}$ (SOMO) and d_{z^2} (SOMO-1) (Single Occupied Molecular Orbitals) orbitals. (Figure 42B).

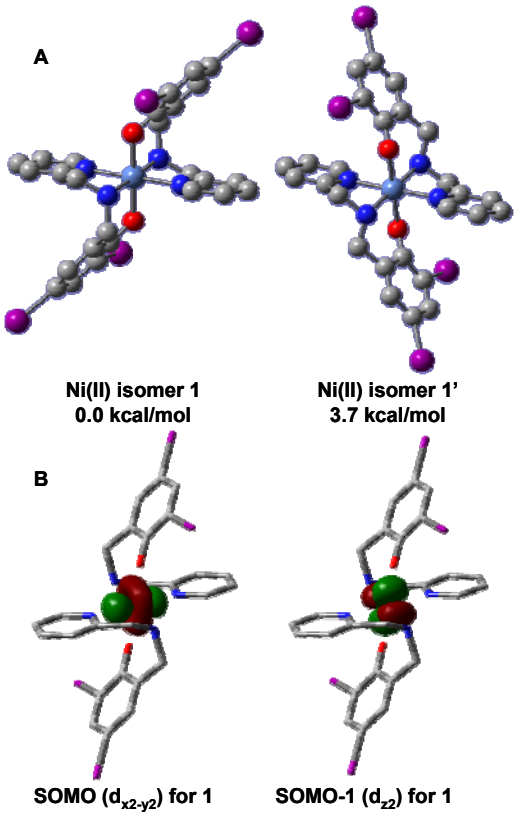

Figure 42. Coordination mode of Nickel isomer complexes

A. Depiction of the two facial $[Ni(L^{IA})_2]$ isomers 1 and 1'. B. Selected MOs (Molecular Orbitals) for unpaired electrons.

Because divalent zinc is a $3d^{10}$ ion, it lacks LFSE (Ligand Field Stabilization Energy) and the coordination mode is most likely the result of ligand sterics. For **2**, we observed a new facial all-cis [$Zn<N_{am1}O_{(phO-)2}><N_{py1}N_{am2}><O_{(phO-)1}\ N_{py2}>$] coordination mode for a doubly deprotonated species, well in contrast with the all-trans counterpart obtained previously with a non-substituted ligand. Thus two different facial isomers were explored for the zinc complex as shown in Figure 43A. The structurally characterized **2** and a hypothetical **2'** that matched the geometry adopted for the nickel containing **1**. Interestingly, the calculations favor **2'** by a small margin of less than 2.0 kcal/mol, thus in disagreement with the observed structure. Therefore, in the absence of a LFSE (Ligand Field Stabilization Energy) the bonding is mainly ionic in nature and other factors such as solvation, crystal packing, or intermolecular force effects must control the final geometry.

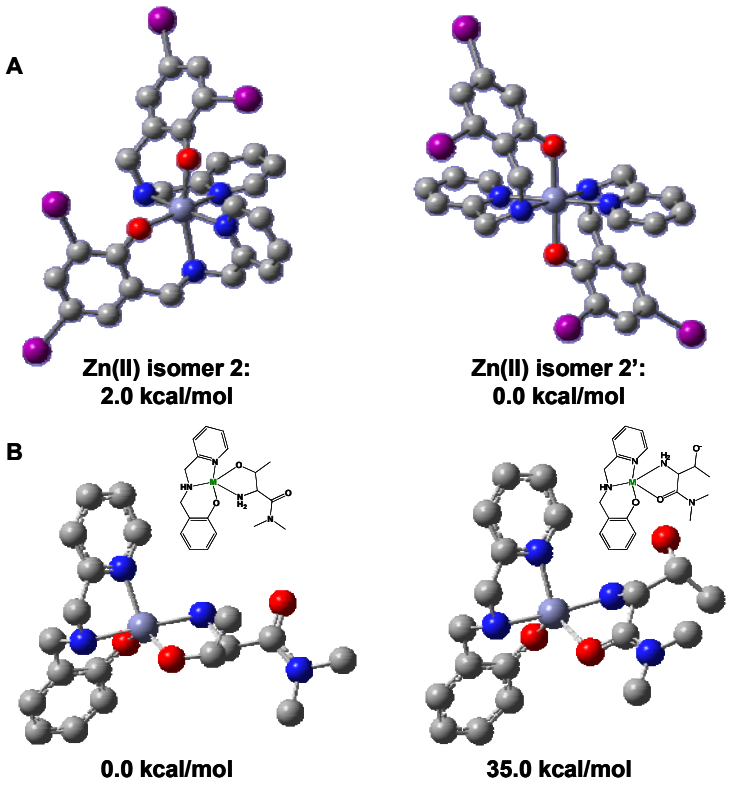

Figure 43. Depiction of zinc isomers and possible interaction of N-terminal threonine.

A. Depiction of the two facial $[Zn(LIA)_2]$ isomers 2 and 2'. B. Possible interaction between the fragment $[Zn(LIA)]^+$ and threonine.

In order to address partial atomic charges, natural bond order (NBO) analysis was performed with both **1** and **2**, the results are shown in Table 3. It is clear from these charge distributions that the interaction between the Ni(II) center in **1** and the ligand is more delocalized, *i.e.* covalent, than the interaction between the Zn(II) center and the ligand in **2**. This can be seen by lower charges on the metal: 1.3 for **1** versus 1.6 for **2**. The values for other atoms in **2** are consistently larger in magnitude reinforcing the notion of more localized, i.e. ionic bonds. These values indicate that there is less stabilization of the positive divalent metal charge unto the ligands for **2** over **1.** This difference is significant, since both complexes are discrete neutral species with an overall zero charge. Thus, it is possible to conclude that an ionic nature would favor ligand dissociation in the biologic milieu for **2** and the equilibrium suggested in Figure 40 should be facilitated.

	Ni **(1)**	Zn **(2)**
M	1.3	1.6
O1	-0.87	-0.90
O2	-0.87	-0.92
N1	-0.56	-0.64
N2	-0.75	-0.77
N3	-0.56	-0.61
N4	-0.75	-0.80

Table 3. NBO (Natural Bond Order) partial atomic charges.

Finally, initial theoretical treatment of the possible binding modes between the fragment $[Zn(L^{IA})]^+$ and a deprotonated threonine residue were also performed. A simplified $[Zn(L)]^+$ fragment with an unsubstituted ligand was used and, in order to model the terminal nature of the threonine residue, a dimethylated amide residue was incorporated, as shown in Figure 43. Two coordination modes were probed; the first considered binding between the zinc center at the $[Zn(L)]^+$ fragment with the terminal (and deprotonated) hydroxyl group and the secondary amine group, whereas the second focused on the binding through the secondary amine and the carbonyl group of the amide residue. The first binding mode is approximately 35 kcal/mol more stable, and although this proposition is merely speculative at this point, it suggests that terminal hydroxo/amine coordination to zinc would be favored. **(The spectroscopic, spectrometric, and structural analyses were generated by the Verani Lab, WSU Department of Chemistry).**

Induction of Cell Death and Inhibition of Cell Proliferation. The cytotoxic effect of $NiCl_2$, $ZnCl_2$, **1**, and **2,** was tested in human leukemia Jurkat T cells treated at different concentrations for 18 h. After each treatment, trypan blue exclusion assay was performed to assess cell death. Cells treated with **2** exhibited a dose-dependent activity reaching 48 %, 70 %, 95 %, and 100 % cell death at 7.5, 10, 15, and 20 μmol/L, respectively (Fig. 44). This turned out to be the single viable species, since the metal salts and **1** had marginal cell-death induction, smaller than ~10 % compared with DMSO-treated cells, at as high as 20 μmol/L (Fig. 44).

To further substantiate this effect, we evaluated whether **2** can suppress cell proliferation of human prostate cancer cells. C4-2B human prostate cancer cells were treated

with $NiCl_2$, $ZnCl_2$, **1**, **2**, and the DMSO control at different concentrations for 18 h, followed by measurement of cell proliferation by MTT assay. It was observed that cells treated with **2** suppressed cell proliferation in a dose-dependent manner (IC_{50} = ~6 µmol/L), reaching 100 % inhibition at 10 µmol/L (Fig. 45). Furthermore, cells treated with **2** at 5 and 7.5 µmol/L decreased cell proliferation by ~35 % and ~85 %, respectively (Fig. 45). Consistently, C4-2B cells treated with the metal salts or **1** showed little or no inhibitory effect even at the highest concentration tested of 20 µmol/L (Fig. 45).

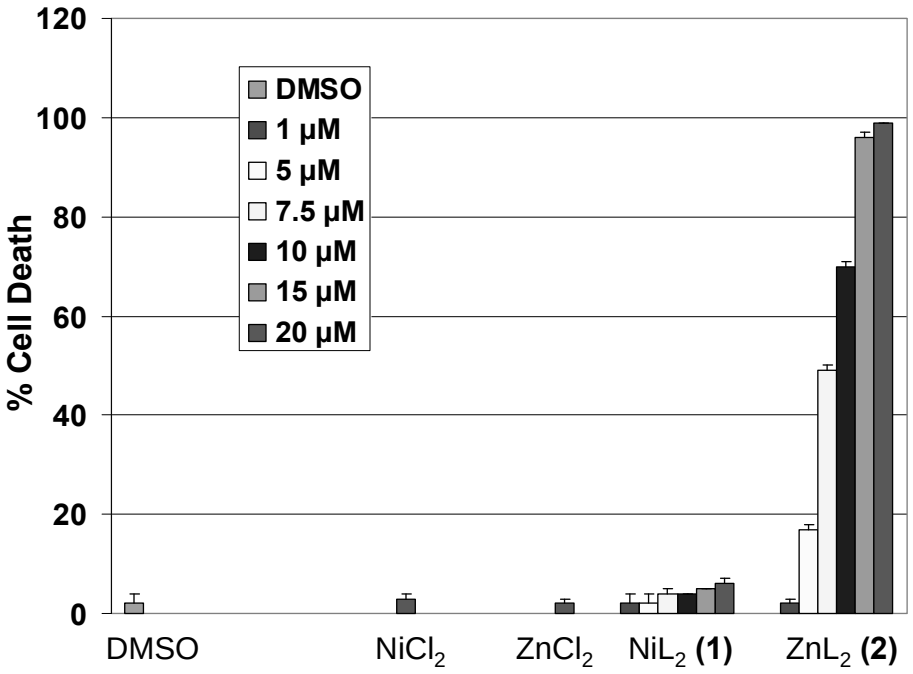

Figure 44. Induction of cell death by zinc complex (1).

Jurkat leukemia T-Cells were treated with $NiCl_2$, $ZnCl_2$, 1, or 2 for 18 h followed by measurement of nonviable cells in a trypan blue exclusion assay.

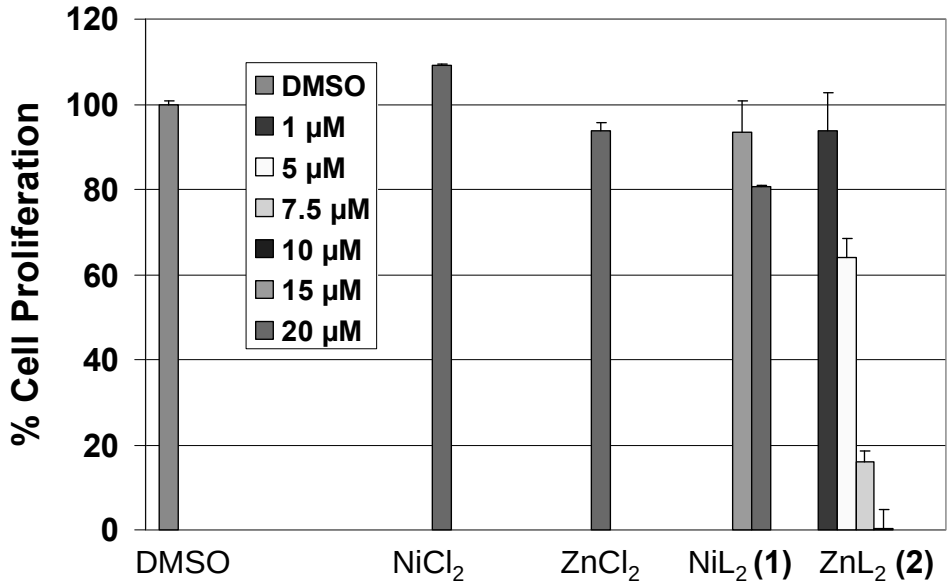

Figure 45. Zinc complex (2) inhibits cell proliferation.

Human prostate cancer C4-2B cells were treated for 18 h with $NiCl_2$, $ZnCl_2$, 1, or 2 followed by MTT assay to measure cell proliferation.

***In Vitro* Proteasome Inhibition.** To test the proteasome inhibitory capacity of these species, a comparison of the inhibitory activity of $NiCl_2$, $ZnCl_2$, **1**, and **2** to the 26S proteasomal activity was performed under cell-free conditions. An extract of C4-2B prostate cancer cells (Fig. 46) was used and the results indicate that both the $ZnCl_2$ salt and **2** have the potential to inhibit the chymotrypsin-like activity of the 26S proteasome with IC_{50} values of 5.7 and 4.4 μmol/L, respectively**.** This result is consistent with our previous finding that zinc dithiocarbamate complexes can target and inhibit the proteasome [Milacic et al., 2008a]. However, extracts treated with **1** at as high as 25 μmol/L showed only ~20 % inhibition (Fig. 46) on the 26S proteasome suggesting that intrinsic distinctive mechanisms of inhibition must be present for **1** and **2**. Consistent with this finding is the fact that $NiCl_2$ at 25 μmol/L could only inhibit the proteasomal activity by ~25 % (Fig. 46).

To provide direct evidence for distinct mechanisms, we incubated a purified rabbit 20S proteasome with $NiCl_2$, $ZnCl_2$, **1**, and **2** at various concentrations, followed by measurement of the chymotrypsin-like activity. We found that this activity was significantly inhibited with the salt $ZnCl_2$ and **2** with similar potencies (IC_{50} = 16.6 and 11.7 μmol/L, respectively) (Fig. 47). Although $NiCl_2$ showed modest inhibitory activity, **1** was rather inactive (Fig. 47). The finding that 1 resulted in an increase in proteasome inhibition suggests the possibility of an irregular fit for nickel into the S1 pocket of the β-5 subunit. Overall, our data remain consistent with the fact that the zinc ion, both as a chloride salt and a complex with the $(L^{IA})^-$ ligand is able to target and inhibit the proteasome under cell-free conditions.

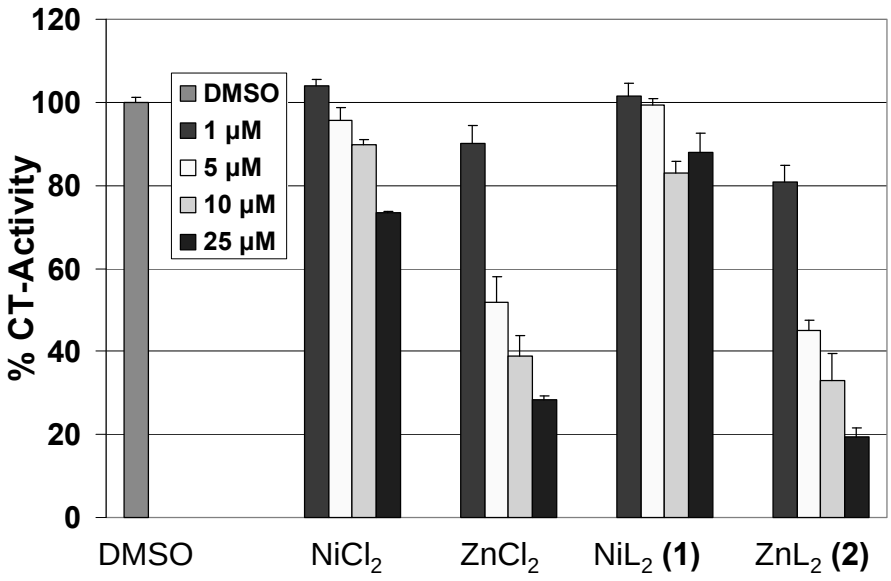

Figure 46. Inhibition of the proteasomal chymotrypsin-like activity in C4-2B cells extracts.

C4-2B cell extract (10 ug) was incubated with a peptide substrate for the proteasomal chymotrypsin-like activity in the presence of $NiCl_2$, $ZnCl_2$, 1, or 2 at indicated concentrations.

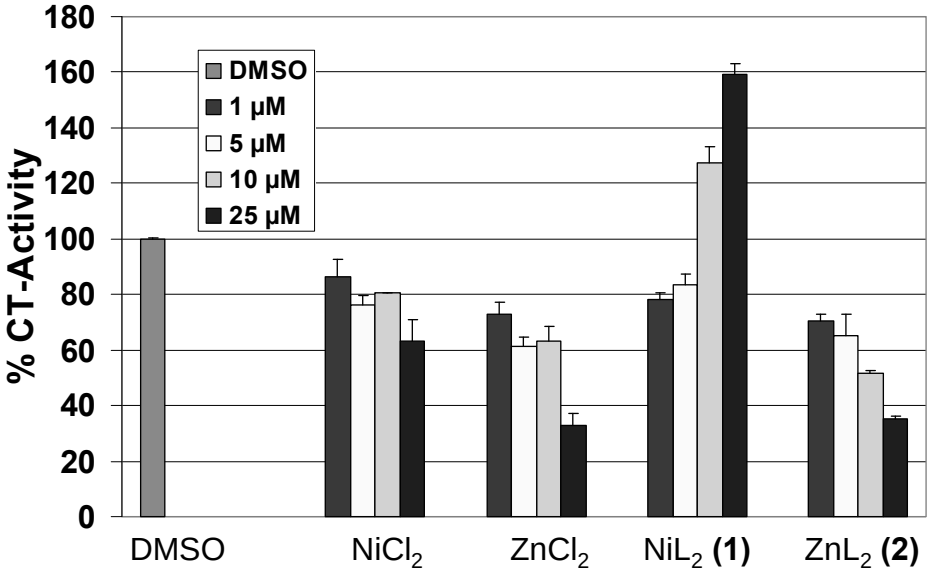

Figure 47. Inhibition of the proteasomal chymotrypsin-like activity of purified 20S.

C4-2B cell extract (35 ng) was incubated with a peptide substrate for the proteasomal chymotrypsin-like activity in the presence of $NiCl_2$, $ZnCl_2$, 1, or 2 at indicated concentrations.

Proteasome inhibition and cell death induction in intact cancer cells. To confirm the ability of **2** to inhibit the proteasomal activity in intact tumor cells, C4-2B human prostate cancer cells were first treated with different concentrations (5, 10, and 25 μmol/L) of $NiCl_2$, $ZnCl_2$, **1**, and **2** for 18 h, followed by measurement of proteasome inhibition. The values for proteasomal chymotrypsin-like activity are given as a percentage in Table 4. The C4-2B cells treated with **2** showed a dose-dependent inhibition of the proteasomal activity by 31 % inhibition at 10 μmol/L and 86 % inhibition at 25 μmol/L. Consistently, levels of ubiquitinated proteins were increased in a dose-dependent manner in C4-2B cells (Fig. 48). In comparison, cells treated with either $NiCl_2$, $ZnCl_2$, or **1** showed negligible proteasome inhibitory effect.

	Dose μM	C4-2B %	SD[a] (+-)	PC3 %	SD[a] (+-)	MCF 10A %	SD (+-)
DMSO	—	100	0.81	100	1.56	100	3.00
$NiCl_2$	25	92	1.41	99	0.10	98	1.83
$ZnCl_2$	25	99	0.90	127	0.45	116	1.56
	5	84	0.87	101	0.01	—	—
$[Ni(L^{IA})_2]$ (1)	10	83	0.96	81	1.59	—	—
	25	80	2.27	92	0.85	89	1.96
	5	111	1.02	114	2.63	118	0.55
$[Zn(L^{IA})_2]$ (2)	10	69	0.14	17	1.38	97	1.48
	25	14	0.68	10	1.13	83	1.59

Table 4. Percentile of CT-activity after treatment with $NiCl_2$, $ZnCl_2$, **1**, and **2**

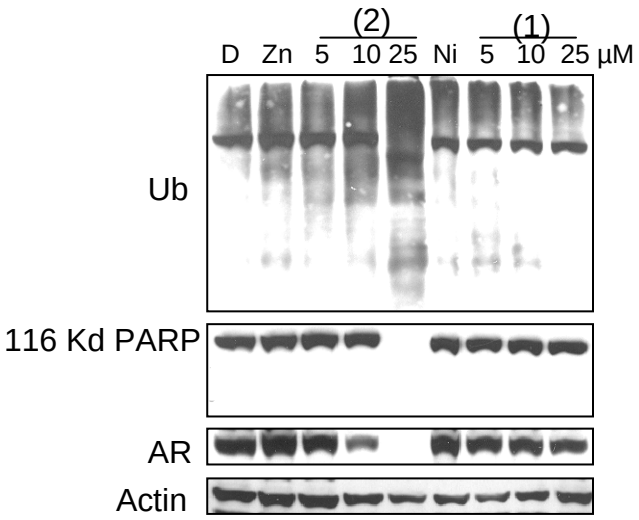

Figure 48. Western analysis of proteasome target proteins.

Human C4-2B cells were treated with ZnCl2, NiCl2, 2, or 1 for 18 h followed by measuring accumulated ubiquitinated proteins (Ub), PARP, and androgen receptor (AR) levels. DMSO (D) was used as solvent control.

It has been shown that proteasome inhibition can lead to decreased levels of androgen receptor (AR) expression [Lin et al., 2002; Yang et al., 2008]. Therefore a decrease in such expression should be observed assuming proteasome activity inhibition by **2**. Consistently, this is the only species that down regulated significantly AR and 25 μmol/L treatment completely abrogated AR expression levels (Fig. 48). These results remain consistent with the ability of **2** to inhibit the proteasome activity.

It has been shown that inhibition of the proteasomal chymotrypsin-like activity selectively in transformed cells could result in the induction of apoptosis [An et al., 1998]. To investigate whether proteasome inhibition and androgen receptor down regulation are associated with cell death, PARP disappearance and morphological changes were measured in the same experiment (Fig. 48 and 49). The results show that only cells treated with 25 μmol/L of **2** were able to completely abrogate full length PARP, whereas cells treated with either $NiCl_2$, $ZnCl_2$, or **1** at the highest concentration tested had little visible effects (Fig. 48). Consistently, morphological changes (detached, shrunken and rounded up) were observed in cells treated with 25 μmol/L **2** and to a significant but lesser extent at 10 μmol/L (Fig. 49). Much less aberrant morphological changes were detected in the cells treated with metal salt or **1** at the highest concentration tested (Fig. 49). These results in this dissertation show that the induction of apoptosis in C4-2B cells by **2** is associated with inhibition of proteasomal chymotrypsin-like activity.

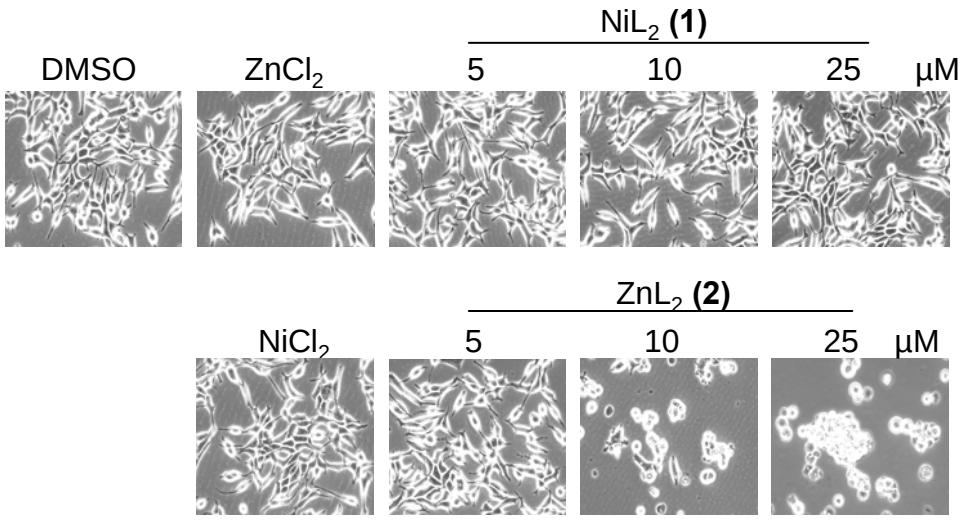

Figure 49. Cellular morphological changes of human prostate C4-2B cells.

Human prostate C4-2B cells were treated with $ZnCl_2$, $NiCl_2$, 1, or 2 for 18 h followed by visualization of morphological changes.

Upon demonstrating the ability of **2** to inhibit the proteasomal chymotrypsin-like activity in AR-dependent C4-2B prostate cancer cells, we then tested the effect of **2** on AR-independent PC-3 human prostate cancer cells. PC-3 cells were treated with 5, 10 and 25 μmol/L of **1** or **2**, and their metal salt for 18 h, followed by measurement of the proteasome activity and apoptosis induction. Percentage of proteasomal chymotrypsin-like activity is designated in Table 4 with DMSO as control. We found that **2** could inhibit the proteasomal activity and induce apoptotic cell death in PC-3 prostate cancer cells, whereas **1**, $NiCl_2$, and $ZnCl_2$ showed little or no effect (Table 4, Fig. 50).

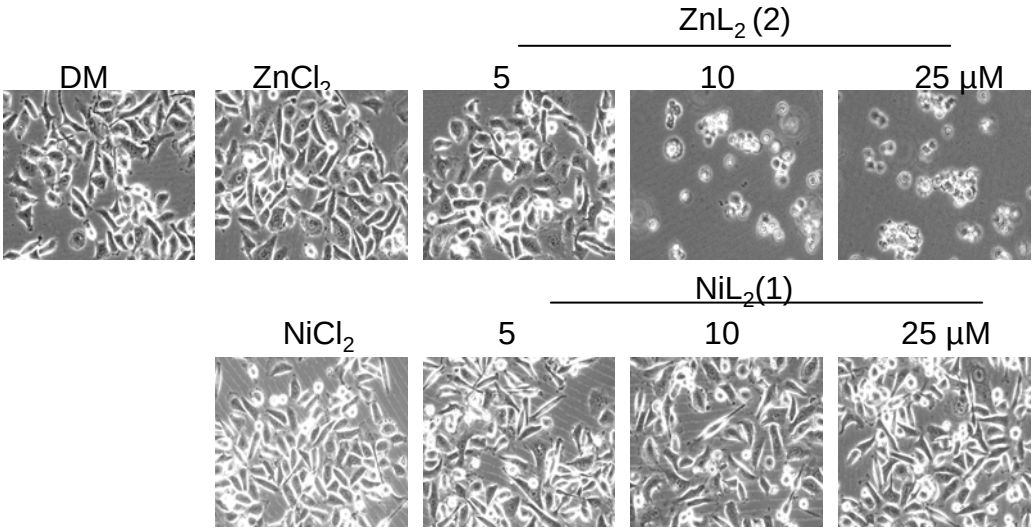

Figure 50. Cellular morphological changes of human prostate PC-3 cells.

Human prostate C4-2B cells were treated with $ZnCl_2$, $NiCl_2$, 1, or 2 for 18 h followed by visualization of morphological changes.

Kinetics of proteasome inhibition and cell death induction. To study the kinetic effect of proteasome inhibition, C4-2B prostate cancer cells were treated with 15 μmol/L **2** over different time points (2-18 h) and their cell lysates were used to measure the proteasomal-chymotrypsin-like activity (Fig. 51A). The proteasomal chymotrypsin-like activity was inhibited by 18 %, 42 %, 57 %, and 63 %, respectively, at 2, 4, 8, and 18 h. This result was consistent with the time-dependent increase in levels of accumulated ubiquitinated proteins. Furthermore, lower levels of AR were detected in cells treated with **2** at all time points and complete abrogation of AR expression is detected in cells after 18 h treatment. Importantly, cell death-associated PARP decrease was detected at later time points with complete PARP disappearance at 18 h (Figure 51B). Cell death induction at later time points is also typified with the appearance of aberrant morphological changes (detached, shrunken and rounded up) (Figure 51C). These results clearly demonstrate that induction of the cell death occurs after proteasome inhibition. Thus, proteasome inhibition appears to be required for cell death induction.

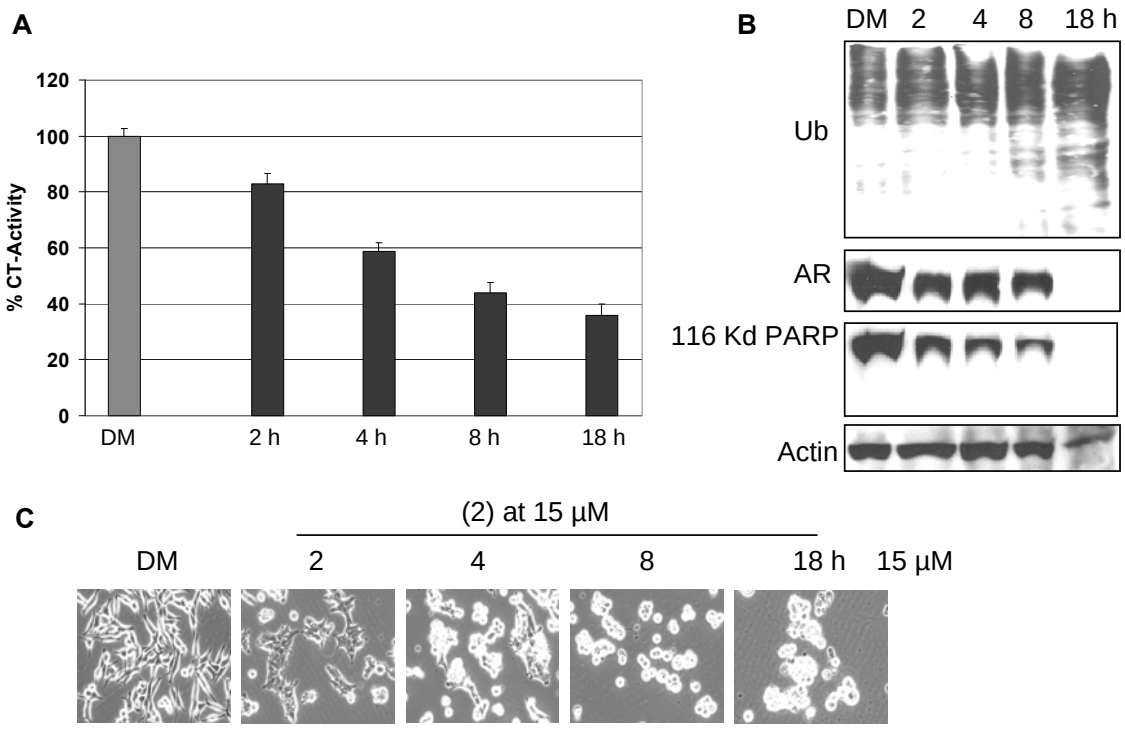

Figure 51. Kinetic effects of proteasome inhibition and cell death induction by zinc complex (2).

C4-2B cells were treated at indicated time points with 15 µmol/L zinc compound followed by measurement of chymotrypsin-like activity (A), Western analysis of ubiquitinated proteins, AR, and PARP (B), and cellular morphological changes (C).

Tumor Cell Selectivity. The ability to distinguish normal from malignant cells is of paramount importance for developing clinically-relevant anticancer drugs. To determine whether inhibition of prostate cancer cellular proteasome activity achieved by **2** is selective toward malignant cells but not normal cells, we used normal-immortalized human breast cell line, MCF-10A. The MCF-10A cells were treated with different concentrations with **2** as high 25 μmol/L for 18 h, followed by measurement of proteasomal chymotrypsin-like activity and cell death. We found that when these nontransformed cells were treated with **2**, only 17 % proteasome inhibition was detected at the highest concentrations tested (Table 4). Other treatments also had little effect on MCF-10A cells (Table 4). To determine whether the inability of **2** to inhibit the proteasome activity at sustainable levels is associated with the lack of cell death induction in these normal immortalized breast cells, cell death associated morphological changes were then assessed in the same experiment. These normal, immortalized MCF-10A cells showed only little, such cell death-related detachment after treatment with **2** up to 18 h at the highest concentration tested (data not shown). Furthermore, the species $NiCl_2$, $ZnCl_2$, and **1** had little or no cytotoxic effect on normal cells. Our data presented in this dissertation suggests that **2** could inhibit the proteasome activity and induce cell death selectively in human cancer cells but not in normal immortalized cells, validating **2** as a promising proteasome inhibitor.

Discussion

In this dissertation we report on two new coordination complexes as potential anticancer candidates, namely, $[Ni(L^{IA})_2]$ **(1)** and $[Zn(L^{IA})_2]$ **(2)**. Both species were characterized by several spectroscopic, spectrometric, and structural methods and display a well established 2:1 ligand-to-metal stoichiometry. DFT calculations considering different isomers of **1** and **2** were performed and show good agreement with the nickel species, but fail to predict the appropriate geometry for the zinc-containing species. Furthermore, initial studies considering coordination of a 1:1 $[Zn(L)]^+$ fragment with threonine suggest a favorable coordination through the terminal hydroxyl group of the amino acid.

The effects of $NiCl_2$, $ZnCl_2$, **1**, and **2** were tested toward a purified rabbit 20S proteasome and 26S proteasome in human prostate cancer cell lines. The results indicate that only **2** and $ZnCl_2$ have a direct inhibitory effect on the proteasome to any significant levels. Furthermore, when $NiCl_2$, $ZnCl_2$, **1**, and **2** were tested on the 26S proteasome of cultured human prostate cancer cells, it was shown that only **2** exhibited potent anti-proliferative and cell death-inducing activity (Fig. 48-51). Similarly, only **2** induced higher levels of ubiquitinated proteins, which were associated with decreased levels of proteasomal chymotrypsin-like activity (Fig. 48; Table 4). In addition, the decrease of proteasomal chymotrypsin-like activity observed for **2** is tightly associated with tumor cell death as seen by the morphological changes and the apparent disappearance of the full length PARP fragment (Fig. 48-51). Species **2** also showed remarkably low cytotoxicity toward normal human breast cells (Table 4; data not shown).

This sharp contrast in proteasome activity inhibition between **1** and **2** is suggested to be related to the nature of the metal ion and its degree of reactivity when combined with

NN'O-containing ligands. As observed in similar complexes from the previous work in this dissertation [Hindo et al., 2009], considerable proteasome inhibition can be attained through 1:1 ligand to metal species that is believed to be the pharmacophore in all these species. Therefore, an equilibrium $[M(L^{IA})_2] \leftrightarrow [M(L^{IA})]^+ + L^{IA-}$ seems necessary to facilitate the formation of the pharmacophore with available coordination sites capable of interaction with the 20S proteasome, likely to be *via* the N-terminal threonine residue. It is observed from the molecular structures and DFT calculations available that covalent interactions prevail in **1**, while **2** is ionic in nature. We, therefore, propose that this intrinsic difference defines the capacity of pharmacophore formation and determines the activity of these species. The lack of activity observed for $ZnCl_2$ in intact cells reinforces the notion offered for the equivalent copper counterparts [Hindo et al., 2009] that the ligand $(L^{IA})^-$ serves as a shuttle vector to cross the cellular membrane. Taken together, it is suggested that the presence of the fragment $[Zn(L^{IA})]^+$ is required for proteasome inhibition. At this point it is not clear whether the ligand dissociation $[Zn(L^{IA})_2] \leftrightarrow [Zn(L^{IA})]^+ + L^{IA-}$ is intra or extracellular, and if intracellular, before or after reaching the 26S proteasome. Furthermore, it is likely that water molecules will coordinate to the zinc ion forming $[Zn(L^{IA})(H_2O)_n]^+$ hydrated species. The investigation of these issues is a current goal of this project and will be properly developed in the future. Nonetheless, the data observed thus far from this dissertation provides a compelling rationale for the clinical development of **2** as a potential anticancer drug.

CHAPTER 5

Inhibition of Tumor Proteasome Activity by Gold Dithiocarbamato Complexes *via* both Redox-Dependent and –Independent Processes

Adapted from published material in Journal of Cellular Biochemistry, 109, 2010; 162-172

We have previously reported on a gold(III) complex, namely [$AuBr_2$(DMDT)] (*N*,*N*-dimethyldithiocarbamate) showing potent *in vitro* and *in vivo* growth inhibitory activities toward human cancer cells and identifying the cellular proteasome as one of the major targets. However, the importance of the oxidation state of the gold center and the involved mechanism of action has yet to be established. The data in this dissertation shows that both gold(III)- and gold(I)-dithiocarbamato species, namely [$AuBr_2$(ESDT)] (AUL12) and [Au(ESDT)]$_2$ (AUL15), could inhibit the chymotrypsin-like activity of purified 20S proteasome and 26S proteasome in human breast cancer MDA-MB-231 cells, resulting in accumulation of ubiquitinated proteins and proteasome target proteins, and induction of cell death, but at significantly different levels. Gold(I) and gold(III) compounds-mediated proteasome inhibition and cell death induction were completely reversed by the addition of a reducing agent, dithiothreitol or *N*-acetyl-*L*-cysteine, suggesting the involvement of redox processes. Furthermore, treatment of MDA-MB-231 cells with gold(III) compound (AUL12), but not the gold(I) analogue (AUL15), resulted in the production of significant level of reactive oxygen species. The data in this dissertation provides strong evidence that the cellular proteasome is an important target of both gold(I) and gold(III) dithiocarbamates, but distinct cellular mechanisms of action are responsible for their different overall effect.

Materials and Methods

Materials. Gold-dithiocarbamato complexes [$AuBr_2$(ESDT)] (AUL12) and [Au(ESDT)]$_2$ (AUL15) were synthesized and characterized as previously described [Ronconi et al., 2005]. 3-[4,5-dimethyltiazol-2-yl)-2,5-diphenyl-tetrazolium bromide (MTT), dithiothreitol (DTT), *N*-acetyl-L-cysteine (NAC), DMSO and other chemicals were purchased from Sigma Aldrich (St. Louis, MO). DMEM/F-12, penicillin, streptomycin and ROS detection kit were purchased from Invitrogen (Carlsbad, CA). Purified rabbit 20S proteasome was purchased from Boston Biochem (Cambridge, MA). Fluorogenic peptide substrate, Suc-LLVY-AMC (for the proteasomal chymotrypsin-like activity) was purchased from Calbiochem (San Diego, CA). Mouse monoclonal antibody against human poly(ADP-ribose)polymerase (PARP) was purchased from BIOMOL International LP (Plymouth Meeting, PA). Mouse monoclonal antibodies against Bax, IκB-α, ubiquitin, goat polyclonal antibody against actin, and secondary antibodies were from Santa Cruz Biotechnology (Santa Cruz, CA).

Cell culture and whole-cell extract preparation. Human breast cancer MDA-MB-231 cells were obtained from American Type Culture Collection (Manassas, VA) and grown in DMEM/F-12 supplemented with 10% fetal bovine serum and 100 units/mL of penicillin and 100 µg/mL of streptomycin. All cells were grown at 37° C in a humidified incubator with a 5% CO_2-enriched atmosphere. A whole-cell extract was prepared as previously described [Daniel et al., 2005].

Inhibition of the purified 20S proteasomal activity by gold compounds. Purified rabbit 20S proteasome (35 ng) was incubated with 20 µmol/L of the fluorogenic substrate Suc-LLVY-AMC (for the proteasomal chymotrypsin-like activity) in 100 µl assay buffer (25

mmol/L Tris-HCl pH 7.5) for 2 h at 37°C in the presence of either gold compound at different concentrations or equivalent v/v percentage of DMSO as control. After incubation, production of hydrolyzed AMC groups was measured with a Wallac Victor^3 multilabel counter with an excitation filter of 365 nm and emission filter of 460 nm.

Proteasome activity assay in intact human breast cancer MDA-MB-231 cells. Human breast cancer MDA-MB-231 cells were grown to 70%-80% confluency, treated with indicated compound or DMSO as a control under various conditions, harvested, and used for whole-cell extract preparation. 10 µg of cell extract was used to determine the chymotrypsin-like activity, as described above.

Cell proliferation assay. MDA-MB-231 cells were seeded in triplicate in a 96-well plate and grown until 70% to 80% confluence, followed by treatment with each compound or DMSO (as a control) for 24 h. After that, the 3-(4,5-dimthylthiazol-2-yl)-2,5-diphenyltetrazolium bromide (MTT) assay was done as previously described [Daniel et al., 2005].

Western Blot analysis. MDA-MB-231 breast cancer cells were treated, harvested, and lysed. Cell lysates (40-50 µg) were separated by SDS-PAGE and transferred to a nitrocellulose membrane followed by visualization using the HyGLO chemiluminescent HRP detection reagent from Denville Scientific (Metuchin, NJ), as previously described [Chen et al., 2005]**.**

Cellular morphological and ROS detection analysis. A Zeiss Axiovert 25 microscope was used for all microscopic imaging with either phase contrast for cellular morphology or fluorescence for ROS detection. MDA-MB-231 cells were seeded in a 6-well plate on top of a cover slip and grown to 70%-80% confluency, followed by treatment with

either AUL12 or AUL15, or DMSO for 3.5 h. TBHP (*t*-butylhydroperoxide), a common ROS inducer, at 100 μM was used as a positive control. Cells that adhered to the cover slips were gently washed once with warm HBSS/Ca/Mg followed by labeling with 1 ml 25 μmol/L carboxy-H_2DCFDA and 25 min incubation at 37°C. Then, 1.0 μmol/L Hoechst 33342 was added to the cells and incubated for another 5 minutes in the dark. The cover slips were gently washed three times with warm HBSS/Ca/Mg before ROS generation was examined using a Zeiss confocal laser microscope.

ROS detection by FACS analysis. MDA-MB-231 cells were plated in p100 dishes and grown to 70-80% confluency, followed by treatment with AUL12 or AUL15, or DMSO control at the indicated concentrations for 3.5 h. Cells were then washed twice with warm HBSS/Ca/Mg followed by incubation with 25 μmol/L of carboxy-H_2DCFDA in a working solution of HBSS/Ca/Mg for 30 min at 37°C protected from light. Cells were then washed with warm HBSS/Ca/Mg and harvested. Prepared samples were then used to measure for ROS induction by FACS analysis.

Annexin V-FITC binding assay. The Annexin V-FITC binding assay was performed using the FITC Annexin V Apoptosis detection kit from BD Biosciences (San Jose, CA). MDA-MB-231 cells were treated with AUL12 or AUL15 at 10-30 μmol/L or DMSO as a control for 4 h. Harvested cells were washed with cold PBS and resuspended with 1X binding buffer, followed by Annexin V-FITC incubation for 15 minutes and PI staining for another 15 minutes at 4°C in the dark. The apoptosis indices were detected by flow cytometry.

Results

Gold(I)-dithiocarbamato complex AUL15 exhibits decreased potency in inhibiting proliferation of human breast cancer cells compared to its gold(III) analogue AUL12. We have previously shown that the gold(III)-dithiocarbamato complex [$AuBr_2$(DMDT)], exhibits potent anti-proliferative activity against different breast cancer cell lines and anti-tumor activity in nude mice bearing breast cancer xenografts [Milacic et al., 2006]. Moreover, our results showed that the cellular proteasome is one of the major targets and that proteasomal inhibition contributes to this gold(III)-mediated cell death. Based on these positive data, we set out to investigate two other gold dithiocarbamato derivatives, namely [$AuBr_2$(ESDT)]$_2$ (AUL12) and [AU(ESDT)]$_2$ (AUL15) (Fig. 52), whose anti-cancer activity was previously reported [Ronconi et al., 2005; Ronconi et al., 2006], in order to elucidate the importance of the oxidation state of the gold center (3+ and 1+, respectively). More importantly, we investigated a potential mechanism of action that may shed insight into the biological effects mediated by gold(III)- and gold(I)-containing compounds.

AUL15

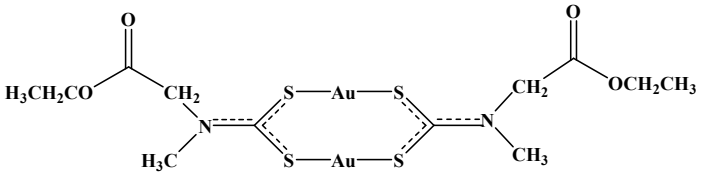

AUL12

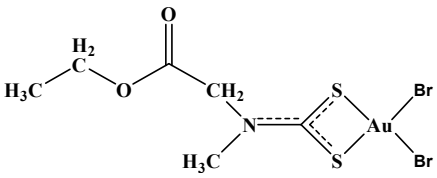

Figure 52. Chemical structures of $[Au(ESDT)]_2$ (AUL15: gold 1+) and $[AuBr_2(ESDT)]$ (AUL12: gold 3+).

We first tested the growth-inhibitory effect of both gold compounds, with the solvent DMSO as a control, toward the highly aggressive breast cancer MDA-MB-231 cell line treated for 24 h, followed by an MTT assay. Although both compounds inhibited cell proliferation in a dose-dependent manner, AUL15 was less potent than AUL12 (Fig. 53). For example, when cells were treated with 10 μmol/L of AUL15 or AUL12, cell proliferation was inhibited by 35% and 70%, respectively (Fig. 53). The IC_{50} values of AUL15 and AUL12 were calculated to be 13.5 μmol/L and 4.5 μmol/L, respectively (Fig. 53).

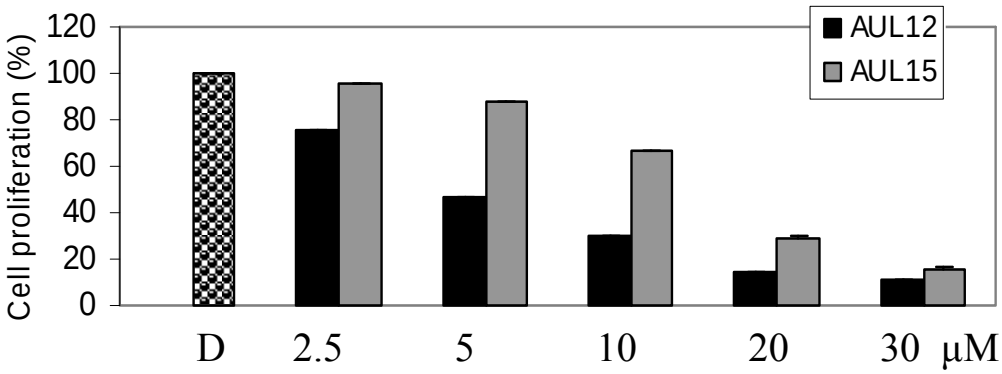

Figure 53. Anti-proliferative effects of the investigated gold compounds.

MDA-MB-231 cells were treated for 24 h with either AUL12 or AUL15 at indicated concentrations, with DMSO as a control. After 24 h, the medium was removed and cells were treated with the MTT reagent.

Gold(I) dithiocarbamato complex AUL15 exhibits lower proteasome-inhibitory activity than its gold(III) analogue AUL12. We have previously shown that the gold(III) compound [$AuBr_2$(DMDT)] could inhibit the chymotrypsin-like activity of purified proteasome [Milacic et al., 2006]. Therefore, we hypothesized that AUL12 could be similarly capable of targeting and inhibiting the proteasome *in vitro*. For comparison purposes, the gold(I) counter-part AUL15 was tested under the same experimental conditions. To provide direct evidence for this, we incubated a purified rabbit 20S proteasome with either AUL12 or AUL15 at various concentrations, with DMSO as a control, followed by measurement of proteasomal activity. We found that AUL15 inhibited the proteasomal chymotrypsin-like activity, but with decreased potency compared to AUL12, with IC_{50} values of 17.7 and 1.13 μmol/L, respectively (Fig. 54).

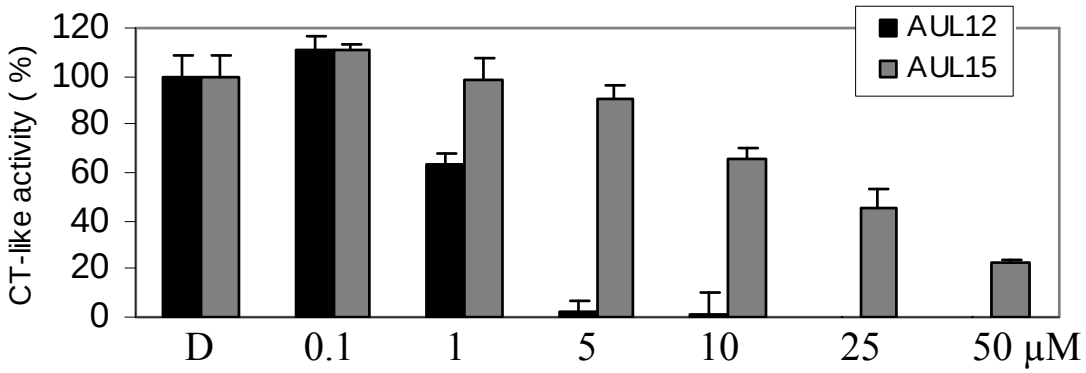

Figure 54. Inhibition of the chymotrypsin-like activity of purified 20S proteasome by gold compounds.

AUL12 and AUL15 were incubated with a purified proteasome at the indicated concentrations, followed by measurement of the chymotrypsin-like activity. DMSO was used as solvent control.

To investigate whether AUL12 and AUL15 could inhibit proteasomal activity in intact cells, breast cancer MDA-MB-231 cells were treated with 10-30 μmol/L of each compound for 4 and 24 h. Cells were treated with DMSO as control. After the treatment, the cell extracts were used to measure proteasomal chymotrypsin-like activity and accumulation of ubiquitinated proteins and proteasome target protein IκB-α. We found that AUL15 had no proteasome-inhibitory effect after 4 h of treatment, even at the highest concentration tested (Fig. 55A). However, after 24 h, it caused proteasome inhibition by 30% and 70% at 20 and 30 μmol/L, respectively (Fig. 55B).

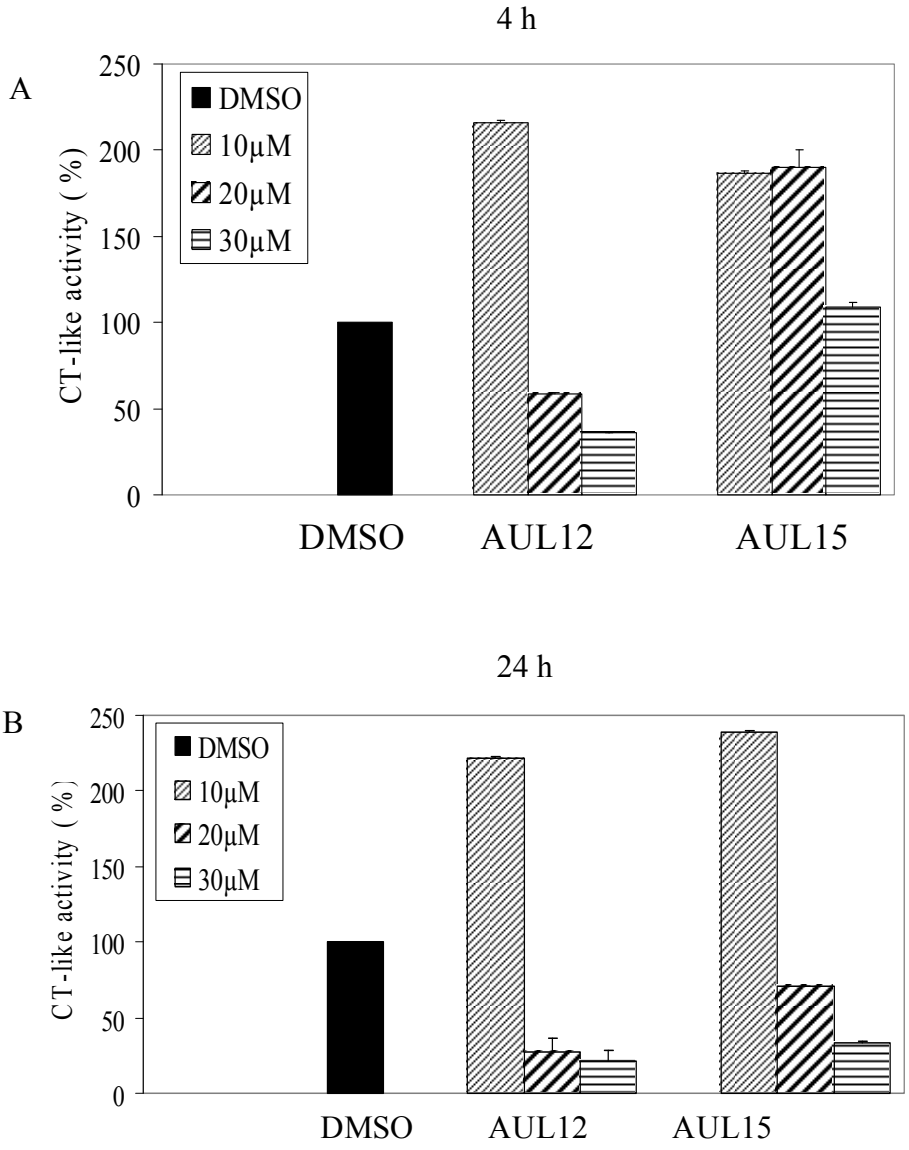

Figure 55. Inhibition of proteasomal chymotrypsin-like activity by gold compounds in MDA-MB-231 cells.

Breast cancer MDA-MB-231 cells were treated with indicated concentrations of AUL12 or AUL15 for **(A)** 4 h or **(B)** 24 h. followed by measurement of the proteasomal chymotrypsin-like activity. DMSO was used as solvent control.

Consistent with this decreased level of proteasomal chymotrypsin-like activity by AUL15 at 24 h, accumulation of ubiquitinated IκB-α was found (Fig. 56A). Interestingly, accumulation of ubiquitinated proteins induced by AUL15 was detected after both 4 and 24 h (Fig. 56B). Since accumulation of ubiquitinated proteins is a transient process, the dose-dependent effect was not seen at 4 h and 24 h, the two time points selected in this experiment. In comparison, cells treated with AUL12 at both 20 and 30 μmol/L significantly inhibited proteasomal chymotrypsin-like activity at both early (4 h) and late time points (24 h) (Fig. 55A-B). In addition, accumulation of ubiquitinated proteins and higher levels of IκB-α and its ubiquitinated form were apparent at both time points (Fig. 56A-B).

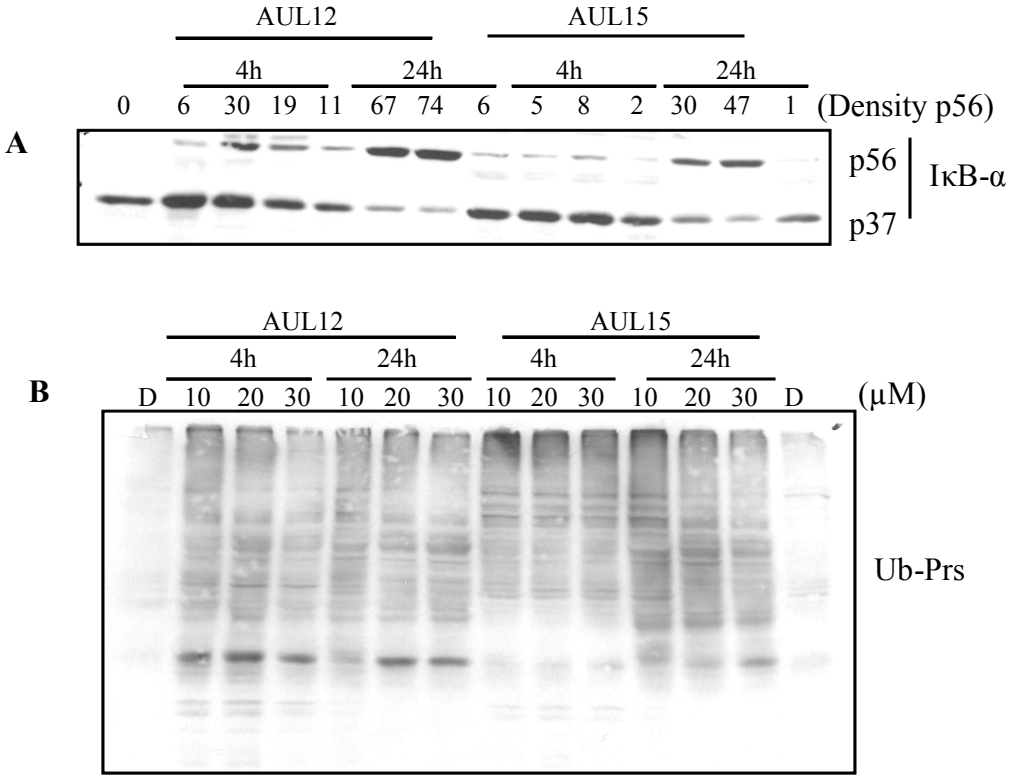

Figure 56. Western Blot analysis of MDA-MB-231 cells treated with AUL12 or AUL15.

Breast cancer MDA-MB-231 cells were treated with indicated concentrations of AUL12 or AUL15 for 4 or 24 h, followed by Western Blot analysis. DMSO solvent was used as a control. **A**. accumulation of IκB-α and ubiquitinated form of IκB-α; **B**. accumulation of ubiquitinated proteins.

Gold(I)-dithiocarbamato complex AUL15 exhibits lower cell death-inducing activity than its gold(III) analogue AUL12 in intact breast cancer MDA-MB-231 cells. To investigate whether inhibition of proteasomal chymotrypsin-like activity was associated with apoptosis or cell death induction, morphological changes, PARP cleavage, Annexin V-FITC, and TUNEL were examined. Changes in cell morphology (shrunken, rounded up and characteristic apoptotic blebbing) were apparent mostly during later time points of the treatment with increasing concentrations of AUL15 (Fig. 57B *vs*. A). Furthermore, we noticed that cells treated with 10 μmol/L AUL12 started rounding up even after 4 h treatment and the effect was greatly enhanced after the treatment with higher concentrations (Fig. 57A). These cell death-associated morphological changes were highly magnified after 24 h; rendering cells predominately rounded up and detached (Fig. 57B).

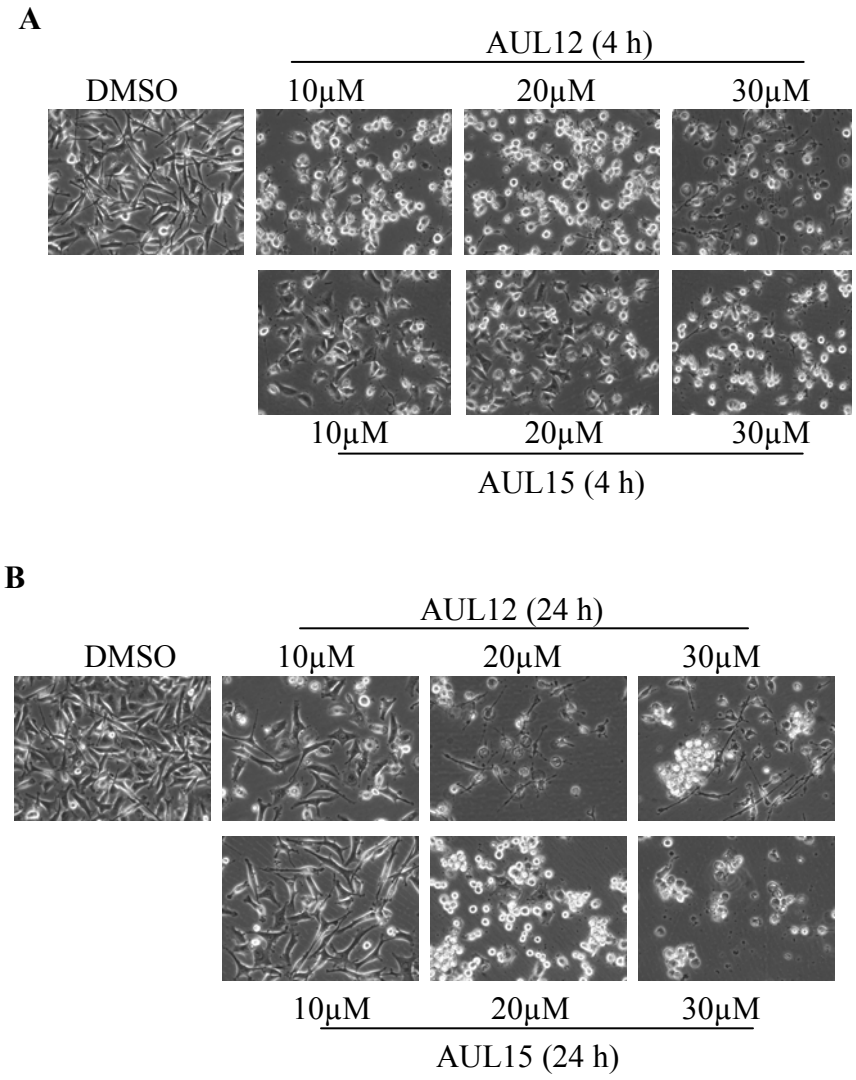

Figure 57. Induction of cell death by gold compounds in MDA-MB-231 cells.

Breast cancer MDA-MB-231 cells were treated with indicated concentrations of AUL12 or AUL15 for (A) 4 h or (B) 24 h, with DMSO as a control, followed by visualization of morphological changes.

To study whether the observed cell death is related to apoptosis, we performed PARP cleavage assay. Treatment of cells with AUL15 at 10-30 μM for 4 h induced the cleavage of the intact PARP protein (p116 kD) into a characteristic p65 fragment (Fig. 58), a by-product of calpain cleavage [Pink et al., 2000]. The complete PARP cleavage was observed when AUL15 was used at higher concentrations for 24 h (Fig. 58). We found the cleavage of the intact PARP protein (p116 kD) into a characteristic p65 fragment in cells treated with either AUL 15 or AUL 12 in both time- and dose-dependent manners (Fig. 58). It is notable to point out that treatment of cells with gold(I) complex AUL15, resulted in PARP disappearance mainly when higher concentrations were used (Fig. 58). On the other hand, treatment with the gold(III) counter-part AUL12, at both early and late time points and at increasing concentrations resulted in complete disappearance of full length PARP and higher levels of the cleaved p65 fragment (Fig. 58).

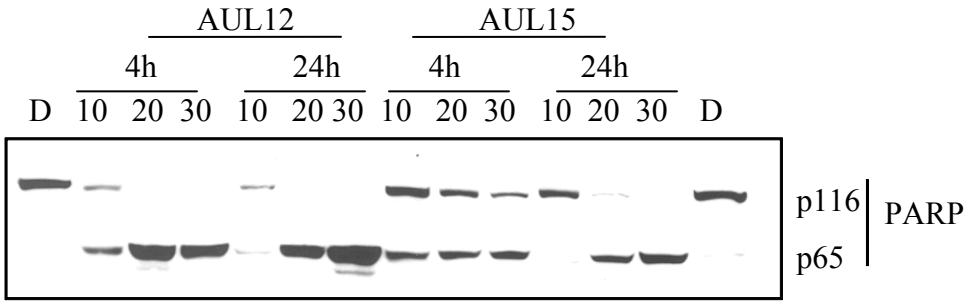

Figure 58. Western Blot analysis of poly-(ADP-Ribose) polymerase PARP cleavage.

Breast cancer MDA-MB-231 cells were treated with indicated concentrations of AUL12 or AUL15 for 4 or 24 h, followed by Western Blot analysis. DMSO solvent was used as a control. PARP cleavage indicates induction of cell death.

We also performed FITC Annexin V staining assay. Treatment with AUL15 at 10 μM for 4 h induced ~21% of cells undergoing late apoptosis while 6% in non-apoptotic death (Fig. 59). When AUL15 was increased to 20 μM, late apoptotic cells and non-apoptotic cell death were increased to 31% and 27%, respectively (Fig. 59). However, further increase of AUL15 to 30 μM induced 72% non-apoptotic cell death (Fig. 59). Treatment of cells with AUL12 at 10 μM for 4 h induced 40% late apoptotic cell death and 25% non-apoptotic cell death, more potent than AUL15 at the same conditions (21% and 6%, respectively; Fig. 59). Similar to AUL15, when AUL12 was used at increased concentrations, the apoptotic death population was decreased while the non-apoptotic death cells were increased (Fig. 59). We also investigated whether treatment with gold compound-induced cytotoxicity is related to DNA damage. Treatment with AUL15 for 4 h at only 30 μM induced TUNEL positivity by ~10% while AUL12 at only 20 and 30 μM generated 2.0 and 30% TUNEL-positive cells (data not shown). Taken together, the data suggest that these gold-dithiocarbamato complexes induced various types of cell death, depending on the status of gold compound, concentrations, and treatment time. However, these data suggest that gold(III) compound has higher proteasome-inhibitory activity and induced higher level of cell death compared to gold(I) dithiocarbamate treatment (see **Discussion**).

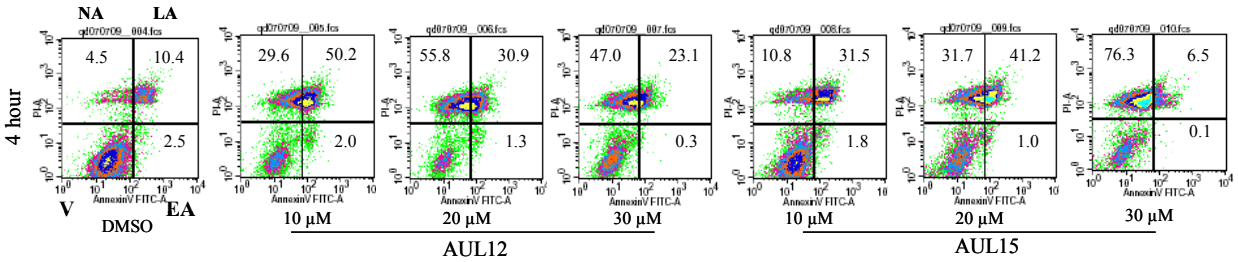

Figure 59. Induction of cell death by gold compounds in MDA-MB-231 cells by Annexin V- FITC binding assay

Human breast cancer MDA-MB-231 were treated with AUL12 or AUL15 for 4 h at the indicated concentrations Annexin V- FITC binding assay was performed to quantify the number of apoptotic cells. The lower right (Annexin V-FITC+/PI-) was considered early stage of apoptotic cells (EA) and upright part (Annexin V-FITC +/PI+) was considered as late stage of apoptotic cells (LA). The lower left part (Annexin V-FITC-/PI-) was considered as viable cells (V) and the upper left part (Annexin V_FITC-/PI+) was considered non-apoptotic cell death (NA).

We and others have previously shown that associated with the cell death commitment, Bax protein (p21/Bax) could be cleaved by calpain, producing a p18/Bax fragment, which then forms a homodimer p36/Bax [Gao and Dou, 2000; Wood and Newcomb, 2000]. Since treatment with gold compounds can lead to calpain activation and p65/PARP fragment production (Fig. 60), we would then expect the appearance of the Bax/p36 homodimer upon treatment. Under our experimental conditions, using breast cancer MDA-MB-231 cells (with DMSO as a control), we detected two forms of Bax protein: p21 and p36 (Fig. 53). When the cells were treated with AUL15, only the treatment with high concentrations for 24 h resulted in higher levels of p18/Bax and p36/ Bax (Fig. 60). In contrast, treatment with AUL12 even at the lowest concentration resulted in higher levels of p18/Bax and p36/Bax during both early and late time points (Fig. 60). This effect was more pronounced upon treatment with higher concentrations of AUL12 (Fig. 60). Together, these results show that the gold(III) compound is able to inhibit proteasomal chymotrypsin-like activity, activate calpain and induce cell death in human breast cancer MDA-MB-231 cells with a higher degree of activity compared to its gold(I) counter-part.

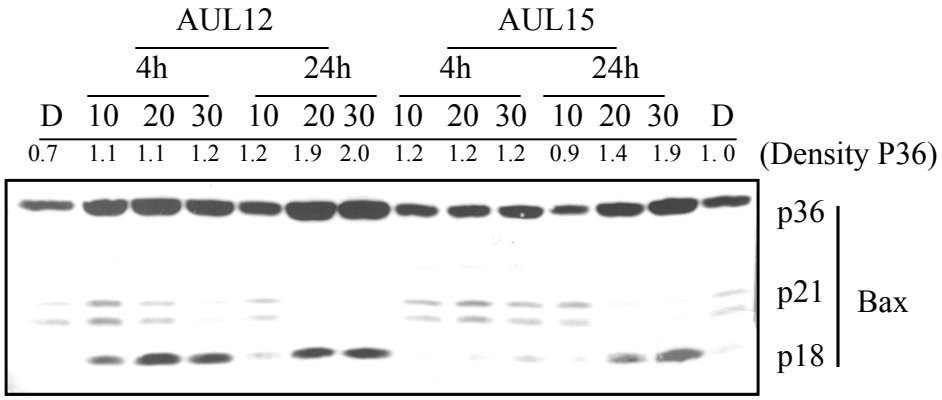

Figure 60. Accumulation of Bax isoforms by Western blot in MDA-MB-231 cells.

Breast cancer MDA-MB-231 cells were treated with AUL12 or AUL15 for 4 or 24 h, followed by performance of Western Blot analysis of Bax isoforms. DMSO solvent was used as a control.

Proteasome inhibition and cell death induction by gold(I)- and gold(III)-dithiocarbamato derivatives is blocked by the reducing agents DTT and NAC. It has been shown that some metals can oxidize cellular proteins and that this process could be blocked by reducing agents such as DTT (dithiothreitol) and NAC (*N*-acetyl- *L*-cysteine) [Godfrey et al., 1994; Rattan and Arad, 1998]. Since both AUL12 and AUL15 could inhibit the chymotrypsin-like activity of purified rabbit 20S proteasome (Fig. 53) and cellular 26S proteasome of cultured breast cancer cells (Figs. 55), we then tested whether reducing agents such as DTT and NAC could affect these events. We found that inhibition of purified 20S proteasome activity by AUL15 was reversed in a dose-dependent manner by addition of DTT and was essentially restored to basal levels with 300 μmol/L DTT (Fig. 61). Similarly, inhibition of purified 20S proteasome by AUL12 could also be reversed by ~80% upon co-incubation of 50 μmol/L of DTT (Fig. 62).

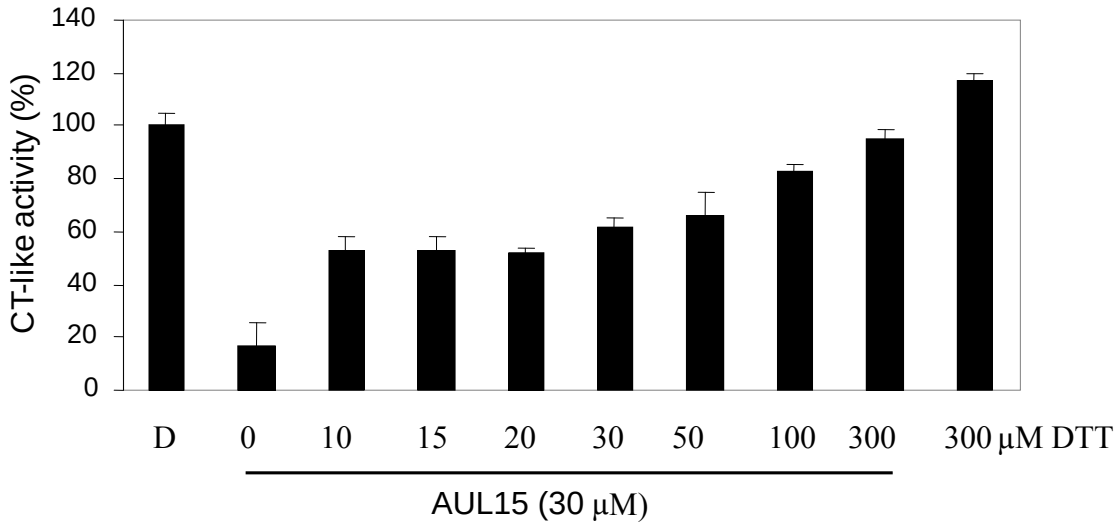

Figure 61. Inhibition of proteasomal activity in purified 20S by AUL15 is blocked by DTT.

Purified rabbit 20S proteasome was incubated with a peptide substrate for the proteasomal chymotrypsin-like activity and indicated concentrations of AUL15 in the absence or presence of DTT at indicated concentrations for 2 hours, followed by the measurement of proteasomal chymotrypsin-like activity. DMSO was used as solvent control.

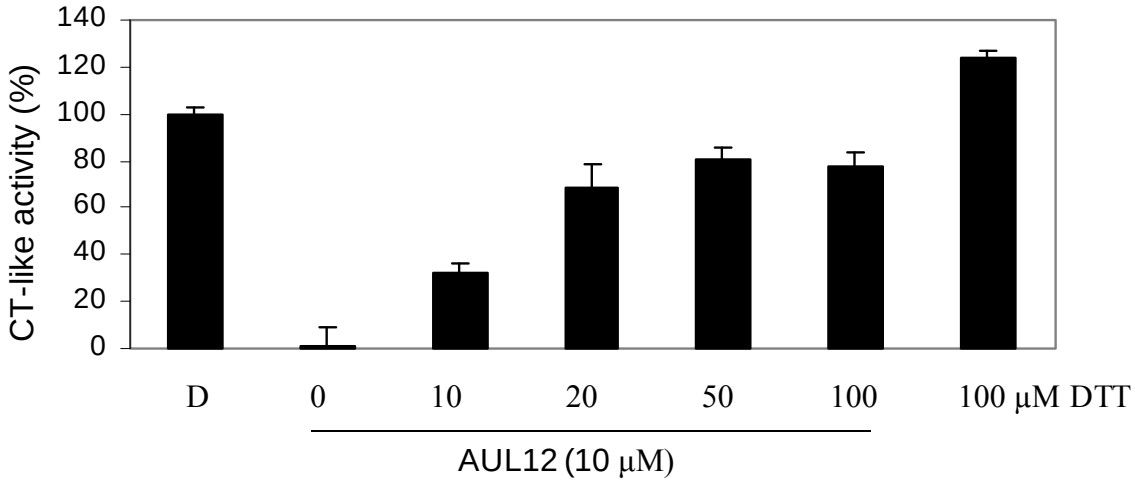

Figure 62. Inhibition of purified 20S proteasomal activity by AUL12 is blocked by DTT.

Purified rabbit 20S proteasome was incubated with a peptide substrate for the proteasomal chymotrypsin-like activity and indicated concentrations AUL12 in the absence or presence of DTT at indicated concentrations for 2 hours, followed by the measurement of the proteasomal chymotrypsin-like activity. DMSO was used as solvent control.

The effect of NAC on AUL12 and AUL15-induced proteasome inhibition in intact MDA-MB-231 cells was also investigated. We found that NAC at 150 μmol/L, effectively restored proteasome activity in the cells treated with 30 μmol/L AUL15 (Fig. 63). Additionally, 100 μmol/L NAC could block proteasome inhibition induced by 20 μmol/L AUL12 after 24 h (Fig. 63).

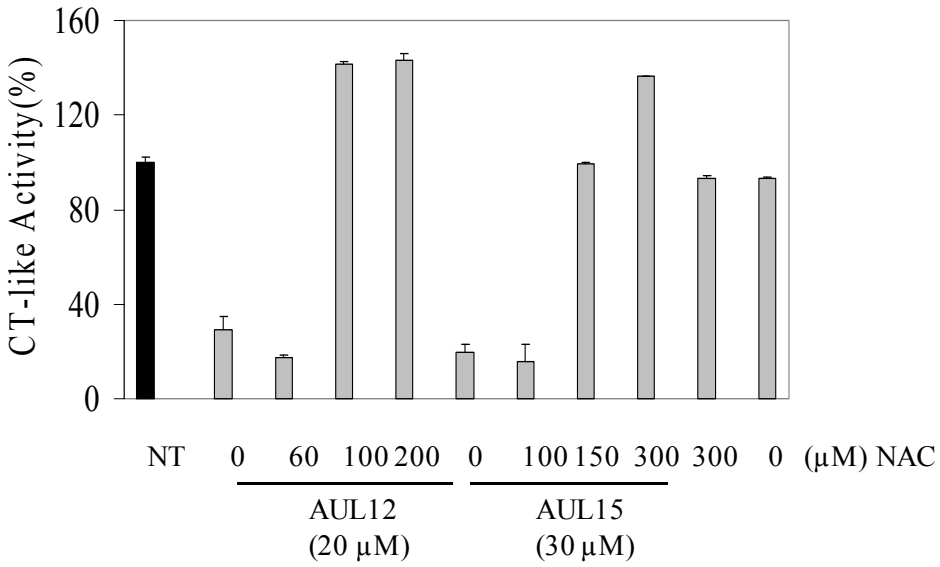

Figure 63. Proteasome inhibition by AUL12 and AUL15 is blocked by NAC in intact MDA-MB-231 cells.

Breast cancer MDA-MB-231 cells were treated with indicated concentrations of AUL12 or AUL15 for 24 h, in the absence or presence of various concentrations of NAC, followed by measurement of the proteasomal chymotrypsin-like activity.

Consistently, co-treatment with each gold compound and NAC blocked accumulation of ubiquitinated proteins and the ubiquitinated form of IκB-α (Fig. 64). Importantly, NAC almost completely blocked gold(I)- and gold(III)-induced production of p65 PARP cleavage (Fig. 64) and cellular morphological changes (Fig. 64). Furthermore, addition of NAC also inhibited the increased levels of p18/Bax to p36/Bax induced by each gold compound, suggesting that NAC inhibits AUL12 and AUL15-induced calpain activation (Fig. 64).

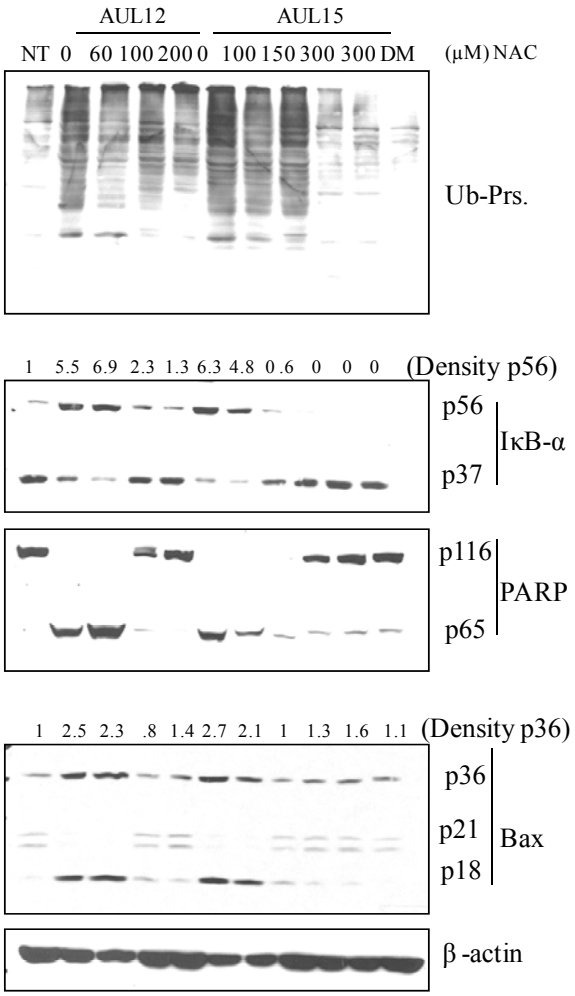

Figure 64. Western Blot analysis showing that proteasome inhibition and cell death induction by AUL12 and AUL15 is blocked by NAC in intact MDA-MB-231 cells.

Breast cancer MDA-MB-231 cells were treated with either AUL12 (20 μM) or AUL15 (30 μM) for 24 h, in the absence or presence of various concentrations of NAC, followed by Western Blot analysis.

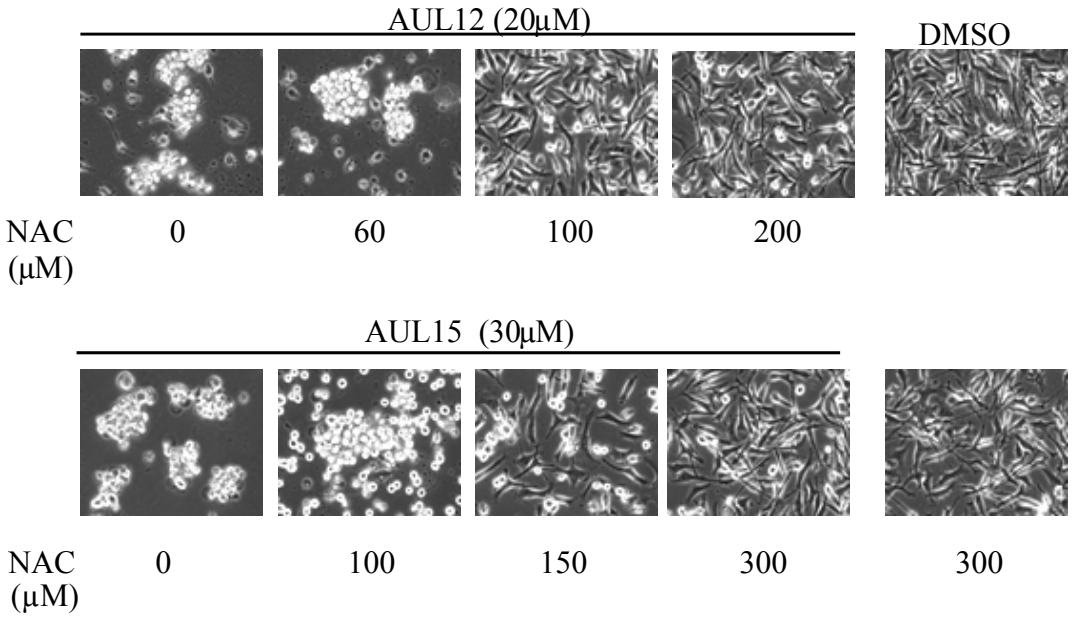

Figure 65. Cell death associated morphological changes in intact MDA-MB-231 cells by AUL12 and AUL15 are blocked by NAC.

Breast cancer MDA-MB-231 cells were treated with indicated concentrations of AUL12 or AUL15 for 24 h, in the absence or presence of various concentrations of NAC, followed by visualization of apoptotic morphological changes by phase-contrast imaging (100x magnification).

Proteasome inhibition and apoptosis induction by gold(III) but not gold(I) dithiocarbamate is mediated through activation of reactive oxygen species (ROS). It has been demonstrated that some chemotherapeutic agents, including proteasome inhibitors, could mediate cell death through increase in oxidative stress [Perez-Galan et al., 2006]. Our data show that gold(I)- and gold(III)-dithiocarbamato derivatives can inhibit the proteasomal chymotrypsin-like activity and induce cell death, which can be completely reversed by the addition of a reducing agent. We next set out to determine if the induction of ROS is responsible for cell death mediated by these complexes. Breast cancer MDA-MB-231 cells were treated with both 20 and 30 μmol/L of AUL12 or AUL15 for 3.5 h along with the oxidation-sensitive probe carboxy-H_2DCFDA, followed by analysis of ROS induction by fluorescence microscopy and FACS analysis. DMSO was used as the negative control and TBHP as positive control under the same experimental conditions. Our results show that treatment with AUL15, at both concentrations was unable to produce reasonably detectable levels of green fluorescence (1.0-1.3% ROS-positive cells)(Fig. 66A-B). However, treatment with AUL12 at both concentrations resulted in the enhancement of bright green fluorescence indicative of the production of ROS (9.6-12.6% ROS-positive cells) (Fig. 66E-F).

Since we have shown that the addition of a reducing agent could completely block the effect of proteasome inhibition and cell death induction, we next investigated whether the addition of NAC could block the production of ROS induced by gold(III) dithiocarbamate. Our data shows that production of ROS in cells treated with the gold(III) complex was almost completely blocked by the addition of 200 μmol/L NAC (1.7%-ROS positive cells) (Fig. 66G). Moreover, the treatment of cells with the gold(I) analogue, with or without co-treatment of NAC failed to induce any significant levels of ROS, thus confirming that the

gold(I) derivative is redox inactive (Fig. 66A-C). The results presented in this dissertation clearly suggest that induction of oxidative stress by gold(III), but not gold(I), is at least partially responsible for its biological activity which can be effectively inhibited through the addition of a reducing agent.

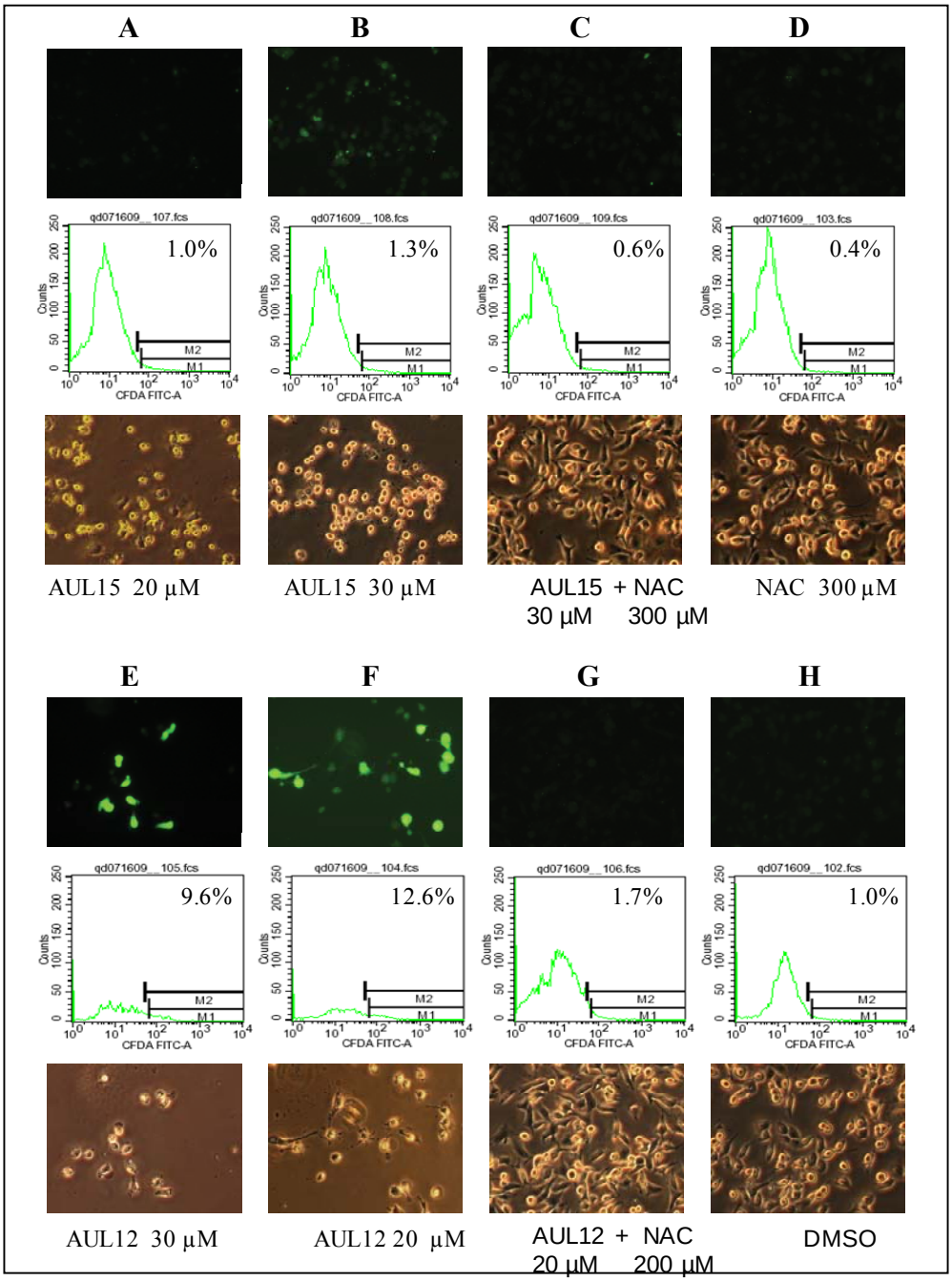

Figure 66. AUL12 [Au(III)] but not AUL15 [Au(I)] induces ROS production in breast cancer cells and is effectively blocked by the addition of NAC.

ROS formation in MDA-MB-231 cells was determined using the oxidation-sensitive probe (carboxy-H_2DCFDA). Cells were treated with AUL12 or AUL15 at the indicated concentrations for 3.5 h with or without the addition of NAC. DMSO and NAC alone were used as negative controls under the same experimental conditions. ROS generation was examined using a Zeiss confocal laser microscope and FACS analysis as explained in Materials and Methods.

Discussion

The clinical impact of platinum-based complexes has precipitated the investigation of other metals which broadens the spectrum of activity and presents modes of action that differ from cisplatin. Although the mechanism of cisplatin has been readily understood, the mechanism of gold compounds responsible for their anti-tumor activity is still under debate. A number of studies suggested that proteins, rather than DNA, may be a more suitable target for gold-containing complexes. Some of the suggested targets for gold compounds include S-donor ligands such as glutathione and cysteine [Milacic et al., 2006], bovine serum albumin [He and Carter, 1992], thioredoxin reductase [Engman et al., 2006], and ERK pathway [Saggioro et al., 2007]. Based on these studies, it was proposed that selective modification of surface protein residues by gold(III) complexes is more likely to be responsible for their biological activity.

We have previously shown that the gold(III) dithiocarbamato derivative ([$AuBr_2$(DMDT)]) was able to inhibit the proteasomal activity and induce apoptosis in cultured breast cancer cells and mice bearing breast cancer xenografts [Milacic et al., 2006]. Furthermore, proteasomal inhibition and apoptosis induction could be effectively reversed by the addition of a reducing agent [Milacic et al., 2006]. The reversal of [$AuBr_2$(DMDT)]–mediated proteasomal inhibition by a reducing agent could be a result of the reaction that pulls the complex away from the proteasome, thereby preventing it from binding and inhibiting the proteasome. This possibility was supported by previous findings that gold(III) complexes can bind S-donor ligands, such as glutathione and cysteine, and cleave their disulfide bond(s) [Milacic et al., 2008b]. It is also possible that NAC or DTT could reduce gold(III) to gold(I), an oxidation state that does not have, or has lower affinity for binding

and inhibiting the proteasome. Another suggested possibility was based on the report that gold(III) porphyrin 1a induces intracellular oxidation, altering reduced glutathione (GSH) levels in the cell [Wang et al., 2005]. Therefore, a possibility that [$AuBr_2$(DMDT)] might stimulate production of ROS that oxidize and inactivate the proteasome was proposed [Milacic et al., 2006]. This hypothesis was supported by a well-established susceptibility of the proteasome to oxidative modification and inactivation upon exposure to free radical–generating systems [Szweda et al., 2002].

In order to evaluate the importance of the 3+ oxidation state for the mechanism of action and overall anti-tumor activity of gold compounds, we compared two gold dithiocarbamato derivatives with different oxidation states of the gold centers, to provide insights into their possible mechanism of action.

When comparing their anti-proliferative activities, it was found that AuL15 was less potent than AUL12 against breast cancer MDA-MB-231 cells (IC_{50} = 13.5 and 4.5 µmol/L, respectively) (Fig. 53). Since both gold compounds own the same ESDT ligand, this finding suggests that the observed effect could be mediated by the different oxidation states of the gold centers.

We then set out to investigate if they share the same molecular target as [$AuBr_2$(DMDT)]- the proteasome. We performed a cell-free activity assay using a purified 20S proteasome incubated with each gold compound (Fig. 54). Interestingly, we found that both complexes inhibited the proteasomal chymotrypsin-like activity, but at significantly different potencies. Similarly to their anti-proliferative activities, AUL15 was less potent in inhibiting the proteasome compared to AUL12 (IC_{50} = 17.7 and 1.13, µmol/L, respectively) (Fig. 54).

To investigate their capability to target and inhibit the cellular proteasome, intact MDA-MB-231 cells were treated and a different effect in activity was found. Proteasomal inhibition was measured by decreased proteasomal activity, increased levels of ubiquitinated proteins, and accumulation of ubiquitinated form of the proteasomal target protein IκB-α (Figs. 55 A-B, 56A-B). Additionally, cell death induction associated with proteasomal inhibition was measured. We found that the effects of the gold(I) compound were again much less pronounced compared to its gold(III) counter-part in the context of cell morphological change, the cleaved PARP fragment p65, annexin V-FITC staining, and TUNEL (Figs. 57-60 and data not shown). We found that at 4 h, cells round up and detachment was observed associated with both apoptotic and non-apoptotic death and calpain-mediated PARP cleavage in to fragment p65, but in the absence of TUNEL-positivity cells detected. This suggests that the cell death observed at 4 h is not apoptosis and it may be calpain-dependent but DNA-damage-independent necrosis. However, at 24 h, both apoptosis and such necrosis occurred. Therefore both necrosis (or DNA-damage-independent cell death) and apoptosis could be induced by these gold compounds and gold(III) has a higher effect while AUL15 at higher concentrations induced more non-apoptotic cell death. Taken together, these findings suggest that the lower potency of AUL15 in inhibiting the proteasome is, at least partly, responsible for its decreased anti-proliferative and cell death-inducing effects, compared to the gold(III) compound, AUL12. We have also found that effects of both gold compounds could be blocked by two different reducing agents (DTT and NAC): both were able to reverse the effects induced by the investigated gold complexes in a cell-free system and in intact MDA-MB-231 cells (Figs. 61-65). We noticed that the similar potent reversion by NAC on cells treated with AUL15 as compared with cells exposed to

AUL12. We found that in addition to inhibition of ROS production, NAC could also react with both gold compounds (unpublished data). Therefore, the reversion of gold compound-mediated effects by NAC could be due to two mechanisms: i) ROS inhibition and ii) direct binding of these two compounds.

It has been shown that many anti-cancer drugs exert their effect through oxidative stress and that the proteasome is susceptible to oxidative modification and inactivation upon exposure to free radical generating systems [Szweda et al., 2002]. Therefore, in an attempt to explain the different potencies of AUL12 and AUL15, we set out to investigate whether they could induce the production of ROS. The results show that treatment with gold(III) compound induces the production of ROS, whereas the gold(I) compound produces much less (Fig. 66 E-F *vs.* A-B). Furthermore, ROS induction by AUL12 could be effectively blocked by the addition of the reducing agent NAC (Fig. 66G). These results show that ROS induced by gold(III) but not gold(I) compound could be, at least partially, responsible for the observed proteasome inhibition. The observation that the treatment with NAC and AUL12 could effectively block the production of ROS, argues that the treatment of NAC may increase the pool of ROS scavengers, thereby preserving cellular integrity. The observation that the gold(I) compound displayed a lower cytotoxic profile may point to the lower affinity of gold(I) to the proteasome, since this different effect was observed under cell free conditions and intact cells. Similarly, it is conceivable that the gold(I) compound may react with all the populations of NAC or DTT molecules, which could partially explain the reversal of gold(I)-mediated events.

Our finding that both gold(I) and gold(III) complexes have the same molecular target is not surprising since it is well known that metal centers are essential for the biological

activity of metal-containing proteins and enzymes, and that metals are often responsible for the activity of organic drugs. The classic example is cisplatin, which exerts its anti-tumor activity by interacting with DNA [Zhu et al., 2005] forming a unique lesion that has not been mimicked by any other organic drugs. However, it has also been known that the activity of metal complexes is not determined only by the presence of the metal, especially when metals exist in different oxidation states and have rich coordination chemistry [Haas and Franz, 2009]. In that case, even subtle changes in the charge of a metal can result in a significant change in the geometry of the complex, leading to dramatic alterations of its biological properties. This might explain the significant differences in the effects of gold(I) and gold(III) compounds investigated here.

AUL12 and AUL15 show different coordination modes at the gold center, that is, tetracoordinate square-planar and dicoordinate linear structure, respectively. It is worth noting that under physiological conditions, AUL12 undergoes hydrolysis, thus delivering two moles of halide per mole of starting complex. Moreover, it has been shown to undergo a subsequent reduction process within 24 h, leading to the corresponding dinuclear gold(I) analogue AUL15 [Ronconi et al., 2006]. However, this reduction process should not affect its cytotoxic properties, since a cytotoxic effect was shown to be exerted mainly within the first twelve hours at nanomolar concentrations [Ronconi et al., 2005] and within 4 hours at micromolar concentrations. All together, these observations strongly suggest that different activities of gold(I) and gold(III) compounds investigated here is a result of the different oxidation states and coordination modes of the gold centers.

Overall, we hypothesize in this dissertation that there are at least two mechanisms responsible for the biological activity of these gold compounds, including ROS production

and direct metal binding to the proteasome. The assertion that gold compounds and other metals can only act nonspecifically and inhibit the proteasome by a secondary effect has been refuted by previous studies from our lab and others. It is notable to point out that treatment with gold(I) at 30 μM for 4 h resulted in the production of ~72% cells undergoing nonapoptotic-related cell death while only producing very low levels of ROS (Figs. 59 vs. 66B). We have also shown that zinc-containing dithiocarbamate derivatives could inhibit the proteasomal activity, but could not be blocked by DTT or NAC, suggesting that these compounds are not acting through ROS (data not shown). Additionally, it has been published previously that zinc does not have a relevant oxidative strength [Amici et al., 2002]. Furthermore, we have also found that Sn could directly bind and inhibit the cellular proteasome [Shi et al., 2009]. Taken together, these results demonstrate that metal-containing compounds do not exert their effect nonspecifically.

In conclusion, the data presented in this dissertation shows that both AUL12 and AUL15 inhibit the proteasome under cell-free conditions and in cultured breast cancer cells, but with different potencies. Furthermore, in either case, proteasome inhibition and cell death induction can be effectively reversed by the addition of DTT or NAC. Interestingly, the gold(III) complex was able to induce production of ROS in intact breast cancer cells, which might be at least partly responsible for the proteasome-inhibitory effect. Although the gold(I) analogue failed to stimulate ROS at any sustained levels, its proteasome-inhibitory and cell death-inducing effects were also completely blocked by the reducing agent. However, further in depth studies are required to delineate this phenomenon completely. Since up to date pharmacologically-employed platinum-containing compounds are strongly

associated with non-specific toxicity, the alternative of metal complexes, especially gold derivatives, as proteasome inhibitors, seems to be a promising approach in cancer therapy.

CHAPTER 6

The Role of Androgen Receptor in Prostate Tumor Cell Death Induced by Proteasome Inhibition and Chemotherapy

Androgen ablation therapy by surgical or medical castration remains the staple of care for most prostate cancer patients. However, most eventually relapse to a hormone-refractory state that no longer responds to androgen withdrawal. Most approaches used in cancer treatment, such as chemotherapy and radiation therapy kill tumor cells by inducing apoptosis. However, cancer cells often acquire resistance to these therapies, and no longer respond these death signals. Therefore, increasing attention has been directed toward alternative mechanisms of cell death that may help circumvent resistance to cytotoxic agents. We have previously shown that decreasing levels of AR correlate with induction of apoptosis by proteasome inhibition. However, the exact role of AR in modulating the cell death response has remained elusive. To study this effect, an experimental model was used consisting of parental PC-3 prostate cancer cells and PC-3 cells stably expressing wild type AR. The data in this dissertation reports that proteasome inhibitor and chemotherapy significantly increased caspase-3 activity in PC-3 cells compared to PC3-AR. Higher levels of caspase-3 activity were associated with apoptotic indices in PC-3 cells. The observation that caspase-3 associated cell death occurs in PC-3 cells, while cell death in PC3-AR cells was associated with much lower levels of caspase-3 was confirmed in cells transiently expressing AR. Interestingly, cotreatment of Velcade and the AR antagonist Casodex caused significant decrease in AR expression associated with an increase in caspase-3 activity in AR(+) LNCaP cells. Taken together, the results provided in this chapter show that AR may influence the

regulatory events involved in cell death, and further understanding these molecular events may have important prognostic and therapeutic potential in the treatment of prostate cancer.

Materials and Methods

Materials. Velcade (Bortezomib) was obtained from Millennium Pharmaceuticals (Cambridge, MA). 3-[4,5-dimethyltiazol-2-yl)-2,5-diphenyl-tetrazolium bromide (MTT), DMSO and other chemicals were purchased from Sigma Aldrich (St. Louis, MO). RPMI-1640, penicillin, streptomycin, pEntr vector, and pLenti-6 vector were purchased from Invitrogen (Carlsbad, CA). Fluorogenic peptide substrates, Suc-LLVY-AMC (for the proteasomal chymotrypsin-like activity) and Ac-DEVD-AMC (for Caspase-3 activity was purchased from Calbiochem (San Diego, CA). Mouse monoclonal antibody against human poly(ADP-ribose)polymerase (PARP) was purchased from BIOMOL International LP (Plymouth Meeting, PA). Mouse monoclonal antibodies against Bax, Bcl-2, caspase-8, caspase-9, rabbit polyclonal against Androgen Receptor (AR-N20), goat polyclonal antibody against actin, and secondary antibodies were from Santa Cruz Biotechnology (Santa Cruz, CA). Cell death ELISA detection kit was purchased from Roche Applied Sciences (Indianapolis, IN). A full-length AR plasmid was purchased from Open Biosystems (Lafayette, CO). Transfection reagent, ExpressFect, was purchased from Denville Scientific (Metuchin, NJ).

Cell culture and whole-cell extract preparation. Human prostate cancer PC-3 and PC-3 cells overexpressing wildtype Androgen Receptor (AR) were obtained from Dr. Fazlul Sarkar (Wayne State University, Det, MI). Human prostate cancer LNCaP cells were obtained from American Type Culture Collection (Manassas, VA). The cell lines were

grown in RPMI-1640 and supplemented with 10% fetal bovine serum and 100 units/mL of penicillin and 100 µg/mL of streptomycin. All cells were grown at 37° C in a humidified incubator with a 5% CO_2-enriched atmosphere. A whole-cell extract was prepared as previously described [Daniel et al., 2005].

Proteasome activity assay in intact human prostate cancer PC-3 and PC-AR cells. Human prostate PC-3 or PC3/AR cells were grown to 70%-80% confluency, treated with indicated compound or DMSO as a control under various conditions, harvested, and used for whole-cell extract preparation. Ten micrograms of cell extract was incubated with 20 µmol/L of the fluorogenic substrate Suc-LLVY-AMC in [50 µmol/L Tris-HCL, pH 7.5] for 2h at 37°C (for the proteasomal chymotrypsin-like activity). After incubation, production of hydrolyzed AMC groups was measured with a Wallac Victor^3 multilabel counter with an excitation filter of 365 nm and emission filter of 460 nm.

Caspase-3 Activity Assay. Cells were treated with indicated agent, harvested, and lysed as described previously. Ac-DEVD-AMC (40 µmol/L) was then incubated with the prepared cell lysates for 24 h and the caspase-3 activity was measured as described above.

Cell proliferation assay. MDA-MB-231 cells were seeded in triplicate in a 96-well plate and grown until 70% to 80% confluence, followed by treatment with Velcade, cisplatin or DMSO (as a control) for 24 h. Following drug exposure time, the 3-(4,5-dimthylthiazol-2-yl)-2,5-diphenyltetrazolium bromide (MTT) assay was done as previously described [Daniel et al., 2005].

Western Blot analysis. PC-3, PC3-AR, and LNCaP breast cancer cells were treated, harvested, and lysed. Cell lysates (40-50 µg) were separated by SDS-PAGE and transferred to a nitrocellulose membrane followed by visualization using the HyGLO chemiluminescent

HRP detection reagent from Denville Scientific (Metuchin, NJ), as previously described [Chen et al., 2005].

Cellular morphology analysis. A Zeiss Axiovert 25 microscope was used for all microscopic imaging with phase contrast for cellular morphology.

Quantification of apoptosis. The Cell Apoptosis ELISA Detection Kit (Roche Applied Sciences) was used to detect apoptosis in PC-3 and PC3-AR cells according to the manufactures protocol.

Expression vector and transient transfection. A full-length AR plasmid was purchased from Open Biosystems (Lafayette, CO). Subsequently, it was subcloned into a pEntr vector (Invitrogen) and recombinated into pLenti-6 vector (Invitrogen). The Invitrogen Lipofectamine 2000 was used for transient transfection of PC-3 cells.

Transient Transfection of AR. PC-3 Cells were grown to 70%-80% confluency followed by addition of the DNA complex using the ExpressFect reagent as mentioned in the manufacturers' protocol. Briefly, 1-2 µl ExpressFect^{TM} was added to 30 µl of DMEM media, mixing gently to create the polymer solution. 30 µl of the polymer solution was added to 30 µl of the DNA solution to create the polymer/DNA complex. The volume of reagents used was based on the final volume of cell culture medium. After 24h, cells were treated with indicated compound and cell lysates were prepared as previously discussed.

Results

Velcade suppresses cell proliferation and proteasomal chymotrypsin-like activity similarly in parental PC-3 and PC-3 cells stably overexpressing AR. In our current study we investigated the regulatory role of the AR (androgen receptor) and how it may influence the molecular events in prostate cancer cells in response to proteasome inhibition and chemotherapy. To test this hypothesis, we used parental PC-3 prostate cancer cells and PC-3 cells stably expressing wild type AR. The identified pair of cell lines was chosen as a relevant experimental model considering that parental PC-3 cells lack endogenous expression of AR, and reengagement of the AR signaling axis through stable overexpression could provide important clues relating to therapeutic intervention in prostate cancer. Importantly our study seeks to provide mechanistic insights into the role of the androgen receptor in prostate cancer cells in response to cytotoxic stimuli.

We first tested the growth inhibitory effect of Velcade toward both prostate cancer lines that differ in AR expression, with the solvent DMSO as a control for 24 h followed by an MTT assay. Velcade (PS-341) is a clinically used proteasome inhibitor used in the treatment of myeloma and mantle cell lymphoma and also being tested against solid tumors [Kane et al., 2003; Kane et al., 2007]. Our results show, although Velcade inhibited cell proliferation in both cell lines in a dose dependent fashion, whereas PC-AR cells appeared to be slightly more sensitive to treatment at lower drug concentrations (Fig. 67). For example, from 50 nM to 0.5 μM cell proliferation was inhibited 20%-25% more in PC3-AR cells compared to its parental cell line, but the trend narrowed between both cell lines in response to higher doses, rendering a similar growth inhibitory profile in response to Velcade (Fig. 67).

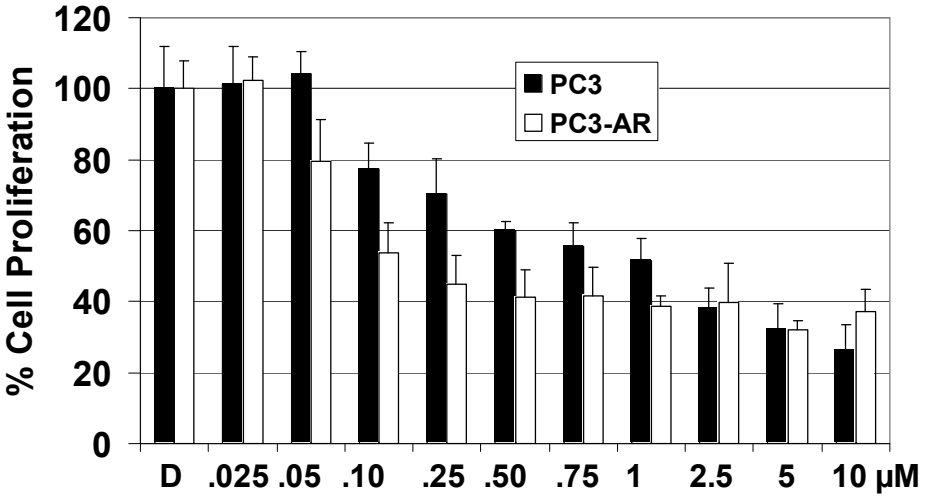

Figure 67. Velcade inhibits cell proliferation at similar levels in both parental PC-3 and PC3 cells stably overexpressing AR.

PC-3 and PC3-AR cells were treated with Velcade for 24 h followed by measurement of cell proliferation by MTT assay.

We next explored whether this pair of cell lines showed a difference in sensitivity to proteasome inhibition in response to Velcade. Both parental PC-3 and PC-AR cells were treated with Velcade (0.25 μM-5 μM) for 24 h. After treatment, cells were harvested, lysed, and cell extract preparations were used to measure proteasomal chymotrypsin-like activity. We found both PC-3 and PC3-AR cells showed a similar sensitivity pattern toward inhibition of chymotrypsin-like activity at all concentrations tested compared with DMSO control treatment (Fig. 68). These results show both prostate cancer lines that differ in AR status show a similar sensitivity toward Velcade as it relates to cell growth and proteasome inhibition.

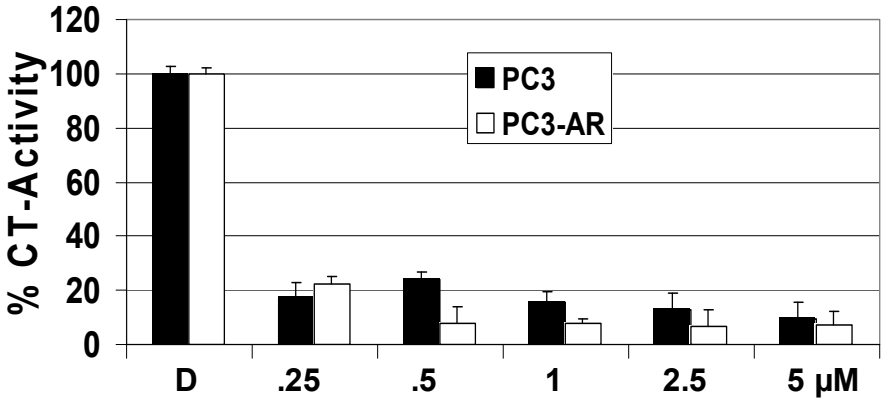

Figure 68. Velcade inhibits proteasomal chymotrypsin-like activity at similar levels in both parental PC-3 and PC3 cells stably overexpressing AR.

PC-3 and PC3-AR cells were treated with indicated concentrations of Velcade for 24 h followed by measurement of proteasomal chymotrypsin-like activities.

Velcade induces Caspase-3 associated cell death in parental PC-3 cells and non-Caspase associated cell death in PC-3 cells stably overexpressing AR. We have previously reported that proteasome inhibitors caused degradation of AR protein in both androgen-dependent LNCaP and androgen-independent C4-2B, suggesting that AR is intimately linked to apoptosis [Chen et al., 2007b; Kim et al., 2008; Yang et al., 2006b]. However, whether this observation is restricted to prostate cancer cells harboring endogenous AR, or whether AR stability is directly implicated in modulating the cell death pathway has yet to be established.

Since both PC-3 and PC3-AR cells showed similar sensitivity to Velcade toward suppression of cell proliferation and proteasomal activity, we next investigated whether the presence of AR could influence the molecular events associated with the cell death program. To test this hypothesis, both cell lines were treated with different concentrations of Velcade (0.25μM-5 μM) for 24 h or DMSO solvent control, and their prepared cell extracts were used for various biochemical assays including caspase activity, PARP cleavage, morphological changes, and histone-DNA ELISA. Significantly higher caspase-3 levels were visible in PC-3 cells, reaching about 26 fold increase compared to DMSO treated cells (Fig. 69). When PC3-AR cells were treated with Velcade, only about 5 fold increase in caspase-3 activity was visible at the highest concentration tested (Fig. 69).

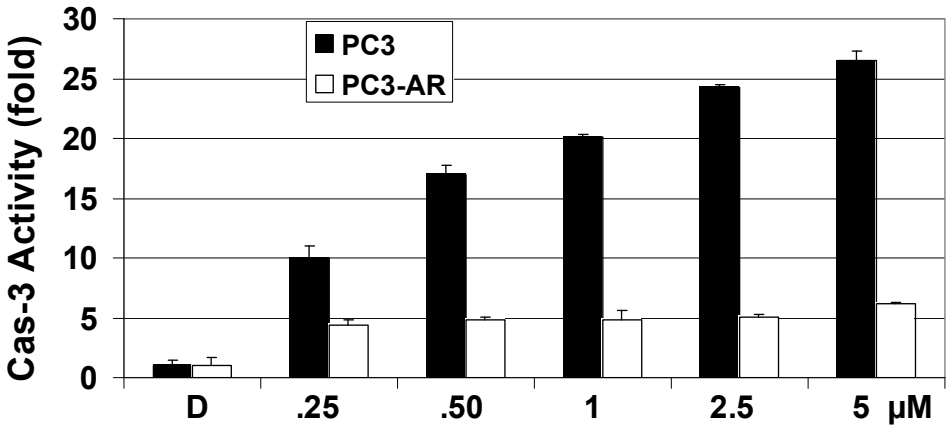

Figure 69. Velcade significantly induces higher levels of Caspase-3 in PC-3 cells compared to PC3 cells stably overexpressing AR.

PC-3 and PC3-AR cells were treated with Velcade at indicated concentrations for 24 h, followed by measurement of capase-3 activity. DMSO (D) was used as solvent control.

This striking difference in caspase-3 activity was verified by western blot analysis, which showed a dose dependent increase in cleaved caspase-3 protein levels compared to PC-AR cells treated with Velcade (Fig. 70). Additionally, significantly higher levels of cleaved caspase-8 and decreased levels of procaspase 9 were visible in aliquots of PC-3 cells, whereas PC3-AR cells showed significantly lower levels (Fig. 70).

It has been shown that PARP can be cleaved by caspase-3 into its characteristic p85 fragment and is characteristic of apoptosis [Lazebnik et al., 1994]. Since higher levels of caspase 3 activity are associated with PC-3 cells in response to Velcade we would expect PARP to be cleaved into its respective p85 fragment. Treatment of PC-3 but not PC3-AR cells resulted in cleaved p85 PARP mostly at higher concentrations, indicative of apoptotic cell death (Fig. 70). Additionally, both the pro- and –antiapoptotic proteins were measured in aliquots from both cell cells lines following treatment with Velcade. We found that both Bcl-2 and Bax were present at much higher levels in PC-3 cells compared to PC-3-AR cells and no discernable difference was found upon treatment (Fig. 70). Furthermore, levels of AR proteins were slightly increased upon exposure to Velcade compared to DMSO treatment (Fig. 70).

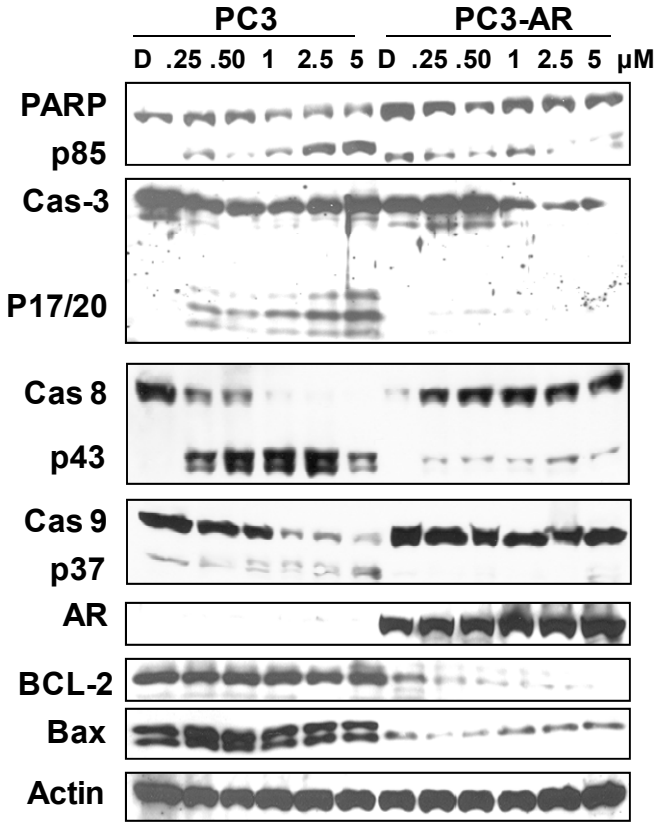

Figure 70. Velcade significantly induces higher levels of apoptotic indices in PC3 cells compared to PC-3 cells stably overexpressing AR.

PC-3 and PC3-AR cells were treated with Velcade for 24 h, followed by Western blot analysis of PARP, caspase-3, 8, 9, AR, BCL-2, and Bax. Actin was used as loading control.

We also observed cell morphology following 24 h treatment as a measurement of cell death. Changes in cell morphology (cell shrunken, and rounded up) were apparent at increasing concentrations of Velcade in both PC-3 and PC3-AR cells (Fig. 71). However, although PC3-AR cells shows significantly lower levels of caspase 3 compared to parental cells, abnormal cell morphology was more pronounced at the lowest concentrations tested (Fig. 71). Therefore, these results suggests that the presence of AR may be influencing the mechanism of cell death induced by cytotoxic insult; PC-3 cells by a caspase associated process and PC3-AR cells by a noncaspase associated mechanism.

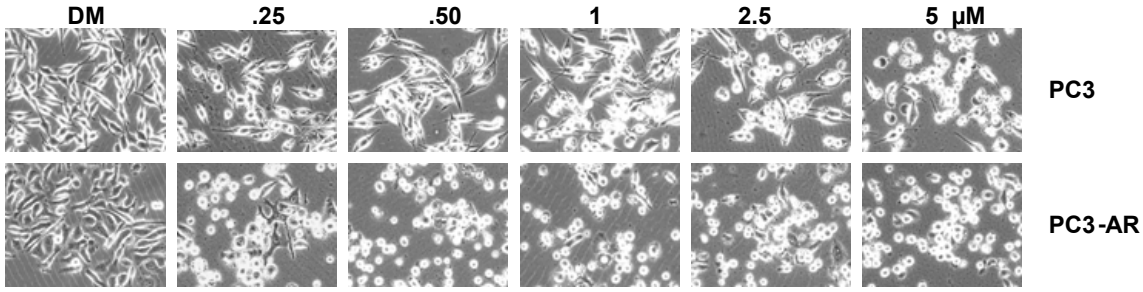

Figure 71. Morphological changes in response to Velcade treatment.

PC-3 and PC3-AR cells were treated with Velcade for 24 h at indicated concentrations, followed by visualization of cellular morphological changes. DMSO (DM) was used as solvent control.

To further investigate the molecular basis of Velcade induced cell death of both PC3 cells and PC-AR cells, histone-DNA ELISA assay was performed to measure apoptosis or non apoptotic cell death. Figure 72 shows a significant increase in apoptotic cells (~7 fold) in PC-3 cells treated with Velcade as measured by ELISA. In contrast, treatment of PC3-AR cells under the same experimental conditions resulted in only minimal levels of apoptotic cells (Fig. 72). These results show that although both cell lines exhibited similar sensitivity to growth inhibition, stably overexpressing AR in AR-independent prostate cancer cells may be influencing the molecular events that facilitate a caspase-associated cell death.

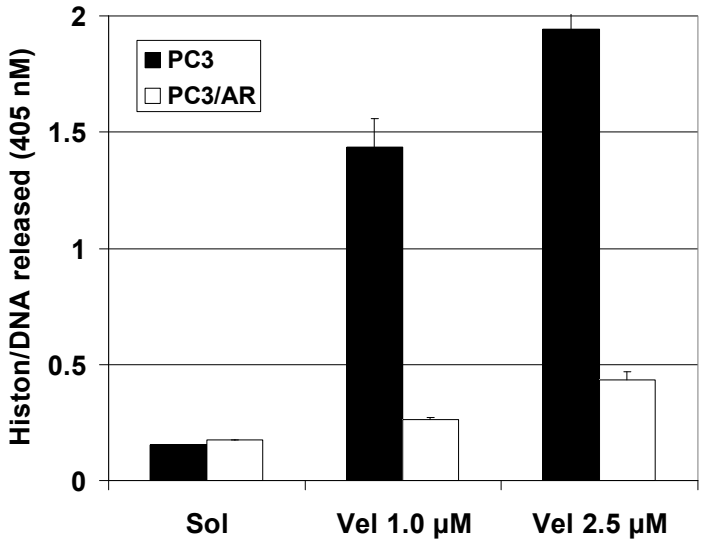

Figure 72. Velcade significantly induces higher levels of apoptotic cell death in PC-3 compared to PC3 cells stably overexpressing AR.

Both cells lines were treated with Velcade at 1 µM or 2.5 µM for 24 h followed by measurement of histone-DNA ELISA for apoptosis.

Cisplatin-induced cytotoxicity elicits Caspase-3 associated cell death (apoptosis) in parental PC-3 cells and non-Caspase associated cell death in PC-3 cells stably overexpressing AR. Our results show that AR may play a pivotal role in influencing the molecular events leading to cell death in response to proteasome inhibitor treatment. To further investigate this claim, PC3 and PC3-AR cells were treated with cisplatin for 24 h followed by measurement of cell proliferation, caspase 3 activity, apoptosis-specific PARP cleavage, and cellular morphological changes. DMSO was used as solvent control. Consistent with our results using Velcade, growth inhibition by cisplatin displayed a similar sensitivity profile between both cell lines at increasing concentrations (25-100 μM) (Fig. 73). Associated with growth inhibition under the same experimental conditions, cisplatin elicited significantly higher activation of caspase 3 in parental PC-3 Cells compared to PC-AR cells (Fig. 74).

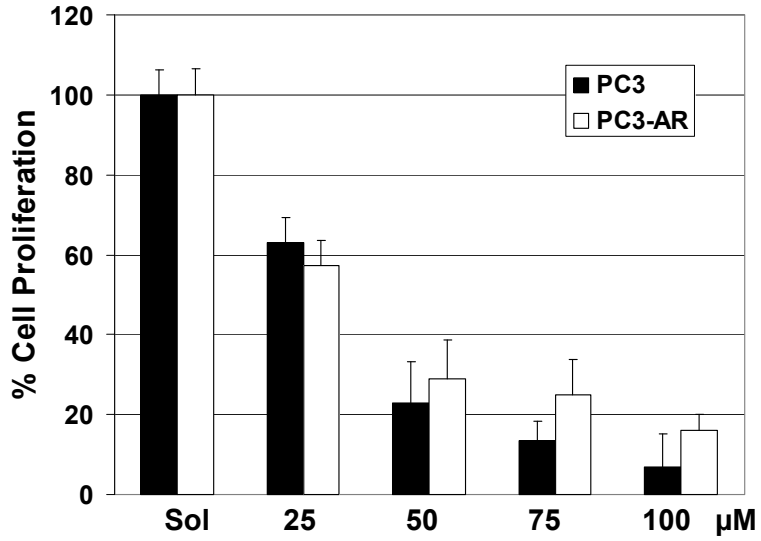

Figure 73. Cisplatin inhibits cell proliferation at similar levels in both parental PC-3 and PC3 cells stably overexpressing AR.

PC-3 and PC3-AR cells were treated with Cisplatin for 24 h followed by measurement of cell proliferation by MTT assay.

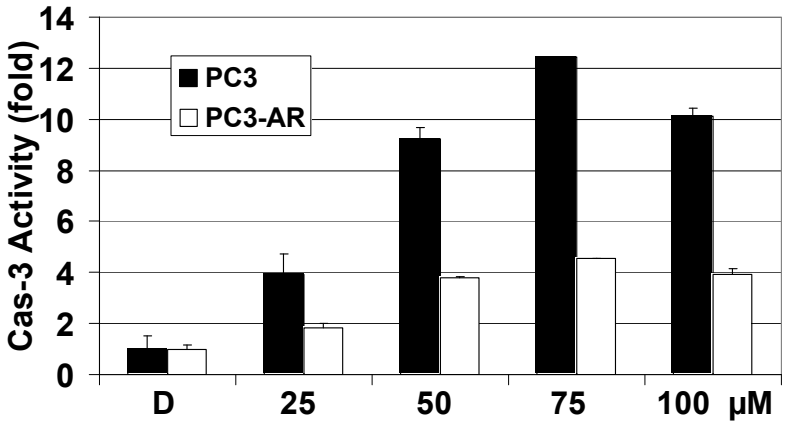

Figure 74. Cisplatin significantly induces higher levels of Caspase-3 in PC-3 compared to PC3 cells stably overexpressing AR.

PC-3 and PC3-AR cells were treated with Velcade for 24 h, followed by measurement of capase-3 activity. DMSO (D) was used as solvent control.

For example, treatment of PC-3 cells with cisplatin at 75 μM resulted in 3-fold higher levels of caspase 3 compared to PC-AR cells at the same concentrations (Fig. 74). Associated with higher levels of caspase 3 in PC-3 cells was p85 PARP cleavage and cleaved caspase 3 protein at higher concentrations of cisplatin (Fig. 75). Additionally, expression of Bcl-2 protein was relatively consistent with that observed in both cell lines with Velcade treatment (Fig. 75). Consistent with a similar growth inhibitory profile, abnormal changes in cell morphology (shrunken, detached) were observed for both cell lines at similar levels that was characteristic of cell death (Fig. 76).

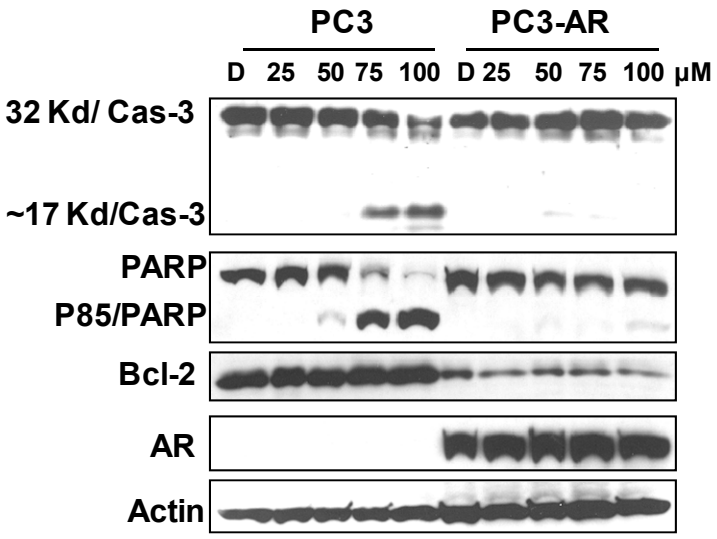

Figure 75. Cisplatin significantly induces higher levels of apoptotic markers in PC-3 cells compared to PC3 cells stably overexpressing AR.

PC-3 and PC3-AR cells were treated with Velcade for 24 h, followed by Western blot analysis of PARP, caspase-3, AR, Bax, and Bcl-2. Actin was used as loading control.

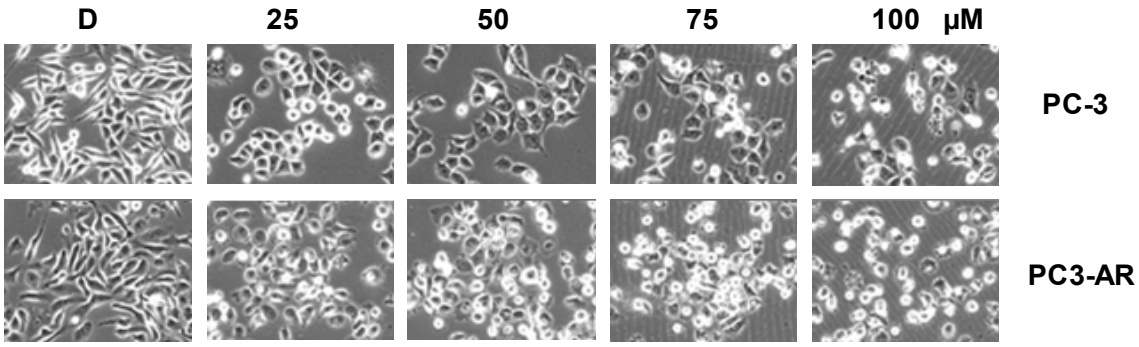

Figure 76. Morphological changes in PC-3 and PC3-AR cells in response to Velcade.

Both cell lines were treated with Velcade for 24 h at indicated concentrations, followed by visualization of cellular morphological changes. DMSO (D) was used as solvent control.

To investigate the kinetic effects of apoptosis induction in parental PC-3 cells, caspase 3 activity, and PARP cleavage were measured and compared to indices in PC3-AR cells treated with 75 μM cisplatin over different time points. We found significantly higher levels of caspase 3 activity primarily during later points compared to PC3-AR cells (Fig. 77). For example, we found a 6.5 and 5.5 fold increase in caspase 3 activity in parental PC-3 cells compared its AR-containing counterpart after 18 h and 24 h exposure of cisplatin, respectively (Fig. 77).

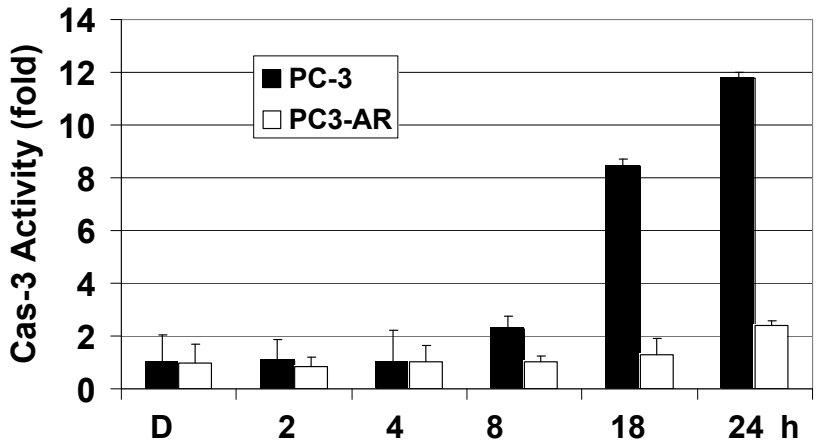

Figure 77. Kinetic effect of cisplatin-induced caspase-3 activity in PC-3 cells.

Human prostate PC-3 and PC3-AR cells were treated with 75 µmol cisplatin at indicated time points followed by measurement of caspase-3 activity. DMSO (D) was used as solvent control.

This observation was confirmed with the appearance of low levels of cleaved procaspase 3 in PC-3 cells (Fig. 78). Consistent with apoptosis induction in PC-3 cells was the appearance of PARP cleavage during later time points (Fig. 78). As observed prior, the appearance of aberrant morphological changes were similar throughout all time points following exposure to cisplatin (data not shown). Furthermore, Bax and Bcl-2 showed relatively stable expression for each cell line in response to treatment compared to DMSO control (Fig. 78). These results show, as demonstrated with Velcade, PC-3 cells undergo cell death in a caspase associated process (characteristic of apoptosis), whereas PC3-AR undergo cell death by a mechanism not associated with high levels of caspase activity.

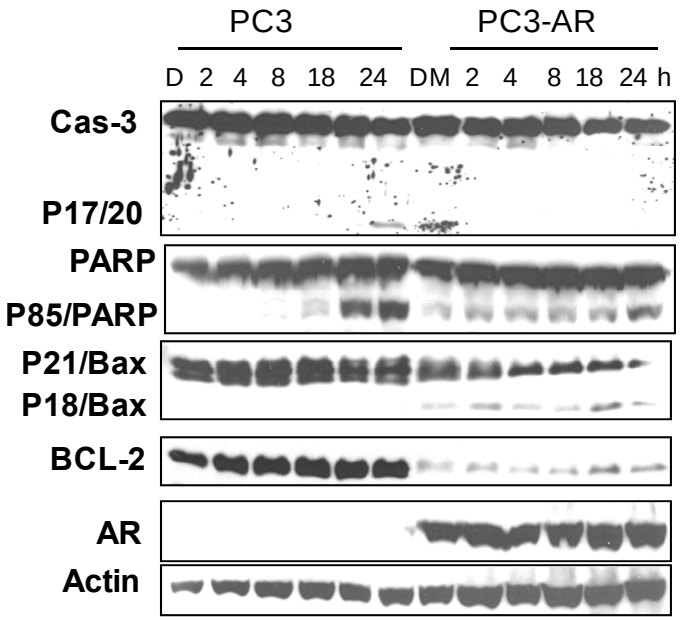

Figure 78. Kinetic effect of apoptotic indices in response to cisplatin**.**

Human prostate PC-3 and PC3-AR cells were treated with 75 µmol cisplatin at indicated time points followed by Western blot analysis of Caspase-3, PARP, Bax, Bcl-2, and AR. Actin was used as loading control.

Proteasome inhibitor and chemotherapy induces caspase 3-associated cell death in parental PC-3 cells and cell death in PC-3 cells transiently overexpressing AR not associated with caspase-3. Our results show that the stable overexpression of AR in AR-independent prostate cancer cells can influence regulatory events that switch the cell death program from apoptotic cell death to a form of cell death that is not associated with caspase-3 activity in response to therapeutic stimuli. To investigate whether transiently expressing AR in PC-3 cells could similarly inhibit caspase-3 activity, we treated parental PC-3 cells and PC-3 cells transiently expressing AR with cisplatin, Velcade, or MG-132 for 24 h. Our results showed inhibition of chymotrypsin-like activity by Velcade in both cell lines at the same concentrations, but PC-3 AR cells were about 3 fold more sensitive to the proteasome inhibitor MG-132 (Fig. 79). Additionally, cisplatin showed minimal proteasome inhibitory activity against either cell line tested compared to DMSO control (Fig. 79).

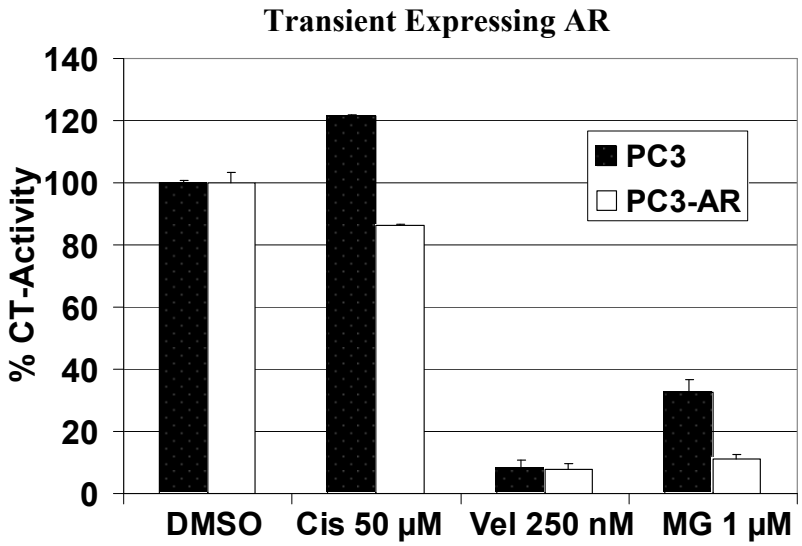

Figure 79. Proteasome inhibitors inhibit proteasomal chymotrypsin-like activity in both parental PC-3 cells PC-3 cells transiently expressing AR at similar levels.

Human prostate PC-3 and PC3 cells transiently expressing AR were treated with cisplatin, MG-132, or Velcade at indicated concentrations for 24 h followed by measurement of proteasomal chymotrypsin-like activity. DMSO was used as solvent control.

Consistent with our finding from cells stably expressing AR, both proteasome inhibitors were unable to induce significant levels of caspase 3 activity in cells transiently expressing AR in response to any therapeutic agent (Fig. 80). For example, we found exposure to Velcade and MG-132 for 24 h induced the activation of Caspase 3 activity about 2.5- fold and 4- fold higher, respectively, in parental PC-3 cells compared to PC3-AR cells (Fig. 80B). Additionally, neither cell line exhibited a significant difference in caspase 3 activity when exposed to 50 μM cisplatin (Fig. 80B). Therefore, consistent with our finding from PC-3 cells stably expressing AR, its transient expression acts as a suppressor of capase-3 activity and may be instrumental in modulating the cell death program to form of cell death that is not heavily associated with caspase-3 activity.

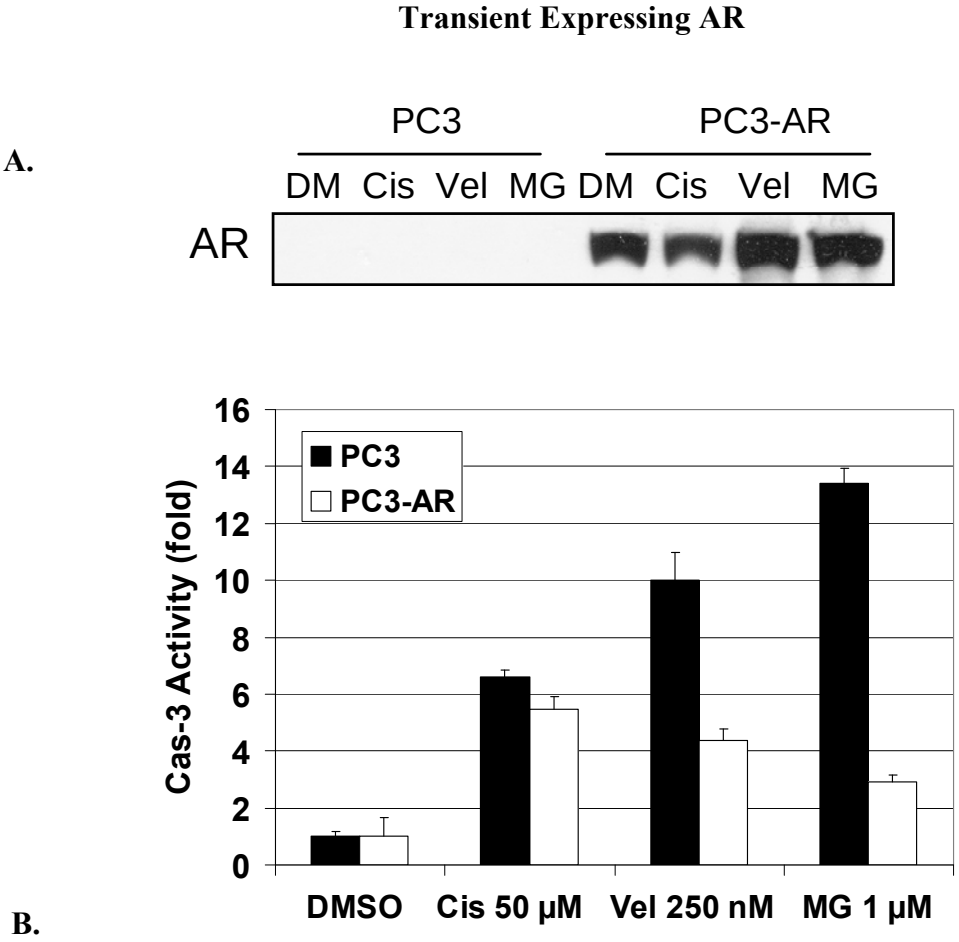

Figure 80. Proteasome inhibitor significantly induces higher caspase-3 activity in parental PC-3 cells compared to PC-3 cells transiently expressing AR.

Human prostate PC-3 and PC3 cells transiently expressing AR were treated with cisplatin, MG-132, or Velcade at indicated concentrations for 24 h followed by measurement of **(A)** AR expression levels, and **(B)** caspase-3 activity. DMSO was used as solvent control.

Androgen receptor suppresses caspase 3 associated cell death in androgen-dependent AR(+) LNCaP cells in response to proteasome inhibitor. Our results clearly show that AR suppresses caspase-3 associated cell death in both stable and transiently expressing PC-3 cells, suggesting the importance AR in regulating cell death. To further investigate its ability to inhibit caspase 3 associated cell death, AR(+) LNCaP cells were treated with either Velcade (0.25 μM-5 μM) or Cisplatin (25 μM-100μM) for 24 h followed by measurement of caspase-3 activity, PARP cleavage, and apoptosis associated proteins. Velcade treatment of parental PC-3 cells was used as a positive control. The results show that treatment of LNCaP cells with Velcade failed to induce any significant levels of caspase-3, cleaved PARP, or induce any discernable difference in apoptotic-associated proteins (Fig. 81A, 82).

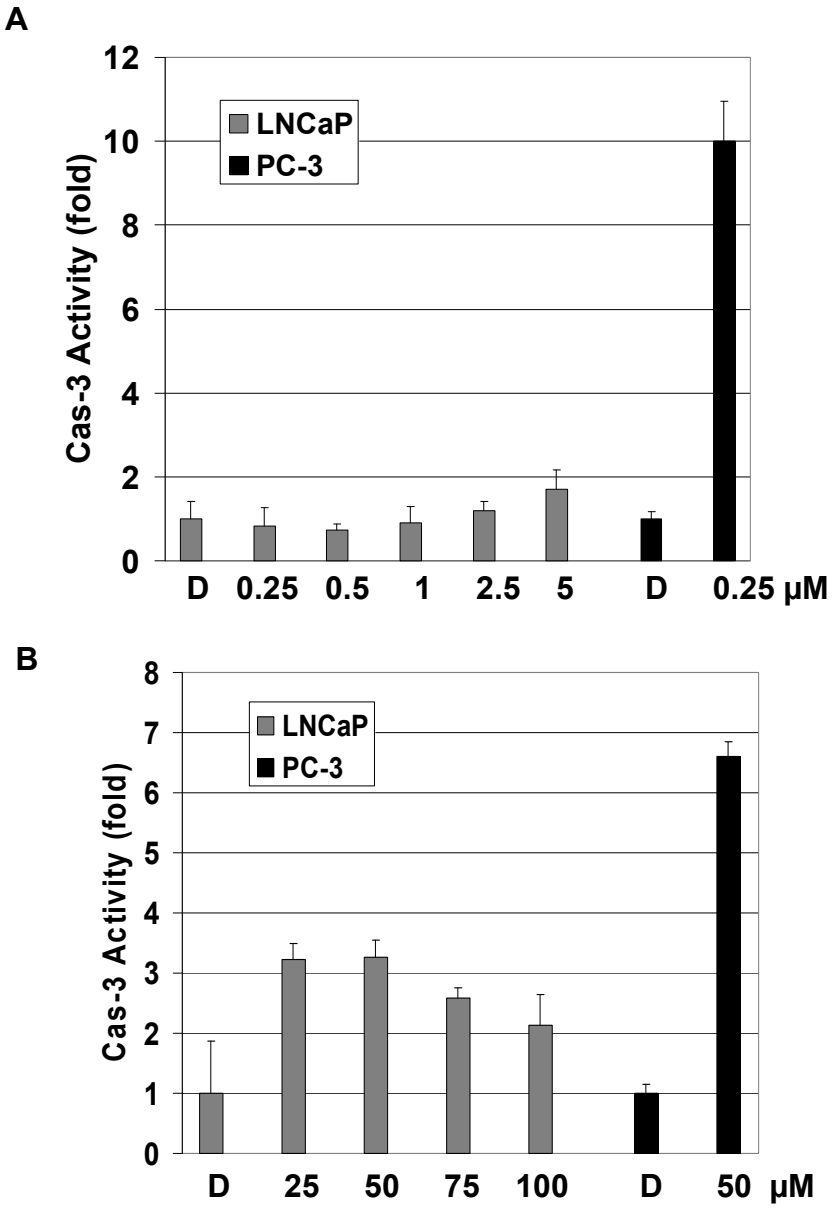

Figure 81. The effect of Velcade (A) and cisplatin (B) on caspase-3 activity in AR(+) LNCaP prostate cancer cells.

Human prostate cancer LNCaP cells were treated for 24 h at indicated concentrations of **(A)** Velcade or **(B)** followed by measurement of caspase-3 activity. Parental PC-3 cells were used as a positive control.

However, cisplatin was able to induce about 3-fold increase in caspase-3 activity 3 at 25 μM and 50 μM, respectively, associated with discernable levels of cleaved PARP (Fig. 81B and 82). Although, proteasome inhibitor failed to induce any significant levels of caspase 3, cisplatin, which operates through a different mechanism of action, was still able to increase caspase-3 activity at lower concentrations tested. These results show LNCaP cells containing endogenous AR expression were considerably resistant to caspase 3-associated cell death by proteasome inhibition, but were increasingly able to activate caspase-3 activity in response to cisplatin.

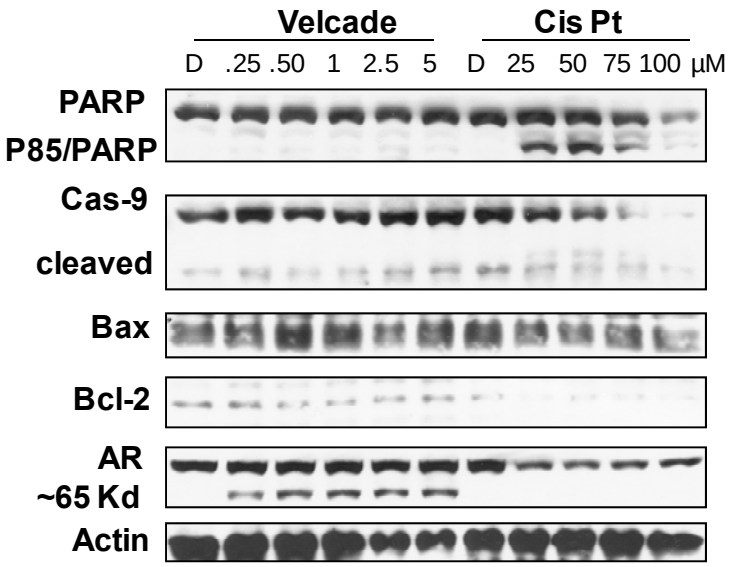

Figure 82. Velcade and cisplatin induce different cell death associated indices in AR-dependent LNCaP prostate cancer cells.

Human prostate cancer LNCaP cells were treated for 24 h with Velcade or cisplatin at indicated concentrations, followed by measurement of PARP, caspase-9, Bax, Bcl-2, and AR by Western Blot analysis.

AR antagonist, Casodex, increases Velcade-induced caspase-3-associated cell death in AR(+) LNCaP cells. Since AR-containing LNCaP cells experienced cell death without significant induction of caspase-3 activity in response to cytotoxic stimuli, we next investigated whether pretreatment with an AR antagonist could rescue caspase-3 dependent cell death. Casodex acts as an anti-androgen by binding to the AR and preventing the activation of its target genes [Furr, 1996]. In addition, casodex accelerates the degradation of the androgen receptor [Waller et al., 2000]. LNCaP cells were treated with Velcade either alone for 24 h or pretreated with casodex (100 μM) for 24h, followed by Velcade treatment at different concentrations (0.25 μM, 1 μM, 25 μM) for an additional 24h, followed by measurement of caspase 3 activity, PARP cleavage, AR, and apoptotic associated proteins. Casodex at 100 μM and DMSO control served as controls. We found that associated with Velcade-induced cell death, caspase 3 activity increased only 2-fold compared to solvent control and casodex alone (Fig. 83). However, cotreatment of Velcade and casodex elicited a dose dependent increase in caspase 3 activity reaching 4.8 fold increase compared to DMSO control and casodex alone (Fig. 83). In comparison, Velcade alone induced caspase 3 activity about 2 fold at the highest concentration tested (Fig. 83).

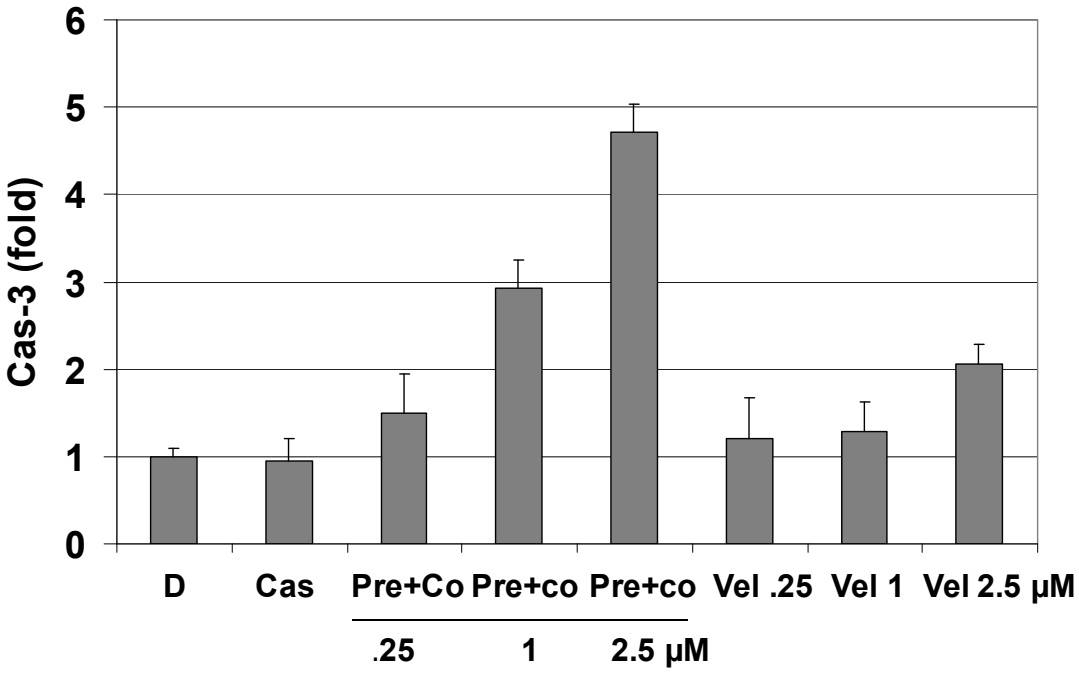

Figure 83. Casodex increases Velcade-induced capase-3-associated cell death in AR(+) LNCaP cells.

LNCaP cells were treated with either casodex alone (100 µM) for 24 h, Velcade alone for 24 h, or pretreatment with casodex followed by cotreatment with Velcade for an additional 24 h at the indicated concentrations, followed by measurement of caspase-3 activity. DMSO (D) was used as solvent control.

Higher levels of caspase-3 activity in cotreated cells were associated with visible levels of PARP cleavage (Fig. 84). Furthermore, If AR was associated with suppression of caspase-3 activity; we'd expect to see decreased levels of AR in cells cotreated with casodex and Velcade. Interestingly, associated with higher levels of caspase-3 was a significant reduction in AR expression (Fig. 84). These results strongly designate AR as a critical player in regulating the cell death program by suppressing caspase-3 activity. Since the majority of hormone resistant prostate cancer (HRPC) remains highly dependent on AR function, elimination of AR may prove to be a viable therapeutic strategy in the treatment of prostate cancer.

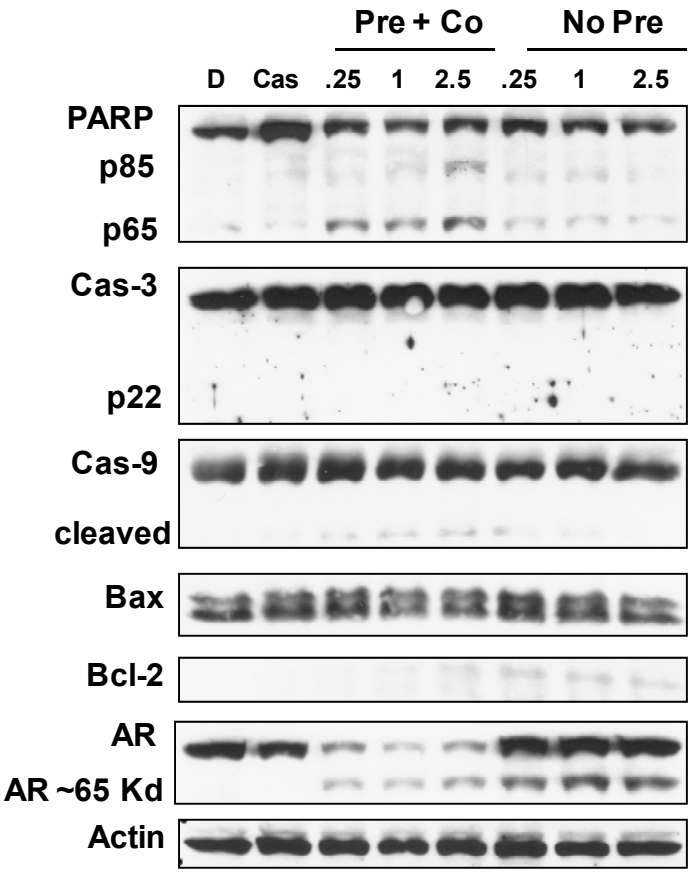

Figure 84. Velcade and casodex partially rescue apoptotic cell death in AR-dependent LNCaP cells.

LNCaP cells were treated with either casodex alone (100 μM) for 24 h, Velcade alone for 24 h, or pretreatment with casodex followed by cotreatment with velcade for an additional 24 h at the indicated concentrations, followed by measurement of PARP, caspase-3, caspase-9, Bax, Bcl-2, and AR by Western Blot analysis. Actin was used as loading control.

Discussion

Many reports have suggested that AR is a critical molecular determinant in driving prostate cancers from a hormone sensitive to a hormone refractory state following ablation of steroidal androgens [Attard et al., 2009a; Cohen and Rokhlin, 2009; Taplin, 2008]. We have previously reported that proteasome inhibitors caused downregulation of AR in both androgen-dependent LNCaP cells and androgen-independent C4-2B cells [Chen et al., 2007b; Yang et al., 2006b], and that calpain involvement is at least partially responsible for this effect [Yang et al., 2008]. The finding that AR degradation by proteasome inhibition is associated with apoptotic cell death stimulated our investigation into examining the regulatory events of AR in driving tumor cell death.

Clinical studies have shown that most anticancer agents induce apoptosis, and that inhibition of the apoptotic program can trigger chemoresistance [Okada and Mak, 2004]. Therefore, targeting alternative forms of cell death may provide effective means for maximal tumor reduction. It is likely that both apoptotic and non-apoptotic pathways contribute to cell death depending on the cell type and degree of therapeutic insult. It has also been shown that many current anticancer therapies, including DNA-alkylating agents can induce necrosis by activation of PARP-1 [Zong et al., 2004]. Increasing evidence suggests that death receptor adaptors, including receptor-interacting protein kinase (RIPK1) and tumor necrosis factor (TNF) receptor associated factor 2 (TRAF2), as important regulators of necrotic cell death [Chan et al., 2003; Holler et al., 2000]. These findings open the possibility of exploiting these as potential molecular targets in cancer therapy. It has also been shown that breast cancer cells treated with tamoxifen can induce autophagy by accumulating autophagic vesicles before tumor cell death [Bursch et al., 1996; Bursch et al.,

2000]. However, the molecular events by which tumors cells can control their fate has remained unanswered. Therefore, assessment of the expression of protein signatures associated with cell death may have significant implications in the selection of treatment strategies for cancer [Bruckheimer and Kyprianou, 2000].

In this study we set out to investigate whether AR can influence the regulatory events in modulating the cell death program in prostate cancer cells in response to proteasome inhibition and chemotherapy. Studies have shown that AR expression in PC-3 cells confers a less aggressive phenotype by decreasing anchorage independent growth and Matrigel invasiveness [Bonaccorsi et al., 2008]. It has also been shown that AR may function as both a suppressor and proliferator to suppress or promote tumor cell metastasis depending on the cellular context [Niu et al., 2008]. However, whether AR can intrinsically modulate the cell death program has yet to be established. The data in this dissertation shows parental PC-3 cells and reexpression of AR into AR(-) PC-3 cells showed similar growth inhibitory effects in response to proteasome inhibition and chemotherapy (Fig. 67, and 73). However, greater than 4-fold increase in caspase-3 activity was seen in PC-3 cells compared to PC3-AR cells at the highest concentration tested, associated with apoptotic indices (Fig. 69, and 70) in response to Velcade treatment. Associated with higher levels of caspase-3 levels in PC-3 cells were significantly higher levels of apoptotic cells as measured by DNA-histone ELISA (Fig. 72). These results suggest that parental PC-3 cells undergo a caspase-associated form of cell death (*e.g.* apoptosis), whereas PC3-AR cells undergo cell death that is not heavily associated with the activation of caspases (*e.g.* caspase-independent apoptosis, nonapoptotic cell death). These interesting results were also seen when this experimental model was treated with cisplatin, although the increase in caspase-3 activity was less pronounced in

parental PC-3 cells (Fig. 74, and 75). Our finding that AR could act as a suppressor of caspase-3-dependent cell death was validated in AR(+) LNCaP cells (Fig. 81-82). Interestingly, when the AR antagonist Velcade was used in cotreatment with Velcade, caspase-3 activity was once again increased, (Fig. 83) demonstrating the intrinsic value AR in modulating the cell death response. Moreover, it was also found that inhibition of caspase activity by AR was not by direct binding (data not shown).

These interesting results suggest that targeting alternative forms of cell death based on protein signatures, such as AR, may provide prognostic and therapeutic opportunities in the treatment of prostate cancer. Furthermore, it is conceivable that targeting AR for its elimination by combination strategies may provide effective means for the treatment of hormone resistant prostate cancer (HRPC), which remains addicted to AR signaling processes.

Future Studies

The data presented in this dissertation presents a compelling rationale for the development of metal complexes with asymmetric [NN'O]-containing ligands with gallium, zinc, and copper as potential proteasome inhibitors for the potential clinical application in the treatment of cancer. However, an in-depth understanding of the mechanism of actions of proteasome inhibitors is essential for their translation into effect drug candidates. A number of studies will be carried out in the future to build upon our initial studies and importantly, to validate the potential use of metal-containing complexes as potential anticancer agents that target the ubiquitin-proteasome pathway. This endeavor requires an interdisciplinary approach that combines the expertises of both molecular biologists and chemists. The first approach will be to determine the optimal electronic and structural properties of the metal ions and ligands necessary for proteasome inhibition. This goal will be obtained through the development of a library of coordination compounds by means of synthesis, structural characterization, and pharmacological studies, both under cell free conditions and cultured human prostate cancer cells. The second approach is to determine the inhibition potential of metal complexes related to (i) the nature of the metal ion (*e.g.* charge, oxidation state), (ii) the nature of the ligand (*e.g.* charge, redox innocence, amphiphilicity), (iii) the nature of the counterions (*e.g.* solubility, cell penetration). To achieve this goal, interactions between complexes, the 20S core and the 19S regulatory caps will be studied, and biomimetic and computational (*in silico*) modeling of the active sites for proteasome inhibition and cell death induction will be considered. The third approach will involve the evaluation of metal complexes toward proteasome inhibition and cell death using cultured human prostate cancer cells and mouse models-bearing human prostate cancer xenografts. A concerted effort will

also be undertaken to identify the biological mechanisms associated with proteasome inhibition. This approach will set out to identify cellular pathways responsible for proteasome inhibition and cell death, including NF-κB, mTOR, AKT, and their association with reactive oxygen species. Identifying critical signaling programs responsible for metal-based proteasome inhibition is essential for their development as anticancer drugs.

An important component of this dissertation demonstrates the critical role of the androgen receptor (AR) in influencing the regulatory events involved in prostate tumor cell death. A series of future studies will be carried out with this project that could have future implications in the treatment of hormone resistant prostate cancer which remains invariably dependent on androgen receptor signaling. An important finding of this study is that cell death in parental PC-3 prostate cancer cells is associated with the induction of capase-3 activity, while cell death in PC3/AR cells are unable to reach high levels of caspase-3. To validate the reliance of PC-3 cells on caspase-3 activity, a future approach would be to measure caspase-3 activity and cell death associated changes in the presence of a caspase-3 inhibitor and either a proteasome inhibitor or chemotherapy. Since treatment of PC-AR cells is not associated with significant levels of caspase-3 activity, a future approach would be to measure protein markers associated with caspase-3 independent cell death, such as necrosis (RIPK-1), and autophagy (e.g. LCM3). Additionally, the results in this dissertation show that treatment of AR(+) LNCaP cells with proteasome inhibitor followed by cotreatment with the AR antagonist Casodex resulted in significant decreased levels of AR protein associated with increased levels of caspase-3 activity. This is a significant finding since elimination of AR may prove to be a curative strategy in hormone resistant prostate cancer. This interesting finding will be validated by future studies in a mouse model-bearing prostate cancer cells that

contain AR and can mimic the hormone resistant state. Mice-bearing prostate cancer xenografts (5-8 mice/group) will be either treated with solvent control, proteasome inhibitor, casodex alone, or combination of proteasome inhibitor and casodex for up to 30 days. Following treatment, tumors will be harvested and used to measure caspase-3 activity, expression levels of AR protein, and also cell death associated changes (e.g. PARP cleavage, Bax, Bcl-2) in tumor tissue. These studies could lead to the generation of therapeutic strategies that target and eliminate AR, and could play a pivotal role in the treatment of prostate cancer.

References

Abou-Jawde R, Choueiri T, Alemany C, Mekhail T. 2003. An overview of targeted treatments in cancer. Clin Ther 25:2121-37.

Adams J. 2002. Proteasome inhibition: a novel approach to cancer therapy. Trends Mol Med 8:S49-54.

Adams J. 2003. The proteasome: structure, function, and role in the cell. Cancer Treat Rev 29 Suppl 1:3-9.

Adams J. 2004. The proteasome: a suitable antineoplastic target. Nat Rev Cancer 4:349-60.

Adams J, Palombella VJ, Sausville EA, Johnson J, Destree A, Lazarus DD, Maas J, Pien CS, Prakash S, Elliott PJ. 1999. Proteasome inhibitors: a novel class of potent and effective antitumor agents. Cancer Res 59:2615-22.

Adams JM, Cory S. 2007. The Bcl-2 apoptotic switch in cancer development and therapy. Oncogene 26:1324-37.

Aghajanian C, Dizon DS, Sabbatini P, Raizer JJ, Dupont J, Spriggs DR. 2005. Phase I trial of bortezomib and carboplatin in recurrent ovarian or primary peritoneal cancer. J Clin Oncol 23:5943-9.

Alama A, Tasso B, Novelli F, Sparatore F. 2009. Organometallic compounds in oncology: implications of novel organotins as antitumor agents. Drug Discov Today 14:500-8.

Alberts SR, Foster NR, Morton RF, Kugler J, Schaefer P, Wiesenfeld M, Fitch TR, Steen P, Kim GP, Gill S. 2005. PS-341 and gemcitabine in patients with metastatic pancreatic adenocarcinoma: a North Central Cancer Treatment Group (NCCTG) randomized phase II study. Ann Oncol 16:1654-61.

Amici M, Forti K, Nobili C, Lupidi G, Angeletti M, Fioretti E, Eleuteri AM. 2002. Effect of neurotoxic metal ions on the proteolytic activities of the 20S proteasome from bovine brain. J Biol Inorg Chem 7:750-6.

An B, Goldfarb RH, Siman R, Dou QP. 1998. Novel dipeptidyl proteasome inhibitors overcome Bcl-2 protective function and selectively accumulate the cyclin-dependent kinase inhibitor p27 and induce apoptosis in transformed, but not normal, human fibroblasts. Cell Death Differ 5:1062-75.

Apelgot S, Coppey J, Fromentin A, Guille E, Poupon MF, Roussel A. 1986. Altered distribution of copper (64Cu) in tumor-bearing mice and rats. Anticancer Res 6:159-64.

Attard G, Cooper CS, de Bono JS. 2009a. Steroid hormone receptors in prostate cancer: a hard habit to break? Cancer Cell 16:458-62.

Attard G, Reid AH, A'Hern R, Parker C, Oommen NB, Folkerd E, Messiou C, Molife LR, Maier G, Thompson E, Olmos D, Sinha R, Lee G, Dowsett M, Kaye SB, Dearnaley D, Kheoh T, Molina A, de Bono JS. 2009b. Selective inhibition of CYP17 with abiraterone acetate is highly active in the treatment of castration-resistant prostate cancer. J Clin Oncol 27:3742-8.

Attard G, Reid AH, Yap TA, Raynaud F, Dowsett M, Settatree S, Barrett M, Parker C, Martins V, Folkerd E, Clark J, Cooper CS, Kaye SB, Dearnaley D, Lee G, de Bono JS. 2008. Phase I clinical trial of a selective inhibitor of CYP17, abiraterone acetate, confirms that castration-resistant prostate cancer commonly remains hormone driven. J Clin Oncol 26:4563-71.

Baldin V, Cans C, Knibiehler M, Ducommun B. 1997. Phosphorylation of human CDC25B phosphatase by CDK1-cyclin A triggers its proteasome-dependent degradation. J Biol Chem 272:32731-4.

Baumeister W, Walz J, Zuhl F, Seemuller E. 1998. The proteasome: paradigm of a self-compartmentalizing protease. Cell 92:367-80.

Becke AD. 1988. Density-functional exchange-energy approximation with correct asymptotic behavior. Phys Rev A 38:3098-3100.

Belch A, Kouroukis CT, Crump M, Sehn L, Gascoyne RD, Klasa R, Powers J, Wright J, Eisenhauer EA. 2007. A phase II study of bortezomib in mantle cell lymphoma: the National Cancer Institute of Canada Clinical Trials Group trial IND.150. Ann Oncol 18:116-21.

Bernardi R, Liebermann DA, Hoffman B. 2000. Cdc25A stability is controlled by the ubiquitin-proteasome pathway during cell cycle progression and terminal differentiation. Oncogene 19:2447-54.

Bernstein LR. 1998. Mechanisms of therapeutic activity for gallium. Pharmacol Rev 50:665-82.

Biswas DK, Iglehart JD. 2006. Linkage between EGFR family receptors and nuclear factor kappaB (NF-kappaB) signaling in breast cancer. J Cell Physiol 209:645-52.

Blagosklonny MV. 2002. P53: an ubiquitous target of anticancer drugs. Int J Cancer 98:161-6.

Blair HC, Teitelbaum SL, Tan HL, Schlesinger PH. 1992. Reversible inhibition of osteoclastic activity by bone-bound gallium (III). J Cell Biochem 48:401-10.

Bonaccorsi L, Nosi D, Quercioli F, Formigli L, Zecchi S, Maggi M, Forti G, Baldi E. 2008. Prostate cancer: a model of integration of genomic and non-genomic effects of the androgen receptor in cell lines model. Steroids 73:1030-7.

Brewer GJ. 2007. Iron and copper toxicity in diseases of aging, particularly atherosclerosis and Alzheimer's disease. Exp Biol Med (Maywood) 232:323-35.

Brewer GJ, Dick RD, Grover DK, LeClaire V, Tseng M, Wicha M, Pienta K, Redman BG, Jahan T, Sondak VK, Strawderman M, LeCarpentier G, Merajver SD. 2000. Treatment of metastatic cancer with tetrathiomolybdate, an anticopper, antiangiogenic agent: Phase I study. Clin Cancer Res 6:1-10.

Bruckheimer EM, Kyprianou N. 2000. Apoptosis in prostate carcinogenesis. A growth regulator and a therapeutic target. Cell Tissue Res 301:153-62.

Budihardjo I, Oliver H, Lutter M, Luo X, Wang X. 1999. Biochemical pathways of caspase activation during apoptosis. Annu Rev Cell Dev Biol 15:269-90.

Burnstein KL. 2005. Regulation of androgen receptor levels: implications for prostate cancer progression and therapy. J Cell Biochem 95:657-69.

Bursch W, Ellinger A, Kienzl H, Torok L, Pandey S, Sikorska M, Walker R, Hermann RS. 1996. Active cell death induced by the anti-estrogens tamoxifen and ICI 164 384 in human mammary carcinoma cells (MCF-7) in culture: the role of autophagy. Carcinogenesis 17:1595-607.

Bursch W, Hochegger K, Torok L, Marian B, Ellinger A, Hermann RS. 2000. Autophagic and apoptotic types of programmed cell death exhibit different fates of cytoskeletal filaments. J Cell Sci 113 (Pt 7):1189-98.

Chakravarty PK, Ghosh A, Chowdhury JR. 1986. Zinc in human malignancies. Neoplasma 33:85-90.

Chan FK, Shisler J, Bixby JG, Felices M, Zheng L, Appel M, Orenstein J, Moss B, Lenardo MJ. 2003. A role for tumor necrosis factor receptor-2 and receptor-interacting protein in programmed necrosis and antiviral responses. J Biol Chem 278:51613-21.

Chang KL, Hung TC, Hsieh BS, Chen YH, Chen TF, Cheng HL. 2006. Zinc at pharmacologic concentrations affects cytokine expression and induces apoptosis of human peripheral blood mononuclear cells. Nutrition 22:465-74.

Chauhan D, Catley L, Li G, Podar K, Hideshima T, Velankar M, Mitsiades C, Mitsiades N, Yasui H, Letai A, Ovaa H, Berkers C, Nicholson B, Chao TH, Neuteboom ST, Richardson P, Palladino MA, Anderson KC. 2005. A novel orally active proteasome inhibitor induces apoptosis in multiple myeloma cells with mechanisms distinct from Bortezomib. Cancer Cell 8:407-19.

Chauhan D, Hideshima T, Anderson KC. 2006. A novel proteasome inhibitor NPI-0052 as an anticancer therapy. Br J Cancer 95:961-5.

Chauhan D, Singh A, Brahmandam M, Podar K, Hideshima T, Richardson P, Munshi N, Palladino MA, Anderson KC. 2008. Combination of proteasome inhibitors bortezomib and NPI-0052 trigger in vivo synergistic cytotoxicity in multiple myeloma. Blood 111:1654-64.

Chauhan D, Singh AV, Ciccarelli B, Richardson PG, Palladino MA, Anderson KC. Combination of novel proteasome inhibitor NPI-0052 and lenalidomide trigger in vitro and in vivo synergistic cytotoxicity in multiple myeloma. Blood 115:834-45.

Chauhan D, Uchiyama H, Akbarali Y, Urashima M, Yamamoto K, Libermann TA, Anderson KC. 1996. Multiple myeloma cell adhesion-induced interleukin-6 expression in bone marrow stromal cells involves activation of NF-kappa B. Blood 87:1104-12.

Chen C, Edelstein LC, Gelinas C. 2000. The Rel/NF-kappaB family directly activates expression of the apoptosis inhibitor Bcl-x(L). Mol Cell Biol 20:2687-95.

Chen CD, Welsbie DS, Tran C, Baek SH, Chen R, Vessella R, Rosenfeld MG, Sawyers CL. 2004a. Molecular determinants of resistance to antiandrogen therapy. Nat Med 10:33-9.

Chen D, Cui QC, Yang H, Barrea RA, Sarkar FH, Sheng S, Yan B, Reddy GP, Dou QP. 2007a. Clioquinol, a therapeutic agent for Alzheimer's disease, has proteasome-inhibitory, androgen receptor-suppressing, apoptosis-inducing, and antitumor activities in human prostate cancer cells and xenografts. Cancer Res 67:1636-44.

Chen D, Cui QC, Yang H, Dou QP. 2006. Disulfiram, a clinically used anti-alcoholism drug and copper-binding agent, induces apoptotic cell death in breast cancer cultures and xenografts via inhibition of the proteasome activity. Cancer Res 66:10425-33.

Chen D, Dou QP. 2008. New uses for old copper-binding drugs: converting the pro-angiogenic copper to a specific cancer cell death inducer. Expert Opin Ther Targets 12:739-48.

Chen D, Frezza M, Shakya R, Cui QC, Milacic V, Verani CN, Dou QP. 2007b. Inhibition of the proteasome activity by gallium(III) complexes contributes to their anti prostate tumor effects. Cancer Res 67:9258-65.

Chen D, Milacic V, Frezza M, Dou QP. 2009. Metal complexes, their cellular targets and potential for cancer therapy. Curr Pharm Des 15:777-91.

Chen D, Peng F, Cui QC, Daniel KG, Orlu S, Liu J, Dou QP. 2005. Inhibition of prostate cancer cellular proteasome activity by a pyrrolidine dithiocarbamate-copper complex is associated with suppression of proliferation and induction of apoptosis. Front Biosci 10:2932-9.

Chen F, Zhang Z, Bower J, Lu Y, Leonard SS, Ding M, Castranova V, Piwnica-Worms H, Shi X. 2002. Arsenite-induced Cdc25C degradation is through the KEN-box and ubiquitin-proteasome pathway. Proc Natl Acad Sci U S A 99:1990-5.

Chen W, Lee J, Cho SY, Fine HA. 2004b. Proteasome-mediated destruction of the cyclin a/cyclin-dependent kinase 2 complex suppresses tumor cell growth in vitro and in vivo. Cancer Res 64:3949-57.

Chen Y, Sawyers CL, Scher HI. 2008. Targeting the androgen receptor pathway in prostate cancer. Curr Opin Pharmacol 8:440-8.

Chen ZJ. 2005. Ubiquitin signalling in the NF-kappaB pathway. Nat Cell Biol 7:758-65.

Chen ZJ, Parent L, Maniatis T. 1996. Site-specific phosphorylation of IkappaBalpha by a novel ubiquitination-dependent protein kinase activity. Cell 84:853-62.

Chitambar CR. 2004a. Apoptotic mechanisms of gallium nitrate: basic and clinical investigations. Oncology (Williston Park) 18:39-44.

Chitambar CR. 2004b. Gallium compounds as antineoplastic agents. Curr Opin Oncol 16:547-52.

Chitambar CR, Matthaeus WG, Antholine WE, Graff K, O'Brien WJ. 1988. Inhibition of leukemic HL60 cell growth by transferrin-gallium: effects on ribonucleotide reductase and demonstration of drug synergy with hydroxyurea. Blood 72:1930-6.

Chitambar CR, Narasimhan J. 1991. Targeting iron-dependent DNA synthesis with gallium and transferrin-gallium. Pathobiology 59:3-10.

Ciechanover A. 1998. The ubiquitin-proteasome pathway: on protein death and cell life. EMBO J 17:7151-60.

Ciechanover A, Orian A, Schwartz AL. 2000. Ubiquitin-mediated proteolysis: biological regulation via destruction. Bioessays 22:442-51.

Cohen MB, Rokhlin OW. 2009. Mechanisms of prostate cancer cell survival after inhibition of AR expression. J Cell Biochem 106:363-71.

Cohen SM. 2007. New approaches for medicinal applications of bioinorganic chemistry. Curr Opin Chem Biol 11:115-20.

Collery P, Domingo JL, Keppler BK. 1996. Preclinical toxicology and tissue gallium distribution of a novel antitumour gallium compound: tris (8-quinolinolato) gallium (III). Anticancer Res 16:687-91.

Coux O, Tanaka K, Goldberg AL. 1996. Structure and functions of the 20S and 26S proteasomes. Annu Rev Biochem 65:801-47.

Crawford LJ, Walker B, Ovaa H, Chauhan D, Anderson KC, Morris TC, Irvine AE. 2006. Comparative selectivity and specificity of the proteasome inhibitors BzLLLCOCHO, PS-341, and MG-132. Cancer Res 66:6379-86.

Culig Z. 2004. Androgen receptor cross-talk with cell signalling pathways. Growth Factors 22:179-84.

Culig Z, Hobisch A, Cronauer MV, Radmayr C, Trapman J, Hittmair A, Bartsch G, Klocker H. 1994. Androgen receptor activation in prostatic tumor cell lines by insulin-like

growth factor-I, keratinocyte growth factor, and epidermal growth factor. Cancer Res 54:5474-8.

Cvek B, Milacic V, Taraba J, Dou QP. 2008. Ni(II), Cu(II), and Zn(II) diethyldithiocarbamate complexes show various activities against the proteasome in breast cancer cells. J Med Chem 51:6256-8.

Daniel KG, Chen D, Orlu S, Cui QC, Miller FR, Dou QP. 2005. Clioquinol and pyrrolidine dithiocarbamate complex with copper to form proteasome inhibitors and apoptosis inducers in human breast cancer cells. Breast Cancer Res 7:R897-908.

Daniel KG, Gupta P, Harbach RH, Guida WC, Dou QP. 2004. Organic copper complexes as a new class of proteasome inhibitors and apoptosis inducers in human cancer cells. Biochem Pharmacol 67:1139-51.

Davies AM, Ho C, Metzger AS, Beckett LA, Christensen S, Tanaka M, Lara PN, Lau DH, Gandara DR. 2007. Phase I study of two different schedules of bortezomib and pemetrexed in advanced solid tumors with emphasis on non-small cell lung cancer. J Thorac Oncol 2:1112-6.

de Gramont A, Figer A, Seymour M, Homerin M, Hmissi A, Cassidy J, Boni C, Cortes-Funes H, Cervantes A, Freyer G, Papamichael D, Le Bail N, Louvet C, Hendler D, de Braud F, Wilson C, Morvan F, Bonetti A. 2000. Leucovorin and fluorouracil with or without oxaliplatin as first-line treatment in advanced colorectal cancer. J Clin Oncol 18:2938-47.

DeMartino GN, Slaughter CA. 1999. The proteasome, a novel protease regulated by multiple mechanisms. J Biol Chem 274:22123-6.

Demo SD, Kirk CJ, Aujay MA, Buchholz TJ, Dajee M, Ho MN, Jiang J, Laidig GJ, Lewis ER, Parlati F, Shenk KD, Smyth MS, Sun CM, Vallone MK, Woo TM, Molineaux CJ, Bennett MK. 2007. Antitumor activity of PR-171, a novel irreversible inhibitor of the proteasome. Cancer Res 67:6383-91.

Deng C, Zhang P, Harper JW, Elledge SJ, Leder P. 1995. Mice lacking p21CIP1/WAF1 undergo normal development, but are defective in G1 checkpoint control. Cell 82:675-84.

Desoize B. 2004. Metals and metal compounds in cancer treatment. Anticancer Res 24:1529-44.

Diehl JA, Zindy F, Sherr CJ. 1997. Inhibition of cyclin D1 phosphorylation on threonine-286 prevents its rapid degradation via the ubiquitin-proteasome pathway. Genes Dev 11:957-72.

Diez M, Arroyo M, Cerdan FJ, Munoz M, Martin MA, Balibrea JL. 1989. Serum and tissue trace metal levels in lung cancer. Oncology 46:230-4.

Dou QP, Li B. 1999. Proteasome inhibitors as potential novel anticancer agents. Drug Resist Updat 2:215-223.

Edwards J, Krishna NS, Grigor KM, Bartlett JM. 2003. Androgen receptor gene amplification and protein expression in hormone refractory prostate cancer. Br J Cancer 89:552-6.

Einhorn L. 2003. Gallium nitrate in the treatment of bladder cancer. Semin Oncol 30:34-41.

Engel RH, Brown JA, Von Roenn JH, O'Regan RM, Bergan R, Badve S, Rademaker A, Gradishar WJ. 2007. A phase II study of single agent bortezomib in patients with metastatic breast cancer: a single institution experience. Cancer Invest 25:733-7.

Engman L, McNaughton M, Gajewska M, Kumar S, Birmingham A, Powis G. 2006. Thioredoxin reductase and cancer cell growth inhibition by organogold(III) compounds. Anticancer Drugs 17:539-44.

Federico A, Iodice P, Federico P, Del Rio A, Mellone MC, Catalano G. 2001. Effects of selenium and zinc supplementation on nutritional status in patients with cancer of digestive tract. Eur J Clin Nutr 55:293-7.

Fesik SW. 2005. Promoting apoptosis as a strategy for cancer drug discovery. Nat Rev Cancer 5:876-85.

Fisher RI, Bernstein SH, Kahl BS, Djulbegovic B, Robertson MJ, de Vos S, Epner E, Krishnan A, Leonard JP, Lonial S, Stadtmauer EA, O'Connor OA, Shi H, Boral AL, Goy A. 2006. Multicenter phase II study of bortezomib in patients with relapsed or refractory mantle cell lymphoma. J Clin Oncol 24:4867-74.

Ford OH, 3rd, Gregory CW, Kim D, Smitherman AB, Mohler JL. 2003. Androgen receptor gene amplification and protein expression in recurrent prostate cancer. J Urol 170:1817-21.

Fraker PJ, Lill-Elghanian DA. 2004. The many roles of apoptosis in immunity as modified by aging and nutritional status. J Nutr Health Aging 8:56-63.

Frankel A, Man S, Elliott P, Adams J, Kerbel RS. 2000. Lack of multicellular drug resistance observed in human ovarian and prostate carcinoma treated with the proteasome inhibitor PS-341. Clin Cancer Res 6:3719-28.

Franklin RB, Costello LC. 2007. Zinc as an anti-tumor agent in prostate cancer and in other cancers. Arch Biochem Biophys 463:211-7.

Franklin RB, Costello LC. 2009. The important role of the apoptotic effects of zinc in the development of cancers. J Cell Biochem 106:750-7.

Frezza M, Hindo SS, Tomco D, Allard MM, Cui QC, Heeg MJ, Chen D, Dou QP, Verani CN. 2009. Comparative Activities of Nickel(II) and Zinc(II) Complexes of Asymmetric [NN'O] Ligands as 26S Proteasome Inhibitors. Inorg Chem.

Fricker SP. 2007. Metal based drugs: from serendipity to design. Dalton Trans:4903-17.

Fuertes MA, Castilla J, Alonso C, Perez JM. 2002. Novel concepts in the development of platinum antitumor drugs. Curr Med Chem Anticancer Agents 2:539-51.

Fulda S, Debatin KM. 2004. Signaling through death receptors in cancer therapy. Curr Opin Pharmacol 4:327-32.

Fulda S, Debatin KM. 2006. Extrinsic versus intrinsic apoptosis pathways in anticancer chemotherapy. Oncogene 25:4798-811.

Furr BJ. 1996. The development of Casodex (bicalutamide): preclinical studies. Eur Urol 29 Suppl 2:83-95.

Galanski M. 2006. Recent developments in the field of anticancer platinum complexes. Recent Pat Anticancer Drug Discov 1:285-95.

Galanski M, Arion VB, Jakupec MA, Keppler BK. 2003. Recent developments in the field of tumor-inhibiting metal complexes. Curr Pharm Des 9:2078-89.

Gao G, Dou QP. 2000. N-terminal cleavage of bax by calpain generates a potent proapoptotic 18-kDa fragment that promotes bcl-2-independent cytochrome C release and apoptotic cell death. J Cell Biochem 80:53-72.

Glotzer M, Murray AW, Kirschner MW. 1991. Cyclin is degraded by the ubiquitin pathway. Nature 349:132-8.

Godfrey EG, Stewart J, Dargie HJ, Reid JL, Dominiczak M, Hamilton CA, McMurray J. 1994. Effects of ACE inhibitors on oxidation of human low density lipoprotein. Br J Clin Pharmacol 37:63-6.

Goldberg AL. 2003. Protein degradation and protection against misfolded or damaged proteins. Nature 426:895-9.

Goldberg AL, Cascio P, Saric T, Rock KL. 2002. The importance of the proteasome and subsequent proteolytic steps in the generation of antigenic peptides. Mol Immunol 39:147-64.

Goy A, Younes A, McLaughlin P, Pro B, Romaguera JE, Hagemeister F, Fayad L, Dang NH, Samaniego F, Wang M, Broglio K, Samuels B, Gilles F, Sarris AH, Hart S, Trehu E, Schenkein D, Cabanillas F, Rodriguez AM. 2005. Phase II study of proteasome inhibitor bortezomib in relapsed or refractory B-cell non-Hodgkin's lymphoma. J Clin Oncol 23:667-75.

Green DR, Reed JC. 1998. Mitochondria and apoptosis. Science 281:1309-12.

Green MA, Welch MJ. 1989. Gallium radiopharmaceutical chemistry. Int J Rad Appl Instrum B 16:435-48.

Gregory CW, He B, Johnson RT, Ford OH, Mohler JL, French FS, Wilson EM. 2001. A mechanism for androgen receptor-mediated prostate cancer recurrence after androgen deprivation therapy. Cancer Res 61:4315-9.

Groll M, Ditzel L, Lowe J, Stock D, Bochtler M, Bartunik HD, Huber R. 1997. Structure of 20S proteasome from yeast at 2.4 A resolution. Nature 386:463-71.

Groll M, Heinemeyer W, Jager S, Ullrich T, Bochtler M, Wolf DH, Huber R. 1999. The catalytic sites of 20S proteasomes and their role in subunit maturation: a mutational and crystallographic study. Proc Natl Acad Sci U S A 96:10976-83.

Groll M, Huber R, Potts BC. 2006. Crystal structures of Salinosporamide A (NPI-0052) and B (NPI-0047) in complex with the 20S proteasome reveal important consequences of beta-lactone ring opening and a mechanism for irreversible binding. J Am Chem Soc 128:5136-41.

Grumont RJ, Rourke IJ, Gerondakis S. 1999. Rel-dependent induction of A1 transcription is required to protect B cells from antigen receptor ligation-induced apoptosis. Genes Dev 13:400-11.

Gupta SK, Singh SP, Shukla VK. 2005. Copper, zinc, and Cu/Zn ratio in carcinoma of the gallbladder. J Surg Oncol 91:204-8.

Gupte A, Mumper RJ. 2009. Elevated copper and oxidative stress in cancer cells as a target for cancer treatment. Cancer Treat Rev 35:32-46.

Haas KL, Franz KJ. 2009. Application of metal coordination chemistry to explore and manipulate cell biology. Chem Rev 109:4921-60.

Habib FK, Dembinski TC, Stitch SR. 1980. The zinc and copper content of blood leucocytes and plasma from patients with benign and malignant prostates. Clin Chim Acta 104:329-35.

Hainsworth JD, Meluch AA, Spigel DR, Barton J, Jr., Simons L, Meng C, Gould B, Greco FA. 2007. Weekly docetaxel and bortezomib as first-line treatment for patients with hormone-refractory prostate cancer: a Minnie Pearl Cancer Research Network phase II trial. Clin Genitourin Cancer 5:278-83.

Hambley TW. 2007. Developing new metal-based therapeutics: challenges and opportunities. Dalton Trans:4929-37.

Hanahan D, Weinberg RA. 2000. The hallmarks of cancer. Cell 100:57-70.

Haq RU, Wereley JP, Chitambar CR. 1995. Induction of apoptosis by iron deprivation in human leukemic CCRF-CEM cells. Exp Hematol 23:428-32.

Harrap KR. 1985. Preclinical studies identifying carboplatin as a viable cisplatin alternative. Cancer Treat Rev 12 Suppl A:21-33.

Hart MM, Adamson RH. 1971. Antitumor activity and toxicity of salts of inorganic group 3a metals: aluminum, gallium, indium, and thallium. Proc Natl Acad Sci U S A 68:1623-6.

Hart MM, Smith CF, Yancey ST, Adamson RH. 1971. Toxicity and antitumor activity of gallium nitrate and periodically related metal salts. J Natl Cancer Inst 47:1121-7.

He XM, Carter DC. 1992. Atomic structure and chemistry of human serum albumin. Nature 358:209-15.

Hedley DW, Tripp EH, Slowiaczek P, Mann GJ. 1988. Effect of gallium on DNA synthesis by human T-cell lymphoblasts. Cancer Res 48:3014-8.

Heinlein CA, Chang C. 2002. Androgen receptor (AR) coregulators: an overview. Endocr Rev 23:175-200.

Heinlein CA, Chang C. 2004. Androgen receptor in prostate cancer. Endocr Rev 25:276-308.

Hengartner MO. 2000. The biochemistry of apoptosis. Nature 407:770-6.

Hershko A, Ciechanover A. 1998. The ubiquitin system. Annu Rev Biochem 67:425-79.

Hideshima T, Richardson P, Chauhan D, Palombella VJ, Elliott PJ, Adams J, Anderson KC. 2001. The proteasome inhibitor PS-341 inhibits growth, induces apoptosis, and overcomes drug resistance in human multiple myeloma cells. Cancer Res 61:3071-6.

Hindo SS, Frezza M, Tomco D, Heeg MJ, Hryhorczuk L, McGarvey BR, Dou QP, Verani CN. 2009. Metals in anticancer therapy: copper(II) complexes as inhibitors of the 20S proteasome. Eur J Med Chem 44:4353-61.

Ho E. 2004. Zinc deficiency, DNA damage and cancer risk. J Nutr Biochem 15:572-8.

Holler N, Zaru R, Micheau O, Thome M, Attinger A, Valitutti S, Bodmer JL, Schneider P, Seed B, Tschopp J. 2000. Fas triggers an alternative, caspase-8-independent cell death pathway using the kinase RIP as effector molecule. Nat Immunol 1:489-95.

Holm RH, Kennepohl P, Solomon EI. 1996. Structural and Functional Aspects of Metal Sites in Biology. Chem Rev 96:2239-2314.

Hoyt MA, Coffino P. 2004. Ubiquitin-free routes into the proteasome. Cell Mol Life Sci 61:1596-600.

Huang DC, Strasser A. 2000. BH3-Only proteins-essential initiators of apoptotic cell death. Cell 103:839-42.

Hunter AM, LaCasse EC, Korneluk RG. 2007. The inhibitors of apoptosis (IAPs) as cancer targets. Apoptosis 12:1543-68.

Imbert C, Hratchian HP, Lanznaster M, Heeg MJ, Hryhorczuk LM, McGarvey BR, Schlegel HB, Verani CN. 2005. Influence of ligand rigidity and ring substitution on the structural and electronic behavior of trivalent iron and gallium complexes with asymmetric tridentate ligands. Inorg Chem 44:7414-22.

Itoh S, Taki M, Takayama S, Nagatomo S, Kitagawa T, Sakurada N, Arakawa R, Fukuzumi S. 1999. Oxidation of Benzyl Alcohol with Cu(II) and Zn(II) Complexes of the Phenoxyl Radical as a Model of the Reaction of Galactose Oxidase. Angew Chem Int Ed Engl 38:2774-2776.

Jabbour E, Cortes JE, Giles FJ, O'Brien S, Kantarjian HM. 2007. Current and emerging treatment options in chronic myeloid leukemia. Cancer 109:2171-81.

Jagannath S, Barlogie B, Berenson J, Siegel D, Irwin D, Richardson PG, Niesvizky R, Alexanian R, Limentani SA, Alsina M, Adams J, Kauffman M, Esseltine DL, Schenkein DP, Anderson KC. 2004. A phase 2 study of two doses of bortezomib in relapsed or refractory myeloma. Br J Haematol 127:165-72.

Jagannath S, Barlogie B, Berenson JR, Siegel DS, Irwin D, Richardson PG, Niesvizky R, Alexanian R, Limentani SA, Alsina M, Esseltine DL, Anderson KC. 2008. Updated survival analyses after prolonged follow-up of the phase 2, multicenter CREST study of bortezomib in relapsed or refractory multiple myeloma. Br J Haematol 143:537-40.

Jakob C, Egerer K, Liebisch P, Turkmen S, Zavrski I, Kuckelkorn U, Heider U, Kaiser M, Fleissner C, Sterz J, Kleeberg L, Feist E, Burmester GR, Kloetzel PM, Sezer O. 2007. Circulating proteasome levels are an independent prognostic factor for survival in multiple myeloma. Blood 109:2100-5.

Jakupec MA, Galanski M, Arion VB, Hartinger CG, Keppler BK. 2008. Antitumour metal compounds: more than theme and variations. Dalton Trans:183-94.

Jakupec MA, Keppler BK. 2004a. Gallium and other main group metal compounds as antitumor agents. Met Ions Biol Syst 42:425-62.

Jakupec MA, Keppler BK. 2004b. Gallium in cancer treatment. Curr Top Med Chem 4:1575-83.

Jamieson ER, Lippard SJ. 1999. Structure, Recognition, and Processing of Cisplatin-DNA Adducts. Chem Rev 99:2467-98.

Jemal A, Siegel R, Ward E, Hao Y, Xu J, Murray T, Thun MJ. 2008. Cancer statistics, 2008. CA Cancer J Clin 58:71-96.

Jemal A, Siegel R, Ward E, Hao Y, Xu J, Thun MJ. 2009. Cancer statistics, 2009. CA Cancer J Clin 59:225-49.

Jia L, Shen HC, Wantroba M, Khalid O, Liang G, Wang Q, Gentzschein E, Pinski JK, Stanczyk FZ, Jones PA, Coetzee GA. 2006. Locus-wide chromatin remodeling and enhanced androgen receptor-mediated transcription in recurrent prostate tumor cells. Mol Cell Biol 26:7331-41.

Joazeiro CA, Anderson KC, Hunter T. 2006. Proteasome inhibitor drugs on the rise. Cancer Res 66:7840-2.

Kalejta RF, Shenk T. 2003. Proteasome-dependent, ubiquitin-independent degradation of the Rb family of tumor suppressors by the human cytomegalovirus pp71 protein. Proc Natl Acad Sci U S A 100:3263-8.

Kane RC, Bross PF, Farrell AT, Pazdur R. 2003. Velcade: U.S. FDA approval for the treatment of multiple myeloma progressing on prior therapy. Oncologist 8:508-13.

Kane RC, Dagher R, Farrell A, Ko CW, Sridhara R, Justice R, Pazdur R. 2007. Bortezomib for the treatment of mantle cell lymphoma. Clin Cancer Res 13:5291-4.

Kelland L. 2007. The resurgence of platinum-based cancer chemotherapy. Nat Rev Cancer 7:573-84.

Kim BE, Nevitt T, Thiele DJ. 2008. Mechanisms for copper acquisition, distribution and regulation. Nat Chem Biol 4:176-85.

King RW, Deshaies RJ, Peters JM, Kirschner MW. 1996. How proteolysis drives the cell cycle. Science 274:1652-9.

Kirin SI, Dubon P, Weyhermuller T, Bill E, Metzler-Nolte N. 2005. Amino acid and peptide bioconjugates of copper(II) and zinc(II) complexes with a modified N,N-bis(2-picolyl)amine ligand. Inorg Chem 44:5405-15.

Kong X, Alvarez-Castelao B, Lin Z, Castano JG, Caro J. 2007. Constitutive/hypoxic degradation of HIF-alpha proteins by the proteasome is independent of von Hippel Lindau protein ubiquitylation and the transactivation activity of the protein. J Biol Chem 282:15498-505.

Kostova I. 2006. Platinum complexes as anticancer agents. Recent Pat Anticancer Drug Discov 1:1-22.

Kuhn DJ, Chen Q, Voorhees PM, Strader JS, Shenk KD, Sun CM, Demo SD, Bennett MK, van Leeuwen FW, Chanan-Khan AA, Orlowski RZ. 2007. Potent activity of carfilzomib, a novel, irreversible inhibitor of the ubiquitin-proteasome pathway, against preclinical models of multiple myeloma. Blood 110:3281-90.

Kuo HW, Chen SF, Wu CC, Chen DR, Lee JH. 2002. Serum and tissue trace elements in patients with breast cancer in Taiwan. Biol Trace Elem Res 89:1-11.

Lanznaster M, Hratchian HP, Heeg MJ, Hryhorczuk LM, McGarvey BR, Schlegel HB, Verani CN. 2006. Structural and electronic behavior of unprecedented five-coordinate iron(III) and gallium(III) complexes with a new phenol-rich electroactive ligand. Inorg Chem 45:955-7.

Lazebnik YA, Kaufmann SH, Desnoyers S, Poirier GG, Earnshaw WC. 1994. Cleavage of poly(ADP-ribose) polymerase by a proteinase with properties like ICE. Nature 371:346-7.

Lee DK, Chang C. 2003. Endocrine mechanisms of disease: Expression and degradation of androgen receptor: mechanism and clinical implication. J Clin Endocrinol Metab 88:4043-54.

Li B, Dou QP. 2000. Bax degradation by the ubiquitin/proteasome-dependent pathway: involvement in tumor survival and progression. Proc Natl Acad Sci U S A 97:3850-5.

Lin HK, Altuwaijri S, Lin WJ, Kan PY, Collins LL, Chang C. 2002. Proteasome activity is required for androgen receptor transcriptional activity via regulation of androgen receptor nuclear translocation and interaction with coregulators in prostate cancer cells. J Biol Chem 277:36570-6.

Lopes UG, Erhardt P, Yao R, Cooper GM. 1997. p53-dependent induction of apoptosis by proteasome inhibitors. J Biol Chem 272:12893-6.

Ma MH, Yang HH, Parker K, Manyak S, Friedman JM, Altamirano C, Wu ZQ, Borad MJ, Frantzen M, Roussos E, Neeser J, Mikail A, Adams J, Sjak-Shie N, Vescio RA, Berenson JR. 2003. The proteasome inhibitor PS-341 markedly enhances sensitivity of multiple myeloma tumor cells to chemotherapeutic agents. Clin Cancer Res 9:1136-44.

Marcon G, Carotti S, Coronnello M, Messori L, Mini E, Orioli P, Mazzei T, Cinellu MA, Minghetti G. 2002. Gold(III) complexes with bipyridyl ligands: solution chemistry, cytotoxicity, and DNA binding properties. J Med Chem 45:1672-7.

Margalioth EJ, Schenker JG, Chevion M. 1983. Copper and zinc levels in normal and malignant tissues. Cancer 52:868-72.

Marzano C, Pellei M, Tisato F, Santini C. 2009. Copper complexes as anticancer agents. Anticancer Agents Med Chem 9:185-211.

Meggers E. 2009. Targeting proteins with metal complexes. Chem Commun (Camb):1001-10.

Melchior M, Rettig SJ, Liboiron BD, Thompson KH, Yuen VG, McNeill JH, Orvig C. 2001. Insulin-enhancing vanadium(III) complexes. Inorg Chem 40:4686-90.

Mertz W. 1993. Essential trace metals: new definitions based on new paradigms. Nutr Rev 51:287-95.

Messersmith WA, Baker SD, Lassiter L, Sullivan RA, Dinh K, Almuete VI, Wright JJ, Donehower RC, Carducci MA, Armstrong DK. 2006. Phase I trial of bortezomib in combination with docetaxel in patients with advanced solid tumors. Clin Cancer Res 12:1270-5.

Messori L, Marcon G, Orioli P. 2003. Gold(III) Compounds as New Family of Anticancer Drugs. Bioinorg Chem Appl:177-87.

Messori L, Orioli P, Tempi C, Marcon G. 2001. Interactions of selected gold(III) complexes with calf thymus DNA. Biochem Biophys Res Commun 281:352-60.

Milacic V, Chen D, Giovagnini L, Diez A, Fregona D, Dou QP. 2008a. Pyrrolidine dithiocarbamate-zinc(II) and -copper(II) complexes induce apoptosis in tumor cells by inhibiting the proteasomal activity. Toxicol Appl Pharmacol 231:24-33.

Milacic V, Chen D, Ronconi L, Landis-Piwowar KR, Fregona D, Dou QP. 2006. A novel anticancer gold(III) dithiocarbamate compound inhibits the activity of a purified 20S

proteasome and 26S proteasome in human breast cancer cell cultures and xenografts. Cancer Res 66:10478-86.

Milacic V, Fregona D, Dou QP. 2008b. Gold complexes as prospective metal-based anticancer drugs. Histol Histopathol 23:101-8.

Minucci S, Pelicci PG. 2006. Histone deacetylase inhibitors and the promise of epigenetic (and more) treatments for cancer. Nat Rev Cancer 6:38-51.

Mirabelli CK, Johnson RK, Hill DT, Faucette LF, Girard GR, Kuo GY, Sung CM, Crooke ST. 1986. Correlation of the in vitro cytotoxic and in vivo antitumor activities of gold(I) coordination complexes. J Med Chem 29:218-23.

Mitsiades N, Mitsiades CS, Richardson PG, Poulaki V, Tai YT, Chauhan D, Fanourakis G, Gu X, Bailey C, Joseph M, Libermann TA, Schlossman R, Munshi NC, Hideshima T, Anderson KC. 2003. The proteasome inhibitor PS-341 potentiates sensitivity of multiple myeloma cells to conventional chemotherapeutic agents: therapeutic applications. Blood 101:2377-80.

Montana AM, Batalla C. 2009. The rational design of anticancer platinum complexes: the importance of the structure-activity relationship. Curr Med Chem 16:2235-60.

Montgomery RB, Mostaghel EA, Vessella R, Hess DL, Kalhorn TF, Higano CS, True LD, Nelson PS. 2008. Maintenance of intratumoral androgens in metastatic prostate cancer: a mechanism for castration-resistant tumor growth. Cancer Res 68:4447-54.

Mortenson MM, Schlieman MG, Virudachalam S, Lara PN, Gandara DG, Davies AM, Bold RJ. 2005. Reduction in BCL-2 levels by 26S proteasome inhibition with bortezomib is associated with induction of apoptosis in small cell lung cancer. Lung Cancer 49:163-70.

Murakami M, Hirano T. 2008. Intracellular zinc homeostasis and zinc signaling. Cancer Sci 99:1515-22.

Nalepa G, Rolfe M, Harper JW. 2006. Drug discovery in the ubiquitin-proteasome system. Nat Rev Drug Discov 5:596-613.

Nayak SB, Bhat VR, Upadhyay D, Udupa SL. 2003. Copper and ceruloplasmin status in serum of prostate and colon cancer patients. Indian J Physiol Pharmacol 47:108-10.

Neidle S, Thurston DE. 2005. Chemical approaches to the discovery and development of cancer therapies. Nat Rev Cancer 5:285-96.

Nencioni A, Grunebach F, Patrone F, Ballestrero A, Brossart P. 2007. Proteasome inhibitors: antitumor effects and beyond. Leukemia 21:30-6.

Niu Y, Altuwaijri S, Lai KP, Wu CT, Ricke WA, Messing EM, Yao J, Yeh S, Chang C. 2008. Androgen receptor is a tumor suppressor and proliferator in prostate cancer. Proc Natl Acad Sci U S A 105:12182-7.

O'Connor OA, Wright J, Moskowitz C, Muzzy J, MacGregor-Cortelli B, Stubblefield M, Straus D, Portlock C, Hamlin P, Choi E, Dumetrescu O, Esseltine D, Trehu E, Adams J, Schenkein D, Zelenetz AD. 2005. Phase II clinical experience with the novel proteasome inhibitor bortezomib in patients with indolent non-Hodgkin's lymphoma and mantle cell lymphoma. J Clin Oncol 23:676-84.

Okada H, Mak TW. 2004. Pathways of apoptotic and non-apoptotic death in tumour cells. Nat Rev Cancer 4:592-603.

Olaleye SB, Farombi EO. 2006. Attenuation of indomethacin- and HCl/ethanol-induced oxidative gastric mucosa damage in rats by kolaviron, a natural biflavonoid of Garcinia kola seed. Phytother Res 20:14-20.

Orlowski RZ. 1999. The role of the ubiquitin-proteasome pathway in apoptosis. Cell Death Differ 6:303-13.

Orlowski RZ, Baldwin AS, Jr. 2002. NF-kappaB as a therapeutic target in cancer. Trends Mol Med 8:385-9.

Orlowski RZ, Kuhn DJ. 2008. Proteasome inhibitors in cancer therapy: lessons from the first decade. Clin Cancer Res 14:1649-57.

Orlowski RZ, Stinchcombe TE, Mitchell BS, Shea TC, Baldwin AS, Stahl S, Adams J, Esseltine DL, Elliott PJ, Pien CS, Guerciolini R, Anderson JK, Depcik-Smith ND, Bhagat R, Lehman MJ, Novick SC, O'Connor OA, Soignet SL. 2002. Phase I trial of the proteasome inhibitor PS-341 in patients with refractory hematologic malignancies. J Clin Oncol 20:4420-7.

Orosz CG, Wakely E, Bergese SD, VanBuskirk AM, Ferguson RM, Mullet D, Apseloff G, Gerber N. 1996. Prevention of murine cardiac allograft rejection with gallium nitrate. Comparison with anti-CD4 monoclonal antibody. Transplantation 61:783-91.

Orvig C, Abrams MJ. 1999. Medicinal inorganic chemistry: introduction. Chem Rev 99:2201-4.

Ott I, Gust R. 2007. Non platinum metal complexes as anti-cancer drugs. Arch Pharm (Weinheim) 340:117-26.

Pagano M, Tam SW, Theodoras AM, Beer-Romero P, Del Sal G, Chau V, Yew PR, Draetta GF, Rolfe M. 1995. Role of the ubiquitin-proteasome pathway in regulating abundance of the cyclin-dependent kinase inhibitor p27. Science 269:682-5.

Palombella VJ, Rando OJ, Goldberg AL, Maniatis T. 1994. The ubiquitin-proteasome pathway is required for processing the NF-kappa B1 precursor protein and the activation of NF-kappa B. Cell 78:773-85.

Papandreou CN, Daliani DD, Nix D, Yang H, Madden T, Wang X, Pien CS, Millikan RE, Tu SM, Pagliaro L, Kim J, Adams J, Elliott P, Esseltine D, Petrusich A, Dieringer P, Perez C, Logothetis CJ. 2004. Phase I trial of the proteasome inhibitor bortezomib in patients with advanced solid tumors with observations in androgen-independent prostate cancer. J Clin Oncol 22:2108-21.

Perez-Galan P, Roue G, Villamor N, Montserrat E, Campo E, Colomer D. 2006. The proteasome inhibitor bortezomib induces apoptosis in mantle-cell lymphoma through generation of ROS and Noxa activation independent of p53 status. Blood 107:257-64.

Peters JM, Cejka Z, Harris JR, Kleinschmidt JA, Baumeister W. 1993. Structural features of the 26 S proteasome complex. J Mol Biol 234:932-7.

Pink JJ, Wuerzberger-Davis S, Tagliarino C, Planchon SM, Yang X, Froelich CJ, Boothman DA. 2000. Activation of a cysteine protease in MCF-7 and T47D breast cancer cells during beta-lapachone-mediated apoptosis. Exp Cell Res 255:144-55.

Prasad AS. 1995. Zinc: an overview. Nutrition 11:93-9.

Prasad AS, Beck FW, Doerr TD, Shamsa FH, Penny HS, Marks SC, Kaplan J, Kucuk O, Mathog RH. 1998. Nutritional and zinc status of head and neck cancer patients: an interpretive review. J Am Coll Nutr 17:409-18.

Provinciali M, Di Stefano G, Fabris N. 1995. Dose-dependent opposite effect of zinc on apoptosis in mouse thymocytes. Int J Immunopharmacol 17:735-44.

Radisky D, Kaplan J. 1999. Regulation of transition metal transport across the yeast plasma membrane. J Biol Chem 274:4481-4.

Rattan AK, Arad Y. 1998. Temporal and kinetic determinants of the inhibition of LDL oxidation by N-acetylcysteine (NAC). Atherosclerosis 138:319-27.

Redman BG, Esper P, Pan Q, Dunn RL, Hussain HK, Chenevert T, Brewer GJ, Merajver SD. 2003. Phase II trial of tetrathiomolybdate in patients with advanced kidney cancer. Clin Cancer Res 9:1666-72.

Reed JC. 1997. Bcl-2 family proteins: regulators of apoptosis and chemoresistance in hematologic malignancies. Semin Hematol 34:9-19.

Reedijk J. 2003. New clues for platinum antitumor chemistry: kinetically controlled metal binding to DNA. Proc Natl Acad Sci U S A 100:3611-6.

Richardson PG, Barlogie B, Berenson J, Singhal S, Jagannath S, Irwin D, Rajkumar SV, Srkalovic G, Alsina M, Alexanian R, Siegel D, Orlowski RZ, Kuter D, Limentani SA, Lee S, Hideshima T, Esseltine DL, Kauffman M, Adams J, Schenkein DP, Anderson KC. 2003. A phase 2 study of bortezomib in relapsed, refractory myeloma. N Engl J Med 348:2609-17.

Richardson PG, Sonneveld P, Schuster M, Irwin D, Stadtmauer E, Facon T, Harousseau JL, Ben-Yehuda D, Lonial S, Goldschmidt H, Reece D, Miguel JS, Blade J, Boccadoro M, Cavenagh J, Alsina M, Rajkumar SV, Lacy M, Jakubowiak A, Dalton W, Boral A, Esseltine DL, Schenkein D, Anderson KC. 2007. Extended follow-up of a phase 3 trial in relapsed multiple myeloma: final time-to-event results of the APEX trial. Blood 110:3557-60.

Richardson PG, Sonneveld P, Schuster MW, Irwin D, Stadtmauer EA, Facon T, Harousseau JL, Ben-Yehuda D, Lonial S, Goldschmidt H, Reece D, San-Miguel JF, Blade J, Boccadoro M, Cavenagh J, Dalton WS, Boral AL, Esseltine DL, Porter JB, Schenkein D, Anderson KC. 2005. Bortezomib or high-dose dexamethasone for relapsed multiple myeloma. N Engl J Med 352:2487-98.

Ronconi L, Giovagnini L, Marzano C, Bettio F, Graziani R, Pilloni G, Fregona D. 2005. Gold dithiocarbamate derivatives as potential antineoplastic agents: design, spectroscopic properties, and in vitro antitumor activity. Inorg Chem 44:1867-81.

Ronconi L, Marzano C, Zanello P, Corsini M, Miolo G, Macca C, Trevisan A, Fregona D. 2006. Gold(III) dithiocarbamate derivatives for the treatment of cancer: solution chemistry, DNA binding, and hemolytic properties. J Med Chem 49:1648-57.

Rorabacher DB. 2004. Electron transfer by copper centers. Chem Rev 104:651-97.

Roth W, Reed JC. 2002. Apoptosis and cancer: when BAX is TRAILing away. Nat Med 8:216-8.

Ryan DP, O'Neil BH, Supko JG, Rocha Lima CM, Dees EC, Appleman LJ, Clark J, Fidias P, Orlowski RZ, Kashala O, Eder JP, Cusack JC, Jr. 2006. A Phase I study of bortezomib plus irinotecan in patients with advanced solid tumors. Cancer 107:2688-97.

Saggioro D, Rigobello MP, Paloschi L, Folda A, Moggach SA, Parsons S, Ronconi L, Fregona D, Bindoli A. 2007. Gold(III)-dithiocarbamato complexes induce cancer cell death triggered by thioredoxin redox system inhibition and activation of ERK pathway. Chem Biol 14:1128-39.

Sarkar FH, Li Y. 2009. Harnessing the fruits of nature for the development of multi-targeted cancer therapeutics. Cancer Treat Rev 35:597-607.

Schwartz AE, Leddicotte GW, Fink RW, Friedman EW. 1974. Trace elements in noraml and malignant human breast tissue. Surgery 76:325-9.

Scott LE, Orvig C. 2009. Medicinal inorganic chemistry approaches to passivation and removal of aberrant metal ions in disease. Chem Rev 109:4885-910.

Serrano M, Gomez-Lahoz E, DePinho RA, Beach D, Bar-Sagi D. 1995. Inhibition of ras-induced proliferation and cellular transformation by p16INK4. Science 267:249-52.

Shah JJ, Orlowski RZ. 2009. Proteasome inhibitors in the treatment of multiple myeloma. Leukemia 23:1964-79.

Shakya R, Imbert C, Hratchian HP, Lanznaster M, Heeg MJ, McGarvey BR, Allard M, Schlegel HB, Verani CN. 2006a. Structural, spectroscopic, and electrochemical behavior of trans-phenolato cobalt(III) complexes of asymmetric NN'O ligands as archetypes for metallomesogens. Dalton Trans:2517-25.

Shakya R, Peng F, Liu J, Heeg MJ, Verani CN. 2006b. Synthesis, structure, and anticancer activity of gallium(III) complexes with asymmetric tridentate ligands: growth inhibition and apoptosis induction of cisplatin-resistant neuroblastoma cells. Inorg Chem 45:6263-8.

Shen HC, Balk SP. 2009. Development of androgen receptor antagonists with promising activity in castration-resistant prostate cancer. Cancer Cell 15:461-3.

Sherr CJ, Roberts JM. 1995. Inhibitors of mammalian G1 cyclin-dependent kinases. Genes Dev 9:1149-63.

Shi G, Chen D, Zhai G, Chen MS, Cui QC, Zhou Q, He B, Dou QP, Jiang G. 2009. The proteasome is a molecular target of environmental toxic organotins. Environ Health Perspect 117:379-86.

Shimazaki Y, Huth S, Odani A, Yamauchi O. 2000. A Structural Model for the Galactose Oxidase Active Site which Shows Counteranion-Dependent Phenoxyl Radical Formation by Disproportionation This work was supported by Grants-in-Aid for Scientific Research (No. 09304062 and 0149219 (Priority Areas) to O.Y. and No. 07CE2004(COE) to A.O.) from the Ministry of Education, Science, Sports, and Culture of Japan, for which we express our thanks. Angew Chem Int Ed Engl 39:1666-1669.

Siddik ZH. 2003. Cisplatin: mode of cytotoxic action and molecular basis of resistance. Oncogene 22:7265-79.

Solit DB, Rosen N. 2006. Hsp90: a novel target for cancer therapy. Curr Top Med Chem 6:1205-14.

Stefanidou M, Maravelias C, Dona A, Spiliopoulou C. 2006. Zinc: a multipurpose trace element. Arch Toxicol 80:1-9.

Steinkamp MP, O'Mahony OA, Brogley M, Rehman H, Lapensee EW, Dhanasekaran S, Hofer MD, Kuefer R, Chinnaiyan A, Rubin MA, Pienta KJ, Robins DM. 2009. Treatment-dependent androgen receptor mutations in prostate cancer exploit multiple mechanisms to evade therapy. Cancer Res 69:4434-42.

Sterz J, von Metzler I, Hahne JC, Lamottke B, Rademacher J, Heider U, Terpos E, Sezer O. 2008. The potential of proteasome inhibitors in cancer therapy. Expert Opin Investig Drugs 17:879-95.

Storr T, Sugai Y, Barta CA, Mikata Y, Adam MJ, Yano S, Orvig C. 2005. Carbohydrate-appended 2,2'-dipicolylamine metal complexes as potential imaging agents. Inorg Chem 44:2698-705.

Szweda PA, Friguet B, Szweda LI. 2002. Proteolysis, free radicals, and aging. Free Radic Biol Med 33:29-36.

Tapiero H, Townsend DM, Tew KD. 2003. Trace elements in human physiology and pathology. Copper. Biomed Pharmacother 57:386-98.

Taplin ME. 2008. Androgen receptor: role and novel therapeutic prospects in prostate cancer. Expert Rev Anticancer Ther 8:1495-508.

Taplin ME, Balk SP. 2004. Androgen receptor: a key molecule in the progression of prostate cancer to hormone independence. J Cell Biochem 91:483-90.

Thalmann GN, Anezinis PE, Chang SM, Zhau HE, Kim EE, Hopwood VL, Pathak S, von Eschenbach AC, Chung LW. 1994. Androgen-independent cancer progression and bone metastasis in the LNCaP model of human prostate cancer. Cancer Res 54:2577-81.

Thompson KH, Orvig C. 2003. Boon and bane of metal ions in medicine. Science 300:936-9.

Tomlins SA, Laxman B, Dhanasekaran SM, Helgeson BE, Cao X, Morris DS, Menon A, Jing X, Cao Q, Han B, Yu J, Wang L, Montie JE, Rubin MA, Pienta KJ, Roulston D, Shah RB, Varambally S, Mehra R, Chinnaiyan AM. 2007. Distinct classes of chromosomal rearrangements create oncogenic ETS gene fusions in prostate cancer. Nature 448:595-9.

Tomlins SA, Rhodes DR, Perner S, Dhanasekaran SM, Mehra R, Sun XW, Varambally S, Cao X, Tchinda J, Kuefer R, Lee C, Montie JE, Shah RB, Pienta KJ, Rubin MA,

Chinnaiyan AM. 2005. Recurrent fusion of TMPRSS2 and ETS transcription factor genes in prostate cancer. Science 310:644-8.

Tran C, Ouk S, Clegg NJ, Chen Y, Watson PA, Arora V, Wongvipat J, Smith-Jones PM, Yoo D, Kwon A, Wasielewska T, Welsbie D, Chen CD, Higano CS, Beer TM, Hung DT, Scher HI, Jung ME, Sawyers CL. 2009. Development of a second-generation antiandrogen for treatment of advanced prostate cancer. Science 324:787-90.

Tsai MJ, O'Malley BW. 1994. Molecular mechanisms of action of steroid/thyroid receptor superfamily members. Annu Rev Biochem 63:451-86.

Turecky L, Kalina P, Uhlikova E, Namerova S, Krizko J. 1984. Serum ceruloplasmin and copper levels in patients with primary brain tumors. Klin Wochenschr 62:187-9.

Vaidyanathan M, Viswanathan R, Palaniandavar M, Balasubramanian T, Prabhaharan P, Muthiah TP. 1998. Copper(II) Complexes with Unusual Axial Phenolate Coordination as Structural Models for the Active Site in Galactose Oxidase: X-ray Crystal Structures and Spectral and Redox Properties of [Cu(bpnp)X] Complexes. Inorg Chem 37:6418-6427.

Waller AS, Sharrard RM, Berthon P, Maitland NJ. 2000. Androgen receptor localisation and turnover in human prostate epithelium treated with the antiandrogen, casodex. J Mol Endocrinol 24:339-51.

Wang CY, Mayo MW, Korneluk RG, Goeddel DV, Baldwin AS, Jr. 1998. NF-kappaB antiapoptosis: induction of TRAF1 and TRAF2 and c-IAP1 and c-IAP2 to suppress caspase-8 activation. Science 281:1680-3.

Wang D, Lippard SJ. 2005. Cellular processing of platinum anticancer drugs. Nat Rev Drug Discov 4:307-20.

Wang Y, He QY, Sun RW, Che CM, Chiu JF. 2005. GoldIII porphyrin 1a induced apoptosis by mitochondrial death pathways related to reactive oxygen species. Cancer Res 65:11553-64.

Weick JK, Stephens RL, Baker LH, Jones SE. 1983. Gallium nitrate in malignant lymphoma: a Southwest Oncology Group study. Cancer Treat Rep 67:823-5.

Whitby FG, Masters EI, Kramer L, Knowlton JR, Yao Y, Wang CC, Hill CP. 2000. Structural basis for the activation of 20S proteasomes by 11S regulators. Nature 408:115-20.

Won KA, Reed SI. 1996. Activation of cyclin E/CDK2 is coupled to site-specific autophosphorylation and ubiquitin-dependent degradation of cyclin E. EMBO J 15:4182-93.

Wood DE, Newcomb EW. 2000. Cleavage of Bax enhances its cell death function. Exp Cell Res 256:375-82.

Yan YK, Melchart M, Habtemariam A, Sadler PJ. 2005. Organometallic chemistry, biology and medicine: ruthenium arene anticancer complexes. Chem Commun (Camb):4764-76.

Yang CH, Gonzalez-Angulo AM, Reuben JM, Booser DJ, Pusztai L, Krishnamurthy S, Esseltine D, Stec J, Broglio KR, Islam R, Hortobagyi GN, Cristofanilli M. 2006a. Bortezomib (VELCADE) in metastatic breast cancer: pharmacodynamics, biological effects, and prediction of clinical benefits. Ann Oncol 17:813-7.

Yang H, Chen D, Cui QC, Yuan X, Dou QP. 2006b. Celastrol, a triterpene extracted from the Chinese "Thunder of God Vine," is a potent proteasome inhibitor and suppresses human prostate cancer growth in nude mice. Cancer Res 66:4758-65.

Yang H, Murthy S, Sarkar FH, Sheng S, Reddy GP, Dou QP. 2008. Calpain-mediated androgen receptor breakdown in apoptotic prostate cancer cells. J Cell Physiol 217:569-76.

Yang H, Zonder JA, Dou QP. 2009. Clinical development of novel proteasome inhibitors for cancer treatment. Expert Opin Investig Drugs 18:957-71.

Zhao G, Lin H. 2005. Metal complexes with aromatic N-containing ligands as potential agents in cancer treatment. Curr Med Chem Anticancer Agents 5:137-47.

Zhao H, Eide D. 1996. The yeast ZRT1 gene encodes the zinc transporter protein of a high-affinity uptake system induced by zinc limitation. Proc Natl Acad Sci U S A 93:2454-8.

Zhou D, Brown SA, Yu T, Chen G, Barve S, Kang BC, Thompson JS. 1999. A high dose of ionizing radiation induces tissue-specific activation of nuclear factor-kappaB in vivo. Radiat Res 151:703-9.

Zhu C, Raber J, Eriksson LA. 2005. Hydrolysis process of the second generation platinum-based anticancer drug cis-amminedichlorocyclohexylamineplatinum(II). J Phys Chem B 109:12195-205.

Zong WX, Ditsworth D, Bauer DE, Wang ZQ, Thompson CB. 2004. Alkylating DNA damage stimulates a regulated form of necrotic cell death. Genes Dev 18:1272-82.

Zowczak M, Iskra M, Torlinski L, Cofta S. 2001. Analysis of serum copper and zinc concentrations in cancer patients. Biol Trace Elem Res 82:1-8.

ABSTRACT

ACTIVATION OF TUMOR CELL DEATH PROGRAM BY TARGETING THE UBIQUITIN-PROTEASOME PATHWAY: SIGNIFICANCE IN CANCER TREATMENT AND PREVENTION

by

MICHAEL FREZZA

August 2010

Advisor: Dr. Q. Ping Dou

Major: Cancer Biology

Degree: Doctor of Philosophy

The ubiquitin-proteasome pathway serves as a quality control mechanism to regulate the degradation of intracellular proteins involved in a wide array of cellular processes including tumorigeneis. Thus targeting key features of protein turnover responsible for the growth and proliferation of cancer have emerged as a favorable approach in cancer therapy. Both *in vitro* and *in vivo* experimental and clinical results have demonstrated the potential use of proteasome inhibitors as novel anticancer drugs. The widespread clinical success of platinum-containing drugs served as a catalyst for investigating other metal complexes for the treatment of human cancer. In an effort to improve upon the limitations of platinum anticancer drugs, different metals and metal complexes that pose different mechanisms of action has been investigated as potential anticancer drugs. We have previously found that different metal containing complexes, including those of copper, zinc, gold, and tin could activate tumor cell death by inhibiting the proteasome. Therefore, it is proposed that gallium could similarly act as a proteasome inhibitor and apoptosis inducer in human tumor cells. The data presented in this dissertation strongly supports this hypothesis. We found that

gallium-cotaining [NN'O] tridentate ligands appended with halogen substituents could inhibit the proteasomal activity *in vitro* and in human prostate cancer cells. Importantly, the most biologically active complex (**5**) could inhibit tumor growth in mice-bearing prostate cancer xenografts associated with inhibition of proteasomal activity and apoptosis. Based on the favorable cytotoxic activity of [NN'O] ligands complexed with gallium, subsequent studies relied on this model architecture complexed to different bivalent transistion metals to gain insight into the pharmacophore responsible for their proteasome-inhibitory effects. Since elevated levels of copper are a trademark of many tumors, targeting heightened levels of copper with copper-binding compounds as a means of tumor growth ablation was proposed. It was found that that these copper complexes (**1-3**), with distinct stoichiometries and protonation states, acted as proteasome inhibitiors and apoptosis inducers in cultured prostate cancer cells, and importantly the species $[CuL^{I}]^{+}$ as the minimal pharmacophore responsible for this effect. This hypothesis was further substantiated by the finding that Zinc-containing [NN'O] complex (**2**), but not Nickel (**1**) could inhibit the proteasomal activity of a purified 20S proteasome and culture prostate cancer cells associated with massive tumor cell death. These results strengthen our current working hypothesis that fast ligand dissociation (Zn-complex) is required to free up the $[ML^{IA}]^{+}$ capable of interaction with the proteasome. This is in agreement with previous studies showing that proteasome inhibition by zinc-containing dithiocarbamate derivatives is assoiciated with apoptosis induction. In contrast, chapters 5 and 6 were primarily focused on the mechanistic properties of proteasome inhibition and its downstream events. Since we have previously reported on a gold(III) complex showing potent *in vitro* and *in vivo* growth inhibitory activity associated with proteasome inhibition and apoptosis, two gold compounds that differ in the oxidation

state of the metal were investigated to gain mechanistic insight into their biological activities. The data in this dissertation provides compelling evidence for the involvement of ROS-mediated proteasome inhibition by gold(III), but not gold(I), and highlights distinct mechanisms of action associated with their biological effects. Since it has been shown that proteasome inhibition is tightly linked to apoptosis in AR (+) prostate cancer cells, it is proposed that AR can influence the regulatory events associated with cell death in prostate cancer cells. Mechanistic studies from chapter 6 provide convincing evidence that proteasome inhibitor- or chemotherapy- induced cell death resulted in significantly higher levels of caspase-3 activity in AR independent prostate cancer cells compared to stably or transiently expressing AR cells. Interestingly, lower levels of caspase 3 activity were partially reversed with the addition of an AR antagonist in AR-dependent prostate cancer cells. These important findings could help facilitate the design of novel therapeutic strategies in the treatment of prostate cancer. Taken together, the studies presented in this dissertation could hold tremendous prognostic and therapeutic potential in the treatment of human cancer.

AUTOBIOGRAPHICAL STATEMENT

Michael J. Frezza

Michael received a Bachelor of Science degree in Biological Sciences from Wayne State University in 2000. He commenced his studies in the Graduate Program in Cancer Biology at the Wayne State University School of Medicine in the fall of 2005 under the guidance of Dr. Q. Ping Dou. During his tenure as a Ph.D. student, Michael published 5 research articles as first author or co-first author. Additionally, he published three review articles as first author, and has contributed to 13 publications in total. A major focus of Michael's research has been on the proteasome as a molecular target in anticancer drug discovery. After receiving his doctorate, he will commence his post-doctoral training under the mentorship of Dr. Q. Ping Dou.